

**Modelling schizophrenia endophenotypes  
by overexpression of Neuregulin-1 isoforms  
in transgenic mice**

Dissertation

for the award of the degree

“Doctor of Philosophy”

Division of Mathematics and Natural Sciences

of the Georg-August-Universität Göttingen

within the doctoral program Molecular Physiology of the Brain  
of the Georg-August University School of Science (GAUSS)

submitted by

María Clara Soto-Bernardini

born in San José, Costa Rica

Göttingen, 2017

## **Thesis Committee**

Priv.-Doz. Dr. Markus Schwab  
Cellular Neurophysiology, Center of Physiology  
Hannover Medical School

Prof. Dr. Nils Brose  
Department of Molecular Neurobiology,  
Max-Planck-Institute of Experimental Medicine Göttingen

Prof. Dr. Till Marquardt  
Medical Faculty (UKA) and Faculty for Mathematics, Computer and Natural Sciences  
RWTH Aachen University

## **Members of the Examination Board**

Prof. Dr. Dr. Hannelore Ehrenreich  
Department of Clinical Neurosciences,  
Max-Planck-Institute of Experimental Medicine Göttingen

Prof. Klaus-Armin Nave, Ph.D.  
Department of Neurogenetics,  
Max-Planck-Institute of Experimental Medicine Göttingen

Prof. Dr. Martin Göpfert  
Department of Cellular Neurobiology,  
Schwann-Schleiden Research Centre, Georg-August-Universität Göttingen

Date of oral examination: 29.05.2017

## **Declaration**

I hereby declare that the PhD thesis entitled “Modelling schizophrenia endophenotypes by overexpression of Neuregulin-1 isoforms in transgenic mice”, was written independently and with no other sources and aids than quoted.

Göttingen, 31.03.2017

María Clara Soto-Bernardini

To Aníbal

“The most beautiful experience we can have is the mysterious. It is the fundamental emotion that stands at the cradle of true art and true science”.

Albert Einstein

## Acknowledgments

I am very grateful to Priv.-Doz. Dr. Markus Schwab for the opportunity to work in this project and his supervision. I am very thankful for his support, motivation and trust. This experience was extremely valuable for my career.

I would like to express my gratitude to Prof. Klaus-Armin Nave, Ph.D. for giving me the opportunity to work in his department. This was a great opportunity that allowed me to develop my scientific competences in an excellent environment. I am also thankful for his support and advices.

I thank the members of my thesis committee, Prof. Dr. Nils Brose and Prof. Dr. Till Marquardt for the helpful discussions in the committee meetings and their support. I further thank the members of my extended thesis committee, Prof. Klaus-Armin Nave, Ph.D., Prof. Dr. Dr. Hannelore Ehrenreich and Prof. Dr. Martin Göpfert for taking part of the final examination of my PhD.

I am very grateful with Dr. Tilmann Unterbarnscheidt for his support, advices and discussions during this years. I am very thankful to him for always being willing to share his scientific experience with me.

I am grateful to our collaborators. I would like to thank Prof. Dr. Dr. Hannelore Ehrenreich, Prof. Dr. Ekrem Dere, and Anja Ronnenberg for the behavioral analysis. I thank Dr. Noa Lipstein for the supervision and great advices regarding the Southern blot and the ES cell work. I thank Dr. Amit Agarwal for the ROSA locus targeting vector, and Dr. Cary Lai for the NRG2 cDNA and the recombinant NRG2 EGF-like domain. Additionally, I thank Prof. Dr. JeonSeop Rhee and Dr. Bekir Altas for the analysis of  $\gamma$ -oscillations. I am grateful with Dr. Ben Cooper for the very valuable advices for immunohistochemical analyses and the antibodies. Finally, I want to thank Dr. Josep Esquerda for receiving me in his lab for a couple of weeks where I learned a lot of very useful tips for immunohistochemical experiments.

I would like to thank the Deutscher Akademischer Austausch Dienst (DAAD), the Göttingen Graduate School for Neurosciences, Biophysics, and Molecular Biosciences (GGNB), the Ministry of Science, Technology and Telecommunications of Costa Rica (MICITT) and the Institute of Technology of Costa Rica (TEC) for the support and funding.

I want to thank Ulli Bode, Gudrun Fricke-Bode and Annette Fahrenholz for the technical support in many ways.

I thank the animal caretakers for looking after my mice, especially Tanja Freerck, Tanja Hoffmeister, Ines Malade, Cornelia Casper.

I thank Fritz Benseler for the advices regarding enzymes and cloning procedures.

I want to thank Hans-Joachim Horn, Lothar Demel and Rolf Merker for the technical support regarding computers and printers.

I am very thankful to Michaela Schmalstieg and Gabriele Endo for their help with administrative issues.

I am really grateful to all the people in the Neurogenetics Department for the very nice working atmosphere. I thank Ulrike, Theresa, Sarah, Iva, Andrea T, Dorota, Bea, Georg for the nice conversations and advices. I am sincerely grateful to the Stassart group especially Ruth, Robert, Andrea M, Dagmar, Vlad and Tamer for treating me as part of their group also for the fun events.

I am very grateful to my family for their love and support, especially Aníbal for his immense support, understanding, love and constant motivation.

## Content

<b>List of figures .....</b>	<b>4</b>
<b>Abbreviations.....</b>	<b>5</b>
<b>Abstract.....</b>	<b>7</b>
<b>1 Introduction .....</b>	<b>8</b>
1.1 Principles of mammalian brain structure and function .....	8
1.2 Schizophrenia.....	12
1.3 Neuregulin 1 .....	14
1.4 ErbB receptor tyrosine kinases .....	16
1.5 The ErbB4 receptor .....	18
1.6 NRG1/ErbB4 signaling in the brain during health and disease.....	19
1.7 NRG2: a NRG1-related ErbB4 ligand with unknown CNS function .....	21
1.8 Aim of the study.....	23
<b>2 Results .....</b>	<b>24</b>
2.1 Generation of a conditional HA-Ig-NRG1 transgenic mouse line.....	24
2.2 Embryonic overexpression of HA-Ig-NRG1 in <i>STOP-Nrg1*<i>NEX-Cre</i></i> mice.....	27
2.3 Chronic NEX-Cre-mediated HA-Ig-NRG1 overexpression in cortical projection causes ErbB4 hyperphosphorylation .....	28
2.4 Absence of neuropathology in the brain of <i>STOP-Nrg1*<i>NEX-Cre</i></i> mice .....	29
2.5 Reduced social inhibition in <i>STOP-Nrg1*<i>NEX-Cre</i></i> mice .....	31
2.6 Reduced hippocampal $\gamma$ -oscillations in Ig-NRG1 transgenic mice.....	35
2.7 The number of Parv <sup>+</sup> interneurons is unaltered in adult <i>STOP-Nrg1*<i>NEX-Cre</i></i> mice.....	35
2.8 Elevated Ig-NRG1 signaling preferentially recruits the AKT signaling pathway.....	37
2.9 Accumulation of Ig-NRG1 in the somatodendritic compartment of projection neurons .....	39
2.10 Analysis of Parv <sup>+</sup> interneuron-specific NRG1 mutants .....	43
2.11 Generation of a “knock in” mouse line for the conditional activation of NRG2 signaling in the brain.....	46
<b>3 Discussion .....</b>	<b>49</b>
3.1 Transgenic approaches to study brain functions.....	49
3.2 Modelling NRG1-ErbB4 hyperstimulation in transgenic mice .....	51
3.3 Embryonic overexpression of HA-Ig-NRG1 impaired social behavior and $\gamma$ -oscillation.....	52
3.4 Elevated Ig-NRG1/ErbB4 signaling preferentially recruits the AKT pathway .....	56
3.5 Ig-NRG1 accumulates in the somatodendritic, not the presynaptic compartment of neurons.....	59



---

3.6	A role for autocrine NRG1 signaling in Parv <sup>+</sup> interneurons?.....	61
3.7	Generation of <i>in vivo</i> and <i>in vitro</i> tools to study NRG2 signaling in cortical synapses .....	62
<b>4</b>	<b>Materials.....</b>	<b>64</b>
4.1	Kits and chemicals.....	64
4.2	Websites referred for online protocols .....	64
4.3	Equipment .....	64
4.4	Molecular biology buffers and solutions .....	66
4.5	Protein biochemistry .....	67
4.5.1	SDS-PAGE and Western blotting .....	67
4.6	DNA and protein markers .....	70
4.7	Immunohistochemistry buffers .....	70
4.8	Histological stains and reagents .....	72
4.9	Primers.....	73
4.9.1	Genotyping primers .....	73
4.9.2	Quantitative real-time PCR primers .....	74
4.10	Strains and bacterial culture media.....	74
4.11	ES cell culture mediums and solutions .....	75
4.12	Chemicals and media for primary cell culture .....	76
4.13	Enzymes.....	77
4.14	Antibodies.....	78
4.14.1	Primary antibodies.....	78
4.14.2	Secondary antibodies .....	79
4.15	Mouse lines .....	79
<b>5</b>	<b>Methods .....</b>	<b>81</b>
5.1	Generation of conditional Ig-NRG1 transgenic mice .....	81
5.2	Breeding of mouse mutants.....	81
5.3	Animal maintenance and handling.....	81
5.4	Phenotyping of tail biopsies of <i>STOP-Nrg1</i> mice .....	81
5.5	Preparation of mouse genomic DNA.....	82
5.5.1	Nexttec™ Tissue & Cells kit-based genomic DNA isolation .....	82
5.5.2	Chloroform DNA extraction.....	82
5.6	Genomic DNA analysis.....	82
5.6.1	DNA amplification <i>in vitro</i> by polymerase chain reaction (PCR) .....	82
5.6.2	Primer design .....	83
5.6.3	PCR programs for genotyping .....	83
5.6.4	Agarose gel electrophoresis separation of DNA fragments.....	85
5.6.5	Measurement of the DNA concentration and purity.....	85
5.6.6	Quantitative Real Time PCR (qRT-PCR) .....	86

---

5.7	Biochemical analysis of protein.....	87
5.7.1	Protein extraction.....	87
5.7.2	Protein concentration measurement .....	87
5.7.3	SDS polyacrylamide gel electrophoresis.....	87
5.7.4	Silver staining of polyacrylamide gels .....	88
5.7.5	Western Blotting .....	88
5.7.6	Immunological detection of proteins and densitometric quantification .....	89
5.8	Histology and immunohistochemistry.....	89
5.8.1	Analysis of the STOP-cassette in different organs .....	89
5.8.2	Perfusion fixation of mouse tissue .....	90
5.8.3	Vibratome sectioning .....	90
5.8.4	Cryoprotection, embedding and cryosectioning .....	90
5.8.5	Paraplast impregnation, embedding and sectioning.....	91
5.8.6	Immunohistological staining procedures .....	92
5.9	Imaging and image analysis .....	94
5.9.1	Cell counting of chromogenic stainings.....	94
5.9.2	Quantification of GFAP <sup>+</sup> and IBA1 <sup>+</sup> areas .....	94
5.10	Behavioral experiments .....	95
5.10.1	Visual cliff test .....	95
5.10.2	Hot plate test .....	95
5.10.3	Exploratory activity in the open field.....	95
5.10.4	Pre-pulse inhibition of the startle response .....	96
5.10.5	Social interaction in pairs.....	96
5.10.6	Statistical analyses .....	97
5.11	Analysis of $\gamma$ -oscillations .....	97
5.12	Primary neuronal culture.....	98
5.12.1	Preparation and maintenance.....	98
5.12.2	Treatment, fixation and staining procedure of primary neurons.....	99
5.13	Generation of conditional NRG2 transgenic mice .....	100
5.13.1	Molecular cloning.....	100
5.13.2	Embryonic stem (ES) cell culture, electroporation, preparation for blastocyst injection .....	102
5.13.3	PCR-based strategy for ES cell clone screening.....	107
<b>6</b>	<b>References .....</b>	<b>109</b>
	<b>Curriculum vitae .....</b>	<b>134</b>

## List of figures

- Figure 1. A cerebral microcircuit.
- Figure 2. Glial cells in the CNS.
- Figure 3. NRG1: alternative splicing, protein structure, and proteolytic processing.
- Figure 4. Ligand binding and activation of ErbB receptors.
- Figure 5. A conditional transgenic mouse line for Cre-mediated expression of Ig-NRG1.
- Figure 6. The  $\beta$ -actin GFP-STOP-flox cassette is widely expressed in nervous and non-nervous tissues of transgenic mice.
- Figure 7.  $\beta$ -actin GFP-STOP-flox cassette is predominantly expressed in projection neurons.
- Figure 8. *NEX-Cre*-mediated overexpression of HA-Ig-NRG1 in *STOP-Nrg1\**NEX-Cre** mice during embryonic stages.
- Figure 9. *NEX-Cre*-mediated HA-Ig-NRG1 expression is restricted to cortical projection neurons during adult stages.
- Figure 10. HA-Ig-NRG1 overexpression in projection neurons causes ErbB4 hyperphosphorylation.
- Figure 11. Normal numbers of cortical neurons in *STOP-Nrg1\**NEX-Cre** mice.
- Figure 12. *STOP-Nrg1\**NEX-Cre** mice show no signs of astrogliosis.
- Figure 13. *STOP-Nrg1\**NEX-Cre** mice show no signs of microgliosis.
- Figure 14. Sensory, exploratory, motor functions, and sensorimotor gating are not affected, but social behavior is altered in *STOP-Nrg1\**NEX-Cre** mice.
- Figure 15. Cortical restricted HA-Ig-NRG1 overexpression in projection neurons reduces the power of hippocampal  $\gamma$ -oscillations.
- Figure 16. Unchanged numbers of Parv<sup>+</sup> cortical interneurons in *STOP-Nrg1\**NEX-Cre** mice.
- Figure 17. Cortical restricted Ig-NRG1 overexpression preferentially stimulates the AKT signaling pathway.
- Figure 18. Ig-NRG1 shows a “punctate” pattern of expression in the somatodendritic compartment of projection neurons.
- Figure 19. NRG1 does not colocalize with presynaptic markers.
- Figure 20. Ig-NRG1 does not colocalize with postsynaptic markers.
- Figure 21. Ig-NRG1 partially colocalizes with the potassium channel Kv2.1.
- Figure 22. Reduced body weight in *Nrg1 f/f\**Parv-Cre** mutants.
- Figure 23. Unaltered numbers of Parv<sup>+</sup> interneurons in the hippocampus of *Nrg1 f/f\**Parv-Cre** mutants.
- Figure 24. Reduction of Parv<sup>+</sup> interneurons in cortical layers II/III of *Nrg1 f/f\**Parv-Cre** mice.
- Figure 25. *In vitro* tools to examine NRG2 functions at CNS synapses.
- Figure 26. Generation of a “knock in” mouse line for conditional NRG2 overexpression.

---

## Abbreviations

AKT	Protein kinase B
AMPA	$\alpha$ -amino-3-hydroxy-5-methyl-4-isoxazolepropionic acid
APP	Amyloid beta precursor protein
bp	Base pairs
°C	Degrees Celsius (centigrades)
CA	Cornu Ammonis
CamKII	Calcium/calmodulin-dependent protein kinase II
ChaT	Choline acetyltransferase
Cm	Centimeters
DAB	3,3'-Diaminobenzidine
DAPI	4'-6-Diamidino-2-phenylindole
Db	Decibel
ddH <sub>2</sub> O	Double distilled (or miliQ) water
DIV	Days <i>in vitro</i>
DMSO	Dimethylsulfoxide
DNA	Deoxyribonucleic acid
DTT	Dithiothreitol
e.g.	<i>Exempli gratia</i>
EDTA	Ethylened acid
ERK	Extracellular signal-regulated kinase
f.c.	Final concentration
g	Gram
GAD67	Glutamate-Decarboxylase of 67 kDa
GFAP	Glial fibrillary acidic protein
GFP	Green fluorescent protein
h	Hours
HA-tag	Human influenza hemagglutinin tag
Hz	Herz
i.e.	<i>Id est</i>
IBA1	Ionized calcium-binding adapter molecule 1
IHC	Immunohistochemistry
kb	Kilobases
kDa	Kilodalton
kg	Kilogram

---

kHz	Kilohertz
M	Molar
mA	Milliampere
MAPK	Mitogen-activated protein kinase
min	Minutes
ml	Milliliter
mM	Millimolar
ms	Milliseconds
mΩ	Milohms
ng	Nanogram
nM	Nanomolar
nm	Nanometer
NMDA	<i>N</i> -Methyl-D-aspartic acid
ON	Overnight
p	P-value
PFA	Paraformaldehyde
pM	Picomolar
PVDF	Polyvinylidene fluoride
rpm	Revolutions per minute
RT	Room temperature
s	Seconds
SEM	Standard error of the mean
TEMED	Tetramethyldiamin
U	Unit (for enzyme activities)
UV	Ultraviolet
V	Volt
v/v	Volume per volume
wt	Wildtype
w/v	Weight per volume
WB	Western blot
xg	$g = 9.81 \text{ ms}^{-1}$ , relative centrifugal force
μF	Microfarads
μg	Microgram
μl	Microliter
μM	Micromolar
μm	Micrometer

## Abstract

Neuregulin 1 (NRG1) is the best characterized member of a family of epidermal growth factor (EGF)-like domain containing proteins that serve as ligands for tyrosine kinase receptors of the ErbB family. NRG1 and its main receptor in the brain, ErbB4, have been involved in neural development, neurotransmission and synaptic plasticity. Additionally, NRG1 isoform-specific expression patterns in the brain have been described, but isoform-specific functions remain unclear. *Nrg1* is a robustly associated schizophrenia susceptibility gene in many populations. Examination of blood cells and *post mortem* brain tissue revealed that increased *Nrg1* expression occurs in schizophrenia patients, including a notable increase in *Ig-Nrg1* mRNA. Together with ErbB4 hyperphosphorylation observed in *post mortem* brains of schizophrenia patients, this suggests that NRG1/ErbB4 hyperstimulation could represent a component of schizophrenia etiology. However, the underlying pathomechanisms are unknown.

In the present study, we investigated brain endophenotypes associated with cortical-restricted Ig-NRG1/ErbB4 hyperstimulation. For this purpose, a conditional transgenic mouse line was produced that permits stage- and cell type-specific overexpression of the Ig-NRG1 isoform under control of the  $\beta$ -actin promoter after Cre-mediated removal of a “floxed” STOP-cassette. A comprehensive analysis of this mouse model revealed that physiologically relevant Ig-NRG1 overexpression in glutamatergic projection neurons resulted in chronic ErbB4 hyperphosphorylation in the neocortex and hippocampus. ErbB4 hyperstimulation was associated with impaired hippocampal  $\gamma$ -oscillation and altered social behavior. Biochemical analyses revealed a preferential activation of the AKT pathway upon Ig-NRG1 overexpression. Furthermore, moderate projection neuron-specific overexpression of Ig-NRG1 allowed us to investigate the subcellular localization of the protein, which appeared to be associated with the potassium channel Kv2.1 in the somatodendritic compartment. These results provide a first insight into possible molecular pathomechanisms and schizophrenia-relevant endophenotypes induced by Ig-NRG1-mediated ErbB4 hyperstimulation in cortical networks.

In a second project, NRG1 signaling functions in ErbB4-expressing GABAergic interneurons have been investigated in conditional NRG1 mutants. Cre-mediated elimination of NRG1 from parvalbumin-positive (Parv<sup>+</sup>) interneurons resulted in body weight reduction, a shivering phenotype, increased motor activity, and a reduced number of interneurons in cortical layers II-III. Thus, in contrast to projection neuron-specific loss- or (moderate) overexpression of NRG1, these findings suggest that NRG1-mediated autocrine signaling in Parv<sup>+</sup> interneurons serves an essential role in the regulation of inhibitory circuit functions.

Finally, in a pilot project a new mouse line for the conditional overexpression of NRG2, a closely related ErbB4 ligand in the brain, has been generated by homologous recombination into the Rosa26 locus of embryonic stem cells.

# 1 Introduction

## 1.1 Principles of mammalian brain structure and function

The central nervous system (CNS) comprises two major parts, the brain and the spinal cord. The brain is an extremely complex organ, whose processes range from simple motor behavior to complex cognitive tasks. It is divided into several functional regions: the brain stem (medulla oblongata, pons and midbrain) receives the sensory information from skin and muscles of the head and provides motor control of head's musculature. It also conveys information from the spinal cord to the brain (and vice versa) and is involved in processing information of hearing, balance and taste senses. The cerebellum is involved in the learning of motor skills and modulates the force and range of movement. The diencephalon (thalamus and hypothalamus) regulates autonomic, endocrine, and visceral functions. Finally, the cerebrum comprises three deep laying structures: the basal ganglia, involved in regulation of motor performance; the hippocampus, which participates in processes of memory storage; and the amygdala, which coordinates autonomic and endocrine responses of emotional states. In addition, the cerebrum contains the two cerebral hemispheres, each with an outer layer called the cerebral cortex. The latter is divided into four lobes with specialized functions: frontal (e.g. short-term memory, motor function, problem solving, spontaneity), parietal (e.g. somatic sensation), occipital (e.g. visual processing), and temporal lobe (e.g. hearing, learning, memory, and emotion) (Kandel, 2013; Markram et al., 2004).

At the beginning of the 20th century, Santiago Ramón y Cajal performed a detailed description of nerve cells and proposed that the nervous system is a network of discrete cells. The principle that neurons are elementary building and signaling elements of the nervous system is called the neuron doctrine. The final proof that confirmed the neuron doctrine came with the introduction of electron microscopy (mid 1950s), when Sandford Palay demonstrated the existence of regions where chemical or electrical signaling between neurons occurs (Palay, 1956; Palay and Palade, 1955). Nowadays, it is known that the human brain consists of approximately  $10^{11}$  electrically excitable neurons that form neuronal networks. Neurons communicate with each other through two kinds of processes that arise from the soma. Dendrites receive incoming signals from other neurons, whereas a single axon conveys electrical signals to other cells. These electrical signals, called action potentials (AP), result from changes in the flux of ions through plasma membrane channels. APs originate at the axon hillock when the electrical excitation of a neuron reaches a certain threshold. APs are all-or-none signals that propagate along the axon and eventually reach fine axonal branches to contact other neurons via synapses. The mammalian brain contains up to  $10^{15}$  synapses (Brose, 1999; Kandel, 2013). In vertebrates, large axons are wrapped by an insulating sheath of lipids called

myelin, which increases AP speed. The myelin is interrupted at the Nodes of Ranvier, where the AP regenerates (Salzer, 2003).

Most of the synapses in the CNS are chemical synapses, in which the pre- and postsynaptic neurons are separated by a synaptic cleft. Chemical synaptic transmission requires the release of neurotransmitters from the presynaptic terminal and movement across the synaptic cleft. Presynaptic terminals contain synaptic vesicles that cluster in active zones. When an AP reaches the active zone, synaptic vesicles fuse with the presynaptic membrane and release neurotransmitters into the synaptic cleft. Afterwards, neurotransmitters bind to receptors on the postsynaptic neuron. Normally, neurotransmitter release produces a single predominant type of synaptic response, e.g. release of glutamate produces excitation, while  $\gamma$ -aminobutyric acid (GABA) or glycine produce inhibitory postsynaptic potentials. Furthermore, besides the differences in biochemical composition, synaptic terminals of excitatory and inhibitory synapse can be distinguished by their morphology. Electrical synapses, by which two cells communicate via gap-junctions also exist. In this case, there is no release of chemical transmitters but the current is transmitted to the postsynaptic cell through the gap-junctions. In contrast to unidirectional transmission at chemical synapses, electrical synapses allow extremely fast bidirectional signal propagation. Even though chemical synapses are not as rapid as electrical synapses, they present an important characteristic called amplification. This phenomenon is based on the fact that from each synaptic vesicle thousands of neurotransmitter molecules are released and activate neurotransmitter receptors in the postsynaptic cell. In many cases, these receptors contain both an extracellular binding site for the neurotransmitter and a membrane spanning-domain that allows ion flux, and are therefore called ionotropic. Another class of receptors, called metabotropic receptors, couple to guanosine triphosphate (GTP)-binding proteins that trigger a second-messenger mediated biochemical cascade or act directly on the opening of ion channels (Kandel, 2013).

The brain comprises different types of neurons that communicate at synapses and form complex circuits. The main neuronal cell type in the brain are excitatory glutamatergic projection neurons. These cells represent 70-80% of neocortical neurons and are located in all cortical layers except for layer I. In general, projection neurons have a characteristic morphology with a long axon and two types of dendrites. Basal dendrites emerge from the same side of the soma as the axon does, whereas apical dendrites originate from the opposite side. Projection neurons form excitatory synapses at specialized protrusions of the dendrites, called dendritic spines (DeFelipe et al., 2013; DeFelipe and Fariñas, 1992; Markram et al., 2004). These postsynaptic microdomains are equipped with a postsynaptic density (PSD) at the cytoplasmic face of the postsynaptic cell in close apposition to the active zone of the presynaptic terminal. The PSD is considered to serve as an organizer of the postsynaptic machinery, in which hundreds of proteins have been identified, including glutamate receptors,



postsynaptic density protein of 95 kDa (PSD95), and many signaling molecules. Pyramidal neurons can also form excitatory synapses with inhibitory interneurons, which usually do not present dendritic spines but are equipped with PSDs (Kandel, 2013; Kennedy, 1997; Ziff, 1997).

The second main component of cortical microcircuits are inhibitory GABAergic interneurons, which possess a short axon that does not leave the cortex, and whose activities are more local. Interneurons represent 20-30% of all neocortical neurons (DeFelipe et al., 2013; Marín, 2012; Markram et al., 2004). GABAergic interneurons are classified into 30 different subtypes based on morphology, molecular and physiological characteristics (Marín and Müller, 2014). As the classification of interneurons by morphological criteria is sometimes difficult, a main classification method is based on the expression of particular proteins. For example, calcium-binding proteins, such as parvalbumin (Parv), calretinin or calbindin. Other interneurons express specific neuropeptides, including somatostatin, cholecystokinin (CCK), neuropeptide Y (NPY), and vasoactive intestinal peptide (VIP) (DeFelipe et al., 2013; Freund and Buzsáki, 1996; Lewis et al., 2005). Different types of these interneurons control the excitability of pyramidal neurons in a unique manner, based on their ability to innervate specific subcellular regions. Martinotti cells, neurogliaform cells and double-bouquet cells form synapses with pyramidal cell dendrites, basket cells form synapses with the soma of pyramidal cells, and chandelier cells innervate the axonal initial segment (Marín, 2012; Markram et al., 2004; Somogyi, 1977). Some classes of interneurons contribute to the coordinate firing of pyramidal cells, which underlays the generation and pacing of different forms of rhythmic activity. Fast-spiking Parv<sup>+</sup> interneurons are responsible for oscillations in the  $\gamma$ -frequency range (30–80 Hz), whereas, non-adjusting, non-fast-spiking somatostatin-expressing interneurons generate  $\beta$ -frequency oscillations (15–30 Hz). Interneurons receive excitatory as well as inhibitory synapses onto their soma (Bartos et al., 2007; Buzsáki and Draguhn, 2004; Marín, 2012).

Inhibitory GABAergic interneurons and excitatory glutamatergic projection neurons are organized in well-defined cell layers in the cerebral cortex (Fig. 1). However, they differ in their developmental origin. Excitatory neurons derive from progenitors in the ventricular zone (VZ) of the pallium and migrate radially into the developing neocortex. In contrast, inhibitory neurons originate from progenitors in the subpallium, from where they migrate along tangential routes to the developing neocortex. Subsequently, interneuron migration switches from tangential to radial migration and interneurons invade different neocortical cell layers (Marín, 2013; Marín and Müller, 2014; Marín and Rubenstein, 2001).

The large majority of cells in the CNS are not neurons, but neuroglia. Glial cells represent more than 80% of the cells in the human brain. These cells differ morphologically (absence of dendrites and axons) and functionally (not directly involved in electric signaling) from neurons.

In vertebrates, glia cells are divided in two major classes. Microglia are immune cells that protect the nervous system and macroglia, which comprise oligodendrocytes and astrocytes.

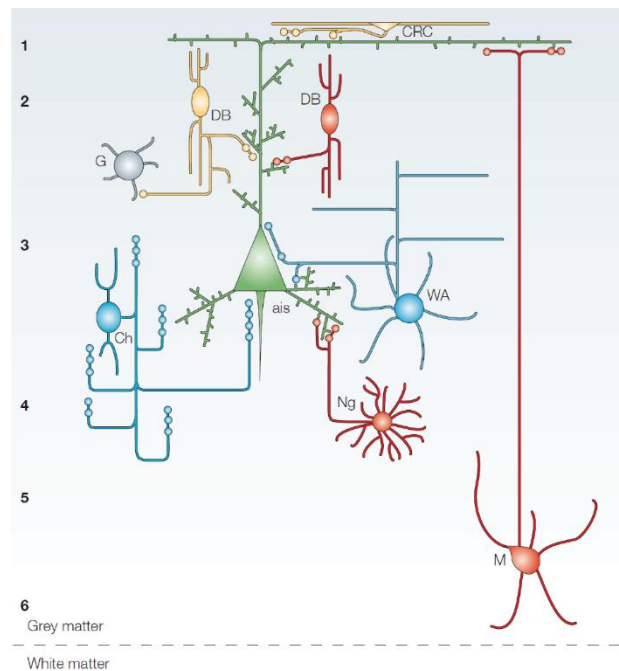


**Figure 1. A cerebral microcircuit.** An excitatory pyramidal neuron is innervated by different classes of interneurons. Chandelier (Ch) and wide arbor (WA) or basket interneurons provide inhibitory input to the axon initial segment (ais) and proximal dendrites, respectively, of pyramidal neurons. Calbindin-expressing double bouquet (red DB), neurogliaform (Ng) and Martinotti (M) interneurons form inhibitory synapses at distal dendrites of pyramidal neurons. Calretinin-expressing (yellow) DB and Cajal–Retzius cells (CRC) target both distal dendrites of pyramidal cells and other GABAergic (G) neurons. 1–6, cortical layers. (Modified from Lewis et al., 2005).

Oligodendrocytes form the myelin sheaths that surround and insulate axons, similar to Schwann cell in the peripheral nervous system (PNS). Unlike Schwann cells that interact with axons in a one-to-one relationship, each oligodendrocyte myelinates up to 30 axonal segments (Fig. 2A; Kandel, 2013; Salzer, 2003). Another important function of oligodendrocytes corresponds to metabolic support and maintenance of the functional integrity of axons (Fünfschilling et al., 2012; Saab et al., 2013, 2016).

Astrocytes have a characteristic star-like shape with large numbers of processes, which contact capillaries and neurons. Astrocytes have an important role in the maintenance of the blood-brain barrier. They regulate extracellular concentrations of ions ( $K^+$ ) and neurotransmitters. Astrocytic processes engulf neuronal synapses, respond to neuronal activity (which increases the  $Ca^{2+}$  concentration in the astrocyte and leads to glutamate or ATP release), and modulation of neuronal activity. This functional integration of pre- and post-synaptic neurons with astrocytes is called the tripartite synapse (Fig. 2B; Kandel, 2013; Lalo et al., 2009; Santello and Volterra, 2009).

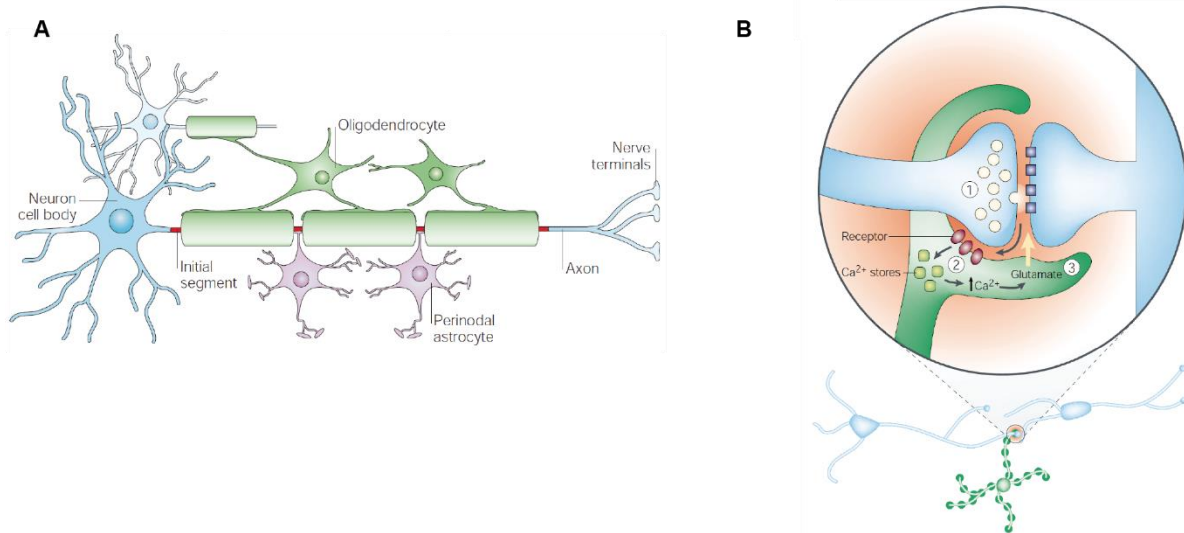


**Figure 2. Glial cells in the CNS. (A)** In the CNS myelin is formed by oligodendrocytes. Each oligodendrocyte engulfs multiple axonal segments with a myelin sheath that speeds up signal propagation by saltatory impulse propagation. Perinodal astrocytes make contact with the nodes of Ranvier (modified from Poliak and Peles, 2003). **(B)** Diagram of a tripartite synapse. An astrocytic process wraps around a synapse. Local signaling between neurons and astrocytes modulates neuronal activity. Astrocytes respond to synaptic activity (1), which acts on astrocytic receptors and triggers  $\text{Ca}^{2+}$  release from internal stores, increasing astrocytic  $\text{Ca}^{2+}$  levels (2). This effect (3) evokes the local release of glutamate and modulates synaptic functions (modified for Haydon, 2001).

The balance between excitation and inhibition and the participation of glial cells in neuron-glia signaling processes is of paramount importance for the correct functioning of cortical circuits. The coordination and communication between these neural cells is the basis for higher cognitive processes, e.g. learning and memory formation, and is regulated by a large number of molecular signaling modules. For example, several neurotrophic factors exert their effects on neurons by signaling through tyrosine kinase receptors to promote neuronal migration, differentiation and survival, synapse formation and synaptic plasticity. Additionally, modules of signaling molecules and their receptors displayed on the cell surface serve as important regulators during the development of the neural network, and for network plasticity in the mature brain. Imbalance between inhibitory and excitatory neurotransmission might result from defects in neuronal communication at all levels above mentioned. Impaired modulation of cortical circuits may also lead to neural network disconnectivity, which has been observed in neuropsychiatric diseases such as schizophrenia (Hayashi-Takagi, 2017; Kandel, 2013; O'Donoghue et al., 2016).

## 1.2 Schizophrenia

Schizophrenia (SZ) is a severe neuropsychiatric disease that affects ~1% of the population worldwide. This disorder is characterized by positive symptoms (such as hallucinations and delusions), negative symptoms (including anhedonia and lack of motivation), and cognitive dysfunction (Insel, 2010). The age of onset is usually during late adolescence or early

adulthood. Due to very disabling condition for patients (Kirov et al., 2005), this disease leads to significant financial and care burden for the families and health care systems.

Reduced cerebral volume and ventricular enlargement are morphological abnormalities that have been frequently found in SZ patients (Vita et al., 2006; Wright et al., 2000). In addition, alterations in synaptic, dendritic and axonal organization have been found, such that SZ can be considered a synaptic disorder. Structural and functional changes in both excitatory and inhibitory circuits have been observed in postmortem brains of individuals with SZ (Chattopadhyaya and Di Cristo, 2012; Garey et al., 1998; Hayashi-Takagi, 2017; Moyer et al., 2015). An imbalance in excitatory and inhibitory activity (E/I imbalance) appears to play a key role in the pathophysiology of SZ (Gao and Penzes, 2015). Furthermore, functional imaging has revealed aberrant activity in cortical circuits, involving the prefrontal cortex (PFC) and hippocampus, as well as subcortical structures, e.g. dorsal thalamus. These functional abnormalities have been suggested to result in disconnectivity between those brain regions (Harrison, 1999).

SZ is considered a multifactorial disease, i.e. multiple genes (each with a small effect) together with environmental factors precipitate the disorder (Risch, 1990; Stepniak et al., 2014). In addition, it is likely that different gene combinations contribute to a similar phenotype in different families and populations (Dawson and Murray, 1996). However, the number of susceptibility loci, the increased risk of developing the disease conferred by each locus, the degree of genetic heterogeneity, and the extent of interaction between loci are not yet known (Owen et al., 2005). Among environmental factors that are thought to be of relevance are prenatal and obstetric complications, such as low birth weight, Rh incompatibility, hypoxia, maternal nutritional deficiencies in the first trimester of pregnancy, exposure to influenza virus, maternal psychological stress (Leask, 2004; Stepniak et al., 2014). Other relevant environmental factors that have been associated with the development of this disease are residence in urban areas and abuse of substances such as amphetamines, cocaine, hallucinogens (Leask, 2004) and marijuana during adolescence (Arseneault et al., 2002).

The importance of a genetic contribution to the etiology of schizophrenia has been demonstrated by twin studies that showed a concordance of 41-65% in monozygotic twins, compared with a concordance of 0-28% in dizygotic twins. Furthermore, the disease exhibits a heritability of around 85% (Cardno and Gottesman, 2000). The absence of unequivocal results in linkage disequilibrium and association studies for SZ might be explained by different environmental factors, the involvement of multiple genes with minor effects, and genetic heterogeneity (Mowry and Nancarrow, 2001). In addition, the complexity and the large number of symptoms manifested by SZ patients as well as the overlapping symptoms with other mental illnesses must be considered (Bahn, 2002; Bramon and Sham, 2001; Gao and Penzes, 2015; Lee et al., 2017). Despite the difficulties to replicate genetic findings, several genomic studies

have demonstrated some consistency. Independent meta-analyses, Badner and Gershon (2002) and Lewis et al., (2003) obtained significant results for chromosome 8p, a region in which Neuregulin 1 (*Nrg1*), one of the most reproducible SZ candidate genes, is located. Several NRG1 genetic variants and haplotypes have been associated with SZ in many (but not all) studies performed in different populations. Most of these variants are located in non-coding regions of the gene (Athanasias et al., 2010; Li et al., 2006; Munafò et al., 2006; Norton et al., 2006; Petryshen et al., 2005; Stefansson et al., 2002). Genetic association between *Nrg1* and its receptor *ErbB4* with SZ has been supported by genome-wide association studies (GWASs) (Agim et al., 2013; Mostaid et al., 2017; Sullivan et al., 2008).

### 1.3 Neuregulin 1

NRG1 is a member of a family of growth factors encoded by four different genes (*Nrg1-4*). NRG1, the best characterized protein of this family, is encoded by one of the largest mammalian genes (~1.4 Mb) located on the short arm of chromosome 8 (8p13) (Harrison and Law, 2006). Alternative splicing and differential promoter usage in the *Nrg1* gene result in the expression of more than 30 isoforms that can be grouped into six different types of proteins (Fig. 3A; Steinhorsdottir et al., 2004). NRG1 type I-VI differ in their N-terminal domains, but all types contain an epidermal growth factor (EGF)-like signaling domain, which is necessary and sufficient to activate tyrosine kinase receptors of the ErbB family (Falls, 2003a; Mei and Xiong, 2008). Two variants of the EGF-like domain exist, which are named  $\alpha$  and  $\beta$ . The  $\beta$ -EGF-like domain has a 100-fold stronger binding affinity to ErbB receptors (Jones et al., 1999). NRG1 type I, II, IV, and V contain a N-terminal immunoglobulin (Ig)-like domain and are referred to as Ig-NRG1 (Harrison and Law, 2006; Mei and Xiong, 2008). The different types of NRG1 have alternative names reflecting their original identification. NRG1 type I was originally named heregulin (Holmes et al., 1992), neu-differentiation factor (NDF) (Wen et al., 1992), or acetylcholine receptor-inducing activity (ARIA) (Falls, 2003a). NRG1 type II is also referred to as glial growth factor (GGF) (Marchionni et al., 1993), or kringle-like domain isoform (Harrison and Law, 2006), because it harbors this domain N-terminally to the Ig-like domain. NRG1 type III contains a cysteine-rich domain (CRD) that serves as a second transmembrane domain. Originally, these variants were named sensory and motor neuron derived factor (SMDF) (Ho et al., 1995), nowadays they are referred to as CRD-NRGs (Falls, 2003a). NRG1 isoforms can also be classified according to the presence of different juxtamembrane stalk regions and cytoplasmic tails (Harrison and Law, 2006; Wen et al., 1994).

The most abundant classes of NRG1 in human and rat brain are type III and type II, followed by type I and type V. Different types of NRG1 isoforms exhibit dynamic expression profiles with expression peaks during early embryonic stages (E13) and around postnatal day (P) 5, suggesting that they exert important functions in neural development. NRG1 isoforms are

expressed in projection neurons of the human and rat cortex and hippocampus, but were also found in GABAergic interneurons and astrocytes (Law et al., 2004; Liu et al., 2011; Okada and Corfas, 2004). The expression of NRG1 isoforms is distinctly regulated by neuronal activity, as observed using a rat model of epileptic seizures induced by kainate treatment in which type I and II isoforms were found to be significantly upregulated, while kainate treatment had no effect on the expression of types III, V and VI isoforms (Liu et al., 2011).

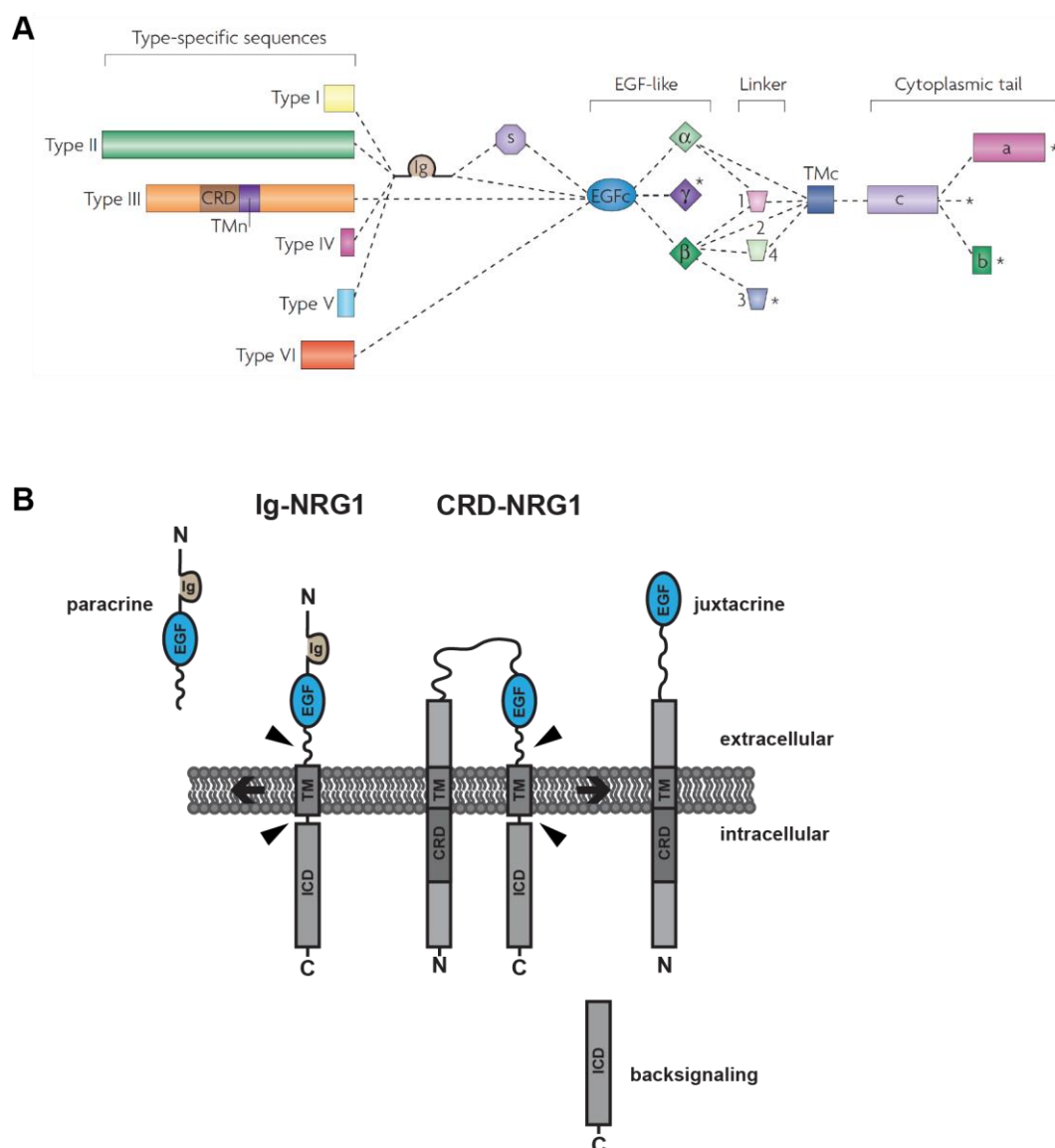


**Figure 3. NRG1: alternative splicing, protein structure, and proteolytic processing.** (A) Alternative splicing and differential promoter usage in the *Nrg1* gene produces NRG1 isoforms with different N-terminal domains. NRG1 type III harbors a cysteine-rich domain (CRD), which serves as a second transmembrane domain (TMn). Types I, II, IV and V contain an N-terminal Ig-like domain. An EGF-like domain is present in all isoforms, a spacer region (S) is lacking in types III and VI in which the N-terminal-specific domain is directly linked to the EGF-like domain. Alternative splicing in the linker region and the C-terminal domain generate additional variants (modified from Mei and Xiong, 2008). (B) Structure of NRG1 type I (Ig-NRG1) and type III (CRD-NRG1). NRG1 isoforms are synthesized as transmembrane pre-proteins (pro-NRG1s). In CRD-NRG1, the N- and C-terminal domains are located in the cytoplasm. Proteolytic cleavage generates mature soluble Ig-NRG1s that act as paracrine signals; in the case of CRD-NRG1 the EGF-like domain remains attached to the membrane after processing, and is thought to function mainly as a juxtacrine signal. The processing of pro-NRG1 type II, IV, V, and VI is similar to type I. Backsignaling via the ICD may also occur. Arrowheads indicate sites of proteolytic processing.

Most NRG1 isoforms are synthesized as transmembrane precursors that subsequently undergo proteolytic cleavage at the juxtamembrane stalk region located C-terminal to the EGF-like domain. In the case of Ig-NRG1 isoforms, this results in the release of a diffusible N-terminal fragment, including the EGF- and Ig-like domains. Therefore, these isoforms seem to act mainly through paracrine signaling by binding to ErbB receptors in neighboring cells. The Ig-like domain binds proteoglycans at the cell surface and extracellular matrix, and this mechanism might increase the concentration of NRG1 at the synapse and subsequent activation of ErbB receptors (Li and Loeb, 2001). Further cleavage that separates the EGF-like domain has been proposed (Falls, 2003b; Harrison and Law, 2006). CRD-NRG1 represents an exception, as it remains attached to the membrane through the CRD domain after proteolytic processing and serves as a juxtacrine signal (Fig. 3B; Harrison and Law, 2006; Mei and Xiong, 2008). The diversity of NRG1 biology is reflected by the findings of several studies in which isoform-specific functions were demonstrated, e.g. for the migration of neurons to the developing cortex (Anton et al., 1997; Flames et al., 2004; Rio et al., 1997).

The complexity of NRG1 signaling is further increased by post-translational modifications, such as glycosylation (Burgess et al., 1995) and proteolytic processing by proteases, such as tumor necrosis factor- $\alpha$  converting enzyme (TACE/ADAM17) (Loeb et al., 1998; Montero et al., 2007),  $\beta$ -site of amyloid precursor protein cleaving enzyme (BACE) (Hu et al., 2006; Willem et al., 2006) and meltrin beta (ADAM19) (Yokozeki et al., 2007). Further processing of NRG1 type III by ADAM17 and BACE1 N-terminal to the EGF-like domain could release this domain, allowing paracrine signaling (Fleck et al., 2013). NRG1 expression and processing seem to be regulated temporally, spatially and by neuronal activity (Eilam et al., 1998; Mei and Xiong, 2008; Ozaki et al., 2004). NRG1 may also act as an ErbB “receptor”, as the intracellular domain (ICD) of NRG1 has been shown to undergo proteolytic cleavage by  $\gamma$ -secretase, triggered by ErbB receptor binding, in addition to synaptic activation or membrane depolarization. After processing and nuclear translocation, this domain may act as a transcription factor to regulate the expression of genes involved in neuronal survival, synaptic maturation and maintenance. ICD-mediated backsignaling has been suggested to regulate growth and branching of cortical dendrites (Bao et al., 2003, 2004; Chen et al., 2010b; Wang et al., 1998). Such backsignaling activity is further supported by direct binding of the NRG1-ICD to LIM kinase 1 (LIMK1), a central regulator of actin dynamics.

#### **1.4 ErbB receptor tyrosine kinases**

ErbB receptors comprise a family of four transmembrane receptor tyrosine kinases (ErbB1-4) that are activated by EGF and related factors, such as members of the NRG family. In total, ErbB receptors integrate signals of more than 15 different ligands. ErbB receptors are widely distributed in many organs and cell types with ectodermal and mesodermal origins, where they

exert important functions in processes related to cell proliferation, growth, migration, and adhesion. These receptors also play an important role in heart development and altered ErbB signaling has been linked to different types of cancer. In the nervous system, ErbB receptors are involved in the regulation of neuronal migration, myelination, axon guidance, synapse and neuromuscular junction formation. ErbB1 (EGFR, HER1) was the first receptor identified based on homology of its gene (*c-erbB*) with the oncogene *v-erbB*, previously identified in avian erythroblastic leukemia virus. Subsequently, additional members of the ErbB family were discovered, including ErbB2 (also known as HER2 and Neu), ErbB3 (HER3), and ErbB4 (HER4) (Iwakura and Nawa, 2013; Mei and Xiong, 2008; Yarden and Sliwkowski, 2001).

All ErbB receptors possess a glycosylated extracellular N-terminal ligand binding domain. The extracellular region also contains two cysteine-rich domains, important for receptor dimerization. In addition, ErbB receptors have a transmembrane domain, a short intracellular juxtamembrane region, a tyrosine kinase domain and a C-terminal tail. Upon ligand binding, monomeric ErbB receptors undergo conformational changes that render the dimerization arm accessible resulting in receptor homo- or heterodimerization. The subsequent activation of tyrosine kinase activity leads to auto-transphosphorylation of tyrosine residues in the intracellular domain, which generates docking sites for adaptor proteins and further activates downstream signaling pathways, e. g. the MAPK (Erk) and PI3K-AKT signaling pathways (Fig. 4; Burgess et al., 2003; Iwakura and Nawa, 2013; Mei and Xiong, 2008; Yarden and Sliwkowski, 2001). Ligand-induced endocytosis of ErbB receptors might have an important role in this process (Yang et al., 2005).

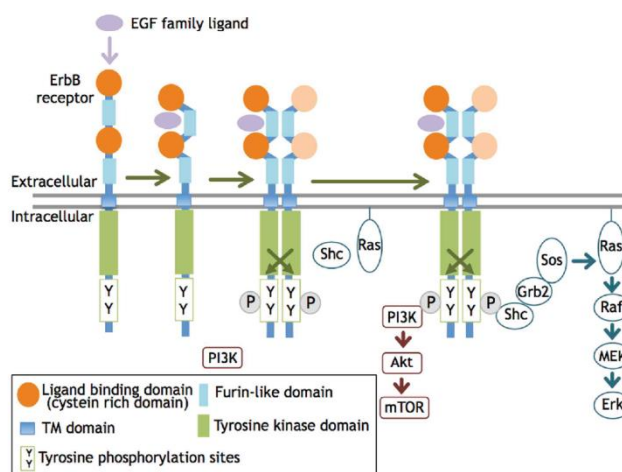


**Figure 4. Ligand binding and activation of ErbB receptors.** Ligand interaction with monomeric ErbB receptors 1, 3, and 4 increases their affinity and induces homo- or heterodimerization. Dimerization activates the tyrosine kinase domain, allowing it to phosphorylate the cytoplasmic region of the ErbB partner. Phosphorylated tyrosine residues recruit various adaptors/effector molecules, such as phosphatidylinositol 3-kinase (PI3K) subunit p85, Src, and Shc, and activates downstream signaling pathways, such as PI3K-AKT and MAPK (Erk). (Modified from Iwakura and Nawa, 2013).



Despite harboring an active kinase domain, ErbB2 has an impaired ligand binding domain and acts as a co-receptor in ErbB heterodimers (Klapper et al., 1999). Interestingly, heterodimers that include ErbB2 have a higher ligand affinity and can bind to additional ligands (Citri et al., 2003). ErbB3 binds NRG1 ligands, but lacks an active kinase domain. Therefore, ErbB3 must form heterodimers with other ErbB receptors to be functional. *In vitro* experiments have shown that ErbB2/ErbB3 form the most potent heterodimer for the regulation of cell growth and transformation (Pinkas-Kramarski et al., 1996; Wallasch et al., 1995). ErbB4 can form heterodimers with all other ErbB receptors, but is also the only receptor that can form functional NRG-binding homodimers. NRG1 also binds and activates ErbB1/ErbB3, ErbB1/ErbB4, ErbB2/ErbB3, ErbB2/ErbB4, and ErbB3/ErbB4 heterodimers.

### 1.5 The ErbB4 receptor

ErbB4 serves as a regulator of mammary gland, cardiovascular and neural development (Citri et al., 2003). The ErbB4 null mutation is lethal at embryonic day (E) 10.5 due to a failure of heart development (Gassmann et al., 1995). In contrast, ErbB4 null mutants survive, in which ErbB4 is expressed under control of a heart-specific myosin-promoter (Tidcombe et al., 2003), demonstrating that ErbB4 is not essential for the development of other organs. Alternative splicing generates four ErbB4 isoforms, which activate distinct signaling pathways. CYT-1 and CYT-2 isoforms differ in the C-terminal cytoplasmic domain, while variants JMa and JMb differ in the juxtamembrane region. Following NRG1-mediated activation CYT-1 and CYT-2 isoforms can activate the Shc–Ras–MAPK signaling pathway and support proliferation. However, only CYT-1 also regulates chemotaxis and survival by activating the PI3K-AKT signaling cascade (Elenius et al., 1997, 1999; Gassmann et al., 1995; Jones et al., 1999; Junttila et al., 2000a; Kainulainen et al., 2000; Sawyer et al., 1998). JMa and JMb variants bind NRG1, but only JMa undergoes proteolytic cleavage by TACE, a process stimulated by ligand binding and protein kinase C (PKC) activity. TACE cleavage sheds the extracellular domain of ErbB4, which contains the binding site for NRG1, from the membrane and is involved in non-canonical forward signaling (Elenius et al., 1997; Mei and Xiong, 2008; Rio et al., 2000; Vecchi et al., 1996; Zhou and Carpenter, 2000). Moreover, TACE-mediated cleavage permits additional processing of the intracellular domain (ICD) of ErbB4 by  $\gamma$ -secretase. Upon cleavage, the ErbB4-ICD can translocate into the nucleus to regulate gene expression by interaction with the transcription factors STAT5 (signal transducer and activators of transcription), YAP1 (Yes-associated protein-1), ETo2 (nuclear transcriptional corepressor), and Mdm2 (p53 regulator). The ErbB4-ICD also forms a complex with the signaling protein TAB2 and the corepressor N-CoR, which then translocates to the nucleus of undifferentiated neural precursors and inhibits their differentiation into astrocytes by repressing the transcription of glial genes

(Arasada and Carpenter, 2005; Komuro et al., 2003; Lee et al., 2002; Linggi and Carpenter, 2006; Mei and Xiong, 2008; Ni et al., 2001; Omerovic et al., 2004; Sardi et al., 2006; Williams et al., 2004). ErbB4 receptors that are mainly expressed in postsynaptic sites of Parv<sup>+</sup> interneurons, contain a C-terminal sequence (T-V-V) that corresponds to the consensus domain necessary for the interaction with PDZ domains, present for instance in PSD95. Interaction of ErbB4 with PSD95 has been shown at glutamatergic postsynapses, and this interaction might play a role in the modulation of synaptic functions (Garcia et al., 2000; Huang et al., 2000; Kim and Sheng, 2004; Ma et al., 2003; Neddens et al., 2011; Neddens and Buonanno, 2010; Vullhorst et al., 2009).

### **1.6 NRG1/ErbB4 signaling in the brain during health and disease**

NRG1 and its main receptor in the brain ErbB4 have been implicated in neurodevelopmental processes that affect the establishment and proper function of neuronal circuits, such as neuronal migration and synaptic neurotransmission. The participation of these proteins in interneuron migration during cortical development has been explained by two models. According to the first model, ErbB4-expressing interneurons migrate from the medial ganglionic eminence (MGE) through a permissive corridor of CRD-NRG1 in the developing striatum, in response to attractive, soluble NRG1 type I in the cortex (Flames et al., 2004). In the second model, NRG1 and NRG3 act as repellants that funnel interneurons as they migrate from the MGE to the cortex (Li et al., 2012a). The involvement of ErbB4 in interneuron migration is supported by a reduced number of GABAergic interneurons in the cortex of heart-rescued ErbB4 null mutants (Flames et al., 2004; Neddens and Buonanno, 2010). In addition to a role of NRG1/ErbB4 signaling in interneuron migration, NRG1/ErbB4 signaling also regulates axon and dendrite development of GABAergic neurons, and promotes the formation and maturation of GABAergic synapses onto pyramidal neurons (del Pino et al., 2013; Fazzari et al., 2010; Krivosheya et al., 2008). NRG1/ErbB4 may also be necessary for maturation of GABAergic synapses in hippocampal interneurons (Krivosheya et al., 2008). Several studies suggest that ErbB4 elimination from interneurons also has an indirect effect on excitatory synapses. Removal of ErbB4 from Parv<sup>+</sup> interneurons resulted in a reduction in dendritic spines (Barros et al., 2009; del Pino et al., 2013; Li et al., 2007; Yin et al., 2013a). In line with this finding, it was recently suggested that NRG1/ErbB4 signaling in Parv<sup>+</sup> interneurons is involved in the regulation of the critical period of visual cortical plasticity by regulation of excitatory synaptic inputs onto Parv<sup>+</sup> neurons (Sun et al., 2016). Moreover, loss of ErbB4 also led to enhanced limbic epileptogenesis, which was reversed by soluble NRG1 (Li et al., 2012b; Tan et al., 2012). Thus, ErbB4 functions in interneurons may indirectly affect excitatory network functions. NRG1/ErbB4 signaling is also involved in the modulation of synaptic functions and neurotransmission in mature networks. *In vitro* studies suggested that treatment of cultured

PFC projection neurons with the EGF-like domain of NRG1 (soluble NRG1) reduces NMDA receptor-mediated excitatory postsynaptic currents (EPSC) (Gu et al., 2005) and AMPA receptor-mediated EPSCs, probably by increasing endocytosis of AMPA receptors in hippocampal neurons (Kwon et al., 2005). Furthermore, treatment of brain slices or neurons with soluble NRG1 also alters the expression or activity of NMDA, glutamate, GABA receptors, and neuronal ACh receptors (Liu et al., 2001; Okada and Corfas, 2004; Ozaki et al., 1997; Ting et al., 2011; Woo et al., 2007).

An additional synaptic function in which NRG1/ErbB4 signaling seems to be involved is synaptic plasticity. Treatment of hippocampal slices with soluble NRG1 was shown to block LTP at the Schaffer collateral/CA1 synapse (Bjarnadottir et al., 2007; Huang et al., 2000; Kwon et al., 2005). This effect was not observed in hippocampal slices from ErbB4 null mice (Pitcher et al., 2008), demonstrating that NRG1 acts via ErbB4. The participation of NRG1/ErbB4 signaling in LTP formation was also demonstrated by *in vivo* studies, in which pan-neuronal or conditional ablation of ErbB4 in Parv<sup>+</sup> interneurons led to enhanced LTP (Chen et al., 2010a; Pitcher et al., 2008; Shamir et al., 2012). In contrast, mice with postnatal elimination of NRG1 from projection neurons (CamKII-Cre) displayed reduced LTP (Agarwal et al., 2014), suggesting that NRG1 mutants not necessarily phenocopy ErbB4 mutants, possibly because ErbB4 integrates signals from several other EGF-like ligands. Consistent with LTP impairment following treatment with soluble NRG1, transgenic mice with neuronal overexpression of CRD-NRG1 showed reduced hippocampal LTP. Further analyses of these transgenic mice and conditional NRG1 mutants (CamKII-Cre and Emx1-Cre) also showed that the excitatory/inhibitory (E/I) balance of CA1 pyramidal neurons was disturbed and that NRG1 overexpression leads to increased inhibitory postsynaptic current (IPSC) frequencies, but not amplitudes. This suggests that NRG1 overexpression leads to enhanced inhibition, probably by increased GABAergic input (Agarwal et al., 2014). These studies suggest that NRG1/ErbB4 signaling is involved in balancing the E/I ratio in cortical circuits. Additionally, it was found that glutamate stimulation increased NRG1 type I expression in cultured rat hippocampal neurons suggesting that this particular isoform may have a role in synaptic activity and plasticity. *In vivo* studies have shown a correlation between memory related performance and the concentration of NRG1 type I in rat hippocampus (Schillo et al., 2005). Thus, in order to understand how different NRG1 isoforms participate in the modulation of cortical circuits, isoform-specific *in vivo* studies are necessary.

Both human *Nrg1* and *ERBB4* genes are on the list of major SZ susceptibility genes (Schizophrenia Gene Resource, Vanderbilt University; <http://bioinfo.mc.vanderbilt.edu/SZGR>). The majority of *Nrg1* variants and haplotypes associated with SZ are located in non-coding regions of the gene (Stefansson et al., 2002; Weickert et al., 2012), suggesting that changes in NRG1 expression levels, rather than altered protein function, could be relevant for SZ. This

is supported by both reduced and increased NRG1 expression levels found in postmortem brain of SZ patients (Bertram et al., 2007; Law et al., 2006). Likewise, NRG1-induced ErbB4 hyperphosphorylation was observed in postmortem brains of SZ patients (Hahn et al., 2006). Dysfunctions in several processes in which NRG1/ErbB4 has been involved, were observed in SZ, including reduced numbers of inhibitory interneurons (Benes et al., 1991; Chance et al., 2005; Heckers and Konradi, 2015; Holt et al., 2005; Levitt, 2005), reduced expression of GAD67 in Parv<sup>+</sup> interneurons of the dorsolateral PFC, and disturbed inhibitory functions (Akbarian et al., 1995; Benes et al., 1991; Farzan et al., 2010; Hashimoto et al., 2003; Lewis et al., 2005; Ongür et al., 2010; Yoon et al., 2010), alterations in dendritic spines (Penzes et al., 2011) and deficits in cortical synchronization, such as impaired  $\gamma$ -oscillations (Kwon et al., 1999; Uhlhaas and Singer, 2010; Wynn et al., 2005).

The investigation of mouse mutants has also revealed similarities with SZ patients. Conventional (*ErbB4*<sup>-/-</sup>) and Parv<sup>+</sup> interneuron-specific ErbB4 mutants (*ErbB4*<sup>-/\*Parv-Cre</sup>) mice manifested novelty-induced hyperactivity and deficits in prepulse inhibition (PPI), in line with findings in SZ patients. Worth mentioning, *ErbB4*<sup>-/-</sup> mice (but not conditional *ErbB4*<sup>-/\*Parv-Cre</sup> mutants) showed reduced anxiety-like behavior and impairments in fear conditioning test (Shamir et al., 2012). Furthermore, ErbB2/B4 double mutant mice that present impaired NMDA receptor/PSD95 clusters, and dendritic spine maturation, showed increased aggressive behavior and reduced PPI (Barros et al., 2009). Additionally, conditional postnatal mutants of NRG1 exhibited hypoactivity and impaired fear-conditioned learning. On the other hand, increased expression of NRG1 was associated with impaired PPI (Agarwal et al., 2014; Deakin et al., 2009; Yin et al., 2013b). Moreover, CRD-NRG1 pan-neuronal overexpression in mice leads to ventricular enlargement, the most replicated endophenotype in SZ patients that was also associated with variants of the *Nrg1* gene (Agarwal et al., 2014; Mata et al., 2009). Taken together, these findings suggest that altered NRG1/ErbB4 signaling activity may be of relevance for the etiopathophysiology of SZ.

### 1.7 NRG2: a NRG1-related ErbB4 ligand with unknown CNS function

The tyrosine kinase receptor ErbB4 interacts not only with NRG1, but also with other members of the NRG family, including NRG2. The *Nrg2* gene was cloned based on sequence similarities with *Nrg1* and harbors a protein domain structure (including a transmembrane and an Ig-like domain) that resembles NRG1 type I (Fig. 3B). As for NRG1, the EGF-like domain of NRG2 has two variants ( $\alpha$  and  $\beta$ ) with differential receptor binding affinities (Jones et al., 1999). Moreover, the NRG2 full-length protein also undergoes proteolytic cleavage that results in shedding of the extracellular domain (Longart et al., 2004). This suggests that NRG2 could be involved in paracrine signaling to ErbB receptors and may serve as an additional regulator of

synapses or other neural network functions in the brain. However, the signaling mechanisms downstream of NRG2-mediated ErbB4 activation have not been studied in detail.

Synaptic changes in *Nrg1* mouse mutants contrast with those reported in *ErbB4* null mutants (Agarwal et al., 2014; Rico and Marín, 2011), suggesting that ErbB4 integrates signals from additional ligands, such as NRG2, during the regulation of cortical circuits. Despite a similar affinity for the ErbB4 receptor, NRG1 and NRG2 show distinct biological properties in cultured cells, probably via differential recruitment of downstream signaling pathways (Crovello et al., 1998). In line with this, analyses of NRG1 and NRG2 knockout mice indicate that these proteins exert different activities during development; e.g. in contrast to NRG1 null mice, NRG2 mutants survive embryogenesis and show no major heart defects (Britto et al., 2004). In conclusion, these findings support the concept that NRG1 and NRG2 stimulate differential cellular responses downstream of activation of a single receptor hetero- or homodimer.

In the nervous system, NRG2 is expressed by spinal cord motor neurons and terminal Schwann cells and may regulate synaptic differentiation at the neuromuscular junctions (NMJ) (Rimer et al., 2004), including expression of muscle acetylcholine receptors (Ponomareva et al., 2006). Expression in the brain increases postnatally and is most prominent in the somatodendritic compartment of neurons, including GABAergic interneurons, in the cortex, hippocampus, and cerebellum (Longart et al., 2004; Vullhorst et al., 2015). Ventricular infusion of the recombinant EGF-like domain of NRG2 (rNRG2) in adult mice enhances the proliferation of putative stem cells in the subventricular zone and their differentiation into interneurons, and these effects were abrogated in ErbB4-deficient mice (Ghashghaei et al., 2006). Recently, it has been suggested that NRG2 may exert regulatory functions at GABAergic and glutamatergic synapses, including autocrine NRG2/ErbB4 signaling in GABAergic interneurons and bidirectional (partly ErbB4-independent) NRG2 signaling in hippocampal granule cells (Lee et al., 2015; Vullhorst et al., 2015). However, downstream signaling pathways in interneurons or granule cells have not been addressed.

In addition, the interaction of human *Nrg1* with *Nrg2* gene variants may result in increased susceptibility to schizophrenia (Benzel et al., 2007). This indicates that association of NRG1 with schizophrenia is mediated not only via ErbB4, but also by functional interaction with other members of the NRG family. However, it is unclear how the interaction of *Nrg1*, *Nrg2*, and *ErbB4* gene variants may contribute to increased disease susceptibility. Further studies to identify the role of NRG2 in the regulation of synaptic functions in the brain, including signaling mechanisms downstream of NRG2-mediated ErbB4 activation in neurons are necessary. This would help to elucidate the participation of NRG/ErbB signaling in the brain during health and disease.

## 1.8 Aim of the study

NRG1/ErbB4 signaling modulates the development and maintenance of cortical circuits, and evidence of cortical disconnectivity has been observed in SZ patients. Higher levels of NRG1 expression and ErbB4 hyperstimulation have been found in post mortem brain tissue of SZ patients. On the other hand, NRG1 isoforms show dynamic and complex expression patterns in the brain, and isoform-specific functions have been suggested. Thus, cell type- or stage-specific changes in the expression of NRG1 isoforms could lead to different consequences. For these reasons, the first aim of this project was to characterize a transgenic mouse line for conditional NRG1 type I (referred hereafter as Ig-NRG1) overexpression, and to model cell type- and stage-specific overexpression of Ig-NRG1 *in vivo*. A subsequent aim of this project was to examine consequences of stage-specific, cortical projection neuron-restricted overexpression of Ig-NRG1 on brain development and behavioral functions. Further, the project's aim was to analyze the subcellular localization of Ig-NRG1, and to obtain a first insight into possible molecular pathomechanism induced by Ig-NRG1 mediated ErbB4 hyperstimulation.

NRG1 is mainly expressed in projection neurons, but it is also present in GABAergic interneurons. Therefore, a second project was to perform a pilot study of autocrine NRG1 functions in interneurons using conditional NRG1 mutants with a specific elimination of NRG1 signaling in Parv<sup>+</sup> interneurons.

NRG2 is a member of the NRG family and also interacts with ErbB4 receptors, but its functions in the brain are not known. The protein structure of NRG2 resembles Ig-NRG1, but its expression patterns in the brain differ. Thus, the third aim of this Ph.D. project was to generate a transgenic mouse line for conditional stimulation of NRG2 signaling *in vivo* by homologous recombination in embryonic stem cells.

## 2 Results

### 2.1 Generation of a conditional HA-Ig-NRG1 transgenic mouse line

NRG1 expression changes during development and differs between isoforms. Ig-NRG1 shows higher levels of expression at E13 and P5 and is reduced in the adult brain (Liu et al., 2011). This suggests important roles in neural development and during the neonatal critical period, for example in interneuron migration and integration into inhibitory circuits. Elevated NRG1 expression has been observed in postmortem brain tissue and blood cells of SZ patients, and a notable increase in *Ig-Nrg1* mRNA has been demonstrated (Hashimoto et al., 2004; Law et al., 2006). To test the hypothesis that hyperstimulation of the Ig-NRG1/ErbB4 signaling pathway may represent a pathomechanism that causes cortical network dysfunctions with relevance for schizophrenia and to investigate the biological effects of this overexpression, a novel mouse model was generated by oocyte injection of a GFP-STOP-flox HA-Ig-Nrg1 (STOP-Nrg1) cassette. *STOP-Nrg1* mice overexpress the full-length, N-terminally HA epitope-tagged Ig-NRG1 $\beta$ 1a isoform under control of the  $\beta$ -actin promoter after Cre-mediated removal of a STOP-cassette flanked by loxP sites (Fig. 5A). Crossbreeding *STOP-Nrg1* mice to Cre recombinase expressing mouse lines (Cre driver lines) permits induction of NRG1 overexpression in a stage- and cell type-specific manner (Fig. 5B).

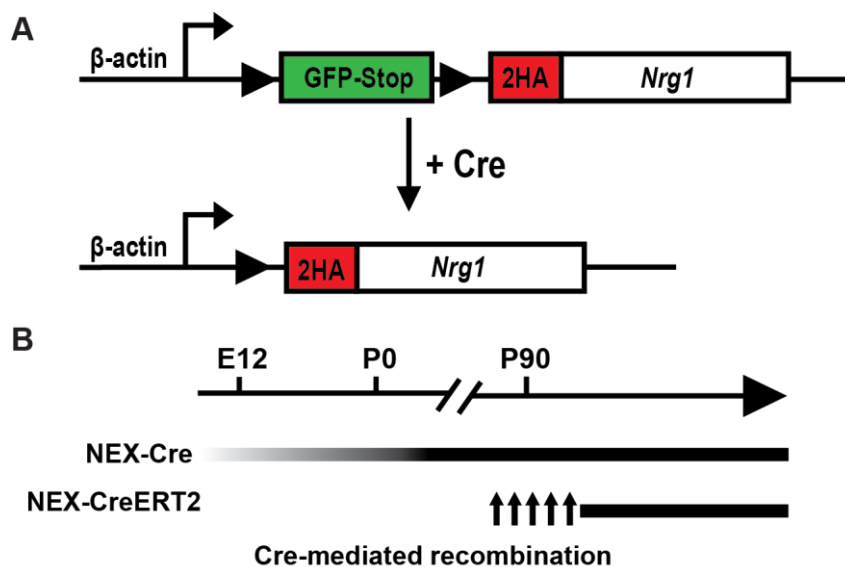


**Figure 5. A conditional transgenic mouse line for Cre-mediated expression of Ig-NRG1. (A)** Transgene cassette used for the generation of transgenic mice that constitutively express GFP under control of the  $\beta$ -actin promoter. Removal of the floxed GFP cassette by Cre recombinase results in the expression of HA-Ig-NRG1. N, N-terminus; C, C-terminus; TM, transmembrane domain; EGF, epidermal growth factor-like domain; Ig, Immunoglobulin-like domain; HA, haemagglutinin. **(B)** Cre driver mouse lines for cell type- and stage-specific overexpression of HA-Ig-NRG1. The *NEX-Cre* driver mouse line enables early embryonic cortical projection neuron-restricted overexpression starting at E12 (Goebbels et al., 2006). *NEX-CreERT2* driver mice enable tamoxifen-induced Cre-mediated recombination and transgene expression in mice at all stages. Arrows indicate tamoxifen injections (Agarwal et al., 2012).

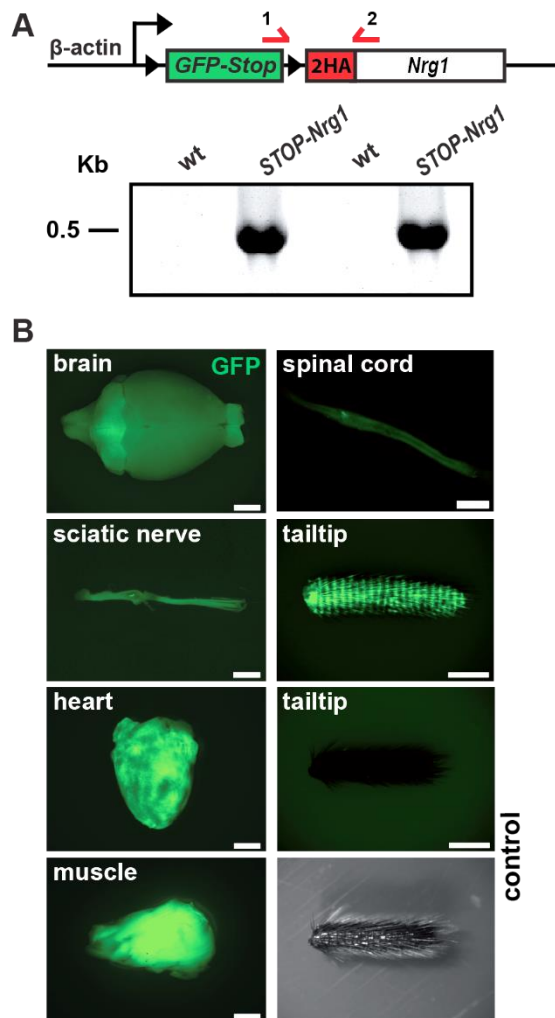


**Figure 6. The  $\beta$ -actin GFP-STOP-flox cassette is widely expressed in nervous and non-nervous tissues of transgenic mice. (A)** Structure of  $\beta$ -actin GFP-STOP-flox HA-Ig-Nrg1 transgene cassette used to generate *STOP-Nrg1* mice with the location of genotyping primers (1 and 2). PCR on tail genomic DNA shows insertion of the *STOP-Nrg1* cassette in *STOP-Nrg1* mice, but not in wt littermates. **(B)** *STOP-Nrg1* mice display green fluorescence in virtually all tissues due to GFP expression from the GFP-STOP-flox cassette. Epifluorescence images of organs of *STOP-Nrg1* mice and epifluorescence images of tail biopsy of a wt littermate. Scale bars, 2 mm (brain, sciatic nerve, heart, spinal cord, tail tip), 4 mm (muscle). GFP, green fluorescent protein.

Ig-NRG1 is mainly expressed in cortical projection neurons (Liu et al., 2011). A mouse model that overexpresses this protein in projection neurons starting during postnatal stages was published after initiation of this project (Yin et al., 2013b). To include embryonic stages in the investigation of Ig-NRG1-mediated functions, *STOP-Nrg1* mice were crossbred to the *NEX-Cre* driver line. *NEX-Cre* mice harbor Cre recombinase as a “knock-in” into the *NeuroD6* locus, which results in a driver line for Cre-mediated recombination in cortical projection neurons starting at E12 (Goebbels et al., 2006). To compare chronic versus adult overexpression of HA-Ig-NRG1, *STOP-Nrg1* mice were also bred to a tamoxifen inducible version of the Cre driver line (*NEX-CreERT2*). CreERT2 results from the N-terminal fusion of Cre recombinase to a mutated human estrogen receptor (ER) ligand-binding domain. Administration of tamoxifen, a synthetic ER ligand, induces the dissociation of CreERT2 from HSP90, nuclear import of CreERT2, and the site-specific recombination of genes that are flanked by loxP sites. This permits tamoxifen induced overexpression of HA-Ig-NRG1 in projection neurons during adult stages (Fig. 5B) (Agarwal et al., 2012). Two transgenic

founder lines were generated by injection of the *STOP-Nrg1* cassette into C57Bl/6N oocytes (Fig. 6A). *STOP-Nrg1* mice were viable and produced offspring according to Mendelian ratios. Organs were examined for GFP expression by fluorescent light microscopy. Mice harboring the *STOP-Nrg1* transgene cassette showed GFP expression in all tissues analyzed, in contrast to control mice (*NEX-Cre* mice) (Fig. 6B). For this reason, genotyping of *STOP-Nrg1* mice can



also be inferred from monitoring GFP expression in tail biopsies. One of the founder lines was frozen after initial characterization.

Expression of the transgene cassette in neural cell types in the brain of *STOP-Nrg1* mice was identified by overlapping GFP fluorescence with fluorescent immunostaining for cell type-specific markers on coronal cryosections. Confocal microscopy revealed expression of the *STOP-Nrg1* transgene in glutamatergic projection neurons, as shown by co-staining for the neuronal marker NeuN and the projection neuron marker neurogranin (NRGN) (Fig. 7A). In contrast, the analysis of interneuron markers GAD67 and Parv revealed that the cassette was expressed only in a few interneurons (Fig. 7A). Among glial cells, the *STOP-Nrg1* transgene was expressed in most oligodendrocytes (Olig2), and a subset of astrocytes (GFAP) and microglia (IBA1). *STOP-Nrg1* expression was also found in spinal cord  $\alpha$ -motoneurons (ChaT) (Fig. 7B). Taken together, these results demonstrate that the *STOP-Nrg1* transgene is expressed in most neural and non-neural tissues and therefore appears suitable to study the role of Ig-NRG1 in several different organs, in addition to the brain.

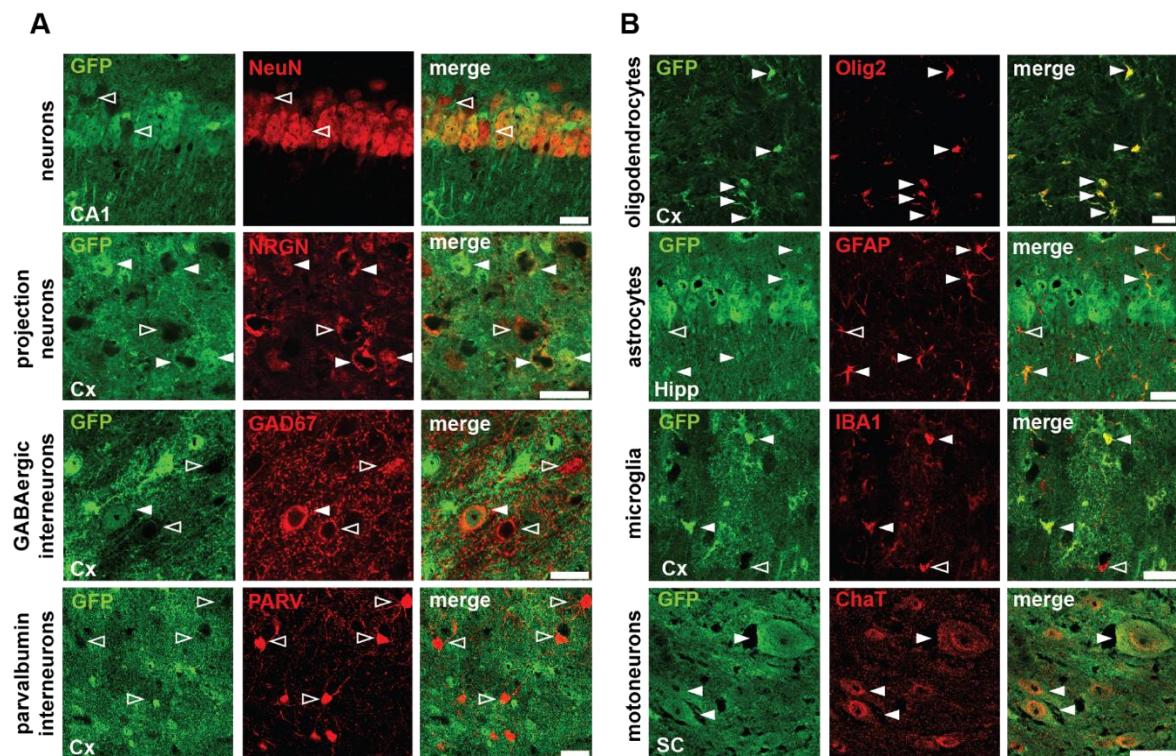


**Figure 7.  $\beta$ -actin GFP-*STOP*-flox cassette is predominantly expressed in projection neurons. (A)** Confocal images of fluorescent immunostainings on 14  $\mu$ m thick coronal cryosections of brains (bregma -1.7) from *STOP-Nrg1* mice at 3 months of age stained for neuronal markers. Immunostaining for NeuN shows overlap with GFP fluorescence and reveals expression of the *STOP-Nrg1* transgene in neurons of the hippocampus of *STOP-Nrg1* mice. *STOP-Nrg1* is expressed in projection neurons (filled arrowheads), indicated by colocalization with neurogranin (NRGN), but only minor expression was found in cortical interneurons (GAD67 and Parv; empty arrowheads). Scale bars, 20  $\mu$ m. **(B)** Immunostainings for glial markers reveals expression of the *STOP-Nrg1* transgene in oligodendrocytes (Olig2), and a subset of astrocytes (GFAP) and microglia (IBA1). The transgene cassette is also expressed in spinal cord motoneurons (ChaT). Scale bars, 25  $\mu$ m (IBA), 20  $\mu$ m (Olig2, GFAP, ChaT). Cx, cortex; CA1, hippocampal CA1 region; SC, spinal cord.

## 2.2 Embryonic overexpression of HA-Ig-NRG1 in *STOP-Nrg1*\**NEX-Cre* mice

NRG1 and its receptor ErbB4 are involved in important aspects of brain development, such as the control of interneuron migration (Flames et al., 2004; Li et al., 2012a). Furthermore, the expression of Ig-NRG1 is higher during early embryonic stages (Liu et al., 2011). To analyze the effect of HA-Ig-NRG1 overexpression in the cortex during embryonic stages, *STOP-Nrg1* mice were bred to the *NEX-Cre* driver line (Fig. 8A). HA-Ig-NRG1 overexpression in *STOP-Nrg1*\**NEX-Cre* mice during embryonic stages was confirmed by immunostaining on coronal cryosections of brains at E16 for Cre-recombinase and NRG1 (using an antibody directed against the N-terminal HA tag) (Fig. 8B-D). Cre-recombinase positive neurons were observed by confocal microscopy in the cortical plate and subplate. Due to recombination of the GFP-

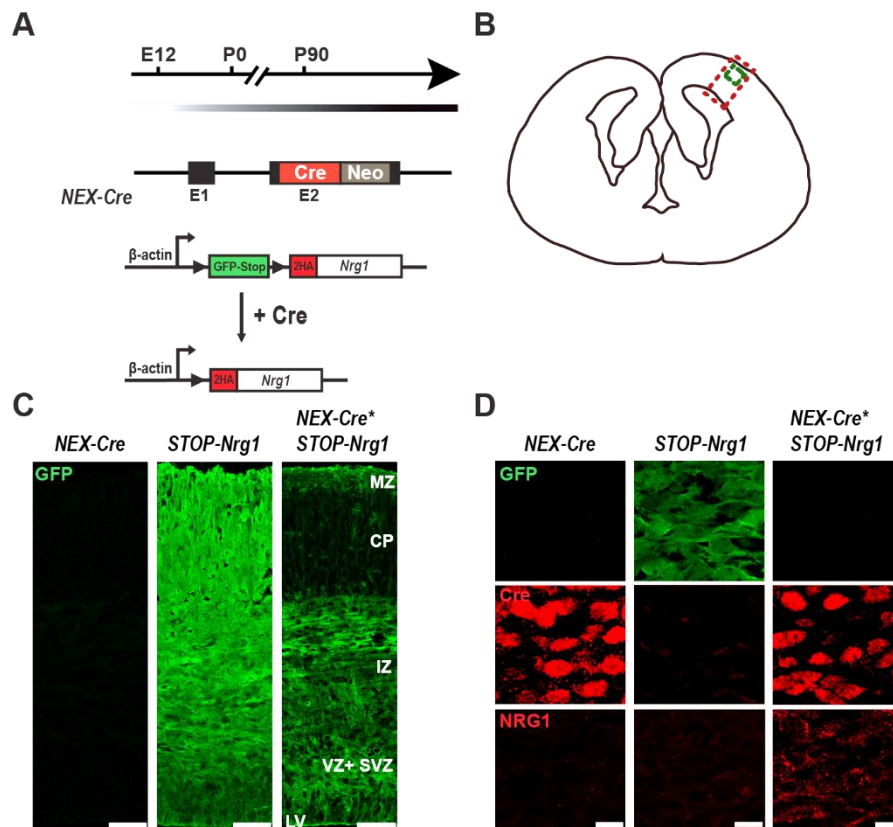


**Figure 8. *NEX-Cre*-mediated overexpression of HA-Ig-NRG1 in *STOP-Nrg1*\**NEX-Cre* mice during embryonic stages.** (A) Cre expression starts at E12 in *NEX-Cre* mice. Structure of the targeted *Neurod6* locus in *NEX-Cre* mice. (E1, Exon1; E2, Exon2; Neo, Neomycin resistance cassette; adapted from (Goebbels et al., 2006)). Structure of the *STOP-Nrg1* cassette and *NEX-Cre*-mediated recombination of the GFP-STOP cassette. (B) Schematic drawing of a coronal brain section at E16 illustrates the position of overview images shown in (C) (dashed red column) and high magnification images shown in (D) (dashed green square). (C) *STOP-Nrg1*\**NEX-Cre* embryos show reduced GFP fluorescence in the cortical plate, subplate and intermediate zone due to the removal of the GFP-STOP cassette by Cre recombinase. CP, cortical plate; IZ, intermediate zone; LV, lateral ventricle; MZ, marginal zone; SP, subplate; SVZ, subventricular zone; VZ, ventricular zone; WM, white matter. Scale bars, 50  $\mu$ m. (D) Immunostainings for GFP, Cre recombinase and NRG1 (using an antibody directed against the HA tag) on cryosections of *STOP-Nrg1*\**NEX-Cre* and control brains (*NEX-Cre* and *STOP-Nrg1*) at E16. Note loss and absence of GFP in *STOP-Nrg1*\**NEX-Cre* and *NEX-Cre* mice, respectively and Cre-expression in *STOP-Nrg1*\**NEX-Cre* and *NEX-Cre*, but not in *STOP-NRG1* mice. NRG1 overexpression is observed only in double transgenic mice. Scale bars, 10  $\mu$ m.

STOP cassette a concomitant reduction of the GFP signal in those regions was detected in *STOP-Nrg1\**NEX-Cre** mice (Fig. 8 C). Overexpression of HA-Ig-NRG1 and concomitantly reduced GFP fluorescence were observed in areas with Cre expression (Fig. 8D). This demonstrates that HA-Ig-NRG1 overexpression in *STOP-Nrg1\**NEX-Cre** mice is initiated in postmitotic cortical projection neurons during embryonic stages, which allows to study the effects of increased Ig-NRG1 expression on cortical development.

### 2.3 Chronic *NEX-Cre*-mediated HA-Ig-NRG1 overexpression in cortical projection neurons causes ErbB4 hyperphosphorylation

*STOP-Nrg1* mice were bred to *NEX-Cre* driver mice to model HA-Ig-NRG1 overexpression in glutamatergic cortical projection neurons. Immunostaining on cryosections confirmed that overexpression of HA-Ig-NRG1 in double transgenic adult mice corresponds to the *NEX-Cre* recombination pattern (Fig. 9A). Furthermore, HA-Ig-NRG1 overexpression in *STOP-Nrg1\**

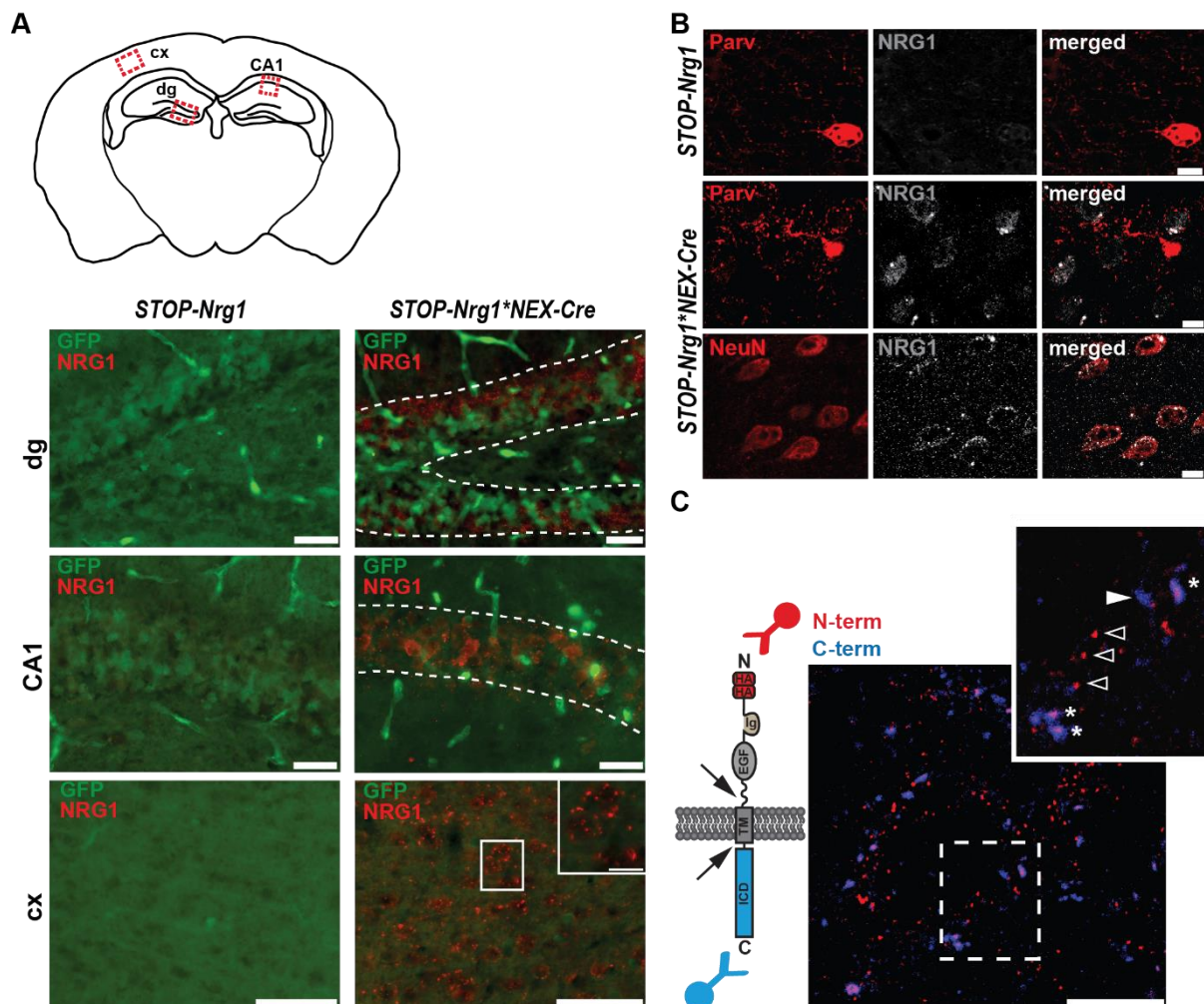


**Figure 9. *NEX-Cre*-mediated HA-Ig-NRG1 expression is restricted to cortical projection neurons during adult stages.** (A) Schematic drawing of an adult coronal brain section illustrates the position of overview images for the dentate gyrus (dg), CA1 region of the hippocampus (CA1), and cortex (cx). Fluorescent immunostaining for the C-terminal domain of HA-Ig-NRG1 on coronal vibratome sections (bregma -1.7) reveals overexpression in *STOP-Nrg1\**NEX-Cre** mice (10 weeks old), consistent with the *NEX-Cre* expression profile. Expression is present in granule cells in the outer shell of the dentate gyrus, the CA1 region of the hippocampus, and in the cortex. Concomitantly, loss of GFP can be detected in *STOP-Nrg1\**NEX-Cre**. Scale bars, 50  $\mu$ m and 10  $\mu$ m (zoom cx).

(B) Fluorescent immunostaining on coronal cryosections of *STOP-Nrg1\**NEX-Cre** mice for HA-Ig-NGR1 (using antibodies directed against the HA tag and neuronal markers). HA-Ig-NGR1 expression is restricted to cortical projection neurons; its signal colocalizes with NeuN, but not with Parv. Scale bars, 15  $\mu$ m. (C) Structure of HA-Ig-NGR1 with binding sites for antibodies directed against N- and C-terminal domains. Arrowheads indicate possible proteolytic cleavage sites. Co-immunostaining on coronal cryosections of *STOP-Nrg1\**NEX-Cre** for the N- and the C-terminal domains of HA-Ig-NGR1 show both colocalization (\*) and non-overlapping signals for the N- and C-terminal domains (empty and filled arrowheads, respectively). Scale bar, 10  $\mu$ m.

*NEX-Cre* mice was specific for cortical projection neurons in cortex and hippocampus (Fig. 9B). Co-immunostaining for the N- and the C-terminal domains of HA-Ig-NGR1 identified domains of co-expression, which most likely reflect the accumulation of the full-length protein. In addition, non-overlapping signals for the N- and C-terminal domains were also detected, consistent with proper proteolytic processing at the juxtamembrane region of HA-Ig-NGR1 and shedding of the N-terminal domain (Fig. 9C). These studies demonstrate that *STOP-Nrg1* transgenic mice serve as a suitable genetic tool for conditional Ig-NGR1 overexpression in the brain.

A biochemical analysis of Cre-dependent transgene expression was performed in the PFC and hippocampus of *STOP-Nrg1\**NEX-Cre** mice at P7, as well as at 16 and 52 weeks of age. “Conventional” Thy1.2 promoter-driven Ig-NGR1 transgenic mice (*Thy1.2 Nrg1*; Michailov et al., 2004) were used as a reference. This study confirmed chronically elevated HA-Ig-NGR1 expression in *STOP-Nrg1\**NEX-Cre** mice and a massive overexpression under control of the Thy1.2 promoter (Fig. 10A-B). Western blot analysis demonstrated that chronic HA-Ig-NGR1 overexpression in *STOP-Nrg1\**NEX-Cre** mice was associated with permanent ErbB4 hyperphosphorylation, using a phospho-ErbB4 (p-ErbB4) antibody directed against tyrosine 1284. This hyperphosphorylation was already present at P7 (Fig. 10C-D). Together, these findings confirm that *STOP-Nrg1\**NEX-Cre** mice allow chronic HA-Ig-NGR1 overexpression in cortical projection neurons, and demonstrate that these mice serve as a suitable genetic tool to model permanent hyperstimulation of ErbB4 receptors in the brain.

#### **2.4 Absence of neuropathology in the brain of *STOP-Nrg1\**NEX-Cre** mice**

*STOP-Nrg1\**NEX-Cre** mice display normal cage behavior and unaltered body weight compared to control littermates. Likewise, Hematoxylin-Eosin (H+E) staining revealed no obvious abnormalities in brain morphology (data not shown). Next, chromogenic immunostainings for the pan-neuronal marker NeuN were performed on brain sections from 16 and 52 weeks old *STOP-Nrg1\**NEX-Cre** mice. A semi-automated quantification method was employed for counting numbers of NeuN<sup>+</sup> neurons based on thresholded images, including watershed-based rendering of positive signals (Fig. 11A-B). Quantification of NeuN<sup>+</sup> neurons in the cortex of these two cohorts of *STOP-Nrg1\**NEX-Cre** mice showed no differences compared to controls. This suggests that chronic HA-Ig-NGR1 overexpression in projection neurons exerts no major effects on the migration and maintenance of cortical neurons.

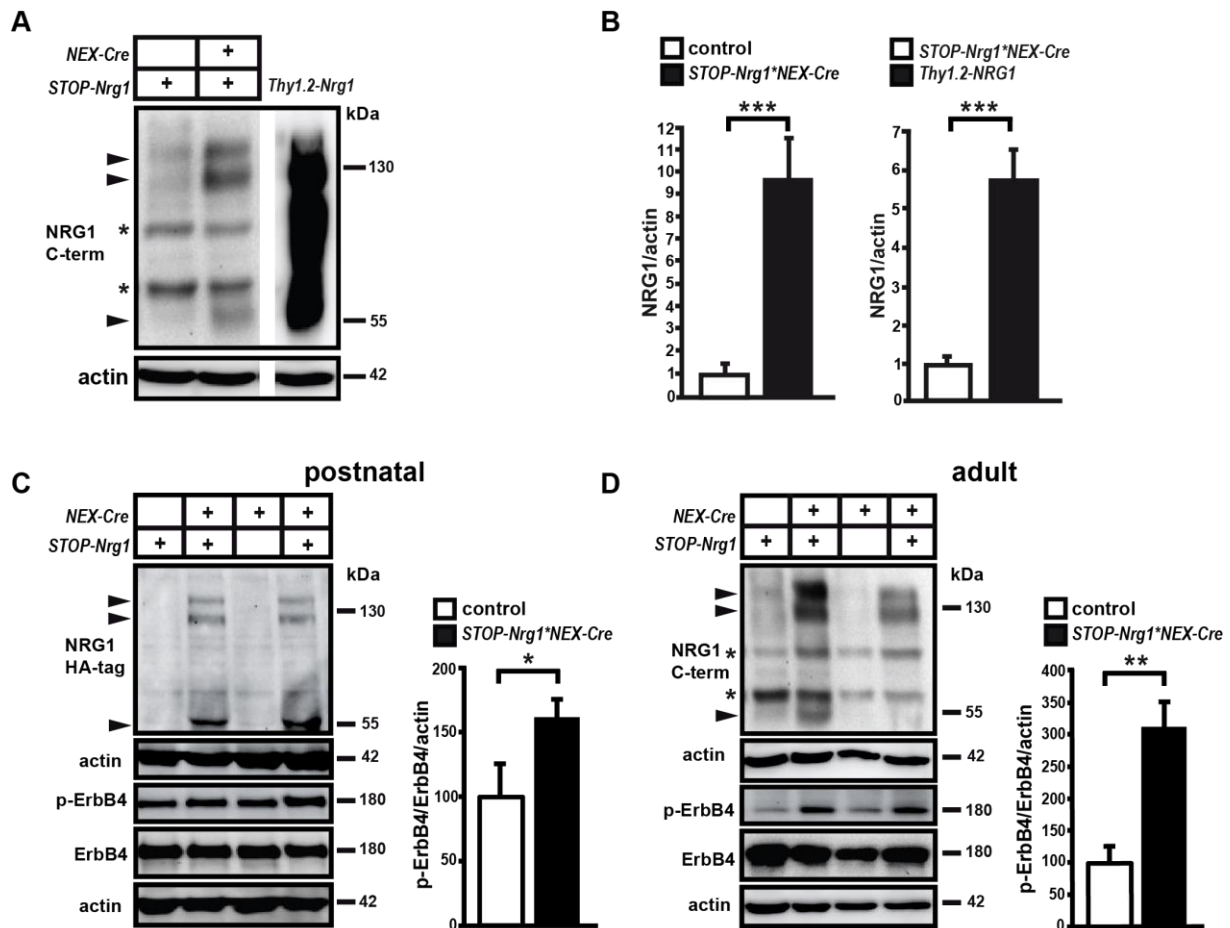


**Figure 10. HA-Ig-NGR1 overexpression in projection neurons causes ErbB4 hyperphosphorylation.** (A) Western blotting of protein lysates from PFC with an antibody directed against the NRG1 C-terminal domain reveals moderate HA-Ig-NGR1 overexpression in *STOP-Nrg1*\*NEX-Cre mice and massive Ig-NGR1 overexpression in *Thy1.2-Nrg1* mice (age 16 weeks). Arrowheads indicate full-length (~130 kDa) and processed protein (~50 kDa). Asterisks indicate non-specific bands. (B) Densitometric quantification of the band corresponding to full-length NRG1. *STOP-Nrg1*\*NEX-Cre mice show ~10-fold overexpression compared to controls (*STOP-Nrg1*, *NEX-Cre*; n=3-4 each; t-test, p=0.0003), in which NRG1 expression is very low at this age. *Thy1.2-Nrg1* mice (n=3) show ~6-fold overexpression compared to *STOP-Nrg1*\*NEX-Cre mice (t-test, p=0.0004). (C) Western blotting of PFC protein lysates with an antibody directed against the HA tag, and an antibody that detects ErbB4 phosphorylated at tyrosine 1284 shows HA-Ig-NGR1 expression and ErbB4 hyperphosphorylation in *STOP-Nrg1*\*NEX-Cre mice at P7. Densitometric quantification of phosphorylated ErbB4 (Tyr1284) bands. Integrated density values were normalized to  $\beta$ -actin loading control (n=4-6; t-test, p=0.011). (D) Biochemical analysis of PFC lysates from *STOP-Nrg1*\*NEX-Cre mice and controls (*STOP-Nrg1*, *NEX-Cre*) shows HA-Ig-NGR1 overexpression and ErbB4 hyperphosphorylation in *STOP-Nrg1*\*NEX-Cre mice (age 16 weeks). Densitometric quantification of phosphorylated ErbB4 (Tyr1284) bands. Integrated density values were normalized to  $\beta$ -actin loading control (n=3 each; t-test, p=0.0011).

Similarly, neuroinflammation and other signs of neuropathology were evaluated by performing chromogenic immunostainings for markers of neuropathology and inflammation on brain sections at 16 and 52 weeks of age. Astrogliosis or microgliosis were tested by staining for GFAP, IBA1 and MAC3. Immunostainings for the astrocytic marker GFAP were quantified with a semi-automated method, which determined the GFAP<sup>+</sup> area in relation to the region of interest. Hippocampus and fimbria were analyzed as examples for gray and white matter regions, respectively (Fig. 12A). No difference in GFAP<sup>+</sup> area was observed in the analyzed brain regions of *STOP-Nrg1*\*NEX-Cre compared to controls (Fig. 12B-C).

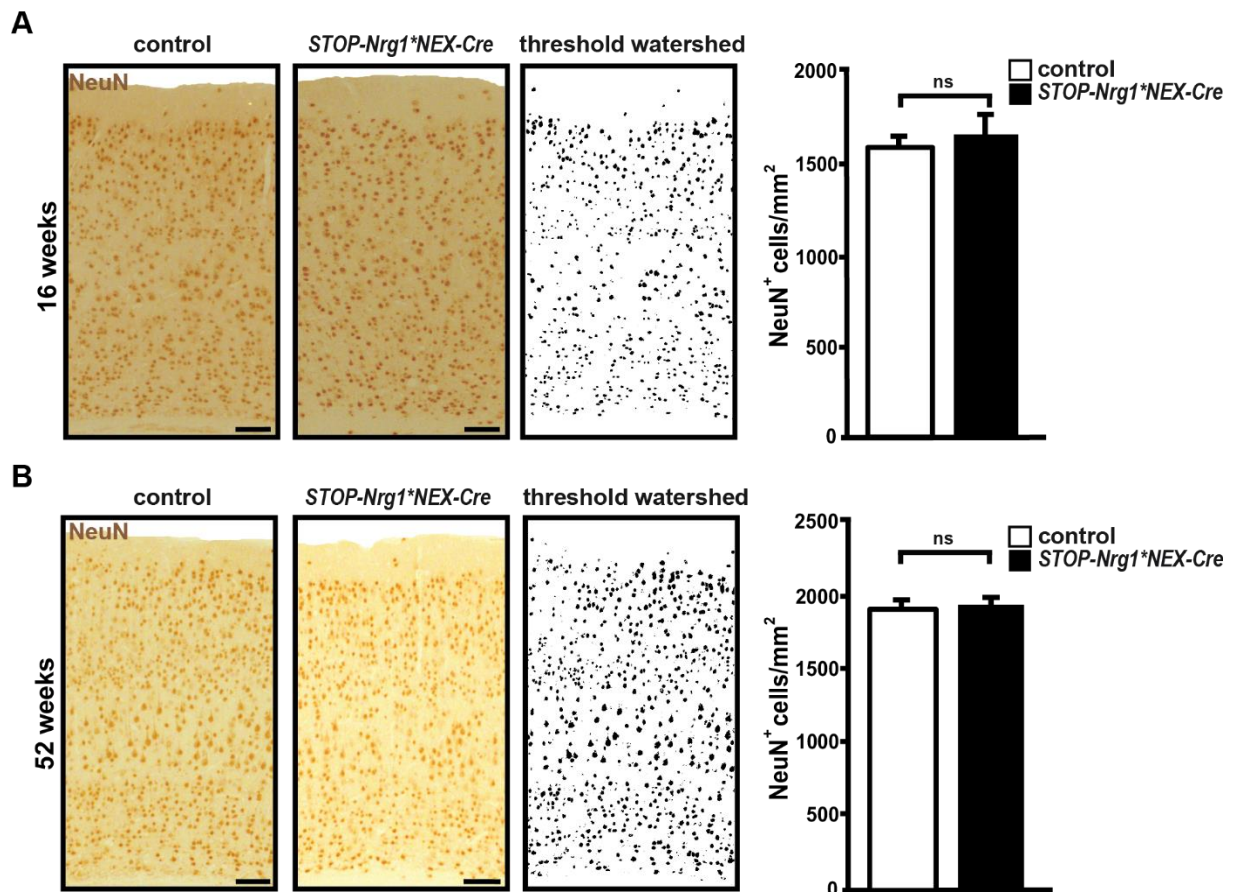


**Figure 11. Normal numbers of cortical neurons in *STOP-Nrg1*\**NEX-Cre* mice.** Chromogenic immunostaining for NeuN on coronal paraffin sections from 16 weeks (**A**) and 52 weeks old mice (**B**) (bregma -1.3 and -1.7, respectively) revealed no changes in neuronal numbers in *STOP-Nrg1*\**NEX-Cre* mice compared to controls (*STOP-Nrg1*, *NEX-Cre*). Semi-automated quantification of columns of the somatosensory cortex (width 600  $\mu$ m) using watershed thresholded images ( $n=3-4$  each; t-test,  $p > 0.05$ ; ns, not significant). Scale bars, 100  $\mu$ m.

A similar semi-automated quantification of chromogenic IBA1 immunostainings was performed to test for microgliosis (Fig. 13A). No differences were identified in *STOP-Nrg1*\**NEX-Cre* mice at 16 or 52 weeks of age compared to controls (Fig. 13B-C). Likewise, no evidence of changes in activated microglia were found in immunostainings for MAC-3. Furthermore, brains were examined for axonal swellings and T-cell infiltration by staining for amyloid precursor protein (APP) and T-cell antigen CD3, respectively. No signs of pathology in *STOP-Nrg1*\**NEX-Cre* were obtained based on these immunostainings (data not shown). In summary, chronic overexpression of HA-Ig-NRG1 derived from projection neurons serves not as a potent signal for neurodegenerative or inflammatory processes in the brain.

## 2.5 Reduced social inhibition in *STOP-Nrg1*\**NEX-Cre* mice

Sensory functions of *STOP-Nrg1*\**NEX-Cre* were examined starting at 2-3 months of age. Behavioral studies were performed by Anja Ronnenberg and Prof. Dr. Ekrem Dere, as part of a collaboration with Prof. Dr. Dr. Hannelore Ehrenreich (MPI-EM, Clinical Neuroscience). In the visual cliff test, HA-Ig-NRG1 overexpressing mice and controls (*NEX-Cre*, *STOP-Nrg1* and

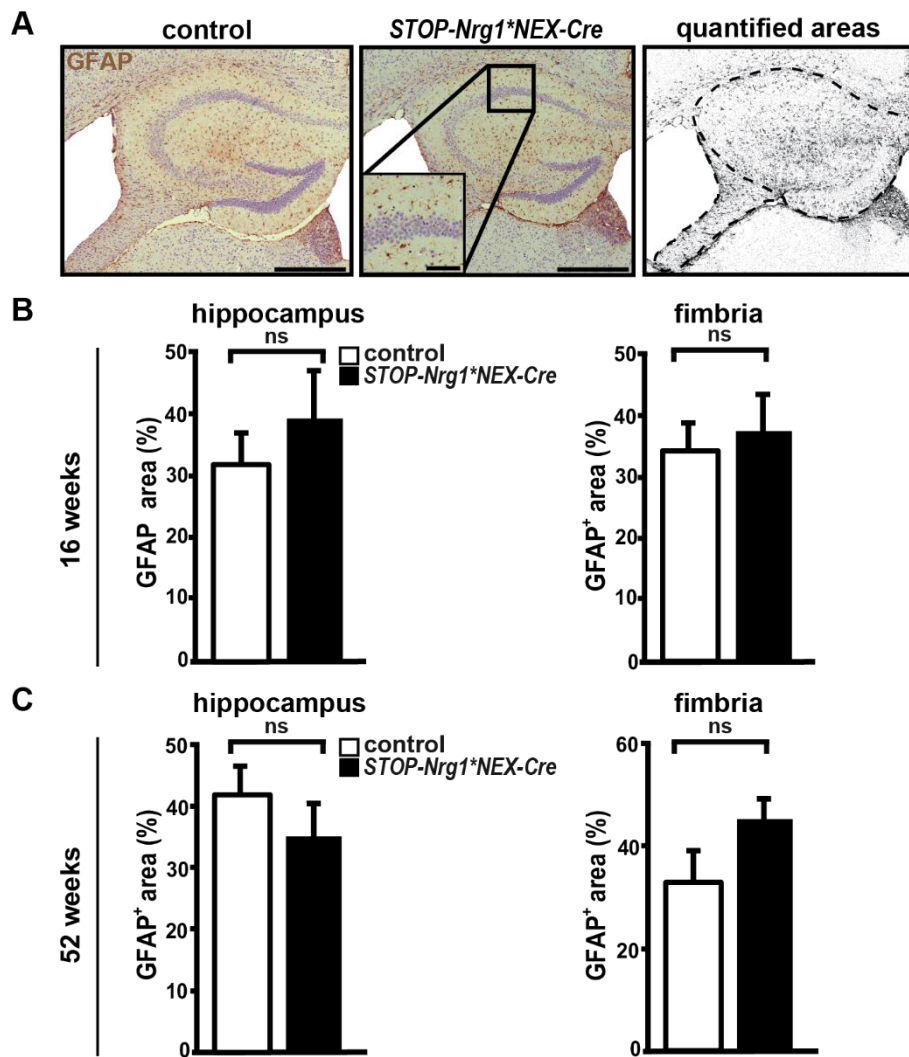


**Figure 12. *STOP-Nrg1*\**NEX-Cre* mice show no signs of astrogliosis.** (A) Chromogenic immunostaining for astrocytes (GFAP) on coronal paraffin sections from 16 weeks old *STOP-Nrg1*\**NEX-Cre* and control mice (bregma -1.3). Quantified areas are marked by dashed lines. Scale bars, 500  $\mu$ m, 100  $\mu$ m (zoom). (B) Semi-automated quantification of GFAP<sup>+</sup> area in hippocampus and fimbria of *STOP-Nrg1*\**NEX-Cre* and control mice (*STOP-Nrg1*, *NEX-Cre*) at 16 weeks of age reveals no difference in GFAP<sup>+</sup> area (n=4-5 each; t-test,  $p > 0.05$ ; ns, not significant). (C) Semi-automated quantification of GFAP<sup>+</sup> area in hippocampus and fimbria of *STOP-Nrg1*\**NEX-Cre* and control mice (*STOP-Nrg1*, *NEX-Cre*) at 52 weeks of age confirms absence of astrogliosis. (n=5-6 each; t-test,  $p > 0.05$ ; ns, not significant).

wt) spent significantly more time on the “safe” ground side as compared to the transparent “air” side (Fig. 14A). Similarly, no significant differences were observed in the hot plate test for pain sensitivity (Fig. 14B).

When exploratory and motor activity was tested no significant genotype effects were observed in the open field test of novelty-induced exploration, as all groups of mice spent similar time in the different zones of the open-field (Fig. 14C). The center zone of the open field is usually avoided by mice since it does not provide shelter. Additionally, motor functions in terms of locomotion and running velocity were not significantly different between genotypes (One-way ANOVA,  $p > 0.05$  for locomotion and velocity; data not shown). In conclusion, these results suggest that HA-Ig-NGR1 overexpression has no major effects on sensory functions, emotionality as well exploratory and motor functions.

A possible effect of HA-Ig-NRG1 overexpression on sensorimotor gating was tested with the pre-pulse inhibition (PPI) test. As expected, the level of inhibition of the startle response after application of the startle pulse increased in dependence of the intensity of the pre-pulse in all genotypes (Fig 14D). However, no significant effects of genotype, genotype per pre-pulse intensity interaction (Fig. 14D) or group differences in terms of the startle response to the 120 dB startle pulse were detected (one-way ANOVA,  $p > 0.05$ ; data not shown). These results suggest that sensorimotor gating and basic acoustic startle reflex pathways are not affected by the increased expression of HA-Ig-NRG1.

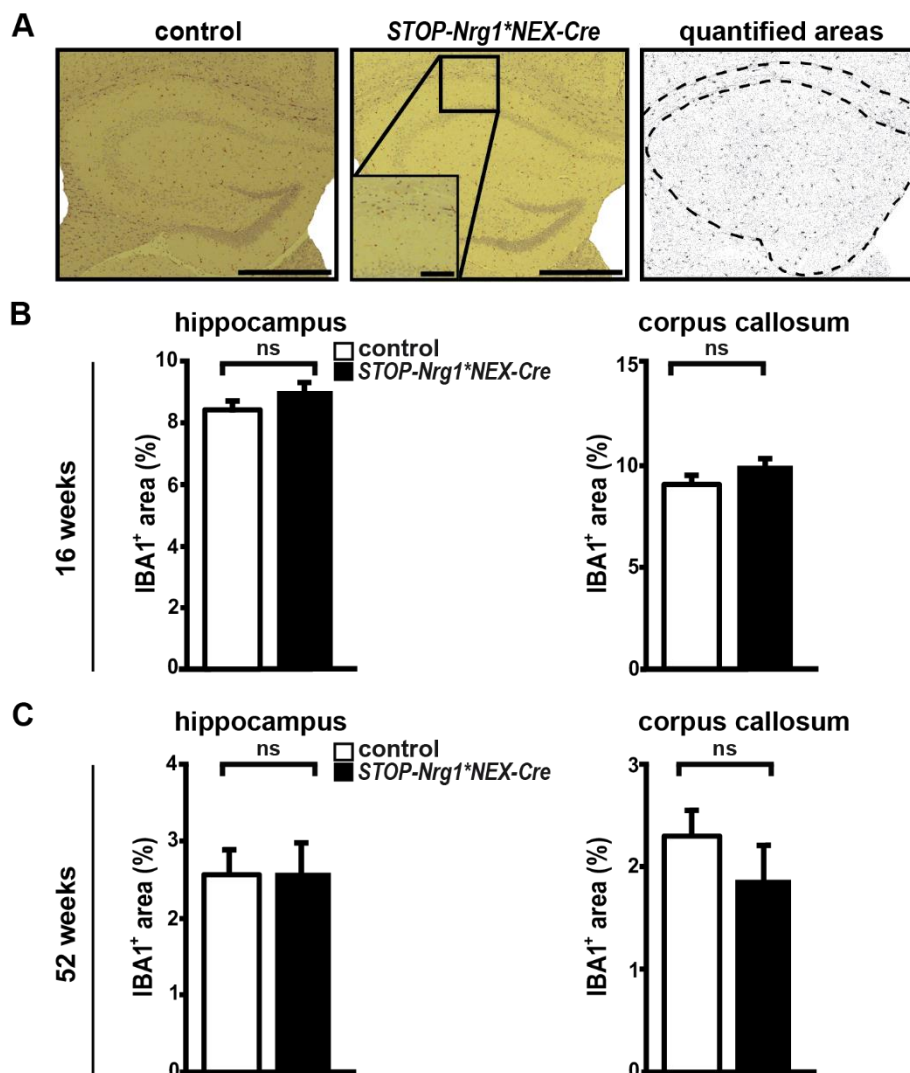


**Figure 13. *STOP-Nrg1*\**NEX-Cre* mice show no signs of microgliosis.** (A) Chromogenic immunostaining for microglia (IBA1) on coronal paraffin sections from 16 weeks old *STOP-Nrg1*\**NEX-Cre* and control mice (bregma -1.3). Quantified areas are shown within dashed lines. Scale bars, 500  $\mu$ m, 100  $\mu$ m (zoom). (B) Semi-automated quantification of IBA<sup>+</sup> area in hippocampus and corpus callosum of *STOP-Nrg1*\**NEX-Cre* and control mice (*STOP-Nrg1*, and *NEX-Cre*) at 16 weeks of age reveals no significant difference in IBA<sup>+</sup> area ( $n=4-5$  each; t-test,  $p > 0.05$ ; ns, not significant). (C) Semi-automated quantification of IBA<sup>+</sup> area in hippocampus and corpus callosum of *STOP-Nrg1*\**NEX-Cre* and control mice (*STOP-Nrg1*, *NEX-Cre*) at 52 weeks of age confirms absence of microgliosis. ( $n=5-6$  each; t-test,  $p > 0.05$ ; ns, not significant).



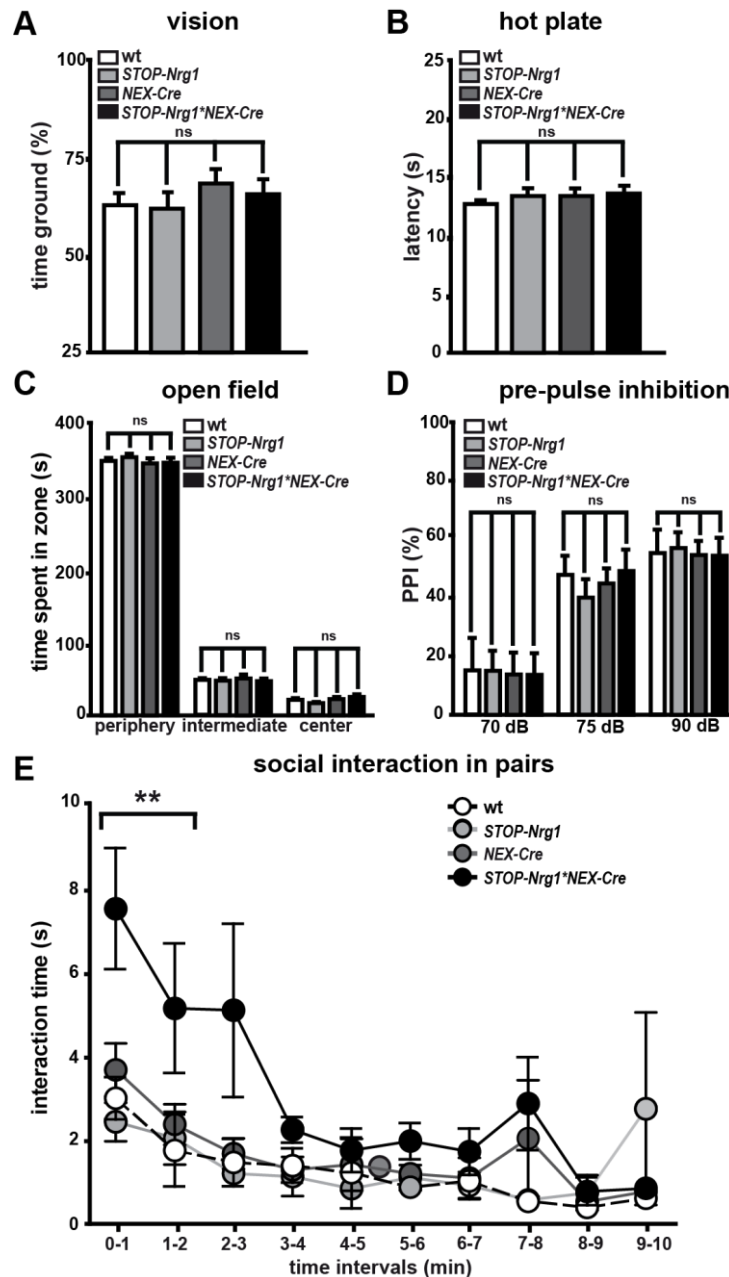


**Figure 14. Sensory, exploratory, motor functions, and sensorimotor gating are not affected, but social behavior is altered in *STOP-Nrg1*\**NEX-Cre* mice.** (A) The visual cliff test showed no differences in the time spent on the “safe” ground side between *STOP-Nrg1*\**NEX-Cre* and control mice (*NEX-Cre*; *STOP-Nrg1*, wt; n=15-17 each; one-way ANOVA,  $p > 0.05$ ; ns, not significant). Bars represent mean $\pm$ SEM percentage of time spend on the ground side. (B) No significant differences between genotypes (*STOP-Nrg1*\**NEX-Cre*, *NEX-Cre*, *STOP-Nrg1*, wt) were observed in the hot plate test (n=14-17; one-way ANOVA,  $p > 0.05$ ; ns, not significant). Bars represent mean $\pm$ SEM latency [s] to show signs of discomfort. (C) No genotype effects were observed in the open filed test (*STOP-Nrg1*\**NEX-Cre*, *NEX-Cre*, *STOP-Nrg1*, wt; n=15-17; one-way ANOVA, p-values for periphery, intermediate zone and center  $> 0.05$ ; ns, not significant). Bars represent mean $\pm$ SEM time spent [s] in different zones. (D) In the PPI test, the startle response after application of the startle pulse increased with the intensity of the pre-pulse in all genotypes (*STOP-Nrg1*\**NEX-Cre*, *NEX-Cre*, *STOP-Nrg1*, wt; n=15-17; one-way ANOVA with repeated measures for main effect of pre-pulse intensity,  $p < 0.0001$ ). No differences for genotype and genotype per pre-pulse intensity interaction were found (one-way ANOVA with repeated measures;  $p > 0.05$ ; ns, not significant). Bars represent mean $\pm$ SEM percentage of inhibition of the startle response. (E) The social interaction test showed a decrease in the time spent in social interaction (across the 10 min of observation) in all genotypes (*STOP-Nrg1*\**NEX-Cre*; *NEX-Cre*; *STOP-Nrg1*; wt; n=6-9 pairs of mice each; one-way ANOVA with repeated measures,  $p < 0.0001$ ). *STOP-Nrg1*\**NEX-Cre* mice showed an effect of genotype (one-way ANOVA with repeated measures,  $p = 0.004$ ) and genotype per time interval interaction (one-way ANOVA with repeated measures,  $p = 0.034$ ). Bars represent mean $\pm$ SEM time of active contact [s].

To test whether HA-Ig-NGR1 overexpression would affect dyadic social interactions, pairs of unfamiliar mice of the same genotype were tested (*STOP-Nrg1\*<sup>+</sup>NEX-Cre*, *NEX-Cre*, *STOP-Nrg1*) in the social interaction test. The time spent with social interactions significantly decreased across the 10 min of observation, indicating that pairs got familiar during the observation period and lost interest in each other towards the end of the observation period. A significant main effect of genotype and genotype per time interval interaction was found for *STOP-Nrg1\*<sup>+</sup>NEX-Cre* mice, which spent significantly more time on social interactions as compared to control groups (wt,  $p=0.005$ ; *STOP-Nrg1*,  $p=0.012$ ; *NEX-Cre*,  $p=0.031$ ; Bonferroni post-hoc test; Fig. 14E). These results revealed that cortical restricted, chronic overexpression of HA-Ig-NGR1 affects social behavior.

## 2.6 Reduced hippocampal $\gamma$ -oscillations in Ig-NGR1 transgenic mice

$\gamma$ -oscillations contribute to cognitive functions and were found to be altered in psychiatric disorders. Importantly, ErbB4 expressing fast-spiking Parv<sup>+</sup> interneurons are key participants in the generation of these oscillations (Bartos et al., 2007). To analyze if projection neuron-specific overexpression of HA-Ig-NGR1 has an effect on  $\gamma$ -oscillations, these oscillations were recorded in the CA3 pyramidal layer of hippocampal slices (in collaboration with Prof. Dr. Jeong Seop Rhee and Dr. Bekir Altas, MPI-EM, Department of Neurobiology). Hippocampal slices were prepared from homozygous *STOP-Nrg1\*<sup>+</sup>NEX-Cre* mice and controls at P30-35. Homozygous *STOP-Nrg1\*<sup>+</sup>NEX-Cre* mice were identified by qPCR (Fig. 15A). Recordings were performed before and after application of kainate (Fig. 15B-C). No changes in the frequency of  $\gamma$ -oscillations were detected in *STOP-Nrg1\*<sup>+</sup>NEX-Cre* compared to *STOP-Nrg1* control mice (Fig. 15D). However, the power of  $\gamma$ -oscillations was reduced in *STOP-Nrg1\*<sup>+</sup>NEX-Cre* mice compared to controls (Fig. 15E). In additional experiments,  $\gamma$ -oscillations were also recorded in *NEX-Cre* and wt mice (P30-35) to exclude possible effects of the *NEX-Cre* driver line. No changes were found in the recordings from *NEX-Cre* compared to wt mice (data not shown). Thus, cortical restricted HA-Ig-NGR1 overexpression results in decreased power of hippocampal  $\gamma$ -oscillations.

## 2.7 The number of Parv<sup>+</sup> interneurons is unaltered in adult *STOP-Nrg1\*<sup>+</sup>NEX-Cre* mice

NGR1 signaling via ErbB4 has been implicated in the migration of cortical interneurons (Flames et al., 2004; Li et al., 2012a). Furthermore, Parv<sup>+</sup> interneurons are usually fast-spiking interneurons that play an important role in the synchronization of pyramidal cell activity and the generation of  $\gamma$ -oscillations (Bartos et al., 2007). Considering the reduced power of  $\gamma$ -oscillations in *STOP-Nrg1\*<sup>+</sup>NEX-Cre* mice, possible effects of chronic HA-Ig-NGR1

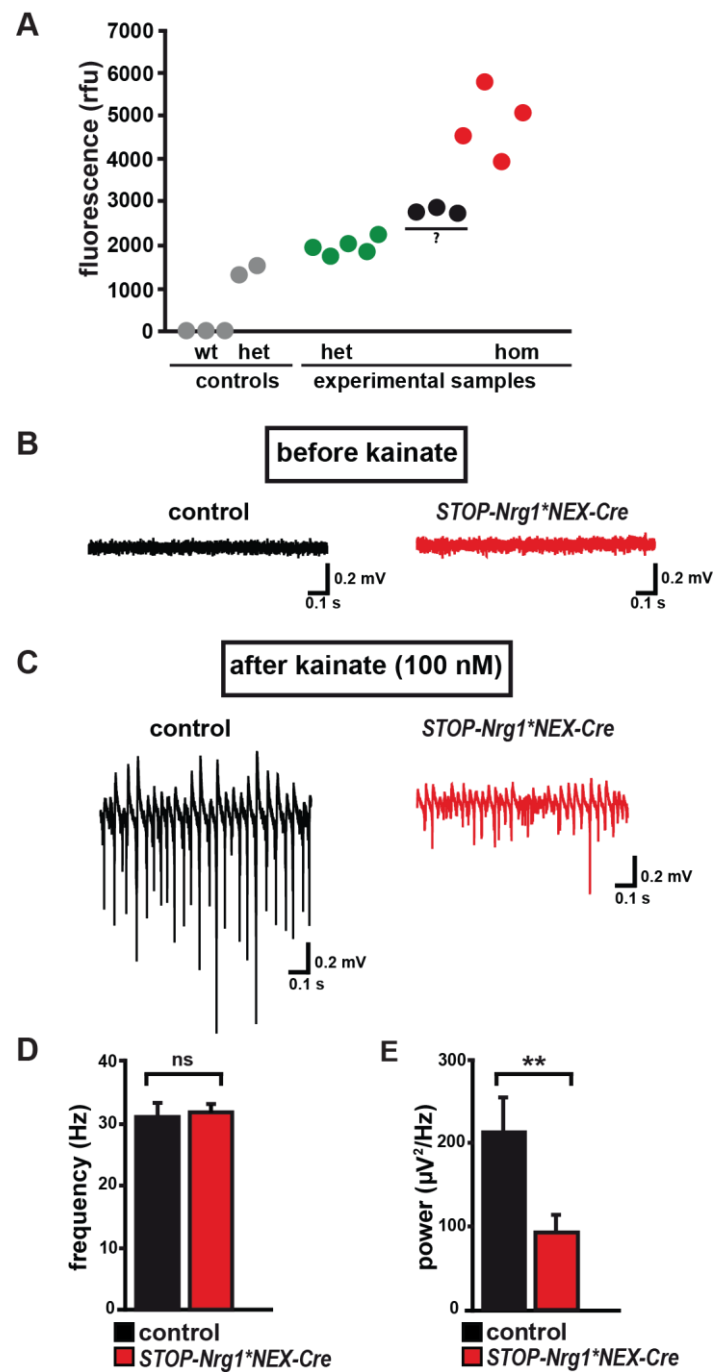


**Figure 15. Cortical restricted HA-Ig-NRG1 overexpression in projection neurons reduces the power of hippocampal  $\gamma$ -oscillations.** (A) qPCR result for the generation of homozygous *STOP-Nrg1\**NEX-Cre** mice. Only mice with the highest values (rfu) were considered homozygous and used in the experiments. wt and heterozygous controls were always included. (B, C) Representative traces of  $\gamma$ -oscillations recorded in the CA3 pyramidal layer before and after kainate application (100 nM) in control (left) and *STOP-Nrg1\**NEX-Cre** mice (right). (D)  $\gamma$ -oscillation frequency was not changed in *STOP-Nrg1\**NEX-Cre** compared to control mice. Mean frequency of  $\gamma$ -oscillations at maximum peak in power spectrum is shown in bar diagram with  $\pm$ SEM. Control,  $31.35 \pm 0.9466$ ,  $N=3$ ,  $n=16$ ; *STOP-Nrg1\**NEX-Cre**,  $32.07 \pm 0.6392$ ,  $N=3$ ,  $n=17$ ;  $p=0.5308$ . (E) Averaged power of  $\gamma$ -oscillations was reduced in *STOP-Nrg1\**NEX-Cre** mice compared to controls. For each recording, the averaged power of  $\gamma$ -oscillations was analyzed between 25-45 Hz frequency in 10 min epochs. Bar diagram represents mean of averaged power of  $\gamma$ -oscillations  $\pm$ SEM. Control,  $215.6 \pm 39.74$ ,  $N=3$ ,  $n=16$ ; *STOP-Nrg1\**NEX-Cre**,  $95.48 \pm 19.23$ ,  $N=3$ ,  $n=17$ ,  $p=0.0093$ .

overexpression beginning at embryonic stages on Parv<sup>+</sup> interneuron numbers were investigated in the hippocampus and cortex. Chromogenic immunostainings were performed on coronal paraffin sections of 16 and 52 weeks old *STOP-Nrg1<sup>+</sup>NEX-Cre* and parental control mice. When manually quantified, no significant differences in the number of Parv<sup>+</sup> interneurons were observed in the cortex and hippocampus of *STOP-Nrg1<sup>+</sup>NEX-Cre* mice compared to controls (Fig. 16A-D). This suggests that increased HA-Ig-NGR1 expression during embryonic development in *STOP-Nrg1<sup>+</sup>NEX-Cre* mice has no major effect on the migration and survival of Parv<sup>+</sup> interneurons in hippocampus and neocortex.

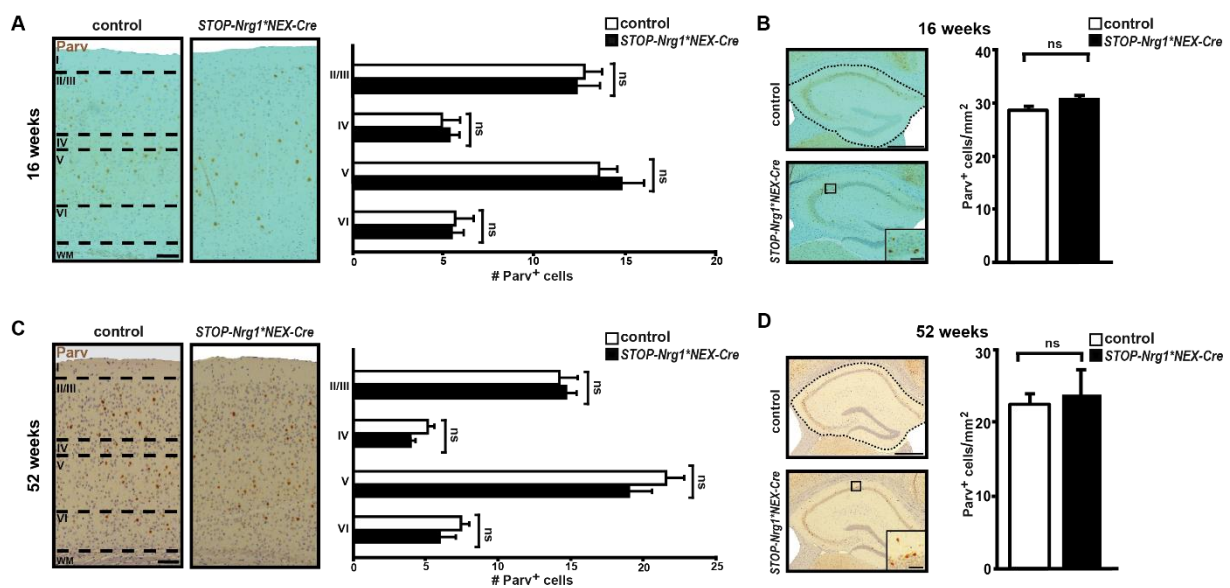


**Figure 16. Unchanged numbers of Parv<sup>+</sup> cortical interneurons in *STOP-Nrg1<sup>+</sup>NEX-Cre* mice.** Chromogenic immunostainings for Parv on coronal paraffin sections from **(A-B)** 16 weeks and **(C-D)** 52 weeks old mice (bregma -1.3 and -1.7, respectively). **(A, C)** Manual quantification of somatosensory cortex columns (width 600  $\mu$ m) showed no differences in numbers of Parv<sup>+</sup> interneurons between *STOP-Nrg1<sup>+</sup>NEX-Cre* mice and controls at 16 weeks and 52 weeks of age (*STOP-Nrg1, NEX-Cre*; n=3-4 each; t-test,  $p > 0.05$ ; ns, not significant). Cortical layers are marked by dashed lines. Scale bar, 100  $\mu$ m. I-VI, cortical layers; WM, white matter. **(B, D)** Quantification of Parv<sup>+</sup> interneurons in the hippocampus of 16 weeks and 52 weeks old *STOP-Nrg1<sup>+</sup>NEX-Cre* mice and controls (*STOP-Nrg1, NEX-Cre*) showed no significant differences (n=3-4 each; t-test,  $p > 0.05$ ; ns, not significant). Dashed line indicates the quantified area. Scale bars, 500  $\mu$ m (hippocampus), 50  $\mu$ m (zoom).

## 2.8 Elevated Ig-NGR1 signaling preferentially recruits the AKT signaling pathway

MAPK and PI3K/AKT are two major signaling pathways downstream of NRG1-mediated ErbB4 stimulation, which regulate many processes required for proper network function, i.e. interneuron migration, dendritic spine formation, and synaptic plasticity (Krivosheya et al., 2008; Kumar et al., 2005; Thomas and Huganir, 2004; Wu et al., 2001). To investigate specific effects of Ig-NGR1 during the regulation of these signaling cascades, biochemical analysis by Western blotting was performed in *STOP-Nrg1<sup>+</sup>NEX-Cre*, *Thy1.2-Nrg1* and control mice. As mentioned above, *Thy1.2-Nrg1* mice showed almost 6-fold Ig-NGR1 overexpression compared to *STOP-Nrg1<sup>+</sup>NEX-Cre* mice (Fig. 10A-B) and consistent with this, ErbB4

hyperphosphorylation in the conventional line is ~5-fold higher than in conditional transgenic mice (Fig. 10C-D; Fig. 17A). This also suggests that ErbB4 is not a rate limiting factor when modelling Ig-NGR1 hyperstimulation in the brain. Biochemical analysis showed no significant differences in p-MAPK levels in *STOP-Nrg1*\**NEX-Cre* compared to controls. However, there was a significant increase in the level of p-MAPK in *Thy1.2-Nrg1* mice compared to controls. Levels of p-MAPK do not differ between conditional and conventional NRG1 transgenic mice (Fig. 17B). On the other hand, levels of p-AKT were increased in both *STOP-Nrg1*\**NEX-Cre* and *Thy1.2-Nrg1* mice compared to controls (Fig. 17C).

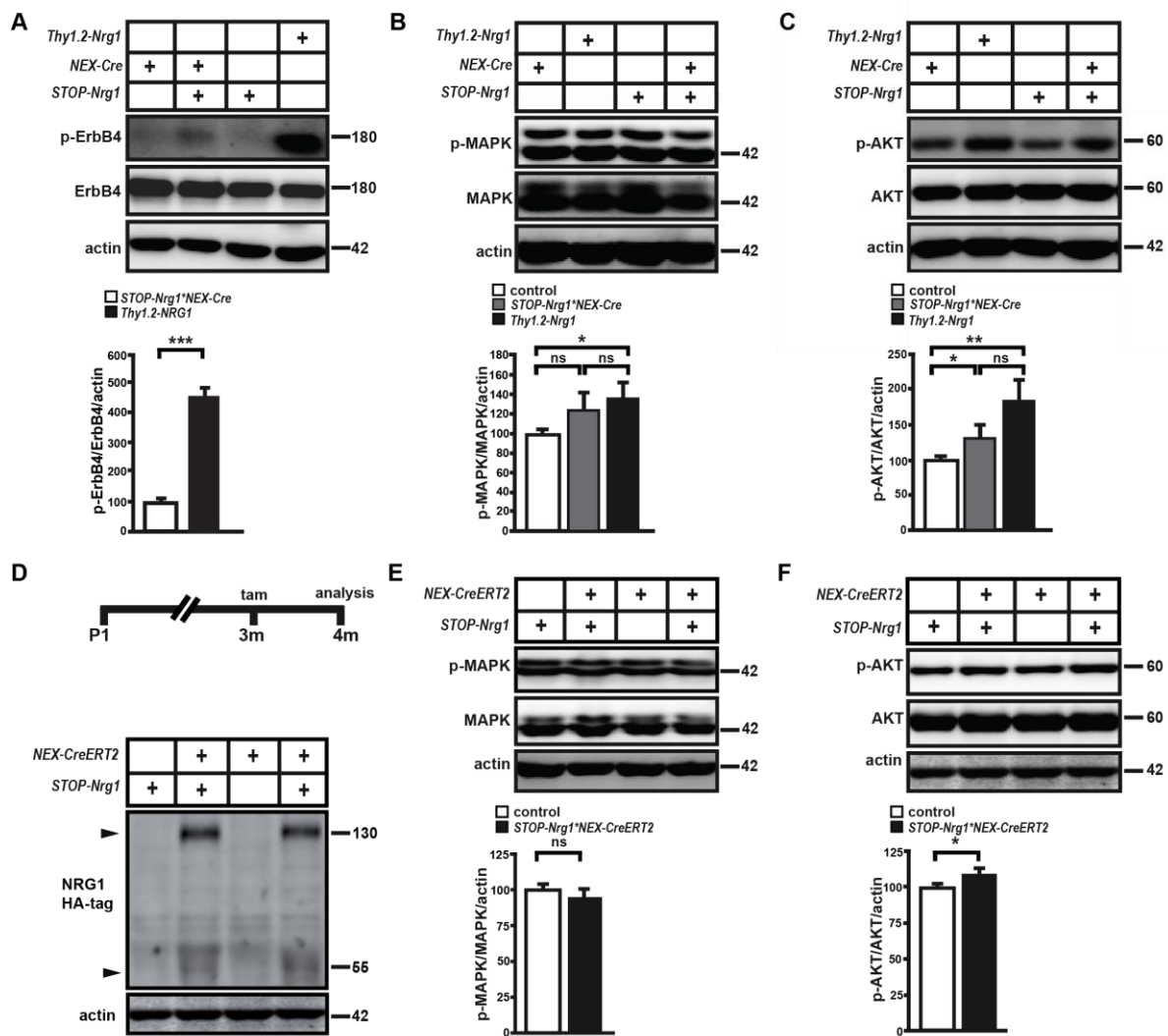


**Figure 17. Cortical restricted Ig-NGR1 overexpression preferentially stimulates the AKT signaling pathway.** (A) Western blotting of PFC protein lysates (age 16 weeks) revealed that ErbB4 hyperphosphorylation is ~5-fold higher in *Thy1.2-NRG1* compared to *STOP-Nrg1*\**NEX-Cre* mice. Densitometric quantification of p-ErbB4 (Tyr1284) bands. Integrated density values were normalized to  $\beta$ -actin loading control (n=3 each; t-test,  $p < 0.0001$ ). (B) Western Blot analysis shows no significant differences in p-MAPK levels in the PFC of *STOP-Nrg1*\**NEX-Cre* mice (16 weeks old) compared to controls (*STOP-Nrg1*, *NEX-Cre*). Levels of p-MAPK are increased in *Thy1.2-NRG1* compared to controls, but are not significantly different from p-MAPK in *STOP-Nrg1*\**NEX-Cre* mice. Densitometric quantification of p-MAPK bands. Integrated density values were normalized to  $\beta$ -actin loading control (n=3-4 each; t-test,  $*p = 0.0222$ ;  $p$  values  $> 0.05$ ; ns, not significant). (C) Western blotting of PFC protein lysates of *STOP-Nrg1*\**NEX-Cre* and *Thy1.2-NRG1* mice (16 weeks old) reveals increased p-AKT levels compared to controls (*STOP-Nrg1*, *NEX-Cre*). Densitometric quantification of p-AKT bands. Integrated density values were normalized

to  $\beta$ -actin loading control (n=3-4 each; t-tests, \*p= 0.0361, \*\*p= 0.0016). **(D)** Western blot analysis shows induction of HA-Ig-NGR1 expression in the hippocampus of tamoxifen injected *STOP-Nrg1\**NEX-CreERT2** mice, but not in injected controls (*STOP-Nrg1*, *NEX-CreERT2*) using an antibody directed against the N-terminal HA tag. Mice were injected with tamoxifen for 5 consecutive days at 3 months of age and collected 4 weeks later. **(E)** Unaltered MAPK phosphorylation in the hippocampus of *STOP-Nrg1\**NEX-CreERT2** mice compared to controls (*STOP-Nrg1*, *NEX-CreERT2*). Densitometric quantification of p-MAPK bands. Integrated density values were normalized to  $\beta$ -actin loading control (n=3-5 each; t-test, p values > 0.05; ns, not significant). **(F)** Increased AKT phosphorylation in the hippocampus of tamoxifen injected *STOP-Nrg1\**NEX-CreERT2** mice compared to controls (*STOP-Nrg1*, *NEX-CreERT2*). Densitometric quantification of phosphorylated AKT bands. Integrated density values were normalized to  $\beta$ -actin loading control (n=3-5 each; t-tests, p= 0.0141).

To achieve HA-Ig-NGR1 overexpression in the adult brain (where levels of NRG1 expression are very low in wildtype), *STOP-Nrg1* transgenic mice were bred to a tamoxifen inducible Cre driver line (*NEX-CreERT2*) (Agarwal et al., 2012). CreERT2-mediated activation of HA-Ig-NGR1 expression was shown by biochemical analysis of protein lysates from the PFC and hippocampus 4 weeks after the final tamoxifen injection (Fig. 17D). Western blot analysis showed no difference in p-MAPK levels between *STOP-Nrg1\**NEX-CreERT2** mice and controls, similar to chronic *STOP-Nrg1\**NEX-Cre** mice (Fig. 17E). In contrast, levels of p-AKT were found to be significantly increased in *STOP-Nrg1\**NEX-CreERT2** compared to controls (Fig 17F). Taken together, these results suggest that Ig-NGR1 overexpression leads to a preferential recruitment of the AKT signaling pathway.

## 2.9 Accumulation of Ig-NGR1 in the somatodendritic compartment of projection neurons

To provide a basis for mechanistic insights into Ig-NGR1-mediated reduction in hippocampal  $\gamma$ -oscillations and altered social behavior, the subcellular localization of this protein was examined in more detail. To obtain more robust signals, homozygous *STOP-Nrg1\**NEX-Cre** and *Thy1.2-Nrg1* mice were included in some of these experiments. Fluorescent immunostainings of conventional and conditional transgenic mice showed a massive overexpression in the brain of *Thy1.2-Nrg1* mice and a moderate overexpression in *STOP-Nrg1\**NEX-Cre** mice (Fig. 18A). These two mouse lines were also used to compare Ig-NGR1 expression patterns by immunohistochemistry. Despite differences in expression levels, both mouse lines showed a similar “punctate” pattern of Ig-NGR1 expression in cortical projection neurons when using an antibody directed against the Ig-NGR1 C-terminus (Fig. 18B). Despite the general concept according to which NRG1 is enriched at presynaptic terminals of projection neurons and interacts with ErbB4 that is mainly expressed in postsynaptic compartments of interneurons, in this study NRG1 was found to be enriched in the somatodendritic compartment of projection neurons (Fig. 18B).

Furthermore, fluorescent immunostainings for synaptic markers in *STOP-Nrg1\**NEX-Cre** and *Thy1.2-Nrg1* mice showed absence of colocalization with the presynaptic markers synaptophysin and VGlut1 (Fig. 19A). A similar finding was obtained in double transgenic mice

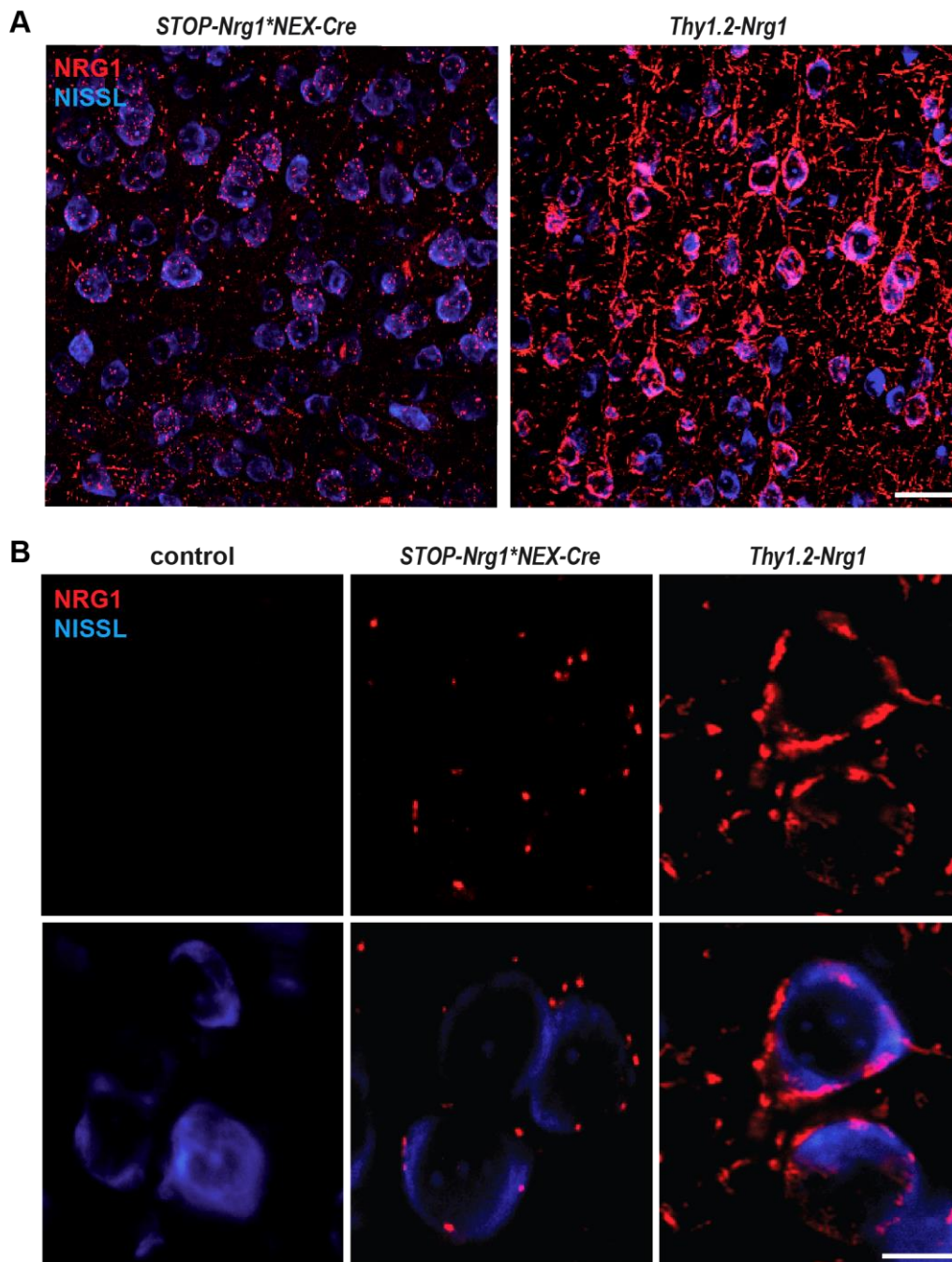


**Figure 18. Ig-NRG1 shows a “punctate” pattern of expression in the somatodendritic compartment of projection neurons. (A)** Fluorescent immunostainings of coronal vibratome sections from *STOP-Nrg1\*NEX-Cre* and *Thy1.2-Nrg1* mice at 8-9 weeks of age using an antibody directed against the C-terminal domain of NRG1 demonstrate a moderate overexpression of Ig-NRG1 in the cortex of *STOP-Nrg1\*NEX-Cre* mice compared to massive overexpression in *Thy1.2-Nrg1* mice. Scale bar, 25  $\mu$ m. **(B)** *STOP-Nrg1\*NEX-Cre* and *Thy1.2-Nrg1* mice showed a similar pattern of subcellular Ig-NRG1 expression in the somatodendritic compartment of cortical projection neurons. Scale bar, 10  $\mu$ m.

that overexpress both Ig-Nrg1 and an “active” variant of CRD-Nrg1 that lacks the C-terminal domain (*Thy1.2-CRD-NRG1<sup>GIEF</sup>*), which mimics BACE1 processing in the juxtamembrane “stalk” region (Velanac et al., 2012; Fig. 19B-C). Additionally, fluorescent immunostainings

were also performed for the serotonin transporter (SERT) to explore the possibility of a close localization of Ig-NRG1 to serotonergic synapses, however this was not the case (Fig. 19D). In addition, fluorescent immunostainings on coronal brain sections from conditional and conventional overexpressors showed no signs of colocalization with the postsynaptic markers PSD95 and Gephyrin (Fig. 20A-B).

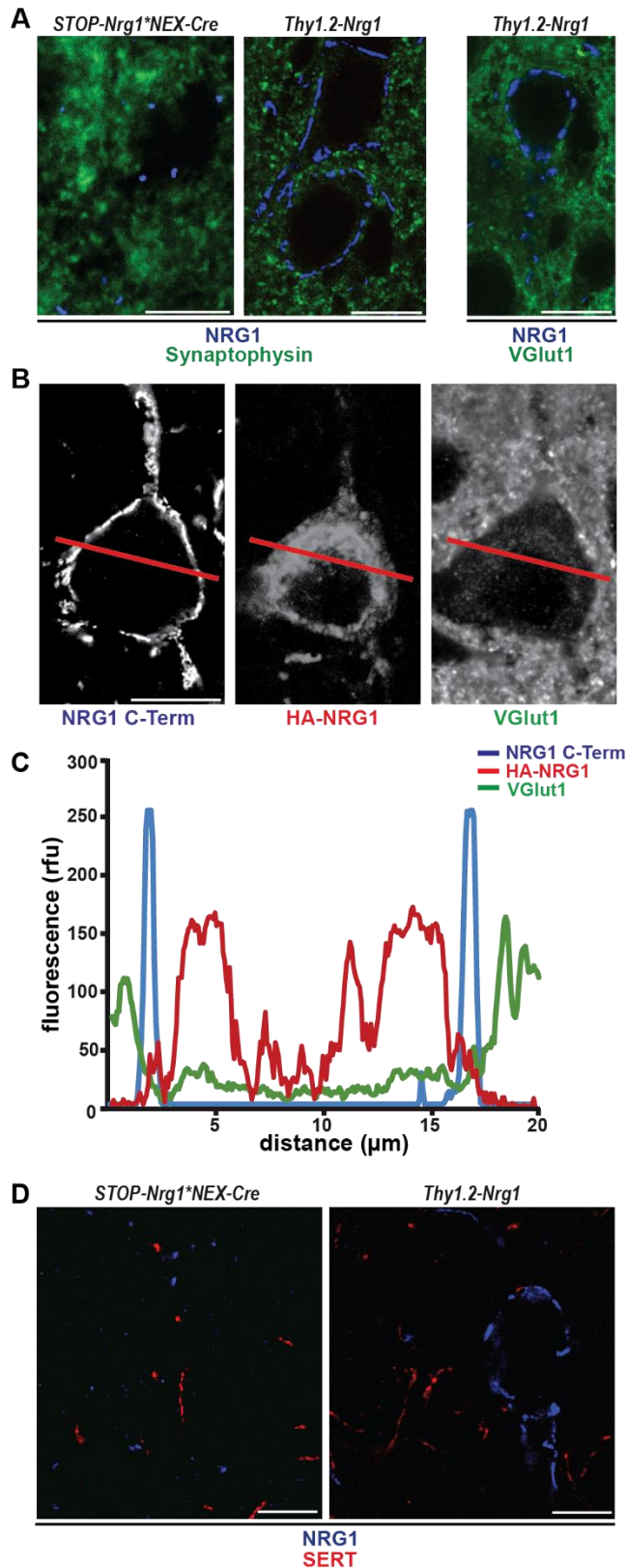


**Figure 19. NRG1 does not colocalize with presynaptic markers.** (A) Fluorescent immunostainings on cryosections from *STOP-Nrg1\*<sup>NEX-Cre</sup>* and *Thy1.2-Nrg1* mice revealed no colocalization of Ig-NRG1 (C-terminal domain) with presynaptic markers synaptophysin and VGlut1. Scale bar, 10 μm. (B) Absence of colocalization of NRG1 with VGlut1 was also found in fluorescent immunostainings of coronal cryosections from *Thy1.2-Nrg1\*<sup>Thy1.2-CRD-NRG1<sup>GIEF</sup></sup>* double transgenic mice. Individual channels of the triple staining for the NRG1 C-terminal domain, HA tag (present at the N-terminus of *CRD-NRG1<sup>GIEF</sup>*) and VGlut1 are shown. A line scan (indicated by a red line) was performed using the plot profile function of Image J. (C) Combined plot reveal no overlap between the fluorescent signal of each marker, consistent with the absence of colocalization of Ig-NRG1 and VGlut1. Scale bar 10 μm. (D) Cryosections of conditional and conventional overexpressors of Ig-NRG1 immunostained for SERT did not show close localization of Ig-NRG1 with the marker. Scale bar, 10 μm.



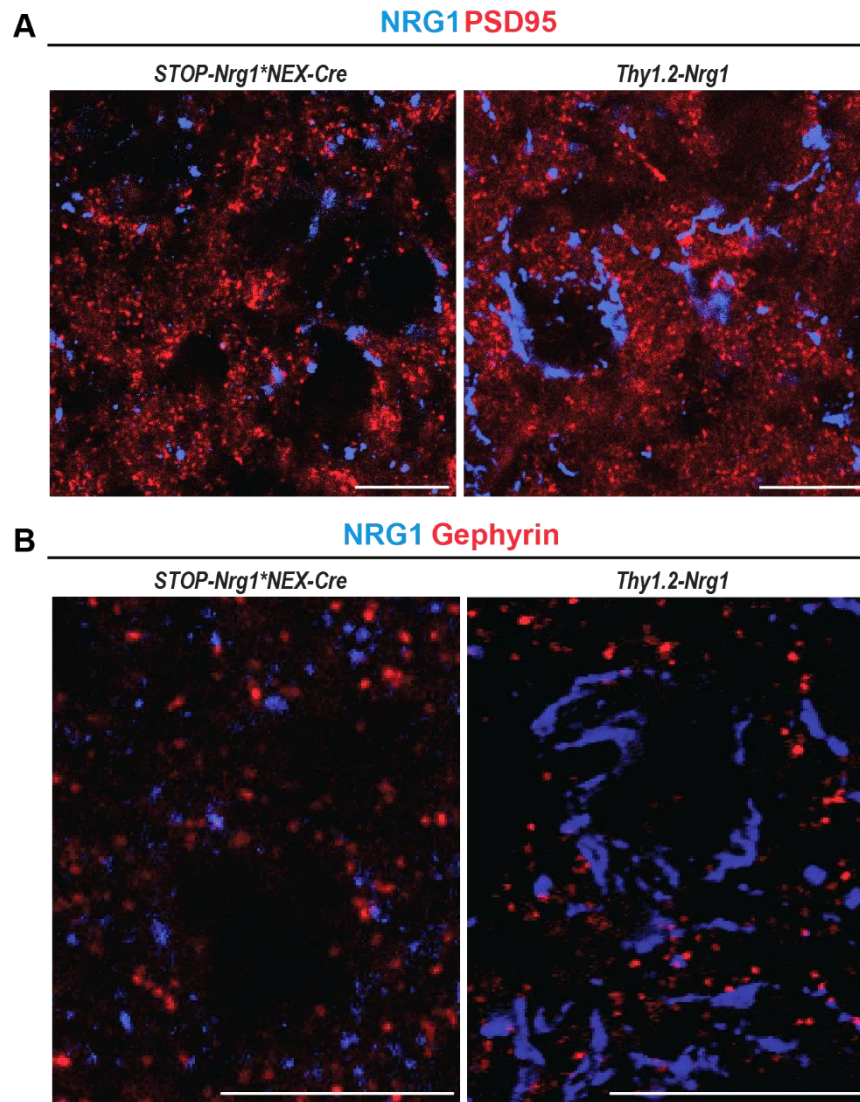


**Figure 20. Ig-NRG1 does not colocalize with postsynaptic markers.** Fluorescent co-immunostainings on cryosections from *STOP-Nrg1\*NEX-Cre* and *Thy1.2-Nrg1* mice for the NRG1 C-terminal domain and postsynaptic markers revealed that Ig-NRG1 does not colocalize with (A) PSD95 and (B) Gephyrin. Scale bars, 10  $\mu$ m.

NRG1 accumulates in ER-derived subsurface cisternae (SSC) in cholinergic synapses (“C-type”) of the spinal cord (Gallart-Palau et al., 2014). Moreover, NRG2 a protein with a similar structure as Ig-NRG1, was found to be associated with Kv2.1, a potassium channel that clusters in the plasma membrane in close proximity to SSCs (Vullhorst et al., 2015). To examine if Ig-NRG1 is also located close to SSCs, fluorescent immunostainings for Kv2.1 were performed, which showed that Ig-NRG1 partially colocalizes with Kv2.1 (Fig. 21A). These results suggest that the higher protein levels in *Thy1.2-Nrg1* mice compared to *STOP-Nrg1\*NEX-Cre* have no considerable impact on the subcellular localization of Ig-NRG1, and that this protein is not located in presynaptic compartments or the PSD of projection neurons (Fig. 21A, I). Instead, Ig-NRG1 appears to accumulate either in the plasma membrane above SSCs (Fig. 21A, II) or even within the SSC membrane (Fig. 21A, III). This argues in favor of somatodendritic functions, including autocrine NRG1 signaling in projection neurons.

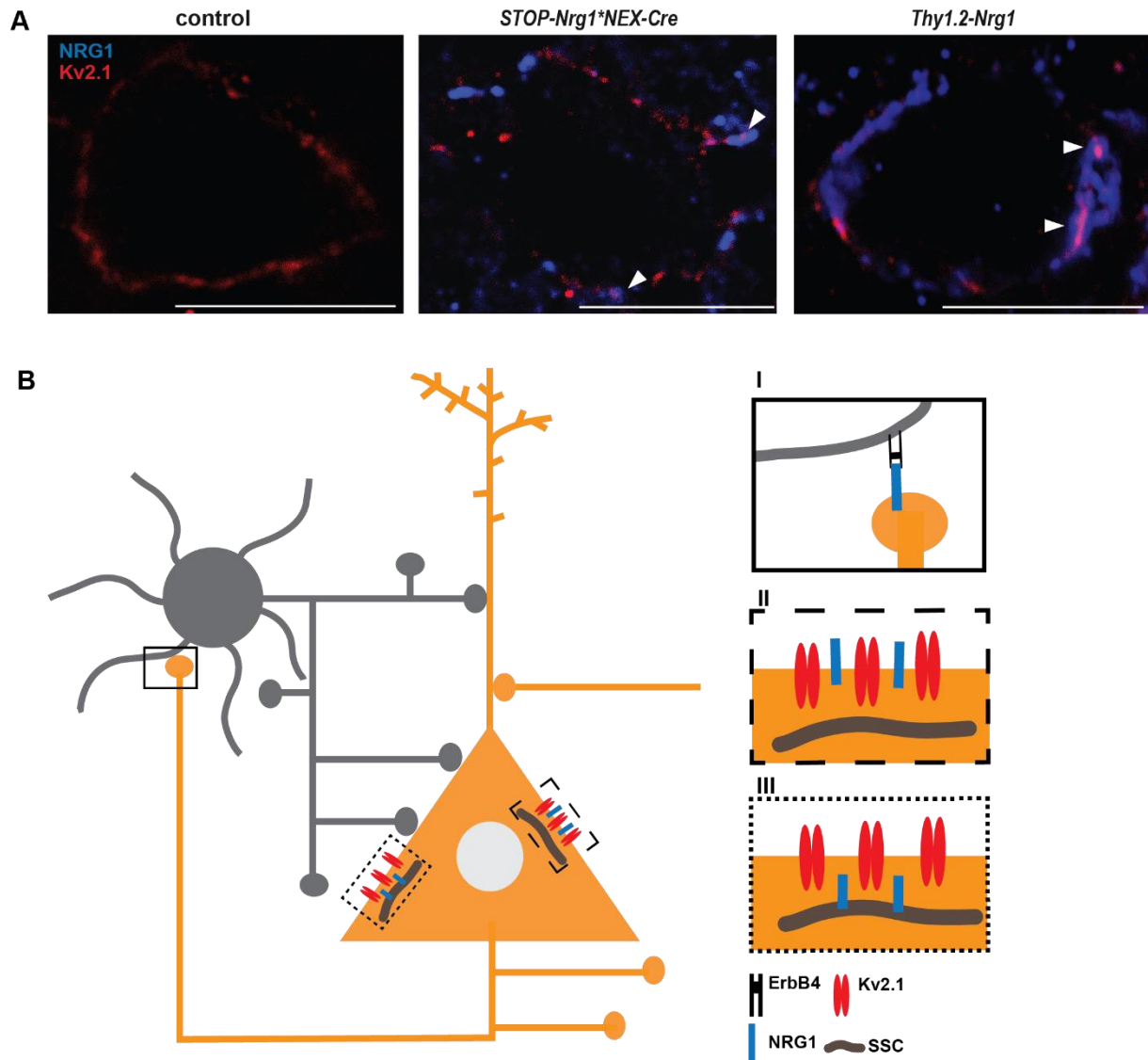


**Figure 21. Ig-NGR1 partially colocalizes with the potassium channel Kv2.1.** (A) Fluorescent immunostainings on cryosections from *STOP-Nrg1\* NEX-Cre* and *Thy1.2-Nrg1* mice revealed that the C-terminal domain of Ig-NGR1 colocalizes with Kv2.1 (arrowheads). Scale bar, 10  $\mu$ m. (B) Model of subcellular Ig-NGR1 localization shows that NRG1 is not enriched in presynaptic compartments of projection neurons (I). Instead, Ig-NGR1 colocalizes with Kv2.1, a potassium channel found in plasma membrane clusters in close proximity to SSCs. Thus, Ig-NGR1 appears to accumulate in the somatodendritic plasma membrane adjacent to (II) or directly within SSCs (III).

## 2.10 Analysis of Parv<sup>+</sup> interneuron-specific NRG1 mutants

NRG1 is prominently expressed by glutamatergic projection neurons, but also present in GABAergic interneurons and astrocytes (Liu et al., 2011). Previous studies indicate that projection neuron-specific loss or (moderate) overexpression of NRG1 are not associated with severe CNS dysfunctions (Agarwal et al., 2014), suggesting that altered paracrine or juxtacrine NRG1 signaling is well tolerated by the brain. Thus, to address autocrine NRG1 signaling functions in ErbB4-expressing, Parv<sup>+</sup> interneurons, a pilot study was performed, in which conditional NRG1 mutants (*Nrg1 f/f*) (Li et al., 2002) were bred to parvalbumin-Cre (*Parv-Cre*) driver mice (Hippenmeyer et al., 2005). First, to determine the Parv-Cre-mediated

recombination pattern, *Parv-Cre* mice were bred to a floxed tdTomato Cre-reporter mouse line (*tdTo*; Madisen et al., 2010). Images from coronal cryosections of *tdTo\*Parv-Cre* mice were obtained. tdTomato reporter fluorescence displayed a recombination pattern, which was in line with the distribution of *Parv*<sup>+</sup> neurons in the brain (Fig. 22A). Next, *Nrg1 f/f\*Parv-Cre* mice were produced, which were born at the expected Mendelian frequencies and survived until adulthood. However, starting at 3-4 weeks of age, *Nrg1 f/f\*Parv-Cre* mice, but not their littermates (*Nrg1 f/f*, *Parv-Cre*, *Nrg1 f/+\*Parv-Cre*) showed a shivering phenotype. In addition, male and female *Nrg1 f/f\*Parv-Cre* mice displayed a significant reduction in their body weight at 5 weeks of age (Fig. 22B), which seems to persist throughout adulthood (data not shown).

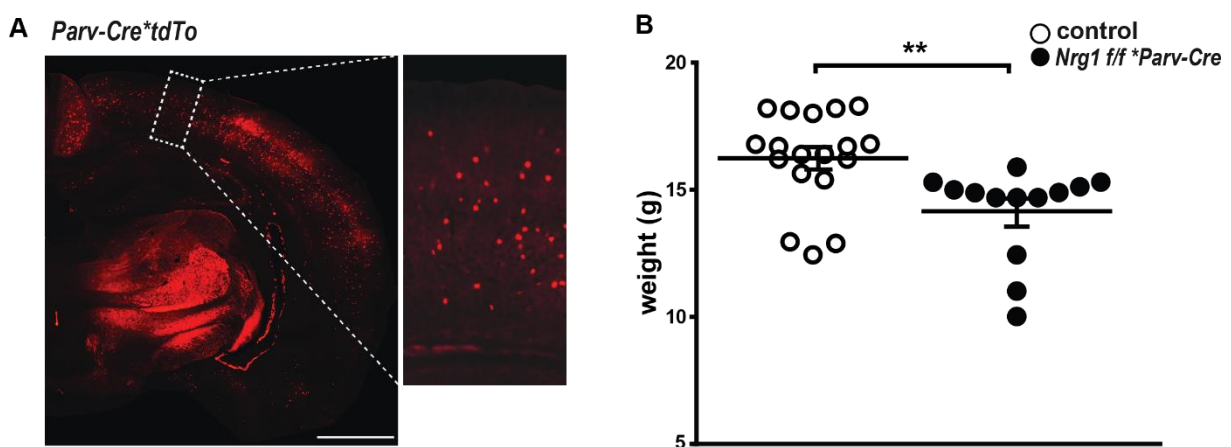


**Figure 22. Reduced body weight in *Nrg1 f/f\*Parv-Cre* mutants.** (A) Cryosection (bregma -1.7) of *tdTo\*Parv-Cre* mouse shows the Cre recombination pattern of the *Parv-Cre* driver line, based on tdTomato reporter fluorescence. Scale bars, 1mm, 100  $\mu$ m (zoom). (B) Body weight reduction in *Nrg1 f/f\*Parv-Cre* females (n=13) compared to controls (*Nrg1 f/f*, n=8; *Parv-Cre*, n=5; *Nrg1 f/+\*Parv-Cre* n=5) at 5 weeks of age. (One-way ANOVA showed no differences between control groups; t-test for mutants vs control group, p=0.006).

To address possible effects on *Parv*<sup>+</sup> interneurons, chromogenic immunostainings were performed on coronal paraffin sections from 5 and 18 weeks old *Nrg1 f/f\*Parv-Cre* and control mice (bregma -1.7; Fig. 23A). Interneuron numbers were manually counted. No significant differences in *Parv*<sup>+</sup> cell numbers were observed in the hippocampus of mutants compared to controls (*Nrg1 f/f*, *Parv-Cre*) at 5 weeks (Fig. 23B). Likewise, no differences were observed in the hippocampus of 18 weeks old *Nrg1 f/f\*Parv-Cre* mutants (Fig. 23C).

Next, columns of the same width from the somatosensory cortex above the CA1 and CA2 region of the hippocampus (Fig. 24A) were used to manually count the number of *Parv*<sup>+</sup> cells. Here, a reduction of *Parv*<sup>+</sup> interneurons was observed in cortical layers II-III in both cohorts of mice (Fig. 24B, D). In contrast, no differences in the numbers of calbindin<sup>+</sup> interneurons were found in *Nrg1 f/f\*Parv-Cre* (n=3) and littermate controls (*Nrg1 f/f*, n=3; *Nrg1 f/+\*Parv-Cre*, n=3) at 18 weeks of age (Fig. 24C), supporting a specific loss of *Parv*<sup>+</sup> cells due to cell autonomous effects of NRG1 elimination.

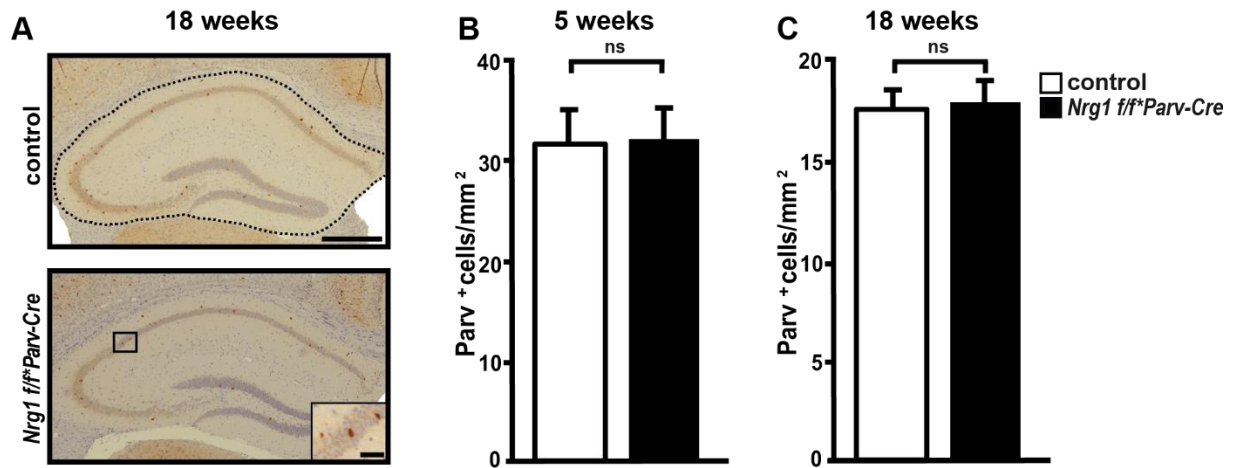


**Figure 23. Unaltered numbers of Parv<sup>+</sup> interneurons in the hippocampus of *Nrg1 f/f\*Parv-Cre* mutants.** (A) Chromogenic immunostainings for Parv<sup>+</sup> cells on coronal paraffin sections (bregma -1.7) from 18 weeks old *Nrg1 f/f\*Parv-Cre* and control mice. (B) Quantification of Parv<sup>+</sup> interneurons in the hippocampus of 5 weeks old females *Nrg1 f/f\*Parv-Cre* (n=4) showed no differences compared to controls (*Nrg1 f/f*, n=3; *Parv-Cre*, n=4). (C) Numbers of Parv<sup>+</sup> interneurons were also unaltered in 18 weeks old males *Nrg1 f/f\*Parv-Cre* (n=3) compared to control mice (*Nrg1 f/f*, n=3; *Nrg1 f/+\*Parv-Cre*, n=3; t-tests,  $p > 0.05$ ; ns, not significant). Scale bars, 500  $\mu\text{m}$  (hippocampus), 50  $\mu\text{m}$  (zoom).

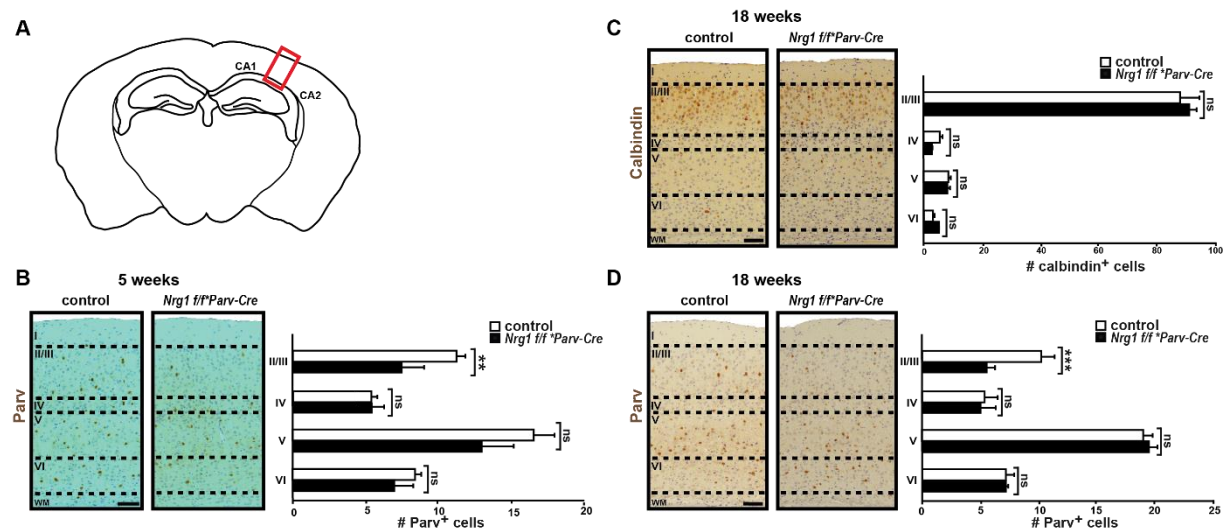


**Figure 24. Reduction of Parv<sup>+</sup> interneurons in cortical layers II/III of *Nrg1 f/f\*Parv-Cre* mice.** (A) Schematic drawing of an adult coronal brain section illustrates the position of images shown in (B-D) (red column between CA1 and CA2 regions of the hippocampus). (B) Chromogenic immunostainings for Parv<sup>+</sup> cells on coronal paraffin sections (bregma -1.7) from 5 weeks old *Nrg1 f/f\*Parv-Cre* and control mice (only females). Manual quantification of columns (width 500  $\mu\text{m}$ ) of the somatosensory cortex showed a reduction in numbers of Parv<sup>+</sup> interneurons in cortical layers II-III of *Nrg1 f/f\*Parv-Cre* mice compared to controls (*Nrg1 f/f*, *Parv-Cre*; n=3-4 each; t-test,  $**p= 0.0253$ ,  $p > 0.05$ ; ns, not significant). Scale bar 100  $\mu\text{m}$ . (C) Chromogenic immunostainings for calbindin<sup>+</sup> interneurons on coronal paraffin sections (bregma -1.7) from 18 weeks old males *Nrg1 f/f\*Parv-Cre* and controls (*Nrg1 f/f*, *Nrg1 f/+\*Parv-Cre*, n=3 each). Manual quantification of columns (width 600  $\mu\text{m}$ ) of the somatosensory cortex showed no changes in cell numbers (t-tests,  $p > 0.05$ ; ns, not significant). Scale bar, 100  $\mu\text{m}$ . (D) Chromogenic immunostainings for Parv<sup>+</sup> cells on coronal paraffin sections (bregma -1.7) from the same cohort of 18 weeks old *Nrg1 f/f\*Parv-Cre* and control mice. Quantification showed a reduction in numbers of of Parv<sup>+</sup> interneurons in cortical layers II-III of mutants compared to controls (t-test,  $***p= 0.0007$ ,  $p > 0.05$ ; ns, not significant). Scale bar, 100  $\mu\text{m}$ .

## 2.11 Generation of a “knock in” mouse line for the conditional activation of NRG2 signaling in the brain

NRG2 is a member of the NRG family with a similar domain structure as Ig-NRG1 and serves as a ligand for ErbB receptors. However, it exhibits different temporal and regional expression patterns in the nervous system (Carraway et al., 1997; Longart et al., 2004). NRG2 is prominently expressed in the adult cortex, dentate gyrus, and cerebellum, but its role in the brain, particularly at cortical synapses, is unknown. In this side project, tools for the investigation of NRG2 functions in CNS synapses were generated and tested. In a first approach, primary hippocampal neurons were treated with the recombinant EGF domain of NRG2 (GST-NRG2; Fig. 25A). After treatment for 24 h, hippocampal neurons (14 DIV) showed increased ErbB4 phosphorylation compared to controls, demonstrating that the EGF domain of NRG2 activates ErbB4 receptors. This effect was significantly reduced after treatment with Lapatinib. Although not yet statistically significant, GST-NRG2-induced ErbB4 phosphorylation was also reduced after treatment with 10  $\mu$ M Spironolactone (Fig. 25B-C), a mineral corticoid

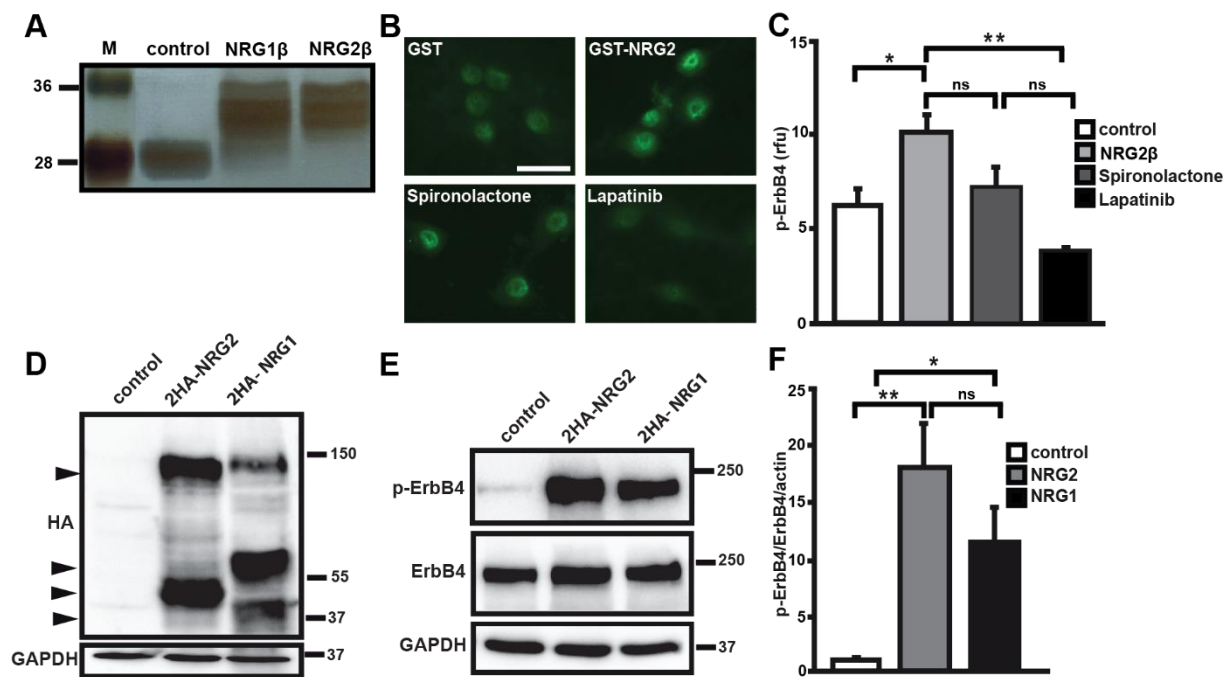


**Figure 25. *In vitro* tools to examine NRG2 functions at CNS synapses.** (A) Silver staining of a polyacrylamide gel shows the integrity of the EGF domain of NRG2 (NRG2 $\beta$ ) fused to GST. NRG1 $\beta$  was used as a positive control, GST as a negative control (700 ng protein/lane were loaded; 12% polyacrylamide gel.) M, marker. (B) Stimulation of hippocampal neurons with GST-NRG2 induces ErbB4 phosphorylation. Spironolactone treatment shows a tendency to reduce NRG2-mediated ErbB4 hyperphosphorylation. Lapatinib treatment was used as a control. Scale bar, 25  $\mu$ m. (C) Quantification of p-ErbB4 levels in hippocampal primary neurons after stimulation with NRG2 $\beta$  and treatment with tyrosine kinase inhibitors. (n= 3-6 replicates per treatment; one-way ANOVA, \*p<0.05, \*\*p<0.005; ns, not significant). (D) Western blotting of lysates from N1E cells transfected with pcDNA3.1-2HA-NRG2 (using an  $\alpha$ HA tag antibody). pCMV-2HA-NRG1 was used as a positive control. Arrowheads indicate full-length (130 kDa) and processed proteins (37 and 50 kDa). (E) ErbB4 hyperphosphorylation in lysates of ErbB4-transfected N1E cells co-transfected with 2HA-NRG2 or pCMV-2HA-NRG1 compared to controls (vector alone; n=3 each). (F) Densitometric quantification of phosphorylated ErbB4 (Tyr1284) bands. Integrated density values were normalized to  $\beta$ -actin loading control (t-tests, \*p=0.0139; \*\*p=0.0063; ns, not significant).

receptor antagonist that was identified as a new ErbB receptor inhibitor (Wehr *et al.*, submitted to EMBO Mol. Med.). Thus, GST-NRG2 could be used in future experiments to examine NRG2-mediated signaling pathways downstream of ErbB4 in cortical neurons. Additionally, a pcDNA3.1-based expression vector harboring 2HA-tagged full-length NRG2 was designed and ordered from GenScript®. Transfection of N1E neuroblastoma cells with pcDNA3.1-2HA-NRG2 showed that the 2HA-NRG2 cassette (used later for the generation of a “knock in” mouse line) was expressed in these cells. Western blotting using an antibody against the HA tag detected full-length and processed protein (Fig. 25D). In addition, phosphorylation of coexpressed ErbB4 was strongly increased in the presence of 2HA-NRG2 (Fig. 25E-F; these data were kindly provided by Ann-Kristin Martens, MHH). In conclusion, these tools are suitable to study effects of ErbB4 signaling on cortical synapses downstream of NRG2 *in vitro*.

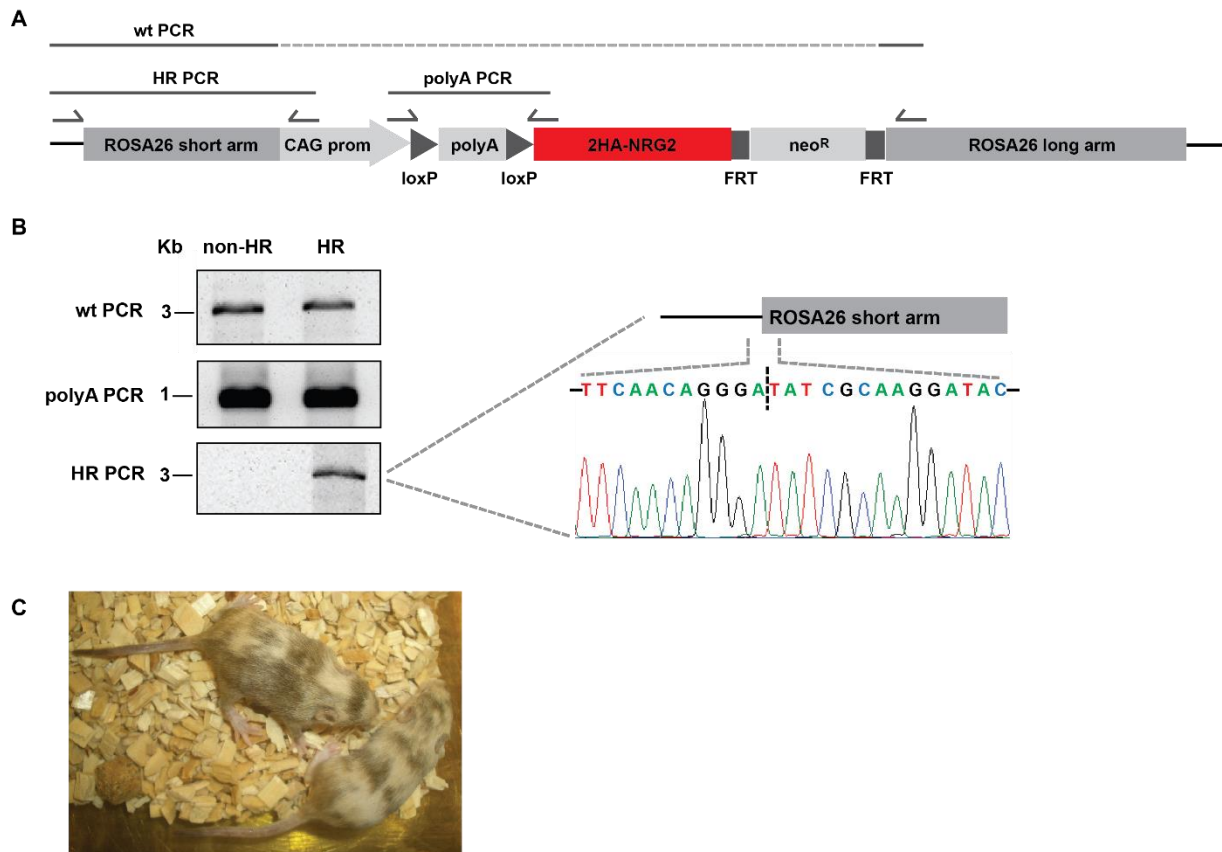


**Figure 26. Generation of a “knock in” mouse line for conditional NRG2 overexpression. (A)** Schematic representation of the targeting vector after integration into the mouse ROSA locus. Arrows indicate PCR primer positions used for the screening of ES cell clones. HR, homologous recombinant. **(B)** PCR results of the screening strategy. wt and polyA PCRs produced a product in HR and non-HR samples. HR PCR was used to amplify the ROSA locus short arm after homologous recombination. Sequencing profile obtained from one of the HR clones shows the transition from the endogenous genomic DNA to the short arm of the targeting vector. **(C)** Chimeric pups born after blastocyst injections of two HR clones.

For the *in vivo* study of NRG2 functions, a conditional NRG2 mouse line was generated. 2HA-NRG2 cDNA was subcloned in a ROSA locus targeting vector (provided by Dr. Agarwal, Johns Hopkins University) and used to electroporate ES cells (Fig. 26A). A PCR strategy was implemented for the screening and identification of homologous recombinant (HR) clones. Identified HR clones were verified by sequencing (Fig. 26B). 10-100% chimeric mice were born after injection of two HR clones into blastocysts (Fig. 26C). 60-70% chimeric males are currently being bred to C57Bl/6N females to confirm germline transmission of targeted ES cells and to establish conditional NRG2 overexpressing mouse lines.

### 3 Discussion

#### 3.1 Transgenic approaches to study brain functions

ErbB4 is the main NRG1 receptor in the brain. However, different NRG1 isoforms show distinct and dynamic expression patterns during development, indicating stage- and isoform-specific functions in the developing and adult nervous system (Carraway et al., 1997; Liu et al., 2011; Mei and Xiong, 2008; Vullhorst et al., 2015). NRG1-ErbB4 signaling has been implicated in a variety of developmental processes in the nervous system, including myelination, interneuron migration and synaptogenesis (Mei and Xiong, 2008). These processes underlay the proper formation of cortical networks, however is not known in detail how different NRG1 isoforms and other NRGs participate in these processes.

Most *Nrg1* variants associated with SZ are located in non-coding regions of the gene (Stefansson et al., 2002; Weickert et al., 2012), which suggests that altered NRG1 expression, rather than protein function *per se*, could be of relevance for this disease. Moreover, analysis of postmortem brains of SZ patients exhibited increased expression of NRG1, and particularly an increment in *Ig-Nrg1* mRNA has been reported (Hashimoto et al., 2004; Law et al., 2006). Additionally, several mouse models with elevated NRG1/ErbB4 signaling display behavioral and morphological impairments that resemble those found in SZ patients (Agarwal et al., 2014; Deakin et al., 2009, 2012; Yin et al., 2013b). This suggests that hyperstimulated NRG1/ErbB4 signaling may increase the susceptibility to develop SZ, however the underlying pathomechanisms have not been elucidated. Thus, the aim of the present study was to validate a transgenic mouse line for the conditional overexpression of Ig-NRG1 and to examine the molecular, cellular, and behavioral consequences of chronic Ig-NRG1 overexpression in glutamatergic projection neurons.

Transgenic mice were generated using a transgene cassette harboring a loxP sites-flanked STOP cassette expressing GFP under control of the  $\beta$ -actin promoter in the absence of Cre recombinase. Thus, analysis of GFP expression was used to determine the expression pattern of the transgene cassette in various organs and cell types. Comparison of GFP fluorescence with cell-type specific markers by fluorescent immunostainings revealed that in the nervous system the STOP cassette is expressed in virtually all glutamatergic projection neurons and oligodendrocytes, and in a subset of astrocytes and microglia. In addition, the cassette is expressed in spinal cord  $\alpha$ -motor neurons and Schwann cells. In contrast, only a few GABAergic interneurons express the STOP cassette. A similar expression pattern was also found in other studies (T. Unterbarscheidt; M. Rossner, personal communication), which suggests that the  $\beta$ -actin promoter is not adequate for transgene expression in interneurons. Outside the brain the transgene cassette is expressed in all organs analyzed, e.g. heart and muscle. This suggests that the mouse line is suitable for the study of Ig-NRG1 functions in



several organs besides the brain. For example, conditional Ig-NGR1 transgenic mice are currently being used to study the role of this isoform for Schwann cell pathology in Charcot-Marie-Tooth disease 1A (R. Stassart and R. Fledrich, personal communication). Outside the nervous system, this mouse line could be valuable for the study of Ig-NGR1 functions in heart development and disease (Kramer et al., 1996; Meyer and Birchmeier, 1995).

An alternative strategy for conditional transgenic approaches, including GABAergic interneurons, is the generation of “knock in” mouse lines using vectors that target the *Rosa26* locus and integrate into the genome by homologous recombination (HR), without the risk of disrupting other genes by random integration. This locus was originally characterized in a gene-trap screen in murine ES cells and drives ubiquitous expression in embryonic and adult mice (Friedrich and Soriano, 1991; Zambrowicz et al., 1997). This strategy was used for the generation of several mouse lines, including the *R26R-floxedTomato* reporter line (Madisen et al., 2010), Charcot-Marie-Tooth mouse models (Bouhy et al., 2016), as well as for the generation of the transgenic mouse line for conditional overexpression of NRG2 developed in the present study.

The Cre-loxP system from the bacteriophage P1 (Hoess et al., 1982) used in this study for the conditional overexpression of Ig-NGR1, is one of the most widely used systems to model stage- and cell- type specific ablation or overexpression of genes of interest. Here, the Cre recombinase recognizes the 34-bp nucleotide sequence of the loxP sites and catalyzes the homologous recombination and subsequent deletion of the DNA between the two loxP sites, in a process that needs no additional elements (Stark et al., 1992; Zhang et al., 2012). Furthermore, these loxP sites are not too large to interrupt the function of the genes, but also not too small to occur randomly within the genome (Zhang et al., 2012). Nowadays multiple mouse lines expressing Cre under control of different promoters are available, including driver lines for cell type- and area-specific Cre expression in the brain (Goebbels et al., 2006; Gorski et al., 2002; Hippenmeyer et al., 2005; Minichiello et al., 1999; Tronche et al., 1999). Moreover, a number of tamoxifen inducible versions of Cre driver lines are also available and permit analyses at the single-cell level (by titrating of tamoxifen dosage) or at later stages of development (Agarwal et al., 2012; Burns et al., 2007; Hirrlinger et al., 2006; Leone et al., 2003; Mori et al., 2006; Pohl et al., 2011; Traka et al., 2010; Weber et al., 2009). However, one limitation of the system is its irreversibility. In contrast, in the tetracycline-inducible system the expression of the target gene depends on the activity of the inducible tetracycline transactivator (tTA). This protein acts as a bacterial transcription factor that recognizes the bacterial *tetO* operon, and its activity is regulated reversibly by the administration of tetracycline derivatives such as doxycycline (Dox). Thus, by using a mouse line that expresses tTA under the control a cell type specific promoter and breeding to a mouse line that expresses the gene of interest attached to the tetO promoter, it is possible to reversibly induce expression of a particular gene

(Kandel, 2013; Zhang et al., 2012). However, only a relatively small number of CNS-specific tTA driver lines are available and its general suitability for brain studies has been debated.

During the early stages of this project a mouse line for conditional overexpression of Ig-NGR1 using the tTA system was published. This mouse model expresses the protein in the presence of tetracycline transactivator (tTA), but in this case the overexpression in projection neurons only starts postnatally (CamKII $\alpha$ -tTA was used as the driver line) (Yin et al., 2013b). The availability of many different Cre-driver lines, including the NEX-Cre driver line in which Cre recombinase expression starts at E12.5 (Goebbels et al., 2006), allowed us in the present study to analyze the effect of Ig-NGR1 overexpression during embryonic stages, when NRG1 has a peak of expression (Liu et al., 2011).

### 3.2 Modelling NRG1-ErbB4 hyperstimulation in transgenic mice

Ig-NGR1 is mainly expressed in projection neurons. Its expression starts during embryonic stages (E12), declines postnatally, and is low in the adult brain (Liu et al., 2011). Ig-NGR1 has been implicated in neurodevelopmental processes, such as interneuron migration (Flames et al., 2004). Thus, to model increased stimulation of Ig-NGR1 signaling during embryonic development, *STOP-Nrg1* mice were bred to the *NEX-Cre* driver line (Goebbels et al., 2006). *STOP-Nrg1*\**NEX-Cre* embryos showed overexpression of HA-Ig-NGR1 at E16 and fluorescent immunostainings confirmed that HA-Ig-NGR1 expression follows the NEX-Cre pattern of expression. Accordingly, fluorescent immunostaining of adult *STOP-Nrg1*\**NEX-Cre* brains showed cortical projection neuron restricted overexpression of HA-Ig-NGR1, in agreement with Cre-recombinase expression in the driver line (Goebbels et al., 2006). Thus, this new mouse model is suitable for the study of the consequences of chronic Ig-NGR1 overexpression starting during embryonic stages.

Ig-NGR1 is synthesized as a transmembrane precursor that subsequently undergoes proteolytic cleavage at the juxtamembrane “stalk” region by proteases, such as ADAM10, ADAM17 and BACE1, which results in shedding of the N-terminal fragment and paracrine signaling (Fleck et al., 2013; Mei and Xiong, 2008). Immunostaining of *STOP-Nrg1*\**NEX-Cre* brain revealed colocalization of the N- and the C- terminal domains of HA-Ig-NGR1 in the cortex, indicating accumulation of the full-length protein. In addition, non-overlapping signals for the N- and C-terminal domains were identified, which probably reflect proteolytic processing at the juxtamembrane region of HA-Ig-NGR1 and shedding of the N-terminal domain. This suggest that HA-Ig-NGR1 undergoes proper proteolytic processing as the endogenous protein, thus *STOP-Nrg1*\**NEX-Cre* mice are suitable to investigate subcellular localisation and proteolytic processing of Ig-NGR1 *in vivo*. Worth mentioning, backsignaling via the NRG1-ICD was described *in vitro* for CRD-NGR1 (Bao et al., 2003, 2004; Talmage, 2008; Wang et al., 1998). NRG1 isoforms are processed by  $\gamma$ -secretase and the NRG1-ICD is highly conserved

between different isoforms (Buonanno and Fischbach, 2001; Mei and Xiong, 2008). Thus, it is possible that some of the signals observed for the C-terminal domain resulted from  $\gamma$ -secretase-mediated cleavage of Ig-NGR1, but this requires further investigation.

Western blot analysis demonstrated more physiological relevant levels of Ig-NGR1 overexpression in *STOP-Nrg1\* $NEX$ -Cre* at all stages analyzed compared to conventional, Thy1.2 promoter-driven NRG1 transgenic mice (Michailov et al., 2004). Importantly, moderate overexpression of Ig-NGR1 was sufficient to induce permanent hyperstimulation of the ErbB4 receptor. Higher levels of p-ErbB4 were present already at P5 and maintained through adulthood. Interestingly, p-ErbB4 levels in *STOP-Nrg1\* $NEX$ -Cre* adult mice resemble those present in postnatal stages, when NRG1 display a peak of expression (Liu et al., 2011). This suggests that the sustained hyperstimulation of NRG1/ErbB4 signaling in *STOP-Nrg1\* $NEX$ -Cre* could mimic the activity of this pathway during postnatal stages in wildtype mice. Moreover, this observation implies that conditional overexpressors of HA-Ig-NGR1 are a suitable tool to study the consequences of NRG1/ErbB4 hyperstimulation *in vivo*.

NGR1 is a growth factor involved not only in developmental processes but also in microglia activation, inflammation, cell proliferation, and cancer. Thus, its overexpression could have pathological effects. Moreover, signaling pathways downstream of NRG1/ErbB4, such as MAPK and AKT signaling pathways are involved in cell survival, proliferation and differentiation, and have been found to be altered under pathological conditions (Fresno Vara et al., 2004; Gu et al., 2016; Pandey et al., 2016). Furthermore, *STOP-Nrg1* mice permanently express GFP in most cells of their body. GFP expression was associated with hypomyelination and axonal pathology in transgenic mice, which express GFP under control of the CNP promoter (Millet et al., 2012). Nevertheless, immunohistochemical analysis showed no change in the number of neurons or signs of astrogliosis, microgliosis, axonal swellings or T-cell infiltration in *STOP-Nrg1\* $NEX$ -Cre* mice at 16 and 52 weeks of age. In conclusion, chronic NRG1-mediated hyperactivation of ErbB4 was not associated with neuropathology in the brains of *STOP-Nrg1\* $NEX$ -Cre*. These findings differ greatly from effects of NRG1 overexpression in Schwann cells. Probably as an effect of autocrine signaling to glial ErbB2/ErbB3 receptors, such transgenic mice display Schwann cell hyperplasia and myelin abnormalities, such as onion bulb formation (Huijbregts et al., 2003; R. Stassart, personal communication).

### **3.3 Embryonic overexpression of HA-Ig-NGR1 impaired social behavior and $\gamma$ -oscillation**

To identify behavioral phenotypes associated with cortical-restricted HA-Ig-NGR1 overexpression a cohort of *STOP-Nrg1\* $NEX$ -Cre* mice and both parental controls were analyzed at 2-3 months of age. Elevated HA-Ig-NGR1 expression was not associated with

altered sensory functions or motor activity. This differs from another study of our group in which cortical-restricted overexpression of CRD-NGR1 starting also during embryonic stages (NEX-Cre) leads to hyperactivity (Unterbarnscheidt et al., *in prep*). This indicates that isoform-specific functions may modulate differently this phenotype. However, it has been shown that Ig-NGR1 overexpression in projection neurons starting postnatally is also associated with hyperactivity (Yin et al., 2013b). Furthermore, pan-neuronal Ig-NGR1 overexpression in *Thy1.2-Nrg1* mice showed initial hypoactivity at 5 months of age followed by hyperactivity at 52 weeks of age (Deakin et al., 2012), whereas mice with pan-neuronal overexpression of CRD-NGR1 under control of Thy1.2 promoter (*Thy1.2-CRD-NGR1*) display anxiety-like behavior but not hyperactivity in the open field test (Agarwal et al., 2014). These contrasting findings suggest that the modulation of motor behavior in adults is influenced differently by cortical and subcortical functions of Ig- and CRD-NGR1, as well as stage-specific patterns of overexpression. Additionally, these results indicate that different levels of Ig- or CRD-NGR1 expression, and consequently different stimulation of ErbB4, also play a role in motor behavior modulation. In fact, conditional NRG1 (CKII-Cre) (Agarwal et al., 2014) and ErbB4 (Nestin-Cre) mutants (Golub et al., 2004) displayed hypoactivity. Interestingly, serotonin and dopamine signaling in the striatum, basal ganglia, and nucleus accumbens seem to be involved in regulation of hyperlocomotion and anxiety (Bishop and Walker, 2003; Brus et al., 2004; Fadda et al., 2005; Jiang et al., 2015; Scott et al., 2006; Taepavarapruk et al., 2000), and it is conceivable that differential levels of expression of NRG1 isoforms could result in distinct regulation of these signaling pathways.

Furthermore, *STOP-Nrg1\*<sup>+</sup>NEX-Cre* mice display no PPI impairment, a measurement of sensorimotor gating relevant in the neuropathology of SZ. PPI impairment has been observed in SZ patients and mouse models for SZ-relevant proteins, such as NRG1 (Agarwal et al., 2014; Braff et al., 1992; Braff and Geyer, 1990; Deakin et al., 2009; Geyer and Braff, 1982; Swerdlow et al., 2008; Yin et al., 2013b). Pan-neuronal overexpression of CRD-NGR1 under control of the Thy1.2 promoter (*Thy1.2-CRD-NGR1*) produces PPI deficits (Agarwal et al., 2014), and this was also present in *Thy1.2-Nrg1* mice (Deakin et al., 2009). Thus, PPI impairment appears not to be NRG1 isoform-specific, also because the conditional mouse line for overexpression of Ig-Nrg1 starting postnatally mentioned above, exhibited a PPI deficit (Yin et al., 2013b). This discrepancy is most likely due to the absence of subcortical overexpression of HA-Ig-NGR1 in *STOP-Nrg1\*<sup>+</sup>NEX-Cre* mice compared to the other models. Striatal projections have been considered important for the generation of PPI (Baldan Ramsey et al., 2011), and in contrast with the other transgenic models *STOP-Nrg1\*<sup>+</sup>NEX-Cre* mice do not show elevated Ig-NGR1 expression in that region.

Interestingly, *STOP-Nrg1\*<sup>+</sup>NEX-Cre* mice displayed increased social interaction in the dyadic social interaction test. This hyper-sociability could represent a social disinhibition phenotype,

which is frequently observed in several neuropsychiatric diseases, as well as in mental retardation (Barak and Feng, 2016; Hirschtritt et al., 2016). Moreover, this phenotype was also found in heterozygous PSD95 knockout mice and homozygous PSD93 mutants, suggesting that these proteins are involved in the processing of social stimuli and the control of social behavior (Winkler et al., 2017). PSD proteins and notably PSD95 are responsible for the organization of the postsynaptic machinery required for synaptic development and plasticity. ErbB4 is enriched at postsynaptic compartments of inhibitory interneurons and interacts with PSD93 and PSD95 (Garcia et al., 2000; Neddens and Buonanno, 2010; Vullhorst et al., 2009). Furthermore, ErbB4-PSD95 interactions may participate in the modulation of glutamatergic synapses (Huang et al., 2000; Kim and Sheng, 2004; Ma et al., 2003). Thus, it is possible that elevated Ig-NGR1 expression starting during embryonic stages, and the consequent ErbB4 hyperstimulation, results in an imbalance that affects the interaction with PSD95 and its control of social stimuli. This behavioral test was not performed in the other two models for Ig-NGR1 overexpression, thus it is not possible to directly compare the effect of different levels of expression or subcortical overexpression of Ig-NGR1 on social behavior. However, in an alternative test for social behavior, postnatal overexpression of Ig-NGR1 lead to less social interaction (Yin et al., 2013b). Again, this might speak for an effect of subcortical functions of hyperstimulated Ig-NGR1/ErbB4 signaling.

The hippocampus plays an important role in social memory formation. In particular, the CA2 region has been involved in social memory. First, expression of the vasopressin 1b receptor (*Avpr1b*), which is critical for social memory and social aggression in rodents, is enriched in the CA2 region (Kohara et al., 2014; Tsien et al., 1996; Wersinger et al., 2002, 2008; Young et al., 2006). Second, restoration of *Avpr1b* expression in dorsal CA2 of *Avpr1b*-null mice was sufficient to rescue social aggression behaviors (Pagani et al., 2015). Third, genetic inactivation of CA2 pyramidal neurons results in a selective loss of social recognition memory (Hitti and Siegelbaum, 2014). More recently, it was demonstrated that CA2 neurons update their spatial representations in response to social or contextual changes in the environment, suggesting that modifications of spatial representations may be a mechanism that these neurons use to encode social and novel contextual information (Alexander et al., 2016). Furthermore, it has been suggested that modulatory influences, such as changes in synaptic strength, may permit behaviorally relevant shifts in place field maps (Savelli and Knierim, 2010). Thus, it will be important to investigate if chronically increased NRG1/ErbB4 signaling could produce synaptic changes that disrupt the mechanism of social memory formation in the CA2 region.

Cognitive processes, such as memory formation, require the synchronization of neuronal network activity in several brain regions. Oscillatory activity is generated by the coordinated interaction of excitatory and inhibitory neurons within neural networks (Bartos et al., 2007; van

Vugt et al., 2010). The frequency of network oscillations includes slow oscillations in the  $\Delta$  (0.5–3 Hz) and  $\theta$  (3–8 Hz) range, as well as fast oscillations in the  $\gamma$  (30–90 Hz) and ultrafast (90–200 Hz) ranges (Buzsáki and Draguhn, 2004).  $\gamma$ -oscillations in the human cortex and hippocampus seem to be important for higher brain functions, such as memory formation, working memory, attention and visual pattern recognition (Bosman et al., 2014). In the present study, embryonic cortical-restricted overexpression of HA-Ig-NRG1 in *STOP-Nrg1\**NEX-Cre** resulted in a reduction in the power, but not the frequency of kainate-induced  $\gamma$ -oscillations. This is in line with several findings showing that NRG1/ErbB4 signaling regulates hippocampal  $\gamma$ -oscillations (Fisahn et al., 2009). Parv<sup>+</sup> fast-spiking basket cells are essential for the generation of  $\gamma$ -oscillations both *in vitro* and *in vivo*, and a large fraction of these interneurons express ErbB4 (Bartos et al., 2007; Fisahn et al., 2009). Interestingly, impaired  $\gamma$ -oscillations and reduced numbers of Parv<sup>+</sup> interneurons in post-mortem hippocampus of SZ patients have been reported (Kwon et al., 1999; Lewis et al., 2005; Wilson et al., 2008; Wynn et al., 2005; Zhang and Reynolds, 2002), providing a possible link between altered NRG1 signaling and SZ.

Reduced power of  $\gamma$ -oscillations in *STOP-Nrg1\**NEX-Cre** mice contrasts findings in *Thy1.2-NRG1* mice, in which a reduction in the frequency, but not the power of  $\gamma$ -oscillations was observed (Deakin et al., 2012).  $\gamma$ -oscillations can be induced in acute hippocampal slices by bath application of carbachol or kainic acid, resulting in the activation of muscarinic acetylcholine or kainate receptors, respectively (Fisahn et al., 1998, 2004). The above difference could be explained by the fact that even though both carbachol- and kainate-induced  $\gamma$ -oscillations are driven by neuronal networks in the CA3 region (Fisahn et al., 1998), carbachol-induced activity depends on the recruitment of AMPA receptors, whereas kainate-induced activity does not (Bartos et al., 2007). This explanation was previously suggested in a study in which soluble NRG1 increased the power of kainate-, but not carbachol-induced  $\gamma$ -oscillations in hippocampal slices (Fisahn et al., 2009). This increment in the power of  $\gamma$ -oscillations contrasts with the reduction observed in kainate-induced  $\gamma$ -oscillations in *STOP-Nrg1\**NEX-Cre** mice. However, it must be taken into account that the treatment with soluble NRG1 simplifies and bypasses important aspects of NRG1 biology and does not reflect isoform-specific effects. In line with this, it was recently suggested that impaired neuropsin-NRG1-ErbB4 signaling leads to an alteration of slow  $\gamma$ -oscillation activity. Neuropsin serves as an extracellular protease shown to cleave mature NRG1 bound to extracellular glycosaminoglycans to remove the heparin-binding domain (Tamura et al 2012). Ablation of neuropsin in mouse mutants caused a decrease in the power of kainate-induced slow  $\gamma$ -oscillations in the CA1 region, which was restored after injection of soluble NRG1 (Kawata et al 2017). These findings imply that changes in NRG1/ErbB4 signaling alter  $\gamma$ -oscillations. The

reduction of the power of  $\gamma$ -oscillations in *STOP-Nrg1\*<sup>NEX</sup>-Cre* mice suggests that HA-Ig-NGR1 overexpression leads to an E/I imbalance, however, this has not been studied in detail. As Parv<sup>+</sup> interneurons play a central role in the generation of  $\gamma$ -oscillations, the consequences of chronic HA-Ig-NGR1 overexpression on the number of Parv<sup>+</sup> interneurons was examined in *STOP-Nrg1\*<sup>NEX</sup>-Cre* mice. Despite the postulated involvement of NRG1/ErbB4 signaling in interneuron migration, no changes in the number of Parv<sup>+</sup> interneurons were found in the hippocampus and cortex of *STOP-Nrg1\*<sup>NEX</sup>-Cre* mice at 16 and 52 weeks of age. However, it cannot be ruled out that further increased levels of HA-Ig-NGR1 in homozygous *STOP-Nrg1\*<sup>NEX</sup>-Cre* mice used in the analysis of  $\gamma$ -oscillations may impact on Parv<sup>+</sup> interneuron functions. Thus, further analyses using homozygous *STOP-Nrg1\*<sup>NEX</sup>-Cre* mice (including earlier developmental stages) are necessary to address this possibility. Furthermore, the absence of changes in interneuron numbers does not preclude a potential impairment in the functional status of these interneurons.

Taken together, these findings demonstrated that a cortical-restricted increase in Ig-NGR1/ErbB4 signaling starting from embryonic stages leads to impaired hippocampal functions, specifically  $\gamma$ -oscillations in the CA3 region and increased social interaction, which seems to be modulated at the CA2 region. Thus, as the CA3 is the primary input of CA2, synaptic alterations in this area could disrupt the connectivity of CA2. In fact, it was demonstrated that  $\gamma$ -oscillations can dynamically coordinate hippocampal networks according to behavioral demands (Montgomery and Buzsáki, 2007). In support of this, it was shown that the  $\gamma$ -oscillation impairment in *Thy1.2 Nrg1* mice is accompanied by an age-dependent working memory deficit (Deakin et al., 2009, 2012), which was also observed after postnatal overexpression of Ig-NGR1 (Yin et al., 2013b). These results and the evidence that the hippocampus is essential for social behavior and spatial short-term memory (Alexander et al., 2016; Deacon et al., 2002; Sanderson et al., 2007), suggest that Ig-NGR1 has a role in hippocampal-dependent cognitive functions.

### **3.4 Elevated Ig-NGR1/ErbB4 signaling preferentially recruits the AKT pathway**

Biochemical analyses demonstrated that *Thy1.2 Nrg1* mice (included as a reference in the present study) displayed an almost 6-fold overexpression of Ig-NGR1 and 5-fold higher ErbB4 hyperphosphorylation compared to *STOP-Nrg1\*<sup>NEX</sup>-Cre* mice. These findings suggest that ErbB4 is not a rate limiting factor for Ig-NGR1 signaling in the brain, consistent with analyses of heterozygous NRG1 and ErbB2/ErbB3 mutants in the PNS, which show that partial elimination of NRG1, but not of ErbB2/ErbB3 receptors, causes hypomyelination (Michailov et al., 2004). On the other hand, ErbB4 activity can be downregulated by dephosphorylation mediated by receptor tyrosine phosphatase  $\beta$  (RPTP $\beta$ ) or tyrosine-protein phosphatase non-receptor type 21 (PTPN21) (Buxbaum et al., 2008; Plani-Lam et al., 2015). Ligand-induced

proteolytic cleavage and ectodomain shedding by TACE has also been proposed as a mechanism for ErbB4 downregulation. Subsequently, levels of the resulting intracellular fragment, which contains the tyrosine kinase activity, are controlled by proteasome function (Rio et al., 2000; Vecchi et al., 1996; Vecchi and Carpenter, 1997; Zhou and Carpenter, 2000). However, since Ig-NGR1 transgenic mice display permanently increased steady-state levels of hyperphosphorylated ErbB4, these mechanisms for downregulation appear not to compensate for Ig-NGR1-mediated hyperactivation. Furthermore, growth factor receptors are internalized upon ligand binding to modulate receptor signaling, in addition to target activated receptors to other intracellular substrates. Nevertheless, ligand-dependent receptor internalization is notably low for ErbB receptors (except ErbB1) (Baulida et al., 1996). Moreover, hippocampal interneurons predominantly express the TACE-mediated cleavage-resistant JMb ErbB4 receptor isoforms, and thus, maintain a high level of ErbB4 at the cell surface (Longart et al., 2007), which can also explain the persistently higher levels of Ig-NGR1-mediated ErbB4 phosphorylation.

In an attempt to analyze the impact of Ig-NGR1-mediated ErbB4 hyperstimulation on two major signaling pathways downstream of NRG1/ErbB4 signaling, biochemical analyses of MAPK and AKT pathways were performed. The MAPK signaling pathway regulates astrocyte proliferation, neuronal survival, synaptic plasticity, dendritic spine morphology, and cognitive processes such as learning and memory (Thomas and Huganir, 2004; Thongrong et al., 2016; Wu et al., 2001). Interestingly, ErbB4 hyperphosphorylation was identified using an antibody directed against Tyr1284, which is the binding site for the SHC1 adapter protein, involved in MAPK signaling (Schulze et al., 2005). Nevertheless, only pan-neuronal massive overexpression of Ig-NGR1 was sufficient to significantly increase levels of phosphorylated MAPK. In *STOP-Nrg1*\**NEX-Cre* mice, although there was a tendency towards increased activation of MAPK, this was not significant, which implies that feedback mechanisms seem to effectively downregulated activation of this signaling pathway.

On the other hand, the level of phosphorylated AKT, a protein acting directly downstream of PI3K, was significantly increased in both conventional and conditional transgenic mice. The PI3K/AKT signaling pathway mediates several processes necessary for the proper function of cortical networks, such as interneuron migration, primary neurite formation and dendritic arborization (Junttila et al., 2000b; Kainulainen et al., 2000; Krivosheya et al., 2008; Polleux et al., 2002). Furthermore, the PI3K/AKT pathway has been implicated in several neurodevelopmental diseases, such as SZ (Emamian, 2012; Emamian et al., 2004; Law et al., 2012; Wang et al., 2017), and an increase of phosphorylated AKT levels in the PFC of schizophrenic patients was recently reported (Hino et al., 2016). Additionally, a genetic association study reported epistasis between SNPs in *Nrg1*, *ErbB4* and *AKT1* that may increase genetic liability for schizophrenia (Nicodemus et al., 2010).



PI3K/AKT signaling is activated by the CYT1 isoform of ErbB4 that binds the PI3K regulatory subunit p85 through its phosphorylated Tyr1056. This interaction leads to the activation of the catalytic subunit of PI3K and subsequent conversion of phosphatidylinositol-4,5-bisphosphate (PI-4,5-P2) to the second messenger phosphatidylinositol-3,4,5-trisphosphate (PI-3,4,5-P3) at the inner plasma membrane. Interaction with these phospholipids recruits AKT to the inner membrane, where it is phosphorylated at Tyr308 and Ser473 by 3'-phosphoinositide-dependent kinases (PDK) 1 and 2, respectively, and subsequently regulates downstream proteins, such as GSK3, Mdm2, and mTOR (Elenius et al., 1999; Fresno Vara et al., 2004; Schulze et al., 2005). Thus, Tyr1056 in ErbB4 CYT1 together with Tyr308 and Ser473 in AKT are key residues involved in the activation of the AKT signaling pathway, whose higher levels may indicate increase stimulation of this pathway. The antibody used to analyze the levels of phosphorylated AKT was directed against Ser473, and full activation of AKT requires phosphorylation of this residue (Wang et al., 2017). However, as mentioned above, ErbB4 hypersphosphorylation was detected at Tyr1284, not at Tyr 1056. Thus, the extent by which Ig-NGR1-mediated ErbB4 activation can stimulate PI3K/AKT pathway is currently unknown, which also prevents an exact molecular explanation for the similar levels of phosphorylated AKT in conditional and conventional Ig-NGR1 transgenic mice, despite distinct levels of phosphorylated ErbB4. Further biochemical analyses of proteins upstream and downstream AKT, eg. PI3K and GSK3, are required to validate the preferential recruitment of this signaling pathway.

To further address a selective recruitment of the AKT pathway under conditions of adult Ig-NGR1 overexpression, *STOP-Nrg1* mice were also bred to a tamoxifen inducible version of the Cre driver line (*NEX-CreERT2*) (Agarwal et al., 2012). Hippocampi were collected four weeks after the last tamoxifen injection. This approach resulted in reduced levels of overexpression (by approximately 40-50%) compared to *STOP-Nrg1\**NEX-Cre** mice, which could be due, at least in part, to absence of Cre recombinase activity in dentate gyrus granule cells of adult mice (Agarwal et al., 2012; Goebbels et al., 2006). No changes in the levels of phosphorylated MAPK were found in this experimental paradigm, consistent with the idea that only massive overexpression of Ig-NGR1 in *Thy1.2 Nrg1* mice is sufficient to stimulate this pathway. In contrast, although at moderate levels, a significant increase of phosphorylated AKT in *STOP-Nrg1\**NEX-CreERT2** mice was present, consistent with a preferential recruitment of the AKT signaling pathway by Ig-NGR1 overexpression. These findings contrast with similar experiments in which CRD-NGR1 overexpression was induced in adult mice. Here, adult activation of CRD-NGR1 expression led to a preferential stimulation of the MAPK signaling pathway (T. Unterbarnscheidt, personal communication). These results suggest isoform-specific, preferential recruitment of AKT versus MAPK signaling pathways. However, as for mice with pan-neuronal overexpression of Ig-NGR1, transgenic mice with strong

expression of a CRD-NRG1 variant that mimics BACE1 processing at the juxtamembrane “stalk” region, stimulate both signaling pathways (T. Unterbarnscheidt, personal communication). Thus, expression levels of Ig- and CRD-NRG1 above a certain threshold permit hyperstimulation of both signaling pathways, and this contrasts with more physiological relevant overexpression in conditional transgenic mice.

Remarkably, compound heterozygous mutants for AKT and NRG1 showed impaired episodic-like memory and impaired sociability (Huang et al., 2015). In line with this finding, hyperactivation of GSK3 $\beta$  (normally inactivated by AKT) in the brain of mice leads to impaired social interaction that could be ameliorated by chronic lithium (GSK3 inhibitor) treatment (Mines et al., 2010). This suggests that impaired inhibition of GSK3 $\beta$  by AKT may affect social behavior. Furthermore, AKT and GSK3 $\beta$  play a critical role in ethanol-induced suppression of kainate-induced  $\gamma$ -oscillations in CA3 (Wang et al., 2017), consistent with the idea that activation of this signaling pathway by elevated NRG1/ErbB4 signaling may be involved in impaired  $\gamma$ -oscillation and subsequent hippocampal-dependent social cognitive deficits.

### **3.5 Ig-NRG1 accumulates in the somatodendritic, not the presynaptic compartment of neurons**

To provide a framework for mechanistic insights into Ig-NRG1-mediated effects on social behavior and hippocampal  $\gamma$ -oscillations, the subcellular localization of this protein was examined in conventional and conditional transgenic mice. Unexpectedly, an enrichment in the somatodendritic compartment of projection neurons was observed, with a punctate pattern of expression. Ig-NRG1 did not colocalize with the presynaptic markers synaptophysin and VGlut1 in both mouse lines. Ig-NRG1 also displayed no close localization to the serotonergic presynaptic marker SERT and excitatory (PSD95) and inhibitory (gephyrin) postsynaptic markers. Furthermore, different expression levels of Ig-NRG1 in *STOP-Nrg1*\*NEX-Cre and *Thy1.2 Nrg1* mice had no effect on subcellular localization. These findings contrast with the general concept according to which NRG1 at presynaptic terminals of projection neurons signals to ErbB4 in the postsynaptic compartment of Parv<sup>+</sup> interneurons.

Importantly, fluorescent immunostainings revealed that Ig-NRG1 partially colocalizes with Kv2.1, a voltage-gated potassium channel that forms large clusters in the plasma membrane in several neuronal cell types, frequently proximal to SSCs (Antonucci et al., 2001; Du et al., 1998). These SSCs are flat membrane-limited vesicles which represent an extension of the endoplasmic reticulum located immediately adjacent to the plasma membrane (Deardorff et al., 2014).

Kv2.1 is highly expressed in virtually all brain regions suggesting a fundamental role in neurons (Misonou et al., 2005). Moreover, it was demonstrated that the phosphorylation state of Kv2.1 rapidly changes in response to increased neuronal excitatory activity in hippocampal pyramidal

neurons, leading to dispersion of Kv2.1 clusters. These effects are mediated by NMDAR activation, followed by Ca<sup>2+</sup>-influx, release of Ca<sup>2+</sup> from intracellular stores, and activation of the Ca<sup>2+</sup>/calmodulin-dependent protein phosphatase 2B/calcineurin, which dephosphorylates Kv2.1 channels. Kv2.1 dispersion is associated with reduced AP firing, suggesting that Kv2.1 plays a role in the modulation of neuronal excitability (Misonou et al., 2004, 2005).

Similar to Ig-NGR1, NRG2 was found to be located in close proximity to Kv2.1 at the plasma membrane of hippocampal interneurons, adjacent to SSCs. It was proposed that inactive transmembrane NRG2 (pro-NGR2) clusters in this region, and that NMDAR activity is required to convert pro-NGR2 to an active ErbB4 receptor ligand. NRG2 promotes the physical association of ErbB4 with GluN2B-containing NMDARs, which causes NMDAR removal from the cell surface and downregulation of NMDAR currents in interneurons (Vullhorst et al., 2015). Additionally, NRG2 was found to be released from its cluster close to SSCs in response to NMDAR activation (Vullhorst et al., 2015). SSCs are believed to be involved in Ca<sup>2+</sup>-dependent Ca<sup>2+</sup> release, due to the presence of the Ca<sup>2+</sup>-release channels inositol trisphosphate receptor (InsP3R) and ryanodine receptors (RyR), as well as a similar ultrastructure compared to triads in skeletal muscle (Henkart et al., 1976; Mandikian et al., 2014). Furthermore, it was suggested that SSCs and the associated plasma membrane act as a signaling microdomain (Vullhorst et al., 2015). Similar to NRG2, Ig-NGR1 could be located in the plasma membrane adjacent to SSCs. Glutamate-induced Ca<sup>2+</sup> release from SSCs then may promote its shedding from clusters, which further leads to proteolytic cleavage of the Ig-NGR1 ectodomain and activation of ErbB4 receptors. Extracellular matrix-bound proteases such as ADAM10 and ADAM17 may be responsible for this processing (Hartmann et al., 2013). In line with this, it was demonstrated that the concentration of the Ig-NGR1 ectodomain increases in response to NMDAR-mediated Ca<sup>2+</sup> transients in rat primary hippocampal neurons (Schillo et al., 2005). Additionally, previous studies demonstrate that NRG1 induces the expression of the NMDA receptor NR2C subunit and that this action requires previous activation of NMDA receptors (Ozaki et al., 1997). Taken together, these observations suggest that, similar to NRG2 in interneurons, pro-Ig-NGR1 in projection neurons is converted to mature Ig-NGR1 in response to NMDAR mediated Ca<sup>2+</sup> transients, which provoke ectodomain shedding and paracrine signaling, possibly involved in the regulation of neuronal excitability. Another, not mutually exclusive, scenario could be that Ig-NGR1 in projection neurons is directly associated with SSCs. NRG1 locates to SSCs in the postsynaptic compartment of cholinergic C-type synapses of spinal cord  $\alpha$ -motoneurons. Moreover, NRG1-containing vesicles were observed in the synaptic cleft, suggesting post- to presynaptic trafficking of NRG1 and signaling to postsynaptic ErbB4 receptors at cholinergic synapses (Gallart-Palau et al., 2014). Additional immunostainings for SSC markers, e.g.  $\sigma$ -1 receptor (Mavlyutov et al., 2010), will be performed to address if Ig-NGR1 is located adjacent to or in SSCs.

### 3.6 A role for autocrine NRG1 signaling in Parv<sup>+</sup> interneurons?

This PhD work and previous studies (Agarwal et al., 2014) demonstrate that projection neuron-specific loss or (moderate) overexpression of NRG1 are not associated with severe CNS dysfunctions, suggesting that altered paracrine or juxtacrine NRG1 signaling originating in these cells is well tolerated by the brain. However, there is evidence that NRG1 overexpression in Schwann cells profoundly stimulates their proliferation, in contrast to axonal NRG1 (R. Stassart and R. Fledrich personal communication), suggesting an important role of NRG1 in autocrine signaling, at least in the PNS. Although NRG1 is enriched in glutamatergic projection neurons, it is also expressed in GABAergic interneurons and astrocytes (Liu et al., 2011), but its function in these cells is largely unknown. As the conditional transgene cassette used in the present and related studies is not expressed in GABAergic interneurons (T. Unterbarscheidt; M. Rossner, personal communication) NRG1-mediated autocrine signaling in ErbB4<sup>+</sup> interneurons currently cannot be addressed by a gain-of-function approach. Thus, a pilot study following a loss-of-function approach was performed, in which conditional NRG1 mutants (*Nrg1 f/f*) (Li et al., 2002) were bred to *Parv-Cre* driver mice (Hippenmeyer et al., 2005). The recombination pattern of the *Parv-Cre* driver line, as revealed by tdTomato reporter fluorescence, was congruent with the distribution of Parv<sup>+</sup> neurons in the brain, suggesting that NRG1 was eliminated from this population of cells in *Nrg1 f/f\*Parv-Cre* mice, which represents ~50% of all GABAergic interneurons (Wonders and Anderson, 2006).

*Nrg1 f/f\*Parv-Cre* mice displayed a shivering phenotype already at 3 weeks of age, and a significant reduction in their body weight at 5 weeks of age, possibly as a result of increased motor activity. Both phenotypic outcomes persisted throughout adulthood. At this initial stage of the study it cannot be ruled out that altered motor function is in part due to elimination of NRG1 from a subset of cells in dorsal root ganglion (DRG) where the *Parv-Cre* driver line is also expressed (Hippenmeyer et al., 2005). A preliminary histological study revealed that conditional ablation of NRG1 in Parv<sup>+</sup> interneurons was associated with a ~50% reduction in the number of Parv<sup>+</sup> interneurons in cortical layers II-III. In contrast, the number of calbindin<sup>+</sup> (ErbB4<sup>+</sup>) interneurons was not altered in *Nrg1 f/f\*Parv-Cre* mutants, suggesting a specific loss of Parv<sup>+</sup> cells that results from elimination of autocrine NRG1 signaling. Additional studies are required to distinguish between cell loss and loss of Parv expression. Several studies have demonstrated effects of environmental factors on Parv expression in the hippocampus, e. g. chronic social isolation (Filipović et al., 2013) and repeated restrained stress (Czeh et al., 2005; Hu et al., 2010). Thus, *Nrg1 f/f\*Parv-Cre* mice may display reduced Parv expression as an indirect consequence of other behavioral dysfunctions. Furthermore, Parv<sup>+</sup> cells have a large energy demand due to their high-frequency AP firing rate. Thus, reduced Parv expression could indicate cellular stress as a result of impaired energy supply. Recently, it was shown that 50% of all myelinated axons in cortical layers II/III derive from Parv<sup>+</sup> interneurons (Micheva et

al., 2016). Their observed “patchy” myelination may not primarily support fast AP conduction, but could be involved in metabolic support of Parv<sup>+</sup> cells. Considering the well established myelination functions of NRG1 (Brinkmann et al., 2008; Michailov et al., 2004), one could speculate about a possible link between autocrine NRG1 signaling, myelination, and metabolic support of neocortical Parv<sup>+</sup> interneurons.

Fast-spiking Parv<sup>+</sup> interneurons have an important role in orchestrating cortical oscillations, maintain the E/I balance, and mediate a variety of cognitive behaviors (Isaacson and Scanziani, 2011; Marín, 2012; Uhlhaas and Singer, 2010). Parv<sup>+</sup> interneurons represent ~30% of interneurons in cortical layers I-III (Petersen and Crochet, 2013) and can be divided into basket cells that target the soma and proximal dendrites of pyramidal neurons (Freund and Katona, 2007; Isaacson and Scanziani, 2011) and axoaxonic or chandelier cells, which innervate the axon initial segment of pyramidal neurons (Somogyi, 1977; Taniguchi et al., 2013). Furthermore, Parv<sup>+</sup> interneurons in cortical layers II-III contribute to associative learning and sensory perception (Allen et al., 2003; Finnerty et al., 1999; Fox, 1992; Petersen and Crochet, 2013; Shepherd et al., 2003). Recently, it was shown that Parv<sup>+</sup> interneurons are involved in inhibitory circuits in the prefrontal cortex that regulate fear behavior. Inhibition of the activity of these interneurons disinhibits prefrontal projection neurons and synchronizes their firing by resetting local  $\theta$ -oscillations, which leads to fear expression (Courtin et al., 2014). To determine if disrupted NRG1 signaling in *Nrg1 f/f\*Parv-Cre* mice affects fear-modulating circuits in the prefrontal cortex, electrophysiological studies are currently being performed (in collaboration with W. Zhang, University of Münster). Preliminary data indicate reduced inhibitory activity and enhanced excitatory synaptic transmission in the PFC of *Nrg1 f/f\*Parv-Cre* mice (W. Zhang, personal communication). Thus, ablation of NRG1 in Parv<sup>+</sup> interneurons may cause defects in fear-regulating circuits in the PFC. Further analyses are necessary to address this question, including immunostaining for Parv (and other inhibitory markers) in PFC, as well as behavioral studies.

### **3.7 Generation of *in vivo* and *in vitro* tools to study NRG2 signaling in cortical synapses**

To study brain functions of NRG2, a closely related NRG family member, several tools to investigate NRG2 functions *in vitro* and *in vivo* have been generated and validated as part of a side project of this PhD thesis. Treatment of primary hippocampal neurons with the recombinant EGF domain of NRG2 demonstrated activation of ErbB4 receptors. In a second approach, transfection of N1E neuroblastoma cells with a NRG2 expression construct showed that the 2HA-NRG2 cassette (used later for the generation of a “knock in” mouse line) was expressed in these cells, and that it induces phosphorylation of co-expressed ErbB4. Thus, these tools are suitable to study NRG2-mediated ErbB4 activation and downstream signaling

pathways in cultured cells. Based on this validation, a new mouse line for conditional overexpression of NRG2 was generated by homologous recombination into the *Rosa26* locus of embryonic stem cells. This locus is not prone to gene silencing effects and has been successfully used for the generation of transgenic mice in which ubiquitous transgene expression has been described in the brain (Bouhy et al., 2016; Friedrich and Soriano, 1991; Irion et al., 2007; Mar et al., 2012; Otsu et al., 2015; Tsika et al., 2014; Zambrowicz et al., 1997). Importantly, the *Rosa26* locus targeting vector used for the generation of this mouse line was found to be expressed in interneurons (A. Agarwal, personal communication). Once fully established, this mouse line (currently at the stage of F0 chimeras) will permit to study NRG2 autocrine signaling in ErbB4<sup>+</sup> interneurons (Vullhorst et al., 2015).

In summary, NRG1 mediates complex signaling processes and NRG1 isoform-specific studies are a prerequisite to elucidate the role of these proteins in the developing and adult brain. Thus, conditional Ig-NRG1 transgenic mice represent a valuable tool to investigate stage- and cell type-specific functions of the Ig-NRG1 during normal and disease conditions.

The results of this study show that cortical restricted overexpression of Ig-NRG1 in glutamatergic projection neurons causes a reduction in the power of  $\gamma$ -oscillations in the hippocampal CA3 region, suggesting an imbalance of E/I neurotransmission. Altered social behavior observed in these mice could be a consequence of impaired coordination of hippocampal networks. Moreover, overexpression of Ig-NRG1 preferentially stimulates the AKT signaling pathway, which could represent an underlying molecular pathomechanism for impaired hippocampal  $\gamma$ -oscillation and altered social behavior. The subcellular localization of Ig-NRG1 in the somatodendritic compartment contrasts with the general concept of NRG1-ErbB4 signaling and suggests that Ig-NRG1 accumulates within or proximal to ER-derived Ca<sup>2+</sup> microdomains. Further studies are necessary to better understand Ig-NRG1-mediated signaling processes in cortical networks.

Finally, a pilot study showed that the selective elimination of NRG1 signaling from Parv<sup>+</sup> interneurons is associated with more severe phenotypic consequences compared to the loss or (moderate) overexpression of NRG1 in projection neurons, suggesting an important function of autocrine NRG1 signaling in inhibitory circuits. Further studies will help to elucidate the role of Parv<sup>+</sup> interneuron-derived NRG1 for inhibitory network functions with relevance for SZ and other neuropsychiatric disorders.

## 4 Materials

### 4.1 Kits and chemicals

All chemicals were purchased from Sigma-Aldrich and Merck unless stated otherwise. All molecular biology and DNA purification kits were purchased from Qiagen, Invitex, BIORAD, Applied Biosystems, Promega, Stratagene, Sigma-Aldrich, Macherey-Nagel, and Nexttec™. General laboratory materials were purchased from Gilson, Sarstedt, Molecular Bio Products, Greiner Bio-One, Falcon, and Eppendorf.

### 4.2 Websites referred for online protocols

Neuroscience	<a href="http://mrw.interscience.wiley.com/emrw/9780471142300/home/">http://mrw.interscience.wiley.com/emrw/9780471142300/home/</a>
Molecular biology	<a href="http://mrw.interscience.wiley.com/emrw/9780471142720/home/">http://mrw.interscience.wiley.com/emrw/9780471142720/home/</a>
Protein	<a href="http://mrw.interscience.wiley.com/emrw/9780471140863/home/">http://mrw.interscience.wiley.com/emrw/9780471140863/home/</a>

### 4.3 Equipment

#### Lab water systems

Sartorius Arium 611

#### Pipettes

Hirschmann Laborgeräte pipetus-akku

Gilson Pipetman (2 µl, 10 µl, 20 µl, 100 µl, 200µl, 1000 µl)

#### Deep-freeze storage

New Brunswick Scientific Co. UltraLow Temperature Freezer U725

#### DNA preparation and analysis

Advanced Biotechnologies Ltd. CombiThermosealer

Biometra Thermocycler T3

Biometra TGradient 96-well

Eppendorf Centrifuge 5415 R

Eppendorf Thermomixer T3

Heraeus Biofuge Pico

INTAS UV-system with camera and printer

Memmert water bath

ÖTTI water bath

New Brunswick Scientific Innova 4000 Incubator Shaker

Heidolph Titramax 1000 T-shaker with Incubator 1000  
Sartorius Extend fine balance  
Industries Inc. G-560E Vortex Genie-2  
Sharp R-202 microwave  
Qiagen Sigma 4K15C centrifuge

### **Protein biochemistry**

Bertin Technologies Precellys 24 Lysis & Homogenization with Peqlab Tubes  
BIORAD PowerPac 300 Power supply  
BIORAD Mini Protean 3 electrophoresis chamber  
BIORAD Mini Trans-Blot® cell  
Hecht Assistant 348 RM5 Rotating mixer  
IKA KS 260 basic shaker  
Intas ChemoCam Imager ECL HR-16-3200  
New Brunswick Scientific Co. TC-7 Tissue culture roller  
Pharmacia LKB-EPS 500/400 Power supply  
ThermoMax Molecular Devices Microplate Reader

### **Perfusion of mice**

Heidolph Pump Drive PD 5101 Peristaltic Pump  
In-house made preparation platform with drainage  
ÖTTI water bath  
Pharmacia Fine Chemicals Peristaltic Pump P-1

### **Histology**

Daewoo microwave  
Inolab wtw Series pH720 pH-meter  
Leica Jung Cryocut CM3000  
Leica Microtome VT1000S vibratome  
Microm AP280-1/-2/-3 paraffin embedding center  
Microm HM400 sliding microtome  
Microm HMP110 embedding station  
PFM water bath 1000  
Polyscience Inc. tissue cassettes IV



### **Microscope and binoculars**

Leica Confocal AOBS SP2 inverted CLSM

Leica MZ16F fluorescent stereomicroscope

Zeiss Imager.Z1 with Power Supply 231, XBO 75W HBO 100W lamp, AxioCam MRc camera and Zeiss Zen 2012 (blue edition) software

Zeiss Observer.Z1 AX10, HXP120 UV-lamp, Power Supply 23, SMC 2009 stage control, ApoTome.2, AxioCam MRm camera and Zeiss Zen 2012 (blue edition) software

### **Softwares**

Adobe Illustrator CC version 17

Adobe Photoshop CC version 14

BioEdit Sequence Alignment Editor version 7.2.5

ImageJ, version 1.47v

GraphPad Prism 5 for Windows version 5.04

Microsoft Excel 2016 version 1611

Microsoft Word 2016 version 1611

SnapGene version 1.1.3

### **4.4 Molecular biology buffers and solutions**

DNA extraction buffer

0.5 % SDS

0.1 M NaCl

0.05 M Tris, pH 8.0

3 mM EDTA

Proteinase K

Stock 10 mg/ml in ddH<sub>2</sub>O

50x Tris acetate EDTA (TAE) buffer

2 M Tris acetate, pH 8

50 mM EDTA

57.1 ml glacial acetic acid

Adjust to the 1000 ml volume with ddH<sub>2</sub>O

1x Tris-EDTA (TE) buffer

10 mM Tris-HCl, pH 8

1 mM EDTA

10 mM dNTP (50x stock)

2 mM each nucleotide (dATP, dCTP, dGTP, dTTP) (Boehringer)

200  $\mu$ M final concentration in a PCR reaction (50  $\mu$ M each nucleotide)

#### 4.5 Protein biochemistry

Phosphatase inhibitors

1 tablet PhosStop phosphatase inhibitor cocktail (Roche)

Added freshly to 10 ml of protein lysis buffer before use.

Protease inhibitors

1 tablet Complete Mini protease inhibitor (Roche)

Added freshly to 10 ml of protein lysis buffer before use.

Sucrose homogenization buffer (protein lysis buffer)

0.32 M Sucrose

0.01 M Tris-HCl, pH 7.4

0.01 M NaHCO<sub>3</sub>

0.01 M MgCl<sub>2</sub>

Phosphatase and protease inhibitors were added freshly to the buffer before use.

##### 4.5.1 SDS-PAGE and Western blotting

4x LDS sample buffer (NuPAGE)

4 ml 100 % Glycerol (f.c. 40 %)

0.682 g Tris base (f.c. 564 mM)

0.666 g Tris-HCl (f.c. 424 mM)

0.8 g LDS (Lithium dodecyl sulfate)

250  $\mu$ l 1 % Phenol red solution (f.c. 2.5 % (v/v))

750  $\mu$ l 1 % Serva Blue G250 solution (f.c. 7.5 % (v/v))

0.006 g EDTA (f.c. 2 mM)

Filled up to 10 ml with ddH<sub>2</sub>O. 1x buffer had a pH of 8.5. No pH adjustment necessary. For a working solution, 20  $\mu$ l of 1 M DTT were added to 50 ml 4x LDS sample buffer.

## 1 M Dithiothreitol (DTT)

1.5425 g DTT

Filled up to 10 ml with ddH<sub>2</sub>O.

## 4x Tris-HCl (Separation gel buffer)

1.5 M Tris-HCl pH 8.8

## 4x Tris-HCl (Stacking gel buffer)

1.0 M Tris-HCl pH 6.8

## 8 % Polyacrylamide separating gel (2 gels of 1.5 mm thickness)

9.3 ml ddH<sub>2</sub>O

5.3 ml 30 % Acrylamide/bis-acrylamide (29:1)

5 ml 1.5 M Tris-HCl pH 8.8

200 µl 10 % SDS (sodium dodecyl sulfate)

200 µl 10 % APS

12 µl TEMED

## Polyacrylamide stacking gel (2 gels of 1.5 mm thickness)

5.5 ml ddH<sub>2</sub>O

1.3 ml 30 % Acrylamide/bis-acrylamide (29:1)

1 ml 1 M Tris-HCl pH 6.8

80 µl 10 % SDS

80 µl 10 % APS

8 µl TEMED

## 5x Trisglycine electrophoresis buffer

125 mM Tris base

1.25 M Glycine

0.5 % SDS

pH ~ 6.8 no adjustment necessary

## 1x Trisglycine electrophoresis buffer

200 ml 5x Trisglycine electrophoresis buffer

800 ml ddH<sub>2</sub>O

---

10x Tris-glycine transfer buffer

250 mM Tris base  
1.9 M Glycine

1x Tris-glycine Transfer buffer

25 mM Tris base  
192 mM Glycine  
20 % Methanol

20x Tris buffered saline (TBS)

1 M Tris base  
3 M NaCl  
pH adjusted to 7.4 with 37 % HCl.

1x TBS with Tween-20 (TBST)

150 mM NaCl  
0.05 % Tween-20  
50 mM Tris-HCl pH 7.5

Blocking Buffer

5 % Non-fat dry milk-powder in 1x TBST  
Not stored longer than one week at 4 °C.

Western blot stripping buffer

0.2 M Glycine-HCl, pH 2.5  
0.1 % Tween-20

Alternatively, 0.5 M NaOH solution was used to strip membranes.

Enhanced Chemiluminescence (ECL) Western-blot detection kit

Western Lightning™ Plus-ECL, Enhanced luminol reagent plus (Perkin Elmer Life Sciences, Inc.).

Roche PVDF Western Blotting Membrane pore size 0.2 µm

#### 4.6 DNA and protein markers

DNA-marker Lambda/HindIII	Promega
GeneRuler 1 kb DNA ladder	Fermentas
GeneRuler 100 bp DNA ladder	Fermentas
Precision Plus prestained protein standard	BioRad

#### 4.7 Immunohistochemistry buffers

##### Avertin (Anesthetic)

1 g	Tribromoethanol (2,2,2-Tribromethanol, 99 %)
0.81 ml	Amyl alcohol
71.49 ml	ddH <sub>2</sub> O

ddH<sub>2</sub>O was heated up to 40 °C and added to the tribromoethanol and amylalcohol and stirred for 10 min. The solution was sterile-filtered, aliquoted and frozen at -20 °C (protected from light). Mice were intraperitoneal (IP) injected with 0.2 ml per 10 g of body weight.

##### Phosphate buffer (Stock Solutions)

0.2 M	Sodium dihydrogen phosphate (NaH <sub>2</sub> PO <sub>4</sub> )
0.2 M	Di-Sodium hydrogen phosphate (Na <sub>2</sub> HPO <sub>4</sub> )
Working Solution (pH 7.4)	
20 ml	0.2 M NaH <sub>2</sub> PO <sub>4</sub>
80 ml	0.2 M Na <sub>2</sub> HPO <sub>4</sub>
100 ml	ddH <sub>2</sub> O

##### 10x Phosphate buffered saline (PBS)

1.7 M	NaCl
34 mM	KCl
40 mM	Na <sub>2</sub> HPO <sub>4</sub> *2H <sub>2</sub> O
18 mM	K <sub>2</sub> HPO <sub>4</sub>

pH adjusted to 7.2 with 1 N NaOH.

##### 1x PBS (Working solution)

100 ml	10x PBS
900 ml	ddH <sub>2</sub> O

---

**Bovine Serum Albumin (PBS/BSA)**

20 ml	0.2 M NaH <sub>2</sub> PO <sub>4</sub>
80 ml	0.2 M Na <sub>2</sub> HPO <sub>4</sub>
1.8 g	NaCl
1 g	Bovine Serum Albumin (BSA)
100 ml	ddH <sub>2</sub> O

**16 % Paraformaldehyde (PFA)**

80 g	Paraformaldehyde
450 ml	ddH <sub>2</sub> O

Heated up to 65 °C while stirring and then stirred for another 20 min. Droplets of 5 M NaOH added until the solution turned clear. Filled up to a final volume of 500 ml with ddH<sub>2</sub>O and left to cool down. Filtered through 500 ml Nalgene sterile filter unit. Aliquoted and frozen at -20 °C.

**4 % Paraformaldehyde (PFA)**

100 ml	0.2 M NaH <sub>2</sub> PO <sub>4</sub>
400 ml	0.2 M Na <sub>2</sub> HPO <sub>4</sub>
250 ml	16 % PFA
8 g	NaCl
250 ml	ddH <sub>2</sub> O

**Citrate Buffer (Stock Solutions)**

0.1 M	Citric acid (C <sub>6</sub> H <sub>8</sub> O <sub>7</sub> *H <sub>2</sub> O)
0.1 M	Sodium citrate (C <sub>6</sub> H <sub>5</sub> O <sub>7</sub> Na <sub>3</sub> *2H <sub>2</sub> O)

Stored at 4 °C.

**Working Solution (0.01 M pH 6)**

9 ml	0.1 M Citric acid
41 ml	0.1 M Sodium citrate
450 ml	ddH <sub>2</sub> O

Always prepared freshly.

**Tris-buffer (Stock Solution)**

0.5 M	Tris base
-------	-----------

pH adjusted to 7.6 with 37 % HCl. Stored at 4 °C.

### Working Solution

100 ml 0.5 M Tris base (pH 7.6)

9 g NaCl

Filled up to a final volume of 1000 ml with ddH<sub>2</sub>O. Always prepared freshly.

2 % Milk-powder in Tris-buffer

20 g Non-fat dry milk-powder

Filled up to a final volume of 1000 ml with Tris-buffer working solution.

### % Triton X-100 in 1x PBS

40 µl 4 % Triton X-100

960 µl 1x PBS

### 5 % Horse-Serum, 0.1 % Triton X-100 in 1x PBS

50 µl Horse Serum

950 µl 0.1 % Triton X-100 in 1x PBS

### Mounting media

Eukit (Kindler)

Aqua-PolyMount (Polyscience)

Shandon Cryomatrix (Thermo Scientific)

## 4.8 Histological stains and reagents

### Mayer's Haematoxylin solution

1 g Haematoxylin

Dissolved in 1000 ml ddH<sub>2</sub>O, then added:

0.2 g Sodium iodate

50 g Potassium aluminum sulfate

under constant shaking. Then added:

50 g Chloralhydrate

1 g Citric acid

Filtered before use.

### Eosin Stock solution (10x)

10 g Eosin

Dissolved in 100 ml of ddH<sub>2</sub>O and left to mature.

Eosin working solution

2.5 ml Eosin Stock solution

Filled up to 250 ml with ddH<sub>2</sub>O and finished by adding 12 drops of glacial acetic acid.

Scott's solution

2 g KHCO<sub>3</sub>

20 g MgSO<sub>4</sub>

Filled up to a final volume of 1000 ml with ddH<sub>2</sub>O.

HCl-Alcohol

1.25 ml Conc. HCl

350 ml 100 % Ethanol

150 ml ddH<sub>2</sub>O

## 4.9 Primers

### 4.9.1 Genotyping primers

<i>STOP-Nrg1</i>	In house No.
Forward: 5'-GGTGGCTATAAAGAGGTCATCAG -3'	15762
Reverse: 5'-CTCCTGGCTTTTCATCTCTTTCAA -3'	28118
<i>NEX-Cre and NEX-CreERT2</i>	
Forward: 5'-GAGTCCTGGAATCAGTCTTTTTTC-3'	3131
Reverse: 5'-CCGCATAACCAGTGAAACAG-3'	2409
Reverse: 5'-AGAATGTGGAGTAGGGTGAC-3'	3132
<i>Thy1.2-Ig-NRG1</i>	
Forward: 5'-TGGCAAAGGACCTTAGGCAGTGT -3'	3776
Reverse: 5'-CTGGTAGAGCTCCTCCGCTTC -3'	3770
<i>Nrg1f/f</i>	
Forward: 5'-TCCTTTTGTGTGTGTTTCAGCACCGG-3'	6744
Reverse: 5'-GCACCAAGTGGTTGCGATTGTTGCT-3'	6743
<i>Parv-Cre</i>	
Forward: 5'-AATGCTTCTGTCCGTTTGCCGGT -3'	5383
Reverse: 5'-CCAGGCTAAGTGCCTTCTCTACA -3'	5382



*R26R-floxtD* Tomato

Forward: 5'-TACGGCATGGACGAGCTGTACAAGTAA-3' 21027

Reverse: 5'-CAGGCGAGCAGCCAAGGAAA-3' 21028

**4.9.2 Quantitative real-time PCR primers***Actin*

Forward: 5'-CTGCTCTTTCCCAGACGAGG -3' 29472

Reverse: 5'-AAGGCCACTTATCACCAGCC -3' 29473

*GFP*

Forward: 5'-ACGGCCACAAGTTCAGC -3' 5271

Reverse: 5'-CAGCTTGCCGGTGGTGCAGA -3' 25586

**4.10 Strains and bacterial culture media**

## Bacterial strains

*Escherichia coli* XL1-Blue (Stratagene)dam-/dcm- Competent *Escherichia coli* (NEB)

## LB medium (Lysogenic Broth)

1 % Bacto-Pepton

0.5 % Yeast extract

1 % NaCl

pH was set to 7 with 1 M NaOH and autoclaved.

Selective LB media was supplemented with following antibiotics:

100 µg/ml Ampicillin

50 µg/ml Kanamycin

## LB-Agar plates

1 % Bacto-Pepton

0.5 % Yeast extract

1 % NaCl

1.2 % Bacto-agar

Solids were suspended in 800 ml ddH<sub>2</sub>O. pH was adjusted to 7 and extra ddH<sub>2</sub>O was added up to 1 L. Solution was autoclaved and left to cool to 55 °C when desired antibiotics are

added. ~20 mL of LB agar were poured per 10 cm polystyrene Petri dish next to a Bunsen burner (bench area was kept sterile).

#### SOC medium

2 %	Tryptone
0.5 %	Yeast extract
10 mM	NaCl
2.5 mM	KCl
10 mM	MgCl <sub>2</sub>
10 mM	Glucose

Tryptone, yeast extract, NaCl, and KCl were mixed and autoclaved. Afterwards, MgCl<sub>2</sub> and glucose were added. 10 ml aliquots were prepared and stored at -20 °C.

#### 4.11 ES cell culture mediums and solutions

##### β-mercaptoethanol 10 mM

360 μl	β-mercaptoethanol stock (Sigma)
500 ml	PBS
~500 ml	total volume

It was filter-sterilized with 0.22 μm filter bottles (Corning) and stored at 4 °C.

##### MEFs medium

500 ml	Knockout-DMEM (Gibco)
95 ml	FBS Hyclone (GE Healthcare)
6 ml	MEM non-essential amino acids (Gibco)
6 ml	Glutamine (Gibco)
6 ml	β-mercaptoethanol 10 mM
3 ml	Pen/Strep (Gibco)
~600 ml	Total volumen

The medium was sterile-filtered with 0.22 μm filter bottles (Corning).

##### Medium for ES cells (129)

50 ml	MEF medium
6.5 μl	LIF (10 <sup>7</sup> U/ml; Millipore)
6 ml	Total volume

The medium was sterile-filtered with 0.22 μm filter bottles (Corning).

#### 2x freezing medium

8 ml MEF medium  
2 ml DMSO (Sigma)  
10 ml Total

The medium was sterile-filtered (0.22  $\mu$ m).

#### Gelatin solution (0.1 %)

1 g porcine gelatin (Sigma) was added to 1 L of ddH<sub>2</sub>O, mixed and autoclaved. Gelatin was added to the culture flasks and plates at least 30 min before using them. Before adding medium and/or cells gelatin was removed.

#### Mitomycin C

50x stock (0.5 mg/ml) mitomycin C (Sigma) was prepared by injecting 4 ml 1x PBS through the lid of a 2 mg bottle, using a syringe (because it is highly toxic to mammalian cells the bottle is never opened). After shaking it manually to dissolve, the bottle was stored at 4 °C.

#### Geneticin (G418)

20 ml of 50 mg/ml G418 was prepared (corrected for active ingredient). It was sterile-filtered (0.22  $\mu$ m), and 1 ml aliquots were prepared. One aliquot was added to 250 ml ES medium.

#### Lysis buffer for DNA isolation

10 mM Tris pH 7.5  
10 mM EDTA pH 8.0  
10 mM NaCl  
0.5 % Sarcosyl  
1 mg/ml Proteinase K (Sigma)

The buffer was prepared with the first four ingredients, and filter-sterile with 0.22  $\mu$ m filter bottles (Corning). The proteinase K was added fresh right before proceeding with DNA extraction.

### 4.12 Chemicals and media for primary cell culture

#### Medium

Neurobasal medium (NBM; Gibco 21103-049) (300 ml): add 6 ml B27 Supplement (Gibco 17504-044), 3 ml P/S (Sigma P0781) and 3 ml Glutamax (Gibco Cat no. 35050-038).

Plating medium: NBM + 5 % FCS (Gibco Cat no. 10106-169) (150 ml)

Medium to stop papain reaction: NBM + 10 % FCS (50ml)

## HBSS

HBSS (BioWhittaker Cambrex BE10-543F)

10 % (w/v) MgSO<sub>4</sub> (sterile filtered)

HBSS †: 500 ml HBSS plus 7.5 ml 10 % (w/v) MgSO<sub>4</sub>

## Poly-L-lysine

Poly-L-lysine (PLL) (Sigma P1274): dilute stock solution (5 mg/ml) 1:50 to 0.1 mg/ml in borate buffer

Borate buffer (400ml):

1.24 g            boric acid

1.9 g            sodium tetraborate

300 ml          ddH<sub>2</sub>O

Adjust pH to 8.5

Add further distilled H<sub>2</sub>O to make 400ml and filter

## Papain

Papain solution (Cell Systems Cat.No. LS003126)

L-cysteine (SIGMA C-7880): 24 mg L-cysteine + 1 ml NBM, sterile filter (0.22 µm), aliquot (12 µl) and store at -20 °C

DNaseI (SIGMA Cat. No. DN25): prepare 10 mg/ml solution, aliquot (42 µl) and store at -20 °C

## 4.13 Enzymes

Restriction enzymes from purchased from New England Biolabs (NEB)

REDTaq DNA polymerase            Sigma-Aldrich

GoTaq polymerase                    Promega

Antartic Phosphatase                New England Biolabs (NEB)

T4 DNA ligase                         Promega

GoTaq® qPCR master mix 2x        Promega

Proteinase K                            Sigma

## 4.14 Antibodies

### 4.14.1 Primary antibodies

Antibody	Species	Dilution	Company	Cat. No	Application
Actin	mono-ms	1000	Millipore	MAB1501	WB
AKT	poly-rb	5000	Cell Signaling	9272	WB
APP	mono-ms	1000	Millipore	MAB348	IHC
Calbindin	mono-ms	1000	Sigma	C 9848	IHC
CD3	mono-rat	150	BioRad	MCA1477A 488	IHC
Cre	poly-rb	1000	Covance	PRB-106C	IHC
ErbB4	mono-rb	1000	Abcam	ab32375	WB
GAD67	mono-ms	100	Millipore	MAB5406	IHC
GADPH	mono-ms	1000	Enzo	ADI-CSA- 335-E	IHC
Gephyrin	mono-ms	500	Synaptic Systems	147 011	IHC
GFAP	poly-rb	500	Dako	Z 0334	IHC
GFP	poly-goat	500	Rockland	600-101- 215	IHC
GM130	mono-ms	200	BD Biosciences	610823	IHC
HA	chicken	100	Sigma Aldrich	GW22511	IHC
HA	Mono-ms	100	Biologends	901502	WB/IHC
IBA1	poly-rb	700	Wako	019-19741	IHC
Kv2.1	mono-ms	500	Neuromab	75-014	IHC
NeuN	mono-ms	100	Chemicon	MAB377	IHC
Neuregulin-1a/b1/2 (C-20)	poly-rb	100	Santa Cruz	SC-348	WB/IHC
Neurogranin	poly-rb	1000	Chemicon	AB1763	IHC
Olig2	poly-rb	200	John Alberta, Harvard	DF308	IHC
Parvalbumin 28	poly-rb	200	Swant	PV-28	IHC
p-AKT (Ser473)(D9E)	poly-rb	5000	Cell Signaling	4060	WB
p-HER4/ErbB4 (Tyr1284)(21A9)	mono-rb	1000	Cell Signaling	4757	WB
p-p44/42 MAPK (Erk1/2) (Thr202/Tyr204)(20G11)	poly-rb	5000	Cell Signaling	4376	WB
p44/42 MAPK (Erk1/2) (137F5)	poly-rb	5000	Cell Signaling	4695	WB
PSD95	mono-ms	500	Neuromab	75-028	IHC
SERT ST C-20	poly-goat	100	Santa Cruz	SC-1458	IHC
Synaptophysin	mono-ms	1000	Synaptic Systems	101 011	WB
VGlut1	poly-guinea pig	100	Synaptic Systems	135 304	IHC

#### 4.14.2 Secondary antibodies

Antibody	Species	Dilution	Company	Application
$\alpha$ -chicken-cy3	donkey	1000	Dianova	IHC
$\alpha$ -chicken-Alexa488	donkey	1000	Dianova	IHC
$\alpha$ -goat-Alexa488	donkey	500	Dianova	IHC
$\alpha$ -guinea pig-cy3	goat	1000	Dianova	IHC
$\alpha$ -guinea pig-cy5	goat	250	Dianova	IHC
$\alpha$ -mouse-cy2	goat	100	Dianova	IHC
$\alpha$ -mouse-cy3	goat	1000	Dianova	IHC
$\alpha$ -mouse-cy5	donkey	250	Dianova	IHC
$\alpha$ -mouse-Alexa488	goat	100	Molecular Probes	IHC
$\alpha$ -mouse-Alexa555	goat	500	Molecular Probes	IHC
$\alpha$ -mouse-DL633	donkey	250	Yopro	IHC
$\alpha$ -mouse-DL649	donkey	250	Dianova	IHC
$\alpha$ -mouse-HRP	goat	5000	Dianova	WB
$\alpha$ - rabbit cy2	goat	100	Dianova	IHC
$\alpha$ - rabbit cy3	goat	1000	Dianova	IHC
$\alpha$ - rabbit cy5	donkey	250	Dianova	IHC
$\alpha$ - rabbit DL633	donkey	250	Yopro	IHC
$\alpha$ - rabbit DL649	donkey	250	Dianova	IHC
$\alpha$ -rabbit-HRP	goat	5000	Promega	WB
$\alpha$ -rabbit-Alexa488	donkey	100	Dianova	IHC
$\alpha$ -rabbit-Alexa555	donkey	500	Dianova	IHC
$\alpha$ -rat-HRP	goat	5000	Dianova	WB

#### 4.15 Mouse lines

##### *STOP-Nrg1*

Conditional  $\beta$ -actin eGFP-STOP-flox 2HA-Ig-Nrg1  $\beta$  1a transgenic mouse (Soto-Bernardini *et al.*, in preparation).

##### *NEX-Cre*

Cre driver mouse line, generated by homologous recombination of Cre into the NEX locus (Goebbels *et al.*, 2006).

*NEX-CreERT2*

Cre driver mouse line, generated by homologous recombination of Tamoxifen-inducible CreERT2 into the NEX locus (Agarwal et al., 2012).

*Thy1.2-Ig-NGR1*

Thy1.2 promoter-driven Ig-Nrg1  $\beta$  1a transgenic mouse (Michailov et al., 2004).

*Nrg1<sup>f/f</sup>*

Conditional floxed NRG1 knockout mouse (Li et al., 2002).

*Parv-Cre*

Cre driver line, generated by homologous recombination of an IRES-Cre cassette at the translational stop codon of parvalbumin gene (Hippenmeyer et al., 2005).

*R26R-floxedTomato*

Rosa26 knock-in floxed tdTomato Cre-reporter mouse line (Madisen et al., 2010).

## 5 Methods

### 5.1 Generation of conditional Ig-NRG1 transgenic mice

*STOP-Nrg1* mice were generated by PCR-amplification and cloning of an Ig-*NRG1* cDNA (kindly provided by Dr. Cary Lai Indiana University) in XhoI restriction site of the polylinker of the  $\beta$ -actin STOP-eGFP-flox cassette in a pBluescriptKS vector. Primers were designed and used to add two HA tags at the 3' to the start codon, and amplify the complete cDNA (forward primer: 5' GTTATCTCGAGGCCACCATGTACCCATACGATGTTCCAGATTACGCTCTTTACC CATCGATGTTCCAGATTACGCTCTTTCTGAGCGCAAAGAAGGCAGAG-3'; reverse primer: 5' -CGCAACTCGAGTTATACAGCAATAGGG-3'). The vector backbone harbored a fragment of a chicken  $\beta$ -actin promoter, a GFP-STOP cassette flanked by two loxP sites, and a bovine growth hormone polyA site. The transgene cassette was excised from the plasmid by digestion with SpeI and AgeI. Afterwards, it was injected into C57Bl/6N oocytes. Initial cloning of the vector backbone was performed by Maike Gummert and HA-Ig-NRG1 cDNA insertion and linearization was conducted by Viktorija Velanac at the Max-Planck-Institute of Experimental Medicine in Göttingen. Three positive founders were born. The transgenic line was maintained on a C57Bl/6N background.

### 5.2 Breeding of mouse mutants

For maintenance and expansion of the colonies, transgenic mice were bred to C57Bl/6N wildtype mice starting at 8 weeks of age.

### 5.3 Animal maintenance and handling

All mice used in this study were maintained and bred in the animal facility of the Max-Planck-Institute of Experimental Medicine. Animals were kept and handled in compliance with animal policies of the Max-Planck-Institute of Experimental Medicine and approved by the German Federal State of Lower Saxony.

### 5.4 Phenotyping of tail biopsies of *STOP-Nrg1* mice

Fluorescence of the loxP sites-flanked eGFP-STOP-cassette was used for routine genotyping of *STOP-Nrg1* mice. For this purpose, tail biopsies were examined under fluorescent light of 488 nm excitation with a fluorescent microscope (Leica MZ16F fluorescent stereomicroscope).



## 5.5 Preparation of mouse genomic DNA

### 5.5.1 Nexttec™ Tissue & Cells kit-based genomic DNA isolation

Nexttec™ Tissue & Cells kit was used to isolate DNA from tail biopsies for further genotyping. Isolation was performed according to manufacturer's protocol. Biopsies were lysed in 300 µl lysis buffer (265 µl buffer G1, 10 µl buffer G2, 25 µl buffer G3) by vigorous shaking for 60-120 min at 1200 rpm and 62 °C. Meanwhile, Nexttec™ cleanPlate96 were equilibrated with 350 µl Prep buffer for 5 min at RT and centrifuged for 1 min at 350 g. 120 µl of the lysates were loaded onto the columns and centrifuged at 750 g for 1 min into fresh tubes. Lysates were diluted 1:5 in ddH<sub>2</sub>O. 1 µl of the lysate was used in genotyping PCR reactions.

### 5.5.2 Chloroform DNA extraction

DNA for genotyping *STOP-NRG1* homozygous mice by quantitative real-time PCR (qPCR) was isolated from tail biopsies with the following protocol. 400 µl of extraction buffer (4.4) were added to each tube. In addition, 75 µl 8 M KAc (sterile-filtered; pH not adjusted), and 400 µl chloroform were added. The solution was mixed by vortexing for approximately 10 s, until a cloudy appearance was obtained. Samples were then centrifuged (5415 D Eppendorf) for 10 min at 4 °C (maximum speed). 200 µl of the supernatant were transferred to a new tube (chloroform waste was kept under fume cupboard and discarded appropriately). 400 µl ethanol were added, and the samples were mixed by inverting the tubes ~ 10 times. In this step the DNA precipitates. Afterwards, samples were centrifuged 10 min at 4 °C (maximum speed). The supernatant was completely removed and the pellets were air dried for ~ 30 min. Finally, 200 µl Tris buffer (10 mM Tris pH8.0) were added to resuspend the DNA. Samples were vortexed and stored at 4 °C for further experiments. This method allows quantification of resulting DNA with UV spectrophotometer, which is indispensable for qPCR analysis.

## 5.6 Genomic DNA analysis

### 5.6.1 DNA amplification *in vitro* by polymerase chain reaction (PCR)

Polymerase chain reaction (PCR) (Mullis et al., 1986) is an *in vitro* method for enzymatic amplification of a DNA sequence of interest. The reaction requires a thermostable DNA polymerase, which is stable at the melting temperature of the double stranded DNA and has an optimal activity at around 72 °C. In this reaction, the sequence of interest is flanked by primers, that bind to the sense and antisense strands of the template. The DNA amplification is carried out in a thermocycler through multiple repetitions of three steps: denaturation, annealing, and extension. Standard PCR master mixes for genotyping were set up with RedTaq polymerase (Sigma) or GoTaq DNA polymerase (Promega) following manufacturer's specification. Specific primers for every mouse line were used (4.9.1).

PCR master mix for RedTaq polymerase:

1 $\mu$ l	DNA (100 pg-100 ng)
1 $\mu$ l	sense primer (10 pM)
1 $\mu$ l	antisense primer (10 pM)
2 $\mu$ l	dNTP mix (2 mM)
2 $\mu$ l	10x RedTaq buffer
1 $\mu$ l	RedTaq polymerase (1 U/ $\mu$ l)
12 $\mu$ l	ddH <sub>2</sub> O

PCR master mix for GoTaq polymerase:

1 $\mu$ l	DNA (100 pg-100 ng)
0.2 $\mu$ l	sense primer (50 pM)
0.2 $\mu$ l	antisense primer (50 pM)
2 $\mu$ l	dNTP mix (2 mM)
4 $\mu$ l	5x GoTaq buffer
0.1 $\mu$ l	GoTaq polymerase (5 U/ $\mu$ l)
12.5 $\mu$ l	ddH <sub>2</sub> O

AccuPrime™ GC-Rich DNA Polymerase or MyFi™ DNA polymerase (Bioline) were used for PCRs in which Taq polymerases with 3' to 5' exonuclease proofreading activity were needed for amplification of big fragments (and/or rich-CG content), used for subsequent cloning.

### 5.6.2 Primer design

Primers were designed based on the template sequence information using the SnapGene software, and OligoAnalyzer 3.1 (<http://eu.idtdna.com/calc/analyzer>). Primers for genotyping had around 20 bp overlap with the template sequence and a melting temperature near 60 °C. Oligonucleotides were synthesized in-house at the AGCTlab (AGCTLab@em.mpg.de) of the Max-Planck-Institute of Experimental Medicine.

### 5.6.3 PCR programs for genotyping

*STOP-Nrg1*

1. 95 °C 5 min
  2. 95 °C 45 sec
  3. 56 °C 30 sec
  4. 72 °C 1 min
- 2 to 4 for 36 cycles
5. 56 °C 1 min

6. 72 °C 10 min
7. 4 °C pause

#### *NEX-Cre and NEX-CreERT2*

1. 95 °C 3 min
2. 54 °C 30 sec
3. 72 °C 1 min
4. 95 °C 30 sec
- 2 to 4 for 39 cycles
5. 54 °C 1 min
6. 72 °C 10 min
7. 4 °C pause

#### *Thy1.2-Ig-NRG1*

1. 95 °C 3 min
2. 95 °C 30 sec
3. 54 °C 30 sec
4. 72 °C 1 min
- 2 to 4 for 39 cycles
5. 54 °C 1 min
6. 72 °C 10 min
7. 4 °C pause

#### *Nrg1f/f*

1. 95 °C 3 min
2. 95 °C 30 sec
3. 57.5 °C 30 sec
4. 72 °C 1 min
- 2 to 4 for 39 cycles
5. 72 °C 20 min
6. 4 °C pause

#### *Parv-Cre*

1. 95 °C 3 min
2. 95 °C 45 sec
3. 56 °C 30 sec
4. 72 °C 1 min

- 2 to 4 for 36 cycles
- 5. 56 °C 1 min
- 6. 72 °C 10 min
- 7. 4 °C pause

#### *R26R-floxtdTomato*

- 1. 95 °C 3 min
- 2. 95 °C 30 sec
- 3. 60 °C 30 sec
- 4. 72 °C 90 sec
- 2 to 4 for 45 cycles
- 5. 60 °C 1 min
- 6. 72 °C 10 min
- 7. 4 °C pause

#### **5.6.4 Agarose gel electrophoresis separation of DNA fragments**

PCR products were analyzed by agarose gel electrophoresis, which separates DNA fragments based on their size. With this method, migration of negatively charged DNA to the positively charged cathode is achieved. Smaller DNA fragments migrate faster through the gel than bigger fragments (Voytas, 2001). 1.5 % agarose gels were prepared in 1x TBE buffer. For DNA visualization 2 to 3 µl of 10x GelRED™ (Biotium) were added to 20 µl DNA sample. Gels were placed into the electrophoresis chambers filled with 1x TBE buffer. DNA marker (1 Kb, SM0311, Thermo Scientific) and DNA samples (with loading buffer included) were loaded into the wells. The chamber was connected to a power supply and the gel was run at 4-10 V/cm (taking into account the distance between anode and cathode). After separation of the desired fragments, snapshots of UV-trans-illuminated gels were taken (Intas UV-Systeme).

#### **5.6.5 Measurement of the DNA concentration and purity**

Spectrophotometric analysis is based on the fact that nucleic acids absorb UV light at a wavelength of 260 nm. A photodetector measures the light that passes through a DNA sample, whereby the light is absorbed by the sample indicating the nucleic acid concentration in the sample. Less light will reach the photodetector if the absorption is high, resulting in a higher OD.

Concentration and purity of DNA samples were measured using the NanoDrop 2000 spectrophotometer (Thermo Scientific). 1 µL of ddH<sub>2</sub>O or TE (depending on the solvent used) was used to measure the blank. Afterwards, 1 µL of each sample was used for the measurement.

### 5.6.6 Quantitative Real Time PCR (qRT-PCR)

qRT-PCR is a PCR variant that allows DNA or RNA quantification in a sample. This is achieved by measuring the amount of amplified product in each cycle of the PCR, using fluorescent probes or fluorescent DNA-binding dyes and a thermal cycler with the capacity to illuminate each sample with beams of light of specific wavelengths and detect the fluorescence emitted by the excited fluorophore. The threshold cycle ( $C_t$ ) is the first cycle at which the fluorescent signal is detected. In this way, the initial DNA amount is calculated based in the  $C_t$ , which is inversely related to the starting quantity of the sample. As the initial DNA amount decreases, the  $C_t$  increases (Biaassoni and Raso, 2014). This technique was used to distinguish between homozygous and heterozygous *STOP-NRG1* mice.

DNA was isolated as described above (5.5.2) and quantified using the NanoDrop 2000 spectrophotometer (Thermo Scientific), as described above. Samples were diluted to a final concentration of 5 ng/ $\mu$ l. Reactions were run in quadruplicates, with primers to amplify the eGFP located in the STOP-cassette (4.9.2). Reactions to amplify  $\beta$ -actin were also performed in quadruplicates. In both cases, a master mix was set up as follows:

4 $\mu$ l	DNA (5 ng/ $\mu$ l)
0.1 $\mu$ l	sense primer (10 pM)
0.1 $\mu$ l	antisense primer (10 pM)
5 $\mu$ l	GoTaq qPCR Master Mix (Promega)
0.8 $\mu$ l	ddH <sub>2</sub> O

qPCR was performed using the standard protocol for relative quantification of the 7500 Fast Real-Time PCR (Applied Biosystems). Post-amplification melting curve analyses were performed to check for primer-dimer artifacts and ensure reaction specificity.  $C_t$  values from the quadruplicates were analyzed, and outliers were eliminated. At least three of the four replicates were included in the analysis. The standard deviation was calculated and considered acceptable up to 0.5. Comparative quantification analysis was performed by the  $\Delta\Delta C_t$  method, that compares results from experimental samples with a calibrator (in this case a negative control which has a higher  $\Delta C_t$ ) and a normalizer ( $\beta$ -actin housekeeping gene).  $C_t$ s for the gene of interest (GFP) in the test samples and the calibrator sample were adjusted in relation to the  $\beta$ -actin gene ( $C_{t \text{ eGFP}} - C_{t \text{ } \beta\text{-actin}}$ ). The resulting  $\Delta\Delta C_t$  ( $\Delta C_{t \text{ sample}} - \Delta C_{t \text{ calibrator}}$ ) value was used to determine the fold difference in expression ( $2^{-\Delta\Delta C_t}$ ). Values obtained were plotted, and normally 3 groups were observed: negative samples, heterozygous and homozygous. Samples that did not clearly correspond to those groups were not considered for further analysis.

## **5.7 Biochemical analysis of protein**

### **5.7.1 Protein extraction**

Sucrose homogenization buffer (320 mM Sucrose, 10 mM Tris (pH7.4), 1 mM NaHCO<sub>3</sub> and 1 mM MgCl<sub>2</sub>) with protease and phosphatase inhibitors (Roche) was used for protein extraction. Dissected frozen prefrontal cortices and hippocampi from one hemisphere were homogenized in 200 µl of the buffer. Homogenization was performed with the Precellys24 homogenizer (5500 rpm, 2x 10 sec, Bertin Technologies). 130 µl of the resulting homogenate were added to 70 µl of 4x LDS sample buffer (NuPAGE) working solution including DTT. The samples were immediately denatured at 70 °C for 10 min and stored at -80 °C. Protein concentration measurement was performed on dilutions (1:1 up to 1:20 in sucrose homogenization buffer) of the leftovers. Afterwards, the rest of the homogenates were stored at -80 °C.

### **5.7.2 Protein concentration measurement**

The protein concentration of samples was determined using the Bio-Rad DC Protein Assay kit. The working principle is based on the Lowry assay described by Lowry et al, 1951. Two steps are included in this assay. One is the reaction between protein and an alkaline copper tartrate solution, followed by the reduction of Folin reagent that produces several reduced species of characteristic blue color with a maximum absorbance at 750 nm. The oxidation of the amino acids tyrosine and tryptophan, (and to a lesser extent cystine, cysteine, and histidine) is responsible for the color development (Lowry et al., 1951; Peterson, 1979). The assay was performed in a 96-well plate (flat bottom) and absorbance was measured at 650 nm with a microtitre plate reader (ThermoMax Molecular Devices). To estimate protein concentrations, dilutions of bovine serum albumin (BSA) were used to produce a standard curve. Protein concentrations were calculated according to the dilution factor.

### **5.7.3 SDS polyacrylamide gel electrophoresis**

Separation of the proteins by size was performed by discontinuous SDS-polyacrylamide gel electrophoresis (SDS-PAGE) (Laemmli, 1970). The working principle of this procedure is based on denaturing the proteins with reducing agents such as dithiothreitol (DTT) or β-mercaptoethanol and heat. This way, disulfide bonds between cysteine residues are cleaved, disrupting the quaternary and tertiary structure of the proteins, which results in linear chains of polypeptides. In addition, the presence of sodium dodecyl sulfate (SDS) or lithium dodecyl sulfate in the buffer renders the proteins with a negative charge, thus proteins migrate based on their molecular weight.

Polyacrylamide gels were cast and poured between Bio-Rad glass plates and 1.75 mm spacer plates. The separation gel (8 % acrylamide) was poured first. 1 ml of isopropanol was added on top of the gels in order to have a flat and straight front. After 20 min of polymerization at RT, the isopropanol was rinsed with ddH<sub>2</sub>O. Afterwards, the stacking gel was poured and a comb (10 or 15 teeth) was inserted into the stacking gel solution. The gels were left to polymerize for 20 min at RT, and stored overnight at 4 °C.

Electrophoresis chambers (Bio-Rad) were assembled according to the manufacturer's manual. 20-30 µg of protein samples and 10 µl of pre-stained protein marker (Fermentas) were loaded onto the gel. The chamber was filled with electrophoresis buffer and connected to a power supply (Bio-Rad). The gels were run at 100 mV for 30 min until samples reached the border between the stacking and the separation gel. Afterwards, the voltage was increased to 150 mV and the gels were run until the tracking dye reached the end of the gel. The gels were removed from the glass plates to proceed with further analysis.

#### **5.7.4 Silver staining of polyacrylamide gels**

The gel was fixed in a solution containing 40 % ethanol, 10 % acetic acid for 1 h on a shaker. Afterwards, it was washed twice in 30 % ethanol for 20 min (shaking). The gel was transferred to ddH<sub>2</sub>O and washed for 20 min (shaking). It was then transferred to sodium thiosulfate (0.8 mM) for 1 min, and washed 3 times in ddH<sub>2</sub>O for 30 s. The gel was placed in a solution of 0.2 % silver nitrate and 0.02 % formaldehyde, for 20 min and rinsed with ddH<sub>2</sub>O for 1 min (twice). To develop, an incubation with 150 ml 2 % sodium carbonate with 0.02 % formaldehyde was performed until the desired intensity of staining was reached (the developer was replaced when it turned yellow). To stop the reaction, the gel was transferred to 150 ml 5 % acetic acid for 10 min. This step was repeated with fresh solution. Finally, the gel was rinsed in ddH<sub>2</sub>O for 5 min.

#### **5.7.5 Western Blotting**

Proteins separated by SDS-PAGE were transferred to PVDF membranes by electrophoresis, as previously described by (Towbin et al., 1979). Using this method, the negatively charged proteins (from SDS-PAGE) migrate from the cathode to the anode and are retained on polyvinylidene difluoride (PVDF) membranes by a combination of dipole and hydrophobic interactions. PVDF membranes (GE Healthcare LifeSciences, pore size 0.45 µm) were activated for 1 min in 100 % methanol, washed twice in ddH<sub>2</sub>O and then placed into cold transfer buffer.

Blotting pads and Whatman papers were placed in cold transfer buffer and the blotting sandwich was assembled taking into account the position of the gel in relation to the membrane and the anode (+). Assembly of the transfer sandwich was performed in a container filled with

transfer buffer. The sandwich was built on the side of the transfer cassette facing the cathode (-) starting with a sponge, followed by Whatman paper, the gel, the membrane, an additional Whatman paper, and a second sponge. Later on, this construct was placed in the transfer cassette and submerged in an electrotransfer tank containing transfer buffer. The protein transfer was performed using Bio-Rad Mini Trans-Blot® cells under a constant current of 350 mA for 90 min at 4 °C.

### **5.7.6 Immunological detection of proteins and densitometric quantification**

Membranes were blocked for 60 min at RT in blocking buffer and then placed into 50 ml falcons containing 5 ml of the primary antibody diluted in the same buffer. Incubation was performed ON at 4 °C with constant rotation. Afterwards, membranes were washed for 10 min in TBST. This washing step was repeated 3 times. Next, membranes were incubated with the HRP-conjugated secondary antibody diluted in blocking buffer for 1 h at RT. Washing steps were performed again four times. This was followed by 1 min incubation with a 1:1 dilution of the two Enhanced Chemiluminescence Detection (ECL) solutions. Membranes were placed into a transparent plastic foil, placed into the Intas ChemoCam Imager, and scanned for 20 min. Images were acquired with the Intas ChemoCam Imager, and saved digitally for subsequent analysis. Membranes were used to analyze different proteins. Stripping of preceding antibodies was performed by incubating the membranes in 0.5 M NaOH for 10-15 min at RT. Before re-probing the membranes with the next primary antibody, another blocking step was performed. For densitometric analyses of western blot bands, the images acquired were opened with ImageJ, converted to 8-Bit and inverted in order to have black bands on white background. ImageJ's gel analyzing function was used to measure the densities of bands of interest. Results were normalized to loading controls ( $\beta$ -actin or GAPDH). Normalized values ( $\pm$ SEM) were analyzed for statistical significance using the GraphPad Prism software package. One-way ANOVA analyses were performed when more than one group of controls were included in the experiment. Bonferroni-post hoc tests for pairwise group comparisons were performed. If no differences between control groups were observed, these were pooled and t-tests were performed.

## **5.8 Histology and immunohistochemistry**

### **5.8.1 Analysis of the STOP-cassette in different organs**

The presence of GFP in the STOP-cassette of the *STOP-Nrg1* mice permits visualization of Cre-dependent stage-specific activation of Ig-NRG1 overexpression (absence of GFP), and can also be used to genotype mice. Expression of the cassette was examined in different organs of the transgenic mice (brain, heart, liver, muscles, tail tips, spinal cord and sciatic



nerve) by checking for GFP fluorescence. Mice were sacrificed by cervical dislocation followed by decapitation. Organs were dissected from the mice, rinsed in 1x PBS, and examined with the Leica MZ16F fluorescent stereomicroscope. Brightfield and fluorescent light images were acquired and analyzed by ImageJ software.

### **5.8.2 Perfusion fixation of mouse tissue**

Mice were perfused and fixed in order to preserve the tissue for later histological analysis. For this purpose, mice were deeply anesthetized by IP injection of Avertin (0.2 ml per 10 g of body weight). After checking the reflexes of the mice, to ensure deep anesthesia, they were fixed onto a platform with drainage.

Two pieces of the tail were collected for re-genotyping. The abdomen and the diaphragm were opened, and the rib cage was cut laterally on both sides to the top and above the sternum. It was then fully removed to expose the heart. A 27 gauge needle butterfly connected to a peristaltic pump was inserted into the left ventricle, making sure not to pierce the septum. Afterwards, the right atrium was opened by a small cut to ensure the perfusion flow. Blood was flushed out of the circulatory system with 20 ml of HBSS (pre-warmed at 37 °C) using a peristaltic pump with a flow rate of 1 ml/min. Then, mice were perfused with 30-40 ml of ice-cold 4 % PFA fixative at the same flow rate. Afterwards, fixed tissues were dissected and placed into cold 4 % PFA ON at 4 °C. Vibratome sectioning was performed the next day. Cryosectioning was performed on the post-fixed tissue after a step of cryoprotection in sucrose solutions. Tissue for paraffin embedding was immediately processed for this purpose after the ON post-fixation.

### **5.8.3 Vibratome sectioning**

After post-fixation, brains were washed in 1x PBS and sliced coronally into 3 three pieces of 4 mm thickness (PFC, hippocampal and cerebellar sections) using a brain slicer. Subsequently, tissues were transferred to the vibratome (Leica VT 1000S). Each section was glued onto the specimen holder of the vibratome using instant glue. The specimen holder was fixed to the stage of the vibratome which was then filled with ice-cold 1x PBS. Coronal sections of 30 µm thickness were collected and transferred to 24-well plates filled with 1x PBS. The sections were kept on ice and immunohistological stainings were immediately performed.

### **5.8.4 Cryoprotection, embedding and cryosectioning**

Incubations in a row of sucrose solutions with ascending sucrose concentrations were performed to cryoprotect tissues. First tissue was shortly rinsed in 1x PBS and then submersed in 10 % (w/v), 20 % (w/v) and 30 % (w/v) sucrose solutions at 4 °C (ON in each solution or until

the tissue was sunk to the bottom of the tube). Brains were sectioned into three 4 mm thick coronal pieces (PFC, hippocampal and cerebellar sections) using a brain slicer, and frozen on aluminum foil on dry ice. Tissues were wrapped in aluminum foil and stored at -80 °C for further sectioning.

Embryonic brains, SC, and sciatic nerves were embedded in Shandon cryomatrix in aluminum foil molds, in order to facilitate sectioning of such small tissues. The bottom of the molds was covered with Shandon cryomatrix at RT and the cryoprotected tissues were placed into the molds with the cutting surface facing to the bottom of the mold. Shandon cryomatrix was used to fill the molds, which were then placed on dry ice to freeze. Tissues were stored at -80 °C for further sectioning. Tissue was transferred from -80 °C to the cryostat (-21 °C) half an hour prior to sectioning. Blocks of tissue embedded in Shandon cryomatrix were trimmed to size using razor blades.

Brains or tissues contained in cryomatrix blocks were glued onto a specimen holder of the cryostat (Leica Jung CM 3000) with Shandon cryomatrix and fixed into the cryostat. 14 µm to 20 µm thick sections were collected using a knife-angle of 4°, a chamber temperature of -21 °C and an object temperature of -19 °C. Sections were either collected on positively charged ultrafrost microscope slides, dried ON at RT in an exicator and then used for immunostainings, or collected as free-floating cryosections in multi-well plates filled with 1x PBS, where they were also processed for stainings.

Cryosections from mouse brains frozen in isopentane were also collected for subsequent fixation in methanol. This method works best for PSD95 and Gephyrin antibodies. A metal box was filled with isopentane, placed on a flat piece of dry ice, surrounded by more dry ice and wet ice, inside a styrofoam box. The temperature was adjusted to -35 °C. Mice were sacrificed by cervical dislocation followed by decapitation and the brains were quickly removed from the skull and drowned in the cold isopentane. They were removed with forceps when no more air bubbles were coming out, and directly transferred to the cryostat. 20 µm thick sections were collected. Sections were then fixed for 15 min in cold (-20 °C) methanol in a cuvette inside the cryostat. Afterwards, sections were washed in 1x PBS for 5 min and then blocked and processed for immunohistochemical analysis.

### **5.8.5 Paraplast impregnation, embedding and sectioning**

After ON post-fixation, brains were shortly rinsed in 1x PBS and sliced into three 4 mm thick pieces (PFC, hippocampal and cerebellar sections). The three pieces were placed in tissue cassettes, dehydrated and infiltrated with paraplast using the paraplast embedding station (Microm HMP110) with the following solution incubation protocol: EtOH 50 % 1 h, EtOH 70 % 2 h, EtOH 70 % 2 h, EtOH 96 % 1 h, EtOH 96 % 1 h, EtOH 100 % 1 h, EtOH 100 % 1 h, Isopropanol 1 h, Xylol 2 h, Xylol 2 h, Paraplast 2 h, Paraplast 2 h. Afterwards,

tissues were embedded in paraplast blocks, using the paraplast embedding center (Microm AP280) and metal molds. Tissue-containing paraplast-blocks were removed from the molds and stored at RT until sectioning.

5  $\mu\text{m}$  sections were sectioned using a sliding microtome (Microm HM 400). Sections were collected in ice-cold distilled water, transferred to a 42 °C water bath for straightening, and mounted on charged microscope slides. Sections of different genotypes were mounted side-by-side on one slide (controls and overexpressors/mutants) for parallel processing. Slides were dried ON at 37 °C and then stored at RT for further immunohistological stainings.

### **5.8.6 Immunohistological staining procedures**

#### **Hematoxylin-Eosin staining**

Hematoxylin-Eosin (H+E) staining is a common histological staining method to obtain information of overall tissue structures. Basophilic nuclei are stained in dark purple by hematoxylin and eosinophilic cytoplasm is stained in pink by the acidic dye Eosin. Paraffin sections were deparaffinized by two 10 min incubations in Xylol and one for 10 min in Xylol/Isopropanol (1:1), followed by rehydration in descending ethanol dilutions (100 %, 90 %, 70 %, and 50 %) for 5 min each. After washing for 5 min in ddH<sub>2</sub>O, sections were stained with 0.1 % hematoxylin for 5 min and washed with ddH<sub>2</sub>O. The dark purple color was differentiated by a short wash in HCl-alcohol solution. The differentiation process was stopped by incubating the sections for 5 min in Scott's solution. Afterwards, sections were shortly rinsed in ddH<sub>2</sub>O, and counterstained in 0.1 % Eosin for 3-5 min. Excess dye was washed off with ddH<sub>2</sub>O. Sections were dehydrated by short incubation steps (10-30 sec) in an ascending row of ethanol (50 %, 70 %, 90 %, and 100 %). Finally, sections were incubated once for 10 min in Xylol/Isopropanol (1:1) and twice for 10 min in Xylol, and mounted with the Xylol based mounting medium Eukitt and dried at RT.

#### **DAB immunostaining of paraffin sections**

An enzymatic reaction of a secondary antibody-linked horseradish peroxidase (HRP) with DAB substrate, which forms a stable brown precipitate that can be visualized by light microscopy, is the working principle of DAB immunostaining (Harlow and Lane, 1988). 5  $\mu\text{m}$  paraffin sections were deparaffinized by two 10 min incubations in Xylol and one for 10 min in Xylol/Isopropanol (1:1), followed by rehydration in descending ethanol dilutions (100 %, 90 %, 70 %, and 50 %) for 5 min each. Afterwards, sections were incubated for 5 min in ddH<sub>2</sub>O followed by 5 min incubation in citrate buffer. Then, sections were cooked for 10 min in boiling citrate buffer at 650 W in the microwave for antigen retrieval. To maintain the buffer molarity after evaporation ddH<sub>2</sub>O was added. Sections were left at RT 20-30 min, washed for 5 min in Tris-buffer with

2 % milk powder and then mounted with plastic cover-plates for the following steps of the protocol. Endogenous peroxidases were inactivated by 5 min incubation with 100  $\mu$ l of 3 % hydrogen peroxide followed by blocking with 100  $\mu$ l of blocking buffer for 20 min at RT. Then 100  $\mu$ l of the primary antibody in PBS/BSA were applied to the slides and incubated ON at 4 °C. Sections were washed with Tris-buffer with 2 % milk-powder, followed by incubation with 100  $\mu$ l of the biotinylated secondary antibody (Dako LSAB2, yellow bottle solution A) for 10 min at RT. After washing in Tris-buffer with 2 % milk-powder, 100  $\mu$ l of Steptavidin conjugated to Horseradish Peroxidase (Dako LSAB2, red bottle solution B) were added to the sections and incubated for 10 min at RT. After washing with Tris-buffer (no milk) for 10 min at RT, the plastic cover-plates were removed and the slides were placed into a box for staining with 100  $\mu$ l of DAB substrate solution (1 ml Dako Substrate buffer with two drops of DAB) for 10 min, followed by washing twice in ddH<sub>2</sub>O for 5 min. In some cases, the sections were counterstained with hematoxylin for 30 sec and then washed once in ddH<sub>2</sub>O for 5 min. Sections were dehydrated in an ascending row of ethanol dilution (50 %, 70 %, 90 %, and 100 %) by incubation steps of 30 sec. Later on, sections were incubated for 10 min in Xylol/Isopropanol (1:1) and twice for 10 min in Xylol. Finally, they were mounted with the Xylol based mounting medium Eukitt and dried at RT.

### **Fluorescent staining of vibratome sections**

Immunostainings of free floating vibratome sections were performed in 24-well plates. First, sections were permeabilized/blocked in 5 % horse serum, 0.1 % Triton X-100 in 1x PBS (200  $\mu$ l per well) for 60 min at RT. Afterwards, blocking solution was carefully removed with a pipette and 200  $\mu$ l of the primary antibodies (diluted in the same blocking solution) were added to each well and incubated overnight at 4 °C in a humidified chamber. On the next day, three washing steps of 10 min in 1x PBS at RT were performed. Later on, 200  $\mu$ l of secondary antibodies and DAPI diluted in the blocking buffer were added to each well. From this step on slides had to be protected from light. Incubation for 120 min at RT, was followed by three washing steps in 1x PBS. Sections were carefully transferred with a soft brush to a deep petri dish filled with tap water and pulled onto charged microscope slides. After a short air drying, sections were mounted with Aqua-PolyMount and stored at 4 °C.

### **Fluorescent staining of cryosections**

Cryosections collected on positively charged ultrafrost microscope slides were washed for 10 min in 1x PBS at RT in a cuvette to remove Shandon cryomatrix. Slides were placed in a humidified chamber. A Hydrophobic Barrier Pen was used to draw a hydrophobic circle around the tissue to avoid loss of solutions and drying of tissue. 200  $\mu$ l of 5 % Horse-Serum, 0.1 % Triton X-100 in 1x PBS were applied onto the slides for permeabilization and blocking for 30

min at RT. Afterwards, 200  $\mu$ l of the primary antibodies (diluted in blocking solution) were applied, and incubation was carried out ON at 4 °C. On the next day, three washing steps of 10 min in 1x PBS at RT in a cuvette were performed, followed by incubation (120 min) in 200  $\mu$ l of secondary antibodies and DAPI diluted in blocking solution. Afterwards, three washes of 10 min in 1x PBS at RT in a cuvette protected from light were performed. Finally, slides were mounted in Aqua-PolyMount and stored at 4 °C.

## **5.9 Imaging and image analysis**

### **5.9.1 Cell counting of chromogenic stainings**

Neuron numbers from cortex and hippocampus of transgenic mice were quantified on 5  $\mu$ m thick coronal paraffin sections (bregma -1.3 or -1.7). These sections were stained chromogenically for neuronal markers and then imaged as tiles overviews at 10x magnification using a Zeiss Imager.Z1 microscope. Cortical and hippocampal cells numbers were blindly counted using the cell counter plugin for ImageJ software. Counted cell numbers were expressed as cell densities (cells per area counted, in  $\text{mm}^2$ ). In some cases, the number of cells per cortical layer in pre-cut columns (of the same width) of the cortex (between CA1 and CA3 region of hippocampus; bregma -1.3 or -1.7) were counted. Cell numbers of both hemispheres were averaged and the data was analyzed using Excel and GraphPad Prism software. One-way ANOVA analyses were performed when more than one group of the controls were included in the experiment. Bonferroni-post hoc tests for pairwise group comparisons were performed. If no differences between control groups were observed, these were pooled and t-tests were performed.

### **5.9.2 Quantification of GFAP<sup>+</sup> and IBA1<sup>+</sup> areas**

GFAP<sup>+</sup> and IBA1<sup>+</sup> areas were quantified on chromogenic stainings of coronal brain sections with a semi-automatic analysis, using a plug-in for ImageJ software (available online at <http://www1.em.mpg.de/gfap>). 10x overview pictures, acquired with the Zeiss Imager.Z1 microscope, were blindly loaded into the software. From regions of interest (hippocampus, fimbria and the corpus callosum) selected in each hemisphere, the software analyzed the DAB-positive area over the total area quantified. Positive area fractions of both hemispheres were averaged and the data was analyzed using GraphPad Prism software. One-way ANOVA analyses were performed when more than one group of the controls were included in the experiment. Bonferroni-post hoc tests for pairwise group comparisons were performed. If no differences between control groups were observed, these were pooled and t-tests were performed.

## 5.10 Behavioral experiments

Mice were group-housed, and brought to the behavioral unit at least one week before the experiment to allow them to adapt to the new environment. Wood chip bedding and nesting material (paper tissue) were provided in their home cages. Animals were maintained on a 12 h light-dark cycle (light-off at 7 pm), at 20-22 °C, with food and water provided *ad libitum*. These experiments were performed by Anja Ronnenberg and Prof. Dr. Ekrem Dere, as part of a collaboration with Prof. Dr. Dr. Hannelore Ehrenreich (MPI-EM, Clinical Neuroscience). Experimentators were blind to the genotypes.

### 5.10.1 Visual cliff test

A Perspex box (70x35x30 cm) with a transparent floor was placed on the edge of an opaque gray box in a way that 50 % of its base was positioned on the box surface (“ground” side). The other 50 % of the base protruded over the edge of the box, suspended 1 m above the floor (“air” side). The light intensity of the testing room was 140 lux. Mice were placed in the middle of the ground side, and the time spent on both sides was measured over 5 min using a video tracking system (Viewer2, Biobserve, Germany) (Dere et al., 2014, 2015; Netrakanti et al., 2015).

### 5.10.2 Hot plate test

The hot plate test (O’Callaghan and Holtzman, 1975) was used to measure pain perception. Mice were placed on a metal plate (UgoBasile Srl, Comerio, Italy) that was preheated up to 55 °C. The latency to show hind paw licking or jumping was recorded. Immediately after showing the response, the mice were removed from the platform. A cut-off time of 40 s ensured that the mice were not injured. Animals were tested at the age of 27-28 weeks (Netrakanti et al., 2015).

### 5.10.3 Exploratory activity in the open field

Exploratory behavior induced by spatial novelty was measured with an open-field set-up. The apparatus consisted of a gray circular Perspex arena (120cm diameter; wall height 25cm) with a light intensity of 140 lux in the center of the arena. Each mouse was placed in the center of the open field and allowed to explore it for 7 min. Latency (s) to cross from the center to the periphery, time spent (s) in the peripheral, intermediate, and center zones of the apparatus and the total distance travelled (m) as well as the mean running velocity (mm/s) were measured using an automated tracking software (Viewer2, Biobserve, Bonn, Germany) (Dere et al., 2014, 2015; Netrakanti et al., 2015).

#### 5.10.4 Pre-pulse inhibition of the startle response

The phenomenon in which a weak pre-stimulus inhibits the reaction of an organism to a subsequent strong startling stimulus is called pre-pulse inhibition. Reduction of the startle reaction reflects the ability of the nervous system to temporarily adapt to a strong sensory stimulus when a preceding weaker signal is given to warn the organism. The inability to filter out the unnecessary information results in deficits in pre-pulse inhibition, and has been linked to abnormalities of sensorimotor gating present in schizophrenia patients (Braff et al., 1992; Geyer and Braff, 1982).

To assess sensorimotor gating as a measure of intact neuronal network function, animals were placed in small metal cages (82x40x40mm) to restrict major movements and exploratory behavior. The cages were equipped with a movable platform floor attached to a sensor that recorded vertical movements of the floor. The cages were placed in sound-attenuating cabinets (TSE Systems, Germany). Startle reflexes were evoked by acoustic stimuli delivered by a loudspeaker that was suspended above the cage and connected to an acoustic generator. Movement of a force-sensitive platform induced by the startle reaction to an acoustic stimulus was recorded over a period of 260 ms beginning with the onset of the pulse. An experimental session consisted of a 2 min habituation period to a 65 dB background white noise (continuous throughout the session), followed by a baseline recording for 1 min at background noise. After baseline recording, 6 pulse-alone trials using startle stimuli of 120 dB intensity and 40 ms duration were applied to decrease the influence of within-session habituation. These data were not included in the 120 dB/40 ms analysis of the pre-pulse inhibition. For tests of pre-pulse inhibition, the startle pulse was applied alone or after a pre-pulse stimulus of 70, 75, or 80 dB intensity and 20 ms duration. A delay of 100 ms with background noise was interposed between the presentation of the pre-pulse and pulse stimulus. The trials were presented in a pseudorandom order with a variable interval ranging from 8 to 22s. The difference between the maximum force detected during the recording window and the force measured immediately before the stimulus onset represents the amplitude of the startle response, and is expressed in arbitrary units. For each animal, the amplitudes were averaged separately for the 2 types of trials (i.e. stimulus alone or stimulus preceded by a pre-pulse). Pre-pulse inhibition was calculated as the percentage of the startle response using the following formula: % pre-pulse inhibition =  $100 - [(startle\ amplitude\ after\ pre-pulse) / (startle\ amplitude\ after\ pulse\ only) \times 100]$  (Netrakanti et al., 2015).

#### 5.10.5 Social interaction in pairs

The dyadic social interaction test was performed at 130 lux light intensity in a neutral testing cage constructed of gray Perspex (30x30x30cm) with fresh sawdust on the ground. Each mouse was individually habituated to the testing cage for 10 min over 2 consecutive days. On

the third day, pairs of unfamiliar mice of the same genotype were placed into the testing cage and allowed to interact for 10 min. Encounters were scored by a trained observer from videotapes of the sessions. The time (s) spent in close contact was registered (Dere et al., 2014).

### 5.10.6 Statistical analyses

Data presented in figures and tables are expressed as mean $\pm$ SEM. Behavior data was analyzed with one-way ANOVA with and without repeated measures. Bonferroni-post hoc tests for pairwise group comparisons were performed in case of significant main effect of genotype. Within-group comparisons were performed with t-tests for dependent samples. All statistics were performed using SPSSv.17 (IBM; New York City, New York, USA). All p values are 2-tailed and considered to be significant if  $<0.05$ .

### 5.11 Analysis of $\gamma$ -oscillations

Hippocampal  $\gamma$ -oscillations are generated by fast-spiking Parv<sup>+</sup> interneurons which are the primary ErbB4-expressing cell population (Bartos et al., 2007; Neddens and Buonanno, 2010). As a collaboration with Prof. Dr. JeonSeop Rhee and Dr. Bekir Altas (MPI-EM, Department of Neurobiology) to investigate if NRG1 type 1/ErbB4 hyperstimulation produces an alteration in  $\gamma$ -oscillatory frequencies, 100 nM kainate application was used to induced  $\gamma$ -oscillations. An interface recording chamber (BSCBU Base Unit with the BSC-HT Haas Top, Harvard Apparatus) with a constant flow of ACSF at 33°C, was used to record these oscillations in the CA3 region of the hippocampus. For this purpose, extracellular recording electrodes (with a resistance between 2.0-3.0 m $\Omega$ ) filled with ACSF solution were placed on the CA3 pyramidal cell layer of slices perfused constantly with the same solution. Baseline recordings were performed before kainate application for 10 min. Oscillatory recordings were performed for 20 min upon perfusion with 100 nM kainate solution. In order to find the maximum oscillations, electrodes were then re-positioned and slices were recorded for additional 20 min with kainate solution application. 700B amplifier (Axon Instruments, Molecular Devices) and Digidata 1440A data acquisition system (Axon Instruments, Molecular Devices) with a Bessel filter at 3 kHz were used to perform measurements. Data analysis was performed using Axograph X software (Axon Instruments). The power spectrum from each trace was calculated for 10 min epochs. Baseline power spectrum was subtracted from the power spectrum of kainate-induced oscillatory recording. The frequency at maximum power peak, average power, area power and maximum power were determined between 25-45 Hz oscillatory frequency band.

T-tests were performed using GraphPad Prism software. Data presented in figures are expressed as mean $\pm$ SEM.



## 5.12 Primary neuronal culture

### 5.12.1 Preparation and maintenance

Primary cortical neurons were prepared from E16 C57Bl/6N mice and hippocampal primary neurons from E18 C57Bl/6N mice. Cells were grown on poly-L-lysine (PLL) coated coverslips (24 wells plates for cortical neurons, 12 wells plates for hippocampal neurons). The day before dissection, coverslips (13 mm or 18 mm according to the plate size) were treated for 2 h with 65 % nitric acid on a roll incubator (50 ml falcon tube, closed with parafilm). Then they were washed 4 times with ddH<sub>2</sub>O (10 min each), two times with 70 % ethanol, and placed on petri dishes covered with filter paper for 1h at 60 °C to dry. Afterwards, coverslips were placed under UV light for 30 min under the sterile hood. Finally, they were sorted in 24 wells plates and 0.5 ml of PLL in borate buffer were added to each well and left ON at 37 °C.

On the dissection day, at least 2 h before dissection, 20 ml of NBM 10 % FBS and enough plating medium were placed in an incubator (37 °C, 5 % CO<sub>2</sub>) to warm the media and to adjust the pH. The PLL was removed from the plates (can be re-used up to 3 times) and they were washed three times with 1x PBS. 0.5 ml of HBSS were added to each well and plates were transferred to the incubator for 1 h. Afterwards, HBSS was removed, half of the final volume of plating medium was added to the plates, and they were transferred to the incubator until dissection. Immediately before dissection 1 ml Neurobasal media was mixed with 40 µl Papain, 10 µl DNaseI (10 mg/ml), and 10 µl L-cysteine. The solution was incubated at 37 °C (water bath) to activate the Papain (at least 10 min before use).

Dissection tools were cleaned with 70 % EtOH. Cold HBSS was added to three petri dishes and to one 15 ml falcon tube. A pregnant mouse was sacrificed outside the cell culture room by cervical dislocation and decapitation and sprayed with 70 % EtOH. The abdomen was opened with a scissor, the uterus was isolated and embryos were transferred into the first HBSS containing petri dish, and taken to the cell culture room. The uterus was opened and embryos were quickly decapitated. Heads were transferred to the second petri dish and kept on ice. Using two forceps, the head was placed onto a lid of a petri dish and the skull was removed. The brain was transferred to the third petri dish using a spoon. The rest of the dissection was performed under a stereo dissecting microscope. Hemispheres were separated, meninges removed (critical step to prevent contamination of non-neuronal cells), and hippocampi (E18) or cortices (E16) were dissected and transferred to the 15 ml falcon tube. Then the tissue was washed twice in 10 ml HBSS with a Pasteur pipette (HBSS was removed when tissue was in the bottom of the tube). HBSS was slowly removed (everything, using a 1000µl pipette to remove the last ml) and 1 ml of activated Papain was added. An incubation of 13 min at RT was performed, inverting the tube every 5 min. 10 ml of NBM 10 % FBS (from the incubator) were added to stop the Papain treatment. Medium was removed

when the tissue was settled at the bottom of the falcon tube. 10 ml of NBM 10 % FBS were added and aspirated again. 2 ml of pre-warmed plating medium were added to the tissue. It was triturated with a P1000 pipette by gently pipetting up and down close to the bottom of the tube (up to 10 times). The cell suspension was pipetted through a Cell strainer into a new 50 ml falcon tube. 10  $\mu$ l of the cell suspension were diluted with 90  $\mu$ l medium and cells were counted in a Neubauer Chamber (only the bright round cells). Cells were diluted with plating medium to the desired cell density and then plated and incubated in a cell culture incubator. The hood, dissection place, and dissection tools were immediately cleaned.

On the next day, the medium was changed to a serum-free medium to prevent overgrowth of astrocytes. 2 h before the medium replacement, the culture medium was transferred to the incubator (37 °C, 5 % CO<sub>2</sub>). The medium was changed plate-by-plate (one plate at a time was taken out of the incubator) with a P1000 pipette. The complete medium was slowly removed from each well and immediately replaced by new medium. One third of the medium was replaced with fresh, warm and pH adjusted culture medium every 3 days.

### **5.12.2 Treatment, fixation and staining procedure of primary neurons**

After 12 DIV, cells were treated with 20 ng/ml of the Glutathione-S-transferase (GST)-fused EGF-like domain of Neuregulin-2 (GST-NRG2  $\beta$ ) (provided by Dr. Cary Lai, Indiana University) for 24h. GST (20 ng/ml) diluted in 1x PBS was added to controls. Afterwards, cells were treated 10  $\mu$ M Spironolactone (Sigma-Aldrich, S3378), 10  $\mu$ M Lapatinib (Lapatinib ditosylate, Axon, 1395) or DMSO (added to controls, as drugs were dissolved and diluted in DMSO) for 24 h. Three coverslips were used for each treatment.

Cells were gently washed three times by adding and removing 1x PBS (50  $\mu$ l per coverslip), fixed in cold 4 % PFA for 20 min, and permeabilized in 100 % MetOH (pre-cooled at -20 °C) for 5 min. Then, cells were washed three times in 1x PBS, and blocked in fish gelatin blocking buffer (2 % FCS, 2 % GS, 2 % fish gelatin in 1x PBS) for 1 h at room temperature.

The p-HER4/ErbB4 antibody (Tyr1284, rabbit, Cell Signaling, 4757) was diluted 1:500 in 10 % fish gelatin blocking buffer, and cells were incubated ON at 4 °C. On the next day, cells were washed three times in 1x PBS. The secondary antibody and Dapi (1:2000) were diluted in 5 % fish gelatin blocking buffer, and cells were incubated for 2h at RT. Finally, coverslips were washed three times in 1x PBS, mounted on microscope slides, and sealed with Aqua-PolyMount. Slides were stored at 4 °C before imaged.

For quantification of ErbB4 phosphorylation levels, images of fluorescently labeled cells were obtained using an Observer Z.1 microscope (Zeiss). From a total of 15 images per treatment (five images per coverslip), the fluorescence of 300 cells (20 cells per image) was quantified using the ImageJ software.

## 5.13 Generation of conditional NRG2 transgenic mice

### 5.13.1 Molecular cloning

#### Generation of chemical competent *E. coli* (XL-1 blue)

*E. coli* XL-1 blue cells were grown in 4 ml LB medium with tetracycline (10 µg/ml) ON at 37 °C with gentle shaking. 200 ml LB-tetracycline media was inoculated with the bacterial culture and grown at 37°C with gentle shaking until OD600 ~0.5. The culture was centrifuged at 5000 xg for 10 min at 4 °C. The supernatant was removed and the bacterial pellet was washed with 80 ml “TB jap” containing 2 % DMSO. A second centrifugation step was performed (10 min at 5000 xg, 4 °C). Afterwards, the pellet was resuspended in 18 ml of “TB jap” containing 7 % DMSO and incubated on ice for 10 min. 100 µl aliquots of bacterial cells were stored at -80 °C. The competence of the cells was  $4 \times 10^7 - 1 \times 10^8$  /µg pUC18 DNA.

#### Transformation of XL1 blue

Competent *E.coli* (100 µl aliquots) were kept on ice. After 10 min 1 µl of plasmid (50-150 ng) was added without mixing, and left on ice for 20 min. Afterwards, bacteria were heat shocked for 30 s at 42 °C and incubated on ice for 5 min. 500 µl of SOC medium was added and incubated for 45 min at 37 °C with constant agitation (1200 rpm, Thermomixer Comfort Eppendorf). 200 µl of the bacterial suspension was plated onto LB plates supplemented with the appropriate antibiotic and incubated ON at 37 °C. Falcon tubes (50 ml) containing 10 ml of LB medium and the proper antibiotic were inoculated with bacterial clones and incubated ON at 37 °C with gentle shaking.

#### Plasmid isolation and purification

##### Small scale DNA purification “mini prep”

Plasmid DNA was purified using a modified 'alkaline lysis' protocol (Bimboim and Doly, 1979) followed by purification with a NucleoSpin® Plasmid kit according to the manufacturer's protocol (Macherey-Nagel).

##### Large scale DNA purification “maxi/midi prep”

Plasmid DNA was purified using the NucleoBond PC500 EF Maxi kit (Macherey-Nagel) based on an 'alkaline lysis' procedure (Bimboim and Doly, 1979) according to the manufacturer's protocol (Macherey-Nagel). Plasmid pellets were resuspended in 300-500 µl endotoxin free ddH<sub>2</sub>O.

### **DNA restriction, dephosphorylation and purification**

50 µl reactions with ~500-1000 ng of DNA were set up. Incubation was performed at 37 °C (2 h to ON depending on the enzyme) with 1-10 units of the enzyme and optimal buffer conditions. Restriction enzymes were inactivated by incubation at 65 °C for 20 min. Digestions were loaded onto agarose gels and fragments purified from gels as described below.

To prevent the re-ligation of digested plasmids, 5'-phosphoryl groups were removed by Antarctic Phosphatase (NEB). 1 µl of the enzyme (5000 U/ml) and 5 µl of 10x Antarctic Phosphatase buffer were added to the digested DNA and incubated at 37 °C for 30 min. Afterwards, the phosphatase was inactivated at 70 °C for 5 min. For isolation and purification of DNA fragments up to 10 kb, the QIAquick Gel Extraction kit (QIAGEN) was used. For this purpose, the DNA product was run on a 0.8-1 % agarose gel in TAE buffer, as described above. The desired DNA fragment was visualized by UV light, cut out of the gel and placed into a safe lock tube. DNA fragments were isolated from agarose following the procedure described in the manufacturer's protocol. Finally, the DNA was eluted in 25 µl of prewarmed ddH<sub>2</sub>O (70 °C) and quantified. DNA fragments >10 kb were purified using NucleoSpin Gel and PCR Clean-up kits (Macherey-Nagel), following manufacturer's specifications.

### **DNA ligation**

20 µl ligation reactions were set up with a molar ratio of 1:5 (vector:insert). 1 µl of T4 DNA ligase (Promega) and 2 µl of 10x buffer ligase were added to the reaction. Ligation was carried out ON at 4 °C, followed by an inactivation step of 10 min at 70 °C. Reactions were used to transform competent cells.

### **DNA sequencing**

DNA samples were sequenced at the sequencing facility of the Max-Planck-Institute of Experimental Medicine. 16 µl of DNA samples (100 ng/µl) were diluted in ddH<sub>2</sub>O and submitted for sequencing together with primer information. Sequences were analyzed using BioEdit Sequence Alignment Editor, SnapGene software and BLAST at National Centre for Biotechnology Information (NCBI) (<http://www.ncbi.nlm.nih.gov/blast/Blast.cgi>).

### **Cloning of conditional NRG2 ROSA locus targeting vectors**

Wildtype mouse NRG2 cDNA (NCBI Reference Sequence: XM\_006525461.3; in pEGFP-N1) was kindly provided by Dr. Cary Lai (Indiana University) and confirmed by sequencing. XL-1 blue and dam<sup>r</sup>/dcm<sup>r</sup> competent cells (NEB) cells were transformed and a miniprep was performed to recover the plasmid. PCR with primers containing restriction sites for FseI (forward: 5'-ataggccgcccATGAGGCGCGACCCGG-3') and PacI (reverse: 5'-gttaattaaTTAGAGGGGCCCGAGTCCTGC-3') were used to amplify and subclone NRG2 cDNA into a ROSA

locus targeting vector (pROSA; kindly provided by Dr. Amit Agarwal; John Hopkins University, Baltimore). PCR reactions of 12.5  $\mu$ l were prepared with 0.62  $\mu$ l of each primer (1 pM), 11.5  $\mu$ l ddH<sub>2</sub>O, 2.5  $\mu$ l 5x AccuPrime™ GC-Rich Buffer A, 5  $\mu$ l pEGFP-NRG2 (10 ng/ $\mu$ l), and 0.5  $\mu$ l AccuPrime™ GC-Rich DNA Polymerase (2U/ $\mu$ l). The thermal profile of the PCR reaction was the following:

1. 95 °C 3 min
2. 95 °C 30 s
3. 60 °C 30 s
4. 72 °C 2.25 min
- 2 to 4 for 30 cycles
5. 72 °C 10 min
7. 4 °C pause

For subcloning pEGFP-N1- NRG2 and pROSA minipreps were prepared from *dam*<sup>-</sup>/*dcm*<sup>-</sup> cells. Digestion reactions with 2  $\mu$ l FseI (2 U/ $\mu$ l; sensible to *dcm* methylation; NEB) and 1  $\mu$ l PaeI (10 U/ $\mu$ l; NEB) were performed ON at 37 °C. After 10 h incubation, 1  $\mu$ l extra of FseI was added to the reaction and incubation was performed for two more hours. After subcloning as described above, pROSA-NRG2 was confirmed by sequencing. A mouse NRG2 cDNA sequence harboring two HA epitope tags located 3' to the NRG2 propeptide sequence as well as 5' FseI and 3' PaeI restriction sites for cloning into pROSA was designed. The composition of the sequence was: 5'-NheI-BamHI-FseI-Kozac-NRG2 propeptide-HA-HA-NRG2 cDNA-PaeI-XbaI-HindIII-3', and its synthesis and subcloning into a pcDNA3.1(+) vector (cloning site: NheI-HindIII) was ordered at GenScript®. The construct (pcDNA3.1-2HA-NRG2) was confirmed by sequencing and a miniprep was produced following transformation into *dam*<sup>-</sup>/*dcm*<sup>-</sup> cells. A restriction digest was performed with FseI and PaeI to subclone 2HA-NRG2 into the pROSA vector (as described above). pROSA-2HA-NRG2 was confirmed by restriction digestion and sequencing.

### **5.13.2 Embryonic stem (ES) cell culture, electroporation, preparation for blastocyst injection**

The procedure described in this section was performed in the Department of Neurobiology at the Max-Planck-Institute of Experimental Medicine under the supervision of Dr. Noa Lipstein. It is based on previous protocols developed in this department and primarily derived from the Allan Bradley lab. or from [www.cellmigration.org](http://www.cellmigration.org). MEFs and ES (OLA/129) cells were obtained from the Department of Neurobiology.

### Establishment of feeder culture or mouse embryonic fibroblasts (MEFs)

MEFs were thawed at RT and MEF medium (up to 5 ml) was added dropwise under constant mixing. Cells were centrifuged for 5 min at 900 rpm. The supernatant was removed, cells were resuspended in 1 ml of medium and transferred to a T75 flask (previously coated with 0.1 % gelatin). After 2-3 days cells were confluent and split by adding 0.05 % Trypsin and incubating for 5 min at 37 °C. Afterwards, MEF medium was added to inactivate Trypsin (8 ml for T75, 10 ml for T175), and cells were gently triturated to break up the clumps. The cells were transferred to new gelatinized flasks containing the necessary volume of medium (T75 total volume: 10ml; T175 total volume: 20ml).

MEFs were used as feeders for ES cells after mitomycin C treatment to avoid MEFs to overgrow ES cells. Inactivation was performed the day before ES cell splitting. Mitomycin C was added to the flasks (from a 0.5 mg/ml stock 200 µl for T75, 400 µl for T175). Flasks were returned to the incubator for 2.5 h. The medium was collected to discard mitomycin C appropriately. Three washes with 1x PBS were performed, the first two were collected with the mitomycin waste. 0.05 % Trypsin was added as described above, and cells were split according to the intended passaging ratio. From a confluent T175 flask with 20 ml of cells after splitting, the cells were plated as follows:

Type of plate	Amount of cells per well (ml)	Volume of medium (ml)	Plates per T175 flask
10 cm plate	3.2	7	6
96 wells plate	0.05	0.1	4
24 wells plate	0.4	0.6	2
6 wells plate	1.6	4.4	2
T75	10	No additional medium	2

MEFs that were not to be split or inactivated, were frozen. The medium was removed and cells were washed with 1x PBS. 0.05 % Trypsin was added, as for regular passaging. One volume of MEF medium was added and cells were gently triturated with a 1 ml pipette. Cells were transferred to a 15 ml Falcon tube, more medium (up to 5 ml) was added and cells were centrifuged for 5 min at 900 rpm. The supernatant was removed and cells were resuspended in 500 µl of MEF medium. 500 µl of 2x freezing medium was added dropwise and the solution was mixed after each addition. Cells were transferred to freezing vial, placed into a freezing container (filled with isopropanol) at -80 °C ON and stored in cryoboxes at -80 °C.

### Thawing of ES cells

ES cells were thawed at RT, ES medium (up to 5 ml) was added dropwise (every 5-10 s) under constant mixing, and cells were centrifuged for 3 min at 900 rpm. The supernatant was removed, cells were resuspended in 1 ml of medium, and transferred to a 10 cm plate with inactivated MEFs covered with ES medium (4 ml). ES medium was replaced twice per day by removing medium, washing with 1x PBS and adding 4 ml of ES medium.

### Expansion of ES cells

ES cells were split when they were still in their exponential growth phase (around 80 % confluence). The medium was changed 3-4 h before splitting. After washing the cells with 1x PBS, 0.25 % trypsin was added as follows:

Type of plate	Volume of trypsin (ml)	Volume of medium for inactivation (ml)
10 cm plate	3	4
96 wells plate	0.04	0.1
24 wells plate	0.16	0.64
6 wells plate	0.64	2.6

Cells were incubated for 15 min at 37 °C. Afterwards, ES medium was added for inactivation as mentioned above. Cells were gently but properly triturated with a pipette to break up the clumps. This was critical as clumps differentiate rapidly, and thus do not have to be passaged. The first 10 cm dish was split (1:3) three days after cells were thawed. After 2 additional days ES cells were split in a ratio of 1:2, to obtain six 10 cm plates the day before electroporation.

### Preparation of DNA for electroporation

Three maxipreps were performed to obtain sufficient DNA for electroporation. The plasmid was linearized with *Asi*I. For this purpose, five restriction digests of 500 µl each were set up with 50 µg of the plasmid pROSA-2HA-NRG2, 50 µl of 10x CutSmart buffer, 5 µl of the enzyme (10 U/µl), and water up to 50 µl, incubated ON at 37 °C, and inactivated 20 min at 80 °C. 2 µl of each reaction were run on a 0.7 % TAE Agarose gel. To purify DNA, 500 µl phenol and one drop of chloroform were added to each tube. A centrifugation step of 15 min at RT and maximum speed was performed. The upper phase was transferred to clean tubes. These two steps were repeated twice. 500 µl of chloroform were added and centrifuged again (repeated 4x). Sodium acetate was added (final concentration 0.25 M). After vigorous mixing, 2 volumes of 100 % ethanol were added. Tubes were manually mixed and placed at -20 °C ON. The next

day, tubes were centrifuged at maximum speed for 15 min at 4 °C. The following steps were performed under the hood. Pellets were washed twice with 1 ml of 70 % ethanol and left open to dry for 30 min. 50 µl of filtered sterile 0.1x TE was added and incubated for 30 min at 37 °C and 300 rpm. The five aliquots were pooled. 186 µg of the linearized construct were obtained, which was sufficient for 7 electroporations.

### **Electroporation of ES cells**

A 1:2 passage of ES cells was performed the day before electroporation, this resulted in six 10 cm plates for electroporation. The medium was changed 3 h before electroporation. Next, cells were triturated as described above, transferred to two 50 ml Falcon tubes and centrifuged for 7 min at 800 rpm. The supernatant was removed and cells were resuspended in 10 ml 1x PBS. A 1:10 dilution was made to count cells. Cells were centrifuged again for 3 min at 800 rpm, the supernatant was removed and cells were resuspended in 6 ml 1x PBS to obtain 11 million cells/ml. Linearized pROSA-2HA-NRG2 was split in half and added to each Falcon tube. Cells were mixed and left at RT for 5 min. 0.9 ml of the mix was transferred to an electroporation cuvette and placed on ice for 2 min. The BioRad GenePulser was set to 230 and 500 µF, and electroporation was performed. Cuvettes were left at RT for 5 min. Cells from each cuvette were plated onto 10 cm dishes with inactivated MEFs.

### **Positive and negative selection of targeted ES cells**

After electroporation, G418 was added to ES medium at a final concentration of 180 µg/ml. The medium was replaced twice per day. The pROSA-2HA-NRG2 construct also contained a negative selection marker, a DTA (diphtheria toxin A) cassette, which is placed outside of the homologous arms and is normally lost during homologous recombination. In the case of a random integration event, it inhibits protein synthesis. This negative selection required no additional drug treatment.

### **Picking of ES cell clones**

Six days after electroporation 10 cm dishes with electroporated ES cells contained colonies at very high density. Therefore, two of the plates were split 1:3. These 6 new plates were left to grow for four days, with medium changes twice a day. When individual colonies were observable colonies were transferred to 96 well plates with inactivated MEFs. For colony picking, a microscope was cleaned and moved into the tissue culture hood. A 96 well plate with round bottom was filled with 25 µl of 0.25 % trypsin per well and placed on ice. ES medium was removed, 10 ml of 1x PBS was added, and the plate was placed under the microscope. Colonies were picked with a P10 pipette (set to 5 µl) and transferred to 96 well plates. Following



picking, plates were incubated for 15 min at 37 °C. Next, 25 µl of ES medium was added to each well and cells were gently triturated with a multichannel pipette. The cell suspension was then transferred to a 96 well plate with feeders. Three days later, when cells reached 80 % confluence (medium was turning orange a few hours after feeding), cells were washed with 1x PBS, 50 µl of trypsin was added and plates were incubated as described before. 100 µl of ES medium was added to inactivate trypsin and triturated. 100 µl of the cell suspension was transferred to two (50 µl each) new 96 wells plates with inactivated MEFs. 50 µl of the cells were transferred to two (25 µl each) 96 well plates without feeders, that were used for DNA isolation. When plates reached 80 % confluence, they were frozen or processed for DNA isolation.

### **Freezing of ES cells in 96 well plates**

The medium was changed 3-4 h before freezing. Two washing steps with 1x PBS were performed. 50 µl of trypsin was added to each well and plates were incubated as before. Afterwards, 50 µl of 2x freezing medium was added to each well and cells were gently triturated. 100 µl sterile-filtered paraffin oil was added on top of the cells. This prevented degassing and evaporation during storage at -80 °C. Plates were sealed with parafilm, placed into a polystyrene box, and transferred to -80 °C. This resulted in slow freezing, and a temperature drop of approximately 1 °C/min.

### **Preparation of 96 well plates for DNA isolation**

Once cells in gelatin plates reached 80 % confluence, DNA was isolated. Plates were washed twice with 1x PBS. 50 µl of lysis buffer (10 mM Tris pH7.5, 10 mM EDTA pH8, 10 mM NaCl, 0.5 % Sarcosyl, 1 mg/ml Proteinase K) were added to each well. Plates were sealed with parafilm and transferred to a humidified chamber where they were incubated ON at 60 °C. On the next day, a fresh solution of 75 mM NaCl in ethanol was prepared, and 100 µl of the NaCl/ethanol solution was added to each well. Plates were stored ON at -20 °C. Precipitated DNA stuck to the bottom of the plate and plates were inverted to discard the solution. 100 µl of 70 % ethanol were added to each well, and the plates were inverted again. This step was repeated 3 times. After the final wash, plates were inverted and allowed to air-dry. Finally, 100 µl 0.1x TE was added to each well and plates were incubated ON at 37 °C.

### **Thawing and expansion of positive clones**

A plate containing 8 homologous recombinant clones was thawed, and these clones were expanded together with four non-homologous recombinant controls. The 96 well plate was transferred from the -80 °C freezer to the 37 °C incubator for 20 min. Mineral oil was removed

from the wells containing the clones that were to be expanded. The clones were transferred to a 24 well plate with inactivated MEFs. Once cells reached 80 % confluence, they were transferred to 6 well plates. Positive clones were split 1:3 once they reached proper confluence. 200  $\mu$ l of all clones (including controls) were transferred to 6 well plates with gelatin for DNA isolation and re-confirmations. The rest of the cell suspensions from negative clones were frozen in freezing vials as previously described. Once triplicates of positive clones reached 80 % confluence, they were frozen in freezing vials.

### **Preparation of homologous recombinant ES cells for blastocyst injection**

Two homologous recombinant clones were chosen for blastocyst injection (based on cell quality before freezing) and reconfirmed by PCR. Cells were thawed and transferred to one well of a 6 well plate (with feeders) 5 days before injection. The medium was changed twice per day. Two days after plating, cells were split 1:3, in 3 wells of a 6 well plate (with feeders), 24 h before injection, cells from one well were split 1:2 and cells in the other two wells were frozen. On injection day, the medium was changed 3-4 h before injection. Cells were washed twice with 1x PBS, 640  $\mu$ l trypsin were added and incubated for 15 min at 37 °C. Afterwards, 1 ml of ES medium was added and cells were gently triturated. The cell suspension was transferred to a 15 ml Falcon tube, medium was added up to 5 ml and cells were centrifuged for 5 min at 900 rpm. The supernatant was removed, cells resuspended in 1 ml of ES cell medium, transferred to a screw-cap tube, placed on ice and taken to the animal facility of the Max-Planck-Institute of Experimental Medicine where injections into C57Bl/6N blastocysts were performed.

#### **5.13.3 PCR-based strategy for ES cell clone screening**

Primers for amplification of the ROSA locus short arm in pROSA-2HA-NRG2 were designed to confirm the correct integration of the construct into the ROSA locus by PCR. The forward primer was located in an endogenous sequence of the mouse genome (upstream of the short arm of the ROSA locus), and the reverse primer aligned within the CAG hybrid promoter. PCR reactions of 12.5  $\mu$ l were prepared with 0.25  $\mu$ l (10  $\mu$ M) of forward primer (5'-GGCAAAGGAATCCAGGTATAGACAAAACC-3'), 0.25  $\mu$ l (10  $\mu$ M) of reverse primer (5'-TATTGGCGTTACTATGGGAACATACGTCAT-3'), 7  $\mu$ l ddH<sub>2</sub>O, 2.5  $\mu$ l 5x MyFi Buffer, 2  $\mu$ l genomic ES cell DNA, and 0.5  $\mu$ l (2U/ $\mu$ l) MyFi™ DNA polymerase (Bioline). The thermal profile of the PCR reaction was the following:

1. 95 °C 3 min
2. 95 °C 30 s
3. 58 °C 30 s

4. 72 °C 2.5 min  
→ 2 to 4 for 35 cycles
5. 72 °C 7 min
7. 4 °C pause

For the implementation of the PCR and as a control, the forward primer was used in a PCR reaction together with a reverse primer located in the long arm of the ROSA locus (5'-TGTCTGGTTTCATGAGTCATCAGACTTCT-3'). This reaction amplified a product only if the construct was not integrated between the two primer sites. Because homologous recombination took place in one chromosome, all cells (homologous and non-homologous recombinant, as well as wildtype) were to be positive for this PCR. Besides the reverse primer, the rest of the conditions in this reaction remained the same as in the homologous recombinant PCR.

## 6 References

- Agarwal, A., Dibaj, P., Kassmann, C. M., Goebbels, S., Nave, K. A., and Schwab, M. H. (2012). In vivo imaging and noninvasive ablation of pyramidal neurons in adult NEX-CreERT2 mice. *Cereb. Cortex* 22, 1473–1486. doi:10.1093/cercor/bhr214.
- Agarwal, A., Zhang, M., Trembak-Duff, I., Unterbarnscheidt, T., Radyushkin, K., Dibaj, P., et al. (2014). Dysregulated expression of neuregulin-1 by cortical pyramidal neurons disrupts synaptic plasticity. *Cell Rep.* 8, 1130–1145. doi:10.1016/j.celrep.2014.07.026.
- Agim, Z. S., Esendal, M., Briollais, L., Uyan, O., Meschian, M., Martinez, L. A. M., et al. (2013). Discovery, validation and characterization of Erbb4 and Nrg1 haplotypes using data from three genome-wide association studies of schizophrenia. *PLoS One* 8, e53042. doi:10.1371/journal.pone.0053042.
- Akbarian, S., Kim, J. J., Potkin, S. G., Hagman, J. O., Tafazzoli, A., Bunney Jr., W. E., et al. (1995). Gene expression for glutamic acid decarboxylase is reduced without loss of neurons in prefrontal cortex of schizophrenics. *Arch Gen Psychiatry* 52, 258–266. doi:10.1001/archpsyc.1995.03950160008002.
- Alexander, G. M., Farris, S., Pirone, J. R., Zheng, C., Colgin, L. L., and Dudek, S. M. (2016). Social and novel contexts modify hippocampal CA2 representations of space. *Nat. Commun.* 7, 10300. doi:10.1038/ncomms10300.
- Allen, C. B., Celikel, T., and Feldman, D. E. (2003). Long-term depression induced by sensory deprivation during cortical map plasticity in vivo. *Nat. Neurosci.* 6, 291–299. doi:10.1038/nn1012.
- Anton, E. S., Marchionni, M. A., Lee, K. F., and Rakic, P. (1997). Role of GGF/neuregulin signaling in interactions between migrating neurons and radial glia in the developing cerebral cortex. *Development* 124, 3501–3510.
- Antonucci, D. E., Lim, S. T., Vassanelli, S., and Trimmer, J. S. (2001). Dynamic localization and clustering of dendritic Kv2.1 voltage-dependent potassium channels in developing hippocampal neurons. *Neuroscience* 108, 69–81. doi:10.1016/S0306-4522(01)00476-6.
- Arasada, R. R., and Carpenter, G. (2005). Secretase-dependent tyrosine phosphorylation of Mdm2 by the ErbB-4 intracellular domain fragment. *J. Biol. Chem.* 280, 30783–30787. doi:10.1074/jbc.M506057200.
- Arseneault, L., Cannon, M., Poulton, R., Murray, R., Caspi, A., and Moffitt, T. E. (2002). Cannabis use in adolescence and risk for adult psychosis: longitudinal prospective study. *BMJ* 325, 1212–1213. doi:10.1136/bmj.325.7374.1212.
- Athanasios, L., Mattingsdal, M., Kähler, A. K., Brown, A., Gustafsson, O., Agartz, I., et al. (2010). Gene variants associated with schizophrenia in a Norwegian genome-wide study are replicated in a large European cohort. *J. Psychiatr. Res.* 44, 748–753. doi:10.1016/j.jpsychires.2010.02.002.

- Badner, J., and Gershon, E. (2002). Meta-analysis of whole-genome linkage scans of bipolar disorder and schizophrenia. *Mol. Psychiatry* 7, 405–411. doi:10.1038/sj/mp/4001012.
- Bahn, S. (2002). Gene expression in bipolar disorder and schizophrenia: new approaches to old problems. *Bipolar Disord.* 4 Suppl 1, 70–72. doi:10.1034/j.1399-5618.2002.40104.x.
- Baldan Ramsey, L. C., Xu, M., Wood, N., and Pittenger, C. (2011). Lesions of the dorsomedial striatum disrupt prepulse inhibition. *Neuroscience* 180, 222–228. doi:10.1016/j.neuroscience.2011.01.041.
- Bao, J., Lin, H., Ouyang, Y., Lei, D., Osman, A., Kim, T.-W. W., et al. (2004). Activity-dependent transcription regulation of PSD-95 by neuregulin-1 and Eos. *Nat. Neurosci.* 7, 1250–1258. doi:10.1038/nn1342.
- Bao, J., Wolpowitz, D., Role, L. W., and Talmage, D. A. (2003). Back signaling by the Nrg-1 intracellular domain. *J. Cell Biol.* 161, 1133–1141. doi:10.1083/jcb.200212085.
- Barak, B., and Feng, G. (2016). Neurobiology of social behavior abnormalities in autism and Williams syndrome. *Nat. Neurosci.* 19, 647–655.
- Barros, C. S., Calabrese, B., Chamero, P., Roberts, A. J., Korzus, E., Lloyd, K., et al. (2009). Impaired maturation of dendritic spines without disorganization of cortical cell layers in mice lacking NRG1/ErbB signaling in the central nervous system. *Proc. Natl. Acad. Sci. U. S. A.* 106, 4507–4512. doi:10.1073/pnas.0900355106.
- Bartos, M., Vida, I., and Jonas, P. (2007). Synaptic mechanisms of synchronized gamma oscillations in inhibitory interneuron networks. *Neuroscience* 8, 45–56.
- Baulida, J., Kraus, M. H., Alimandi, M., Di Fiore, P. P., and Carpenter, G. (1996). All ErbB receptors other than the epidermal growth factor receptor are endocytosis impaired. *J. Biol. Chem.* 271, 5251–5257. doi:10.1074/jbc.271.9.5251.
- Benes, F. M., McSparren, J., Bird, E. D., SanGiovanni, J. P., and Vincent, S. L. (1991). Deficits in small interneurons in prefrontal and cingulate cortices of schizophrenic and schizoaffective patients. *Arch. Gen. Psychiatry* 48, 996–1001. doi:10.1001/archpsyc.1991.01810350036005.
- Benzel, I., Bansal, A., Browning, B. L., Galwey, N. W., Maycox, P. R., McGinnis, R., et al. (2007). Interactions among genes in the ErbB-neuregulin signalling network are associated with increased susceptibility to schizophrenia. *Behav. Brain Funct.* 3, 31. doi:10.1186/1744-9081-3-31.
- Bertram, I., Bernstein, H.-G., Lendeckel, U., Bukowska, A., Dobrowolny, H., Keilhoff, G., et al. (2007). Immunohistochemical evidence for impaired neuregulin-1 signaling in the prefrontal cortex in schizophrenia and in unipolar depression. *Ann. N. Y. Acad. Sci.* 1096, 147–156. doi:10.1196/annals.1397.080.
- Biassoni, R., and Raso, A. (2014). *Quantitative real-time PCR: methods and protocols*. Humana Press.

- Bimboim, H. C., and Doly, J. (1979). A rapid alkaline extraction procedure for screening recombinant plasmid DNA. *Nucleic Acids Res.* 7, 1513–1523. doi:10.1093/nar/7.6.1513.
- Bishop, C., and Walker, P. D. (2003). Combined intrastriatal dopamine D1 and serotonin 5-HT2 receptor stimulation reveals a mechanism for hyperlocomotion in 6-hydroxydopamine-lesioned rats. *Neuroscience* 121, 649–657. doi:10.1016/S0306-4522(03)00516-5.
- Bjarnadottir, M., Misner, D. L., Haverfield-Gross, S., Bruun, S., Helgason, V. G., Stefansson, H., et al. (2007). Neuregulin1 (NRG1) signaling through Fyn modulates NMDA receptor phosphorylation: differential synaptic function in NRG1+/- knock-outs compared with wild-type mice. *J. Neurosci.* 27, 4519–4529. doi:10.1523/JNEUROSCI.4314-06.2007.
- Bosman, C. A., Lansink, C. S., and Pennartz, C. M. A. (2014). Functions of gamma-band synchronization in cognition: From single circuits to functional diversity across cortical and subcortical systems. *Eur. J. Neurosci.* 39, 1982–1999. doi:10.1111/ejn.12606.
- Bouhy, D., Geuens, T., De Winter, V., Almeida-Souza, L., Katona, I., Weis, J., et al. (2016). Characterization of new transgenic mouse models for two Charcot-Marie-Tooth-causing HspB1 mutations using the Rosa26 locus. *J. Neuromuscul. Dis.* 3, 183–200. doi:10.3233/JND-150144.
- Braff, D. L., and Geyer, M. A. (1990). Sensorimotor gating and schizophrenia. Human and animal model studies. *Arch Gen Psychiatry* 47, 181–188.
- Braff, D. L., Grillon, C., and Geyer, M. A. (1992). Gating and habituation of the startle reflex in schizophrenic patients. *Arch Gen Psychiatry* 49, 206–215.
- Bramon, E., and Sham, P. C. (2001). The common genetic liability between schizophrenia and bipolar disorder: a review. *Curr. Psychiatry Rep.* 3, 332–337. doi:10.1007/s11920-001-0030-1.
- Brinkmann, B. G., Agarwal, A., Sereda, M. W., Garratt, A. N., Müller, T., Wende, H., et al. (2008). Neuregulin-1/ErbB signaling serves distinct functions in myelination of the peripheral and central nervous system. *Neuron* 59, 581–595. doi:10.1016/j.neuron.2008.06.028.
- Britto, J. M., Lukehurst, S., Weller, R., Fraser, C., Qiu, Y., Hertzog, P., et al. (2004). Generation and characterization of neuregulin-2-deficient mice. *Mol. Cell. Biol.* 24, 8221–8226. doi:10.1128/MCB.24.18.8221-8226.2004.
- Brose, N. (1999). Synaptic cell adhesion proteins and synaptogenesis in the mammalian central nervous system. *Naturwissenschaften* 86, 516–524. doi:10.1007/s001140050666.
- Brus, R., Nowak, P., Szkilnik, R., Mokolajun, U., and Kostrzewa, R. M. (2004). Serotonergics attenuate hyperlocomotor activity in rats. Potential new therapeutic strategy for hyperactivity. *Neurotox. Res.* 6, 317–326.
- Buonanno, A., and Fischbach, G. D. (2001). Neuregulin and ErbB receptor signaling pathways

- in the nervous system. *Curr. Opin. Neurobiol.* 11, 287–296. doi:10.1016/j.conb.2015.04.003.
- Burgess, A. W., Cho, H. S., Eigenbrot, C., Ferguson, K. M., Garrett, T. P. J., Leahy, D. J., et al. (2003). An open-and-shut case? Recent insights into the activation of EGF/ErbB receptors. *Mol. Cell* 12, 541–552. doi:10.1016/S1097-2765(03)00350-2.
- Burgess, T. L., Ross, S. L., Qian, Y., Brankow, D., and Hu, S. (1995). Biosynthetic processing of neu differentiation factor. *J. Biol. Chem.* 270, 19188–19196.
- Burns, K. A., Ayoub, A. E., Breunig, J. J., Adhami, F., Weng, W. L., Colbert, M. C., et al. (2007). Nestin-CreER mice reveal DNA synthesis by nonapoptotic neurons following cerebral ischemia-hypoxia. *Cereb. Cortex* 17, 2585–2592. doi:10.1093/cercor/bhl164.
- Buxbaum, J. D., Georgieva, L., Young, J. J., Plescia, C., Kajiwara, Y., Jiang, Y., et al. (2008). Molecular dissection of NRG1-ERBB4 signaling implicates PTPRZ1 as a potential schizophrenia susceptibility gene. *Mol. Psychiatry* 13, 162–172. doi:10.1038/sj.mp.4001991.
- Buzsáki, G., and Draguhn, A. (2004). Neuronal oscillations in cortical networks. *Science* 304, 1926–1929. doi:10.1126/science.1099745.
- Cardno, A. G., and Gottesman, I. I. (2000). Twin studies of schizophrenia: From bow-and-arrow concordances to star wars Mx and functional genomics. *Am. J. Med. Genet. - Semin. Med. Genet.* 97, 12–17. doi:10.1002/(SICI)1096-8628(200021)97:1<12::AID-AJMG3>3.0.CO;2-U.
- Carraway, K. L., Weber, J. L., Unger, M. J., Ledesma, J., Yu, N., Gassmann, M., et al. (1997). Neuregulin-2, a new ligand of ErbB3/ErbB4-receptor tyrosine kinases. *Nature* 387, 512–516. doi:10.1038/387512a0.
- Chance, S. A., Walker, M., and Crow, T. J. (2005). Reduced density of calbindin-immunoreactive interneurons in the planum temporale in schizophrenia. *Brain Res.* 1046, 32–37. doi:10.1016/j.brainres.2005.03.045.
- Chattopadhyaya, B., and Di Cristo, G. (2012). GABAergic circuit dysfunctions in neurodevelopmental disorders. *Front. Psychiatry* 3, 51. doi:10.3389/fpsy.2012.00051.
- Chen, Y.-J., Zhang, M., Yin, D.-M., Wen, L., Ting, A., Wang, P., et al. (2010a). ErbB4 in parvalbumin-positive interneurons is critical for neuregulin 1 regulation of long-term potentiation. *Proc. Natl. Acad. Sci. U. S. A.* 107, 21818–21823. doi:10.1073/pnas.1010669107.
- Chen, Y., Hancock, M. L., Role, L. W., and Talmage, D. A. (2010b). Intramembranous valine linked to schizophrenia is required for neuregulin 1 regulation of the morphological development of cortical neurons. *J. Neurosci.* 30, 9199–9208. doi:10.1523/JNEUROSCI.0605-10.2010.
- Citri, A., Skaria, K. B., and Yarden, Y. (2003). The deaf and the dumb: The biology of ErbB-2

- and ErbB-3. *Exp. Cell Res.* 1, 54–65. doi:10.1016/B978-012160281-9/50005-0.
- Courtin, J., Chaudun, F., Rozeske, R. R., Karalis, N., Gonzalez-Campo, C., Wurtz, H., et al. (2014). Prefrontal parvalbumin interneurons shape neuronal activity to drive fear expression. *Nature* 505, 92–96. doi:10.1038/nature12755.
- Crovello, C. S., Lai, C., Cantley, C., Iii, K. L. C., Cantley, L. C., and Carraway, K. L. (1998). Differential signaling by the epidermal growth factor-like growth factors neuregulin-1 and Neuregulin-2. *J. Biol. Chem.* 273, 26954–26961. doi:10.1074/jbc.273.41.26954.
- Czeh, B., Simon, M., van der Hart, M. G., Schmelting, B., Hesselink, M. B., and Fuchs, E. (2005). Chronic stress decreases the number of parvalbumin-immunoreactive interneurons in the hippocampus: prevention by treatment with a substance P receptor (NK1) antagonist. *Neuropsychopharmacology* 30, 67–79. doi:10.1038/sj.npp.1300581.
- Dawson, E., and Murray, R. (1996). A gene at 6p? Schizophrenia. *Curr Biol* 6, 268–271.
- Deacon, R. M. J., Bannerman, D. M., Kriby, B. P., Croucher, A., and Rawlins, J. N. P. (2002). Effects of cytotoxic hippocampal lesions in mice on a cognitive test battery. *Behav. Brain Res.* 133, 57–68. doi:10.1016/S0166-4328(01)00451-X.
- Deakin, I. H., Law, A. J., Oliver, P. L., Schwab, M. H., Nave, K. A., Harrison, P. J., et al. (2009). Behavioural characterization of neuregulin 1 type I overexpressing transgenic mice. *Neuroreport* 20, 1523–1528. doi:10.1097/WNR.0b013e328330f6e7.
- Deakin, I. H., Nissen, W., Law, A. J., Lane, T., Kanso, R., Schwab, M. H., et al. (2012). Transgenic overexpression of the type i isoform of neuregulin 1 affects working memory and hippocampal oscillations but not long-term potentiation. *Cereb. Cortex* 22, 1520–1529. doi:10.1093/cercor/bhr223.
- Deardorff, A. S., Romer, S. H., Sonner, P. M., and Fyffe, R. E. W. (2014). Swimming against the tide: investigations of the C-bouton synapse. *Front. Neural Circuits* 8, 106. doi:10.3389/fncir.2014.00106.
- DeFelipe, J., and Fariñas, I. (1992). The pyramidal neuron of the cerebral cortex: morphological and chemical characteristics of the synaptic inputs. *Prog Neurobiol* 39, 563–607. doi:10.1016/0301-0082(92)90015-7.
- DeFelipe, J., López-Cruz, P. L., Benavides-Piccione, R., Bielza, C., Larrañaga, P., Anderson, S., et al. (2013). New insights into the classification and nomenclature of cortical GABAergic interneurons. *Nat. Rev. Neurosci.* 14, 202–216. doi:10.1038/nrn3444.
- del Pino, I., García-Frigola, C., Dehorter, N., Brotons-Mas, J., Alvarez-Salvado, E., Martínez de Lagrán, M., et al. (2013). ErbB4 Deletion from Fast-Spiking Interneurons Causes Schizophrenia-like Phenotypes. *Neuron* 79, 1152–1168. doi:10.1016/j.neuron.2013.07.010.
- Dere, E., Dahm, L., Lu, D., Hammerschmidt, K., Ju, A., Tantra, M., et al. (2014). Heterozygous *ambra1* deficiency in mice: A genetic trait with autism-like behavior restricted to the female



- gender. *Front. Behav. Neurosci.* 8, 181. doi:10.3389/fnbeh.2014.00181.
- Dere, E., Winkler, D., Ritter, C., Ronnenberg, A., Poggi, G., Patzig, J., et al. (2015). Gpm6b deficiency impairs sensorimotor gating and modulates the behavioral response to a 5-HT<sub>2A/C</sub> receptor agonist. *Behav. Brain Res.* 277, 254–263. doi:10.1016/j.bbr.2014.04.021.
- Du, J., Tao-Cheng, J. H., Zerfas, P., and McBain, C. J. (1998). The K<sup>+</sup> channel, Kv2.1, is apposed to astrocytic processes and is associated with inhibitory postsynaptic membranes in hippocampal and cortical principal neurons and inhibitory interneurons. *Neuroscience* 84, 37–48. doi:10.1016/S0306-4522(97)00519-8.
- Eilam, R., Pinkas-Kramarski, R., Ratzkin, B. J., Segal, M., and Yarden, Y. (1998). Activity-dependent regulation of Neu differentiation factor/neuregulin expression in rat brain. *Proc. Natl. Acad. Sci. U. S. A.* 95, 1888–1893. doi:10.1073/pnas.95.4.1888.
- Elenius, K., Choi, C. J., Paul, S., Santiestevan, E., Nishi, E., and Klagsbrun, M. (1999). Characterization of a naturally occurring ErbB4 isoform that does not bind or activate phosphatidylinositol 3-kinase. *Oncogene* 18, 2607–2615. doi:10.1038/sj.onc.1202612.
- Elenius, K., Corfas, G., Paul, S., Choi, C. J., Rio, C., Plowman, G. D., et al. (1997). A novel juxtamembrane domain isoform of HER4/ErbB4. Isoform-specific tissue distribution and differential processing in response to phorbol ester. *J. Biol. Chem.* 272, 26761–26768. doi:10.1074/jbc.272.42.26761.
- Emamian, E. S. (2012). AKT/GSK3 signaling pathway and schizophrenia. *Front. Mol. Neurosci.* 5, 33. doi:10.3389/fnmol.2012.00033.
- Emamian, E. S., Hall, D., Birnbaum, M. J., Karayiorgou, M., and Gogos, J. a (2004). Convergent evidence for impaired AKT1-GSK3 $\beta$  signaling in schizophrenia. *Nat. Genet.* 36, 131–137. doi:10.1038/ng1296.
- Fadda, P., Scherma, M., Fresu, A., Collu, M., and Fratta, W. (2005). Dopamine and serotonin release in dorsal striatum and nucleus accumbens is differentially modulated by morphine in DBA/2J and C57BL/6J mice. *Synapse* 56, 29–38. doi:10.1002/syn.20122.
- Falls, D. L. (2003a). Neuregulins: Functions, forms, and signaling strategies, in *The EGF Receptor Family: Biologic Mechanisms and Role in Cancer*, 15–31. doi:10.1016/B978-012160281-9/50003-7.
- Falls, D. L. (2003b). Neuregulins and the neuromuscular system: 10 Years of answers and questions. *J. Neurocytol.* 32, 619–647. doi:10.1023/B:NEUR.0000020614.83883.be.
- Farzan, F., Barr, M. S., Levinson, A. J., Chen, R., Wong, W., Fitzgerald, P. B., et al. (2010). Evidence for gamma inhibition deficits in the dorsolateral prefrontal cortex of patients with schizophrenia. *Brain* 133, 1505–1514. doi:10.1093/brain/awq046.
- Fazzari, P., Paternain, A. V., Valiente, M., Pla, R., Luján, R., Lloyd, K., et al. (2010). Control of cortical GABA circuitry development by Nrg1 and ErbB4 signalling. *Nature* 464, 1376–

1380. doi:10.1038/nature08928.
- Filipović, D., Zlatković, J., Gass, P., and Inta, D. (2013). The differential effects of acute vs. chronic stress and their combination on hippocampal parvalbumin and inducible heat shock protein 70 expression. *Neuroscience* 236, 47–54. doi:10.1016/j.neuroscience.2013.01.033.
- Finnerty, G. T., Roberts, L. S., and Connors, B. W. (1999). Sensory experience modifies the short-term dynamics of neocortical synapses. *Nature* 400, 367–371. doi:10.1038/22553.
- Fisahn, A., Contractor, A., Traub, R. D., Buhl, E. H., Heinemann, S., and McBain, C. J. (2004). Distinct roles for the kainate receptor subunits GluR5 and GluR6 in kainate-induced hippocampal gamma oscillations. *J. Neurosci.* 24, 9658–9668. doi:10.1523/JNEUROSCI.2973-04.2004.
- Fisahn, A., Neddens, J., Yan, L., and Buonanno, A. (2009). Neuregulin-1 modulates hippocampal gamma oscillations: Implications for schizophrenia. *Cereb. Cortex* 19, 612–618. doi:10.1093/cercor/bhn107.
- Fisahn, A., Pike, F. G., Buhl, E. H., and Paulsen, O. (1998). Cholinergic induction of network oscillations at 40 Hz in the hippocampus in vitro. *Nature* 394, 186–189. doi:10.1038/28179.
- Flames, N., Long, J. E., Garratt, A. N., Fischer, T. M., Gassmann, M., Birchmeier, C., et al. (2004). Short- and long-range attraction of cortical GABAergic interneurons by neuregulin-1. *Neuron* 44, 251–561. doi:10.1016/j.neuron.2004.09.028.
- Fleck, D., van Bebber, F., Colombo, A., Galante, C., Schwenk, B. M., Rabe, L., et al. (2013). Dual cleavage of neuregulin 1 type III by BACE1 and ADAM17 liberates its EGF-like domain and allows paracrine signaling. *J. Neurosci.* 33, 7856–7869. doi:10.1523/JNEUROSCI.3372-12.2013.
- Fox, K. (1992). A critical period for experience-dependent synaptic plasticity in rat barrel cortex. *J. Neurosci.* 12, 1826–1838.
- Fresno Vara, J. A., Casado, E., de Castro, J., Cejas, P., Belda-Iniesta, C., and González-Barón, M. (2004). PI3K/Akt signalling pathway and cancer. *Cancer Treat. Rev.* 30, 193–204. doi:10.1016/j.ctrv.2003.07.007.
- Freund, T. F., and Buzsáki, G. (1996). Interneurons of the hippocampus. *Hippocampus* 6, 347–470. doi:10.1002/(SICI)1098-1063(1996)6:4<347::AID-HIPO1>3.0.CO;2-I.
- Freund, T. F., and Katona, I. (2007). Perisomatic inhibition. *Neuron* 56, 33–42. doi:10.1016/j.neuron.2007.09.012.
- Friedrich, G., and Soriano, P. (1991). Promoter traps in embryonic stem cells a genetic screen to identify and mutate developmental genes in mice. *Gene Dev.* 5, 1513–1523.
- Fünfschilling, U., Supplie, L. M., Mahad, D., Boretius, S., Saab, A. S., Edgar, J., et al. (2012). Glycolytic oligodendrocytes maintain myelin and long-term axonal integrity. *Nature* 485,

- 517–521. doi:10.1038/nature11007.
- Gallart-Palau, X., Tarabal, O., Casanovas, A., Sábado, J., Correa, F. J., Hereu, M., et al. (2014). Neuregulin-1 is concentrated in the postsynaptic subsurface cistern of C-bouton inputs to  $\alpha$ -motoneurons and altered during motoneuron diseases. *FASEB J.* 28, 3618–3632. doi:10.1096/fj.13-248583.
- Gao, R., and Penzes, P. (2015). Common mechanisms of excitatory and inhibitory imbalance in schizophrenia and autism spectrum disorders. *Curr. Mol. Med.* 15, 146–67. doi:10.1016/j.jaac.2013.12.025.
- Garcia, R. A., Vasudevan, K., and Buonanno, A. (2000). The neuregulin receptor ErbB-4 interacts with PDZ-containing proteins at neuronal synapses. *Proc. Natl. Acad. Sci. U. S. A.* 97, 3596–3601. doi:10.1073/pnas.070042497.
- Garey, L. J., Ong, W. Y., Patel, T. S., Kanani, M., Davis, A., Mortimer, A. M., et al. (1998). Reduced dendritic spine density on cerebral cortical pyramidal neurons in schizophrenia. *J. Neurol. Neurosurg. Psychiatry* 65, 446–453. doi:10.1136/jnnp.65.4.446.
- Gassmann, M., Casagrande, F., Orioli, D., Simon, H., Lai, C., Klein, R., et al. (1995). Aberrant neural and cardiac development in mice lacking the ErbB4 neuregulin receptor. *Nature* 378, 390–394. doi:10.1017/CBO9781107415324.004.
- Geyer, M. A., and Braff, D. L. (1982). Habituation of the blink reflex in normals and schizophrenic patients. *Psychophysiology* 19, 1–6. doi:10.1111/j.1469-8986.1982.tb02589.x.
- Ghashghaei, H. T., Weber, J., Pevny, L., Schmid, R., Schwab, M. H., Lloyd, K. C., et al. (2006). The role of neuregulin-ErbB4 interactions on the proliferation and organization of cells in the subventricular zone. *Proc. Natl. Acad. Sci. U. S. A.* 103, 1930–1935. doi:10.1073/pnas.0510410103.
- Goebbels, S., Bormuth, I., Bode, U., Hermanson, O., Schwab, M. H., and Nave, K. A. (2006). Genetic targeting of principal neurons in neocortex and hippocampus of NEX-Cre mice. *Genesis* 44, 611–621. doi:10.1002/dvg.20256.
- Golub, M. S., Germann, S. L., and Lloyd, K. C. K. (2004). Behavioral characteristics of a nervous system-specific erbB4 knock-out mouse. *Behav. Brain Res.* 153, 159–170. doi:10.1016/j.bbr.2003.11.010.
- Gorski, J. A., Talley, T., Qiu, M., Puellas, L., Rubenstein, J. L. R., and Jones, K. R. (2002). Cortical excitatory neurons and glia, but not GABAergic neurons, are produced in the Emx1-expressing lineage. *J. Neurosci.* 22, 6309–6314. doi:20026564.
- Gu, J.-J., Zhang, J.-H., Chen, H.-J., and Wang, S.-S. (2016). TPX2 promotes glioma cell proliferation and invasion via activation of the AKT signaling pathway. *Oncol. Lett.* 12, 5015–5022.
- Gu, Z., Jiang, Q., Fu, A., Ip, N., and Yan, Z. (2005). Regulation of NMDA receptors by

- neuregulin signaling in prefrontal cortex. *J. Neurosci.* 25, 4974–4984. doi:10.1523/JNEUROSCI.1086-05.2005.
- Hahn, C.-G., Wang, H.-Y., Cho, D.-S., Talbot, K., Gur, R. E., Berrettini, W. H., et al. (2006). Altered neuregulin 1-erbB4 signaling contributes to NMDA receptor hypofunction in schizophrenia. *Nat. Med.* 12, 824–828. doi:10.1038/nm1418.
- Harrison, P. J. (1999). The neuropathology of schizophrenia: A critical review of the data and their interpretation. *Brain* 122, 593–624. doi:10.1093/brain/122.4.593.
- Harrison, P. J., and Law, A. J. (2006). Neuregulin 1 and schizophrenia: Genetics, gene expression, and neurobiology. *Biol. Psychiatry* 60, 132–140. doi:10.1016/j.biopsych.2005.11.002.
- Hartmann, M., Herrlich, A., and Herrlich, P. (2013). Who decides when to cleave an ectodomain? *Trends Biochem. Sci.* 38, 111–120. doi:10.1016/j.tibs.2012.12.002.
- Hashimoto, R., Straub, R. E., Weickert, C. S., Hyde, T. M., Kleinman, J. E., and Weinberger, D. R. (2004). Expression analysis of neuregulin-1 in the dorsolateral prefrontal cortex in schizophrenia. *Mol. Psychiatry* 9, 299–307. doi:10.1038/sj.mp.4001434.
- Hashimoto, T., Volk, D. W., Eggan, S. M., Mirnics, K., Pierri, J. N., Sun, Z., et al. (2003). Gene expression deficits in a subclass of GABA neurons in the prefrontal cortex of subjects with schizophrenia. *J. Neurosci.* 23, 6315–6326. doi:10.2967/jnumed.108.060368.
- Hayashi-Takagi, A. (2017). Synapse pathology and translational applications for schizophrenia. *Neurosci. Res.* 114, 3–8. doi:10.1016/j.neures.2016.09.001.
- Haydon, P. G. (2001). GLIA: listening and talking to the synapse. *Nat. Rev. Neurosci.* 2, 185–193. doi:10.1038/35058528.
- Heckers, S., and Konradi, C. (2015). GABAergic mechanisms of hippocampal hyperactivity in schizophrenia. *Schizophr. Res.* 167, 4–11. doi:10.1016/j.schres.2014.09.041.
- Henkart, M., Landis, D. M. D., and Reese, T. S. (1976). Similarity of junctions between plasma membranes and endoplasmic reticulum in muscle and neurons. *J. Cell Biol.* 70, 338–347.
- Hino, M., Kunii, Y., Matsumoto, J., Wada, A., Nagaoka, A., Niwa, S. ichi, et al. (2016). Decreased VEGFR2 expression and increased phosphorylated Akt1 in the prefrontal cortex of individuals with schizophrenia. *J. Psychiatr. Res.* 82, 100–108. doi:10.1016/j.jpsychires.2016.07.018.
- Hippenmeyer, S., Vrieseling, E., Sigrist, M., Portmann, T., Laengle, C., Ladle, D. R., et al. (2005). A developmental switch in the response of DRG neurons to ETS transcription factor signaling. *PLoS Biol.* 3, 878–890. doi:10.1371/journal.pbio.0030159.
- Hirrlinger, P. G., Scheller, A., Braun, C., Hirrlinger, J., and Kirchhoff, F. (2006). Temporal control of gene recombination in astrocytes by transgenic expression of the tamoxifen-inducible DNA recombinase variant CreERT2. *Glia* 54, 11–20. doi:10.1002/glia.20342.
- Hirschtritt, M. E., Darrow, S. M., Illmann, C., Osiecki, L., Grados, M., Sandor, P., et al. (2016).

- Social disinhibition is a heritable subphenotype of tics in Tourette syndrome. *Neurology* 87, 497–504. doi:10.1212/WNL.0000000000002910.
- Hitti, F. L., and Siegelbaum, S. A. (2014). The hippocampal CA2 region is essential for social memory. *Nature* 508, 88–92. doi:10.1038/nature13028.
- Ho, W. H., Armanini, M. P., Nuijens, A., Phillips, H. S., and Osheroff, P. L. (1995). Sensory and motor neuron-derived factor. A novel heregulin variant highly expressed in sensory and motor neurons. *J. Biol. Chem.* 270, 14523–14532. doi:10.1074/jbc.270.24.14523.
- Hoess, R. H., Ziese, M., and Sternberg, N. (1982). P1 site-specific recombination: nucleotide sequence of the recombining sites. *Proc. Natl. Acad. Sci. U. S. A.* 79, 3398–3402. doi:10.1073/pnas.79.11.3398.
- Holmes, W. E., Sliwkowski, M. X., Akita, R. W., Henzel, W. J., Lee, J., Park, J. W., et al. (1992). Identification of heregulin, a specific activator of p185 erbB2. *Science* 256, 1205–1210.
- Holt, D. J., Bachus, S. E., Hyde, T. M., Wittie, M., Herman, M. M., Vangel, M., et al. (2005). Reduced density of cholinergic interneurons in the ventral striatum in schizophrenia: an in situ hybridization study. *Biol. Psychiatry* 58, 408–416. doi:10.1016/j.biopsych.2005.04.007.
- Hu, W., Zhang, M., Czéh, B., Flügge, G., and Zhang, W. (2010). Stress impairs GABAergic network function in the hippocampus by activating nongenomic glucocorticoid receptors and affecting the integrity of the parvalbumin-expressing neuronal network. *Neuropsychopharmacology* 35, 1693–1707. doi:10.1038/npp.2010.31.
- Hu, X., Hicks, C. W., He, W., Wong, P., Macklin, W. B., Trapp, B. D., et al. (2006). Bace1 modulates myelination in the central and peripheral nervous system. *Nat. Neurosci.* 9, 1520–1525. doi:10.1038/nn1797.
- Huang, C.-H., Pei, J.-C., Luo, D.-Z., Chen, C., Chen, Y.-W., and Lai, W.-S. (2015). Investigation of gene effects and epistatic interactions between Akt1 and neuregulin 1 in the regulation of behavioral phenotypes and social functions in genetic mouse models of schizophrenia. *Front. Behav. Neurosci.* 8, 455. doi:10.3389/fnbeh.2014.00455.
- Huang, Y. Z., Won, S., Ali, D. W., Wang, Q., Tanowitz, M., Du, Q. S., et al. (2000). Regulation of neuregulin signaling by PSD-95 interacting with ErbB4 at CNS synapses. *Neuron* 26, 443–455. doi:10.1016/S0896-6273(00)81176-9.
- Huijbrechts, R. P. H., Roth, K. A., Schmidt, R. E., and Carroll, S. L. (2003). Hypertrophic neuropathies and malignant peripheral nerve sheath tumors in transgenic mice overexpressing glial growth factor  $\beta$ 3 in myelinating Schwann cells. *J. Neurosci.* 23, 7269–7280.
- Insel, T. R. (2010). Rethinking schizophrenia. *Nature* 468, 187–193. doi:10.1038/nature09552.
- Irion, S., Luche, H., Gadue, P., Fehling, H. J., Kennedy, M., and Keller, G. (2007). Identification and targeting of the ROSA26 locus in human embryonic stem cells. *Nat. Biotechnol.* 25,

- 1477–1482. doi:10.1038/nbt1362.
- Isaacson, J. S., and Scanziani, M. (2011). How inhibition shapes cortical activity. *Neuron* 72, 231–243. doi:10.1016/j.neuron.2011.09.027.
- Iwakura, Y., and Nawa, H. (2013). ErbB1-4-dependent EGF/neuregulin signals and their cross talk in the central nervous system: pathological implications in schizophrenia and Parkinson's disease. *Front. Cell. Neurosci.* 7, 4. doi:10.3389/fncel.2013.00004.
- Jiang, L., O'Leary, C., Kim, H. A., Parish, C. L., Massalas, J., Waddington, J. L., et al. (2015). Motor and behavioral phenotype in conditional mutants with targeted ablation of cortical D1 dopamine receptor-expressing cells. *Neurobiol. Dis.* 76, 137–158. doi:10.1016/j.nbd.2015.02.006.
- Jones, J. T., Akita, R. W., and Sliwkowski, M. X. (1999). Binding specificities and affinities of egf domains for ErbB receptors. *FEBS Lett.* 447, 227–231. doi:10.1016/S0014-5793(99)00283-5.
- Junttila, T. T., Sundvall, M., Määttä, J. A., and Elenius, K. (2000a). ErbB4 and its isoforms: Selective regulation of growth factor responses by naturally occurring receptor variants. *Trends Cardiovasc. Med.* 10, 304–310. doi:10.1016/S1050-1738(01)00065-2.
- Junttila, T. T., Sundvall, M., Määttä, J. A., and Elenius, K. (2000b). ErbB4 and its isoforms selective regulation of growth factor responses by naturally occurring receptor variants. *Trends Cardiovasc. Med.* 10, 304–310. doi:10.1016/S1050-1738(01)00065-2.
- Kainulainen, V., Sundvall, M., Määttä, J. A., Santiestevan, E., Klagsbrun, M., and Elenius, K. (2000). A natural ErbB4 isoform that does not activate phosphoinositide 3-kinase mediates proliferation but not survival or chemotaxis. *J. Biol. Chem.* 275, 8641–8649. doi:10.1074/jbc.275.12.8641.
- Kandel, E. R. (2013). *Principles of Neural Science*. Fifth Edit. McGraw-Hill Education.
- Kennedy, M. B. (1997). The postsynaptic density at glutamatergic synapses. *Trends Neurosci.* 20, 264–268. doi:10.1016/S0166-2236(96)01033-8.
- Kim, E., and Sheng, M. (2004). PDZ domain proteins of synapses. *Nat. Rev. Neurosci.* 5, 771–781. doi:10.1038/nrn1517.
- Kirov, G., O'Donovan, M. C., and Owen, M. J. (2005). Finding schizophrenia genes. *J. Clin. Invest.* 115, 1440–1448. doi:10.1172/JCI24759.
- Klapper, L. N., Glathe, S., Vaisman, N., Hynes, N. E., Andrews, G. C., Sela, M., et al. (1999). The ErbB-2/HER2 oncoprotein of human carcinomas may function solely as a shared coreceptor for multiple stroma-derived growth factors. *Proc. Natl. Acad. Sci.* 96, 4995–5000. doi:10.1073/pnas.96.9.4995.
- Kohara, K., Pignatelli, M., Rivest, A. J., Jung, H.-Y., Kitamura, T., Suh, J., et al. (2014). Cell type-specific genetic and optogenetic tools reveal hippocampal CA2 circuits. *Nat. Neurosci.* 17, 269–279. doi:10.1038/nn.3614.

- Komuro, A., Nagai, M., Navin, N. E., and Sudol, M. (2003). WW domain-containing protein YAP associates with ErbB-4 and acts as a co-transcriptional activator for the carboxyl-terminal fragment of ErbB-4 that translocates to the nucleus. *J. Biol. Chem.* 278, 33334–33341. doi:10.1074/jbc.M305597200.
- Kramer, R., Bucay, N., Kane, D. J., Martin, L. E., Tarpley, J. E., and Theill, L. E. (1996). Neuregulins with an Ig-like domain are essential for mouse myocardial and neuronal development. *Proc. Natl. Acad. Sci. U. S. A.* 93, 4833–4838. doi:10.1073/pnas.93.10.4833.
- Krivosheya, D., Tapia, L., Levinson, J. N., Huang, K., Kang, Y., Hines, R., et al. (2008). ErbB4-neuregulin signaling modulates synapse development and dendritic arborization through distinct mechanisms. *J. Biol. Chem.* 283, 32944–32956. doi:10.1074/jbc.M800073200.
- Kumar, V., Zhang, M.-X., Swank, M. W., Kunz, J., and Wu, G.-Y. (2005). Regulation of dendritic morphogenesis by Ras-PI3K-Akt-mTOR and Ras-MAPK signaling pathways. *J. Neurosci.* 25, 11288–11299. doi:10.1523/JNEUROSCI.2284-05.2005.
- Kwon, J. S., O'Donnell, B. F., Wallenstein, G. V, Greene, R. W., Hirayasu, Y., Nestor, P. G., et al. (1999). Gamma frequency-range abnormalities to auditory stimulation in schizophrenia. *Arch. Genet. Psychiatry* 56, 1001–1005.
- Kwon, O.-B., Longart, M., Vullhorst, D., Hoffman, D. A., and Buonanno, A. (2005). Neuregulin-1 reverses long-term potentiation at CA1 hippocampal synapses. *J. Neurosci.* 25, 9378–9383. doi:10.1523/JNEUROSCI.2100-05.2005.
- Laemmli, U. K. (1970). Cleavage of structural proteins during assembly of head of bacteriophage-T4. *Nature* 227, 680–685. doi:10.1038/227680a0.
- Lalo, U., Andrew, J., Palygin, O., and Pankratov, Y. (2009). Ca<sup>2+</sup>-dependent modulation of GABAA and NMDA receptors by extracellular ATP: implication for function of tripartite synapse. *Biochem. Soc. Trans.* 37, 1407–1411. doi:10.1042/BST0371407.
- Law, A. J., Lipska, B. K., Weickert, C. S., Hyde, T. M., Straub, R. E., Hashimoto, R., et al. (2006). Neuregulin 1 transcripts are differentially expressed in schizophrenia and regulated by 5' SNPs associated with the disease. *Proc. Natl. Acad. Sci. U. S. A.* 103, 6747–6752. doi:10.1073/pnas.0602002103.
- Law, A. J., Shannon Weickert, C., Hyde, T. M., Kleinman, J. E., and Harrison, P. J. (2004). Neuregulin-1 (NRG-1) mRNA and protein in the adult human brain. *Neuroscience* 127, 125–136. doi:10.1016/j.neuroscience.2004.04.026.
- Law, A. J., Wang, Y., Sei, Y., O'Donnell, P., Piantadosi, P., Papaleo, F., et al. (2012). Neuregulin 1-ErbB4-PI3K signaling in schizophrenia and phosphoinositide 3-kinase-p110 $\delta$  inhibition as a potential therapeutic strategy. *Proc. Natl. Acad. Sci. U. S. A.* 109, 12165–70. doi:10.1073/pnas.1206118109.
- Leask, S. (2004). Environmental influences in schizophrenia: the known and the unknown. *Adv.*

- Psychiatric Treat.* 10, 323–330.
- Lee, H. J., Jung, K. M., Huang, Y. Z., Bennett, L. B., Lee, J. S., Mei, L., et al. (2002). Presenilin-dependent  $\gamma$ -secretase-like intramembrane cleavage of ErbB4. *J. Biol. Chem.* 277, 6318–6323. doi:10.1074/jbc.M110371200.
- Lee, J., Rizzo, S., Altshuler, L., Glahn, D. C., Miklowitz, D. J., Sugar, C. A., et al. (2017). Deconstructing bipolar disorder and schizophrenia: A cross-diagnostic cluster analysis of cognitive phenotypes. *J. Affect. Disord.* 209, 71–79. doi:10.1016/j.jad.2016.11.030.
- Lee, K.-H., Lee, H., Yang, C. H., Ko, J.-S., Park, C.-H., Woo, R.-S., et al. (2015). Bidirectional signaling of neuregulin-2 mediates formation of GABAergic synapses and maturation of glutamatergic synapses in newborn granule cells of postnatal hippocampus. *J. Neurosci.* 35, 16479–16493. doi:10.1523/JNEUROSCI.1585-15.2015.
- Leone, D. P., Genoud, S., Atanasoski, S., Grausenburger, R., Berger, P., Metzger, D., et al. (2003). Tamoxifen-inducible glia-specific Cre mice for somatic mutagenesis in oligodendrocytes and Schwann cells. *Mol. Cell. Neurosci.* 22, 430–440. doi:10.1016/S1044-7431(03)00029-0.
- Levitt, P. (2005). Disruption of interneuron development. *Epilepsia* 46, 22–28. doi:10.1111/j.1528-1167.2005.00305.x.
- Lewis, C. M., Levinson, D. F., Wise, L. H., DeLisi, L. E., Straub, R. E., Hovatta, I., et al. (2003). Genome scan meta-analysis of schizophrenia and bipolar disorder, part II: Schizophrenia. *Am. J. Hum. Genet.* 73, 34–48. doi:10.1086/376549.
- Lewis, D. a, Hashimoto, T., and Volk, D. W. (2005). Cortical inhibitory neurons and schizophrenia. *Nat. Rev. Neurosci.* 6, 312–324. doi:10.1038/nrn1648.
- Li, B., Woo, R. S., Mei, L., and Malinow, R. (2007). The neuregulin-1 receptor ErbB4 controls glutamatergic synapse maturation and plasticity. *Neuron* 54, 583–597. doi:10.1016/j.neuron.2007.03.028.
- Li, D., Collier, D. A., and He, L. (2006). Meta-analysis shows strong positive association of the neuregulin 1 (NRG1) gene with schizophrenia. *Hum. Mol. Genet.* 15, 1995–2002. doi:10.1093/hmg/ddl122.
- Li, H., Chou, S.-J., Hamasaki, T., Perez-Garcia, C. G., and O’Leary, D. D. M. (2012a). Neuregulin repellent signaling via ErbB4 restricts GABAergic interneurons to migratory paths from ganglionic eminence to cortical destinations. *Neural Dev.* 7, 10. doi:10.1186/1749-8104-7-10.
- Li, K.-X., Lu, Y.-M., Xu, Z.-H., Zhang, J., Zhu, J.-M., Zhang, J.-M., et al. (2012b). Neuregulin 1 regulates excitability of fast-spiking neurons through Kv1.1 and acts in epilepsy. *Nat. Neurosci.* 15, 267–273. doi:10.1038/nn.3006.
- Li, L., Cleary, S., Mandarano, M. A., Long, W., Birchmeier, C., and Jones, F. E. (2002). The breast proto-oncogene, HRGalpha regulates epithelial proliferation and lobuloalveolar



- development in the mouse mammary gland. *Oncogene* 21, 4900–4907. doi:10.1038/sj.onc.1205634.
- Li, Q., and Loeb, J. A. (2001). Neuregulin-HSPG interactions produce sustained ErbB receptor activation required for the induction of AChRs in muscle. *J. Biol. Chem.* 276, 38068–38075. doi:10.1074/jbc.M104485200.
- Linggi, B., and Carpenter, G. (2006). ErbB-4 s80 intracellular domain abrogates ETO2-dependent transcriptional repression. *J. Biol. Chem.* 281, 25373–25380. doi:10.1074/jbc.M603998200.
- Liu, X., Bates, R., Yin, D.-M., Shen, C., Wang, F., Su, N., et al. (2011). Specific regulation of NRG1 isoform expression by neuronal activity. *J. Neurosci.* 31, 8491–8501. doi:10.1523/JNEUROSCI.5317-10.2011.
- Liu, Y., Ford, B., Mann, M. A., and Fischbach, G. D. (2001). Neuregulins increase  $\alpha 7$  nicotinic acetylcholine receptors and enhance excitatory synaptic transmission in GABAergic interneurons of the hippocampus. *J. Neurosci.* 21, 5660–5669. doi:21/15/5660 [pii].
- Loeb, J. A., Susanto, E. T., and Fischbach, G. D. (1998). The neuregulin precursor proARIA is processed to ARIA expression of the cell surface by a protein kinase C-enhanced mechanism. *Mol. Cell. Neurosci.* 91, 77–91.
- Longart, M., Chatani-Hinze, M., Gonzalez, C. M., Vullhorst, D., and Buonanno, A. (2007). Regulation of ErbB-4 endocytosis by neuregulin in GABAergic hippocampal interneurons. *Brain Res. Bull.* 73, 210–219. doi:10.1016/j.brainresbull.2007.02.014.
- Longart, M., Liu, Y., Karavanova, I., and Buonanno, A. (2004). Neuregulin-2 is developmentally regulated and targeted to dendrites of central neurons. *J. Comp. Neurol.* 472, 156–172. doi:10.1002/cne.20016.
- Lowry, O. H., Rosebrough, N. J., Farr, L., Randall, R. J., and Randall, R. J. (1951). Protein measurement with the folin phenol reagent. *J. Biol. Chem.* 193, 265–275. doi:10.1016/0304-3894(92)87011-4.
- Ma, L., Huang, Y. Z., Pitcher, G. M., Valtschanoff, J. G., Ma, Y. H., Feng, L. Y., et al. (2003). Ligand-dependent recruitment of the ErbB4 signaling complex into neuronal lipid rafts. *J. Neurosci.* 23, 3164–3175. doi:23/8/3164 [pii].
- Madisen, L., Zwingman, T. A., Sunkin, S. M., Oh, S. W., Zariwala, H. A., Gu, H., et al. (2010). A robust and high-throughput Cre reporting and characterization system for the whole mouse brain. *Nat. Neurosci.* 13, 133–140. doi:10.1038/nn.2467.
- Mandikian, D., Bocksteins, E., Parajuli, L. K., Bishop, H. I., Cerda, O., Shigemoto, R., et al. (2014). Cell type-specific spatial and functional coupling between mammalian brain Kv2.1 K<sup>+</sup> channels and ryanodine receptors. *J. Comp. Neurol.* 522, 3555–3574. doi:10.1002/cne.23641.
- Mar, L., Yang, F.-C., and Ma, Q. (2012). Genetic marking and characterization of Tac2-

- expressing neurons in the central and peripheral nervous system. *Mol. Brain* 5, 3. doi:10.1186/1756-6606-5-3.
- Marchionni, M. A., Goodearl, A. D., Chen, M. S., Bermingham-McDonogh, O., Kirk, C., Hendricks, M., et al. (1993). Glial growth factors are alternatively spliced erbB2 ligands expressed in the nervous system. *Nature* 362, 312–318. doi:10.1038/362312a0.
- Marín, O. (2012). Interneuron dysfunction in psychiatric disorders. *Nat. Rev. Neurosci.* 13, 107–120. doi:10.1038/nrn3155.
- Marín, O. (2013). Cellular and molecular mechanisms controlling the migration of neocortical interneurons. *Eur. J. Neurosci.* 38, 2019–2029. doi:10.1111/ejn.12225.
- Marín, O., and Müller, U. (2014). Lineage origins of GABAergic versus glutamatergic neurons in the neocortex. *Curr. Opin. Neurobiol.* 26, 132–141. doi:10.1016/j.conb.2014.01.015.
- Marín, O., and Rubenstein, J. L. (2001). A long, remarkable journey: tangential migration in the telencephalon. *Nat. Rev. Neurosci.* 2, 780–790. doi:10.1038/35097509.
- Markram, H., Toledo-Rodriguez, M., Wang, Y., Gupta, A., Silberberg, G., and Wu, C. (2004). Interneurons of the neocortical inhibitory system. *Nat. Rev. Neurosci.* 5, 793–807. doi:10.1038/nrn1519.
- Mata, I., Perez-Iglesias, R., Roiz-Santiañez, R., Tordesillas-Gutierrez, D., Gonzalez-Mandly, A., Vazquez-Barquero, J. L., et al. (2009). A neuregulin 1 variant is associated with increased lateral ventricle volume in patients with first-episode schizophrenia. *Biol. Psychiatry* 65, 535–540. doi:10.1016/j.biopsych.2008.10.020.
- Mavlyutov, T. A., Epstein, M. L., Andersen, K. A., Ziskind-Conhaim, L., and Ruoho, A. E. (2010). The sigma-1 receptor is enriched in postsynaptic sites of C-terminals in mouse motoneurons. An anatomical and behavioral study. *Neuroscience* 167, 247–255. doi:10.1016/j.neuroscience.2010.02.022.
- Mei, L., and Xiong, W. C. (2008). Neuregulin 1 in neural development, synaptic plasticity and schizophrenia. *Nat. Rev. Neurosci.* 9, 437–452.
- Meyer, D., and Birchmeier, C. (1995). Multiple essential functions of neuregulin in development. *Nature* 378, 386–390. doi:10.1038/378753a0.
- Michailov, G. V., Sereda, M. W., Brinkmann, B. G., Fischer, T. M., Haug, B., Birchmeier, C., et al. (2004). Axonal Neuregulin-1 regulates myelin sheath thickness. *Science* 304, 700–703.
- Micheva, K. D., Wolman, D., Mensh, B. D., Pax, E., Buchanan, J., Smith, S. J., et al. (2016). A large fraction of neocortical myelin ensheathes axons of local inhibitory neurons. *eLife* 5, e15784. doi:10.7554/eLife.15784.
- Millet, V., Marder, M., and Pasquini, L. A. (2012). Adult CNP::EGFP transgenic mouse shows pronounced hypomyelination and an increased vulnerability to cuprizone-induced demyelination. *Exp. Neurol.* 233, 490–504. doi:10.1016/j.expneurol.2011.11.028.

- Mines, M. A., Yuskaitis, C. J., King, M. K., Beurel, E., and Jope, R. S. (2010). GSK3 influences social preference and anxiety-related behaviors during social interaction in a mouse model of fragile X syndrome and autism. *PLoS One* 5, e9706. doi:10.1371/journal.pone.0009706.
- Minichiello, L., Korte, M., Wolfner, D., Kühn, R., Unsicker, K., Cestari, V., et al. (1999). Essential role for TrkB receptors in hippocampus-mediated learning. *Neuron* 24, 401–414. doi:10.1016/S0896-6273(00)80853-3.
- Misonou, H., Mohapatra, D. P., Park, E. W., Leung, V., Zhen, D., Misonou, K., et al. (2004). Regulation of ion channel localization and phosphorylation by neuronal activity. *Nat. Neurosci.* 7, 711–718. doi:10.1038/nn1260.
- Misonou, H., Mohapatra, D. P., and Trimmer, J. S. (2005). Kv2.1: A voltage-gated K<sup>+</sup> channel critical to dynamic control of neuronal excitability. *Neurotoxicology* 26, 743–752. doi:10.1016/j.neuro.2005.02.003.
- Montero, J. C., Rodríguez-Barrueco, R., Yuste, L., Juanes, P. P., Borges, J., Esparís-Ogando, A., et al. (2007). The extracellular linker of pro-Neuregulin-a2c is required for efficient sorting and juxtacrine function. *Mol. Biol. Cell* 18, 380–393. doi:10.1091/mbc.E06.
- Montgomery, S. M., and Buzsáki, G. (2007). Gamma oscillations dynamically couple hippocampal CA3 and CA1 regions during memory task performance. *Proc. Natl. Acad. Sci. U. S. A.* 104, 14495–14500. doi:10.1073/pnas.0701826104.
- Mori, T., Tanaka, K., Buffo, A., Wurst, W., Kühn, R., and Gotz, M. (2006). Inducible gene deletion in astroglia and radial glia - A valuable tool for functional and lineage analysis. *Glia* 54, 21–34. doi:10.1002/glia.20350.
- Mostaid, M. S., Mancuso, S. G., Liu, C., Sundram, S., Pantelis, C., Everall, I. P., et al. (2017). Meta-analysis reveals associations between genetic variation in the 5' and 3' regions of Neuregulin-1 and schizophrenia. *Nat. Publ. Gr.* 7, e1004-5. doi:10.1038/tp.2016.279.
- Mowry, B. ., and Nancarrow, D. J. (2001). Molecular genetics of schizophrenia. *Clin. Exp. Pharmacol. Physiol.* 28, 66–69.
- Moyer, C. E., Shelton, M. A., and Sweet, R. A. (2015). Dendritic spine alterations in schizophrenia. *Neurosci. Lett.* 601, 46–53. doi:10.1016/j.neulet.2014.11.042.
- Mullis, K., Faloona, F., Scharf, S., Saiki, R., Horn, G., and Erlich, H. (1986). Specific enzymatic amplification of DNA in vitro: The polymerase chain reaction. *Cold Spring Harb Symp Quant Biol* 51 Pt 1, 263–273.
- Munafò, M. R., Thiselton, D. L., Clark, T. G., and Flint, J. (2006). Association of the NRG1 gene and schizophrenia: a meta-analysis. *Mol. Psychiatry* 11, 539–546. doi:10.1038/sj.mp.4001840.
- Neddens, J., and Buonanno, A. (2010). Selective populations of hippocampal interneurons express ErbB4 and their number and distribution is altered in ErbB4 knockout mice.

- Hippocampus* 20, 724–744. doi:10.1002/hipo.20675.
- Neddens, J., Fish, K. N., Tricoire, L., Vullhorst, D., Shamir, A., Chung, W., et al. (2011). Conserved interneuron-specific ErbB4 expression in frontal cortex of rodents, monkeys, and humans: Implications for schizophrenia. *Biol. Psychiatry* 70, 636–645. doi:10.1016/j.biopsych.2011.04.016.
- Netrakanti, P. R., Cooper, B. H., Dere, E., Poggi, G., Winkler, D., Brose, N., et al. (2015). Fast cerebellar reflex circuitry requires synaptic vesicle priming by Munc13-3. *Cerebellum* 14, 264–283. doi:10.1007/s12311-015-0645-0.
- Ni, C.-Y., Murphy, M. P., Golde, T. E., and Carpenter, G. (2001).  $\gamma$ -Secretase cleavage and nuclear localization of ErbB-4 receptor tyrosine kinase. *Science* 294, 2179–2181. doi:10.1126/science.1065412.
- Nicodemus, K. K., Law, A. J., Radulescu, E., Luna, A., Kolachana, B., Vakkalanka, R., et al. (2010). Biological validation of increased schizophrenia risk with NRG1, ERBB4, and AKT1 epistasis via functional neuroimaging in healthy controls. *Arch. Gen. Psychiatry* 67, 991–1001. doi:10.1001/archgenpsychiatry.2010.117.
- Norton, N., Moskvina, V., Morris, D. W., Bray, N. J., Zammit, S., Williams, N. M., et al. (2006). Evidence that interaction between neuregulin 1 and its receptor erbB4 increases susceptibility to schizophrenia. *Am. J. Med. Genet.* 141 B, 96–101. doi:10.1002/ajmg.b.30236.
- O’Callaghan, J. P., and Holtzman, S. G. (1975). Quantification of the analgesic activity of narcotic antagonists by a modified hot-plate procedure. *J. Pharmacol. Exp. Ther.* 192, 497–505.
- O’Donoghue, S., Holleran, L., Cannon, D. M., and McDonald, C. (2016). Anatomical Dysconnectivity in Bipolar Disorder Compared with Schizophrenia: A selective review of structural network analyses using diffusion MRI. *J. Affect. Disord.* 209, 217–228. doi:10.1016/j.jad.2016.11.015.
- Okada, M., and Corfas, G. (2004). Neuregulin1 downregulates postsynaptic GABAA receptors at the hippocampal inhibitory synapse. *Hippocampus* 14, 337–344. doi:10.1002/hipo.10185.
- Omerovic, J., Puggioni, E. M. R., Napoletano, S., Visco, V., Fraioli, R., Frati, L., et al. (2004). Ligand-regulated association of ErbB-4 to the transcriptional co-activator YAP65 controls transcription at the nuclear level. *Exp. Cell Res.* 294, 469–479. doi:10.1016/j.yexcr.2003.12.002.
- Ongür, D., Prescott, A. P., McCarthy, J., Cohen, B. M., and Renshaw, P. F. (2010). Elevated gamma-aminobutyric acid levels in chronic schizophrenia. *Biol. Psychiatry* 68, 667–670. doi:10.1016/j.biopsych.2010.05.016.
- Otsu, Y., Couchman, K., Lyons, D. G., Collot, M., Agarwal, A., Mallet, J., et al. (2015). Calcium

- dynamics in astrocyte processes during neurovascular coupling. *Nat. Neurosci.* 18, 210–218. doi:10.1038/nn.3906.
- Owen, M. J., Craddock, N., and O'Donovan, M. C. (2005). Schizophrenia: Genes at last? *Trends Genet.* 21, 518–525. doi:10.1016/j.tig.2005.06.011.
- Ozaki, M., Itoh, K., Miyakawa, Y., Kishida, H., and Hashikawa, T. (2004). Protein processing and releases of neuregulin-1 are regulated in an activity-dependent manner. *J. Neurochem.* 91, 176–188. doi:10.1111/j.1471-4159.2004.02719.x.
- Ozaki, M., Sasner, M., Yano, R., Lu, H. S., and Buonanno, A. (1997). Neuregulin-beta induces expression of an NMDA-receptor subunit. *Nature* 390, 691–694. doi:10.1038/37795.
- Pagani, J. H., Zhao, M., Cui, Z., Avram, S. K. W., Caruana, D. A., Dudek, S. M., et al. (2015). Role of the vasopressin 1b receptor in rodent aggressive behavior and synaptic plasticity in hippocampal area CA2. *Mol. Psychiatry* 20, 490–499. doi:10.1038/mp.2014.47.
- Palay, S. L. (1956). Synapses in the central nervous system. *J. Biophys. Biochem. Cytol.* 2, 193–201.
- Palay, S. L., and Palade, G. E. (1955). The fine structure of neurons. *J. Biophys. Biochem. Cytol.* 1, 69–88.
- Pandey, V., Bhaskara, V. K., and Babu, P. P. (2016). Implications of mitogen-activated protein kinase signaling in glioma. *J. Neurosci. Res.* 94, 114–127. doi:10.1002/jnr.23687.
- Penzes, P., Cahill, M. E., Jones, K. A., VanLeeuwen, J.-E., and Woolfrey, K. M. (2011). Dendritic spine pathology in neuropsychiatric disorders. *Nat. Neurosci.* 14, 285–293. doi:10.1038/nn.2741.
- Petersen, C. C. H., and Crochet, S. (2013). Synaptic computation and sensory processing in neocortical layer 2/3. *Neuron* 78, 28–48. doi:10.1016/j.neuron.2013.03.020.
- Peterson, G. L. (1979). Review of the folin phenol protein quantitation method of Lowry, Rosebrough, Farr and Randall. *Anal. Biochem.* 100, 201–220. doi:10.1016/0003-2697(79)90222-7.
- Petryshen, T. L., Middleton, F. a, Kirby, A., Aldinger, K. a, Purcell, S., Tahl, a R., et al. (2005). Support for involvement of neuregulin 1 in schizophrenia pathophysiology. *Mol. Psychiatry* 10, 366–374. doi:10.1038/sj.mp.4001661.
- Pinkas-Kramarski, R., Soussan, L., Waterman, H., Levkowitz, G., Alroy, I., Klapper, L., et al. (1996). Diversification of Neu differentiation factor and epidermal growth factor signaling by combinatorial receptor interactions. *EMBO J.* 15, 2452–2467.
- Pitcher, G. M., Beggs, S., Woo, R.-S., Mei, L., and Salter, M. W. (2008). ErbB4 is a suppressor of long-term potentiation in the adult hippocampus. *Neuroreport* 19, 139–143. doi:10.1097/WNR.0b013e3282f3da10.
- Plani-Lam, J. H. C., Chow, T. C., Siu, K. L., Chau, W. H., Ng, M. H. J., Bao, S., et al. (2015). PTPN21 exerts pro-neuronal survival and neuritic elongation via ErbB4/NRG3 signaling.

- Int. J. Biochem. Cell Biol.* 61, 53–62. doi:10.1016/j.biocel.2015.02.003.
- Pohl, H. B. F., Porcheri, C., Mueggler, T., Bachmann, L. C., Martino, G., Riethmacher, D., et al. (2011). Genetically induced adult oligodendrocyte cell death is associated with poor myelin clearance, reduced remyelination, and axonal damage. *J. Neurosci.* 31, 1069–1080. doi:10.1523/JNEUROSCI.5035-10.2011.
- Poliak, S., and Peles, E. (2003). The local differentiation of myelinated axons at nodes of Ranvier. *Nat. Rev. Neurosci.* 4, 968–980. doi:10.1038/nrn1253.
- Polleux, F., Whitford, K. L., Dijkhuizen, P. A., Vitalis, T., and Ghosh, A. (2002). Control of cortical interneuron migration by neurotrophins and PI3-kinase signaling. *Development* 129, 3147–3160.
- Ponomareva, O. N., Fischer, T. M., Lai, C., and Rimer, M. (2006). Schwann cell-derived neuregulin-2 alpha can function as a cell-attached activator of muscle acetylcholine receptor expression. *Glia* 54, 630–637. doi:10.1002/glia.20413.
- Rico, B., and Marín, O. (2011). Neuregulin signaling, cortical circuitry development and schizophrenia. *Curr. Opin. Genet. Dev.* 21, 262–270. doi:10.1016/j.gde.2010.12.010.
- Rimer, M., Prieto, A. L., Weber, J. L., Colasante, C., Ponomareva, O., Fromm, L., et al. (2004). Neuregulin-2 is synthesized by motor neurons and terminal Schwann cells and activates acetylcholine receptor transcription in muscle cells expressing ErbB4. *Mol. Cell. Neurosci.* 26, 271–281. doi:10.1016/j.mcn.2004.02.002.
- Rio, C., Buxbaum, J. D., Peschon, J. J., and Corfas, G. (2000). Tumor necrosis factor- $\alpha$ -converting enzyme is required for cleavage of erbB4/HER4. *J. Biol. Chem.* 275, 10379–10387. doi:10.1074/jbc.275.14.10379.
- Rio, C., Rieff, H. I., Qi, P., Khurana, T. S., and Corfas, G. (1997). Neuregulin and erbB receptors play a critical role in neuronal migration. *Neuron* 19, 39–50. doi:S0896-6273(00)80346-3 [pii].
- Risch, N. (1990). Linkage strategies for genetically complex traits. 1. Multilocus Models. *Am. J. Hum. Genet.* 46, 222–228. doi:papers2://publication/uuid/040CE8D5-AA72-4C07-8C7C-071B3AE3E19F.
- Saab, A. S., Tzvetanova, I. D., and Nave, K. A. (2013). The role of myelin and oligodendrocytes in axonal energy metabolism. *Curr. Opin. Neurobiol.* 23, 1065–1072. doi:10.1016/j.conb.2013.09.008.
- Saab, A. S., Tzvetavona, I. D., Trevisiol, A., Baltan, S., Dibaj, P., Kusch, K., et al. (2016). Oligodendroglial NMDA receptors regulate glucose import and axonal energy metabolism. *Neuron* 91, 119–132. doi:10.1016/j.neuron.2016.05.016.
- Salzer, J. L. (2003). Polarized domains of myelinated axons. *Neuron* 40, 297–318. doi:10.1016/S0896-6273(03)00628-7.
- Sanderson, D. J., Gray, A., Simon, A., Taylor, A. M., Deacon, R. M. J., Seeburg, P. H., et al.

- (2007). Deletion of glutamate receptor-A (GluR-A) AMPA receptor subunits impairs one-trial spatial memory. *Behav. Neurosci.* 121, 559–569. doi:10.1037/0735-7044.121.3.559.
- Santello, M., and Volterra, A. (2009). Synaptic modulation by astrocytes via Ca<sup>2+</sup>-dependent glutamate release. *Neuroscience* 158, 253–259. doi:10.1016/j.neuroscience.2008.03.039.
- Sardi, S. P., Murtie, J., Koirala, S., Patten, B. A., and Corfas, G. (2006). Presenilin-dependent ErbB4 nuclear signaling regulates the timing of astrogenesis in the developing brain. *Cell* 127, 185–197. doi:10.1016/j.cell.2006.07.037.
- Savelli, F., and Knierim, J. J. (2010). Hebbian analysis of the transformation of medial entorhinal grid-cell inputs to hippocampal place fields. *J. Neurophysiol.* 103, 3167–3183. doi:10.1152/jn.00932.2009.
- Sawyer, C., Hiles, I., Page, M., Crompton, M., and Dean, C. (1998). Two erbB-4 transcripts are expressed in normal breast and in most breast cancers. *Oncogene* 17, 919–924. doi:10.1038/sj.onc.1202015.
- Schillo, S., Pejović, V., Hunzinger, C., Hansen, T., Poznanović, S., Kriegsmann, J., et al. (2005). Integrative proteomics: Functional and molecular characterization of a particular glutamate-related neuregulin isoform. *J. Proteome Res.* 4, 900–908. doi:10.1021/pr050012p.
- Schulze, W. X., Deng, L., and Mann, M. (2005). Phosphotyrosine interactome of the ErbB-receptor kinase family. *Mol. Syst. Biol.* 1, 1–13. doi:10.1038/msb4100012.
- Scott, D. J., Heitzeg, M. M., Koeppe, R. A., Stohler, C. S., and Zubieta, J.-K. (2006). Variations in the human pain stress experience mediated by ventral and dorsal basal ganglia dopamine activity. *J. Neurosci.* 26, 10789–10795. doi:10.1523/JNEUROSCI.2577-06.2006.
- Shamir, A., Kwon, O.-B., Karavanova, I., Vullhorst, D., Leiva-Salcedo, E., Janssen, M. J., et al. (2012). The importance of the NRG-1/ErbB4 pathway for synaptic plasticity and behaviors associated with psychiatric disorders. *J. Neurosci.* 32, 2988–2997. doi:10.1523/JNEUROSCI.1899-11.2012.
- Shepherd, G. M. ., Pologruto, T. A., and Svoboda, K. (2003). Circuit analysis of experience-dependent plasticity in the developing rat barrel cortex. *Neuron* 38, 277–289. doi:10.1016/S0896-6273(03)00152-1.
- Somogyi, P. (1977). A specific “axo-axonal” interneuron in the visual cortex of the rat. *Brain Res.* 136, 345–350. doi:10.1016/0006-8993(77)90808-3.
- Stark, W. M., Boocock, M. R., and Sherratt, D. J. (1992). Catalysis by site-specific recombinases. *Trends Genet* 8, 432–439. doi:10.1016/0168-9525(92)90327-Z.
- Stefansson, H., Sigurdsson, E., Steinthorsdottir, V., Bjornsdottir, S., Sigmundsson, T., Ghosh, S., et al. (2002). Neuregulin 1 and susceptibility to schizophrenia. *Am. J. Hum. Genet.* 71,

- 877–892. doi:10.1086/342734.
- Steinthorsdottir, V., Stefansson, H., Ghosh, S., Birgisdottir, B., Bjornsdottir, S., Fasquel, A. C., et al. (2004). Multiple novel transcription initiation sites for NRG1. *Gene* 342, 97–105. doi:10.1016/j.gene.2004.07.029.
- Stepniak, B., Papiol, S., Hammer, C., Ramin, A., Everts, S., Hennig, L., et al. (2014). Accumulated environmental risk determining age at schizophrenia onset: A deep phenotyping-based study. *The Lancet Psychiatry* 1, 444–453. doi:10.1016/S2215-0366(14)70379-7.
- Sullivan, P. F., Lin, D., Tzeng, J.-Y., van den Oord, E., Perkins, D., Stroup, T. S., et al. (2008). Genomewide association for schizophrenia in the CATIE study: results of stage 1. *Mol. Psychiatry* 13, 570–584. doi:10.1038/mp.2008.25.
- Sun, Y., Ikrar, T., Davis, M. F., Gong, N., Zheng, X., Luo, Z. D., et al. (2016). Neuregulin-1/ErbB4 signaling regulates visual cortical plasticity. *Neuron* 92, 160–173. doi:10.1016/j.neuron.2016.08.033.
- Swerdlow, N. R., Weber, M., Qu, Y., Light, G. A., and Braff, D. L. (2008). Realistic expectations of prepulse inhibition in translational models for schizophrenia research. *Psychopharmacology (Berl)*. 199, 331–388. doi:10.1007/s00213-008-1072-4.
- Taepavarapruk, P., Floresco, S. B., and Phillips, A. G. (2000). Hyperlocomotion and increased dopamine efflux in the rat nucleus accumbens evoked by electrical stimulation of the ventral subiculum: role of ionotropic glutamate and dopamine D1 receptors. *Psychopharmacology (Berl)*. 151, 242–251. doi:10.1007/s002130000376.
- Talmage, D. A. (2008). Mechanisms of neuregulin action. *Novartis Found. Symp.* 289, 74–93.
- Tan, G.-H., Liu, Y.-Y., Hu, X.-L., Yin, D.-M., Mei, L., and Xiong, Z.-Q. (2012). Neuregulin 1 represses limbic epileptogenesis through ErbB4 in parvalbumin-expressing interneurons. *Nat. Neurosci.* 15, 258–266. doi:10.1038/nn.3005.
- Taniguchi, H., Lu, J., Huang, Z. J., Markram, H., Gelman, D. M., Marín, O., et al. (2013). The spatial and temporal origin of chandelier cells in mouse neocortex. *Science* 339, 70–74. doi:10.1126/science.1227622.
- Thomas, G. M., and Huganir, R. L. (2004). MAPK cascade signalling and synaptic plasticity. *Neuroscience* 5, 173–183.
- Thongrong, S., Hausott, B., Marvaldi, L., Agostinho, A. S., Zangrandi, L., Burtscher, J., et al. (2016). Sprouty2 and -4 hypomorphism promotes neuronal survival and astrocytosis in a mouse model of kainic acid induced neuronal damage. *Hippocampus* 26, 658–667. doi:10.1002/hipo.22549.
- Tidcombe, H., Jackson-Fisher, A., Mathers, K., Stern, D. F., Gassmann, M., and Golding, J. P. (2003). Neural and mammary gland defects in ErbB4 knockout mice genetically rescued from embryonic lethality. *Proc Natl Acad Sci U S A* 100, 8281–8286. doi:10.1073/



- pnas.1436402100.
- Ting, A. K., Chen, Y., Wen, L., Yin, D.-M., Shen, C., Tao, Y., et al. (2011). Neuregulin 1 promotes excitatory synapse development and function in GABAergic interneurons. *J. Neurosci.* 31, 15–25. doi:10.1523/JNEUROSCI.2538-10.2011.
- Towbin, H., Staehelin, T., and Gordon, J. (1979). Electrophoretic transfer of proteins from polyacrylamide gels to nitrocellulose sheets: procedure and some applications. *Proc. Natl. Acad. Sci. U. S. A.* 76, 4350–4354. doi:10.1002/bies.950190612.
- Traka, M., Arasi, K., Avila, R. L., Podojil, J. R., Christakos, A., Miller, S. D., et al. (2010). A genetic mouse model of adult-onset, pervasive central nervous system demyelination with robust remyelination. *Brain* 133, 3017–3029. doi:10.1093/brain/awq247.
- Tronche, F., Kellendonk, C., Kretz, O., Gass, P., Anlag, K., Orban, P. C., et al. (1999). Disruption of the glucocorticoid receptor gene in the nervous system results in reduced anxiety. *Nat. Genet.* 23, 99–103. doi:10.1038/12703.
- Tsien, J., Huerta, P., and Tonegawa, S. (1996). The essential role of hippocampal CA1 NMDA receptor-dependent synaptic plasticity in spatial memory. *Cell* 87, 1327–1338. doi:10.1016/S0092-8674(00)81827-9.
- Tsika, E., Kannan, M., Foo, C. S. Y., Dikeman, D., Glauser, L., Gellhaar, S., et al. (2014). Conditional expression of Parkinson's disease-related R1441C LRRK2 in midbrain dopaminergic neurons of mice causes nuclear abnormalities without neurodegeneration. *Neurobiol. Dis.* 71, 345–358. doi:10.1016/j.nbd.2014.08.027.
- Uhlhaas, P. J., and Singer, W. (2010). Abnormal neural oscillations and synchrony in schizophrenia. *Nat. Rev. Neurosci.* 11, 100–113. doi:10.1038/nrn2774.
- van Vugt, M. K., Schulze-Bonhage, A., Litt, B., Brandt, A., and Kahana, M. J. (2010). Hippocampal gamma oscillations increase with working memory load. *J. Neurosci.* 30, 2694–2699. doi:10.1523/JNEUROSCI.0567-09.2010.
- Vecchi, M., Baulida, J., and Carpenter, G. (1996). Selective cleavage of the heregulin receptor ErbB-4 by protein kinase C activation. *J. Biol. Chem.* 271, 18989–18995. doi:10.1074/jbc.271.31.18989.
- Vecchi, M., and Carpenter, G. (1997). Constitutive proteolysis of the ErbB-4 receptor tyrosine kinase by a unique, sequential mechanism. *J. Cell Biol.* 139, 995–1003. doi:10.1083/jcb.139.4.995.
- Velanac, V., Unterbarnscheidt, T., Hinrichs, W., Gummert, M. N., Fischer, T. M., Rossner, M. J., et al. (2012). Bace1 processing of NRG1 type III produces a myelin-inducing signal but is not essential for the stimulation of myelination. *Glia* 60, 203–217. doi:10.1002/glia.21255.
- Vita, A., De Peri, L., Silenzi, C., and Dieci, M. (2006). Brain morphology in first-episode schizophrenia: A meta-analysis of quantitative magnetic resonance imaging studies.

- Schizophr. Res.* 82, 75–88. doi:10.1016/j.schres.2005.11.004.
- Voytas, D. (2001). Resolution and recovery of DNA fragments. *Curr. Protoc. Mol. Biol.* 51, II:2.5A:2.5A.1–2.5A.9. doi:10.1002/0471142735.im1004s02.
- Vullhorst, D., Mitchell, R. M., Keating, C., Roychowdhury, S., Karavanova, I., Tao-Cheng, J.-H., et al. (2015). A negative feedback loop controls NMDA receptor function in cortical interneurons via neuregulin 2/ErbB4 signalling. *Nat. Commun.* 6, 7222. doi:10.1038/ncomms8222.
- Vullhorst, D., Neddens, J., Karavanova, I., Tricoire, L., Petralia, R. S., McBain, C. J., et al. (2009). Selective expression of ErbB4 in interneurons, but not pyramidal cells, of the rodent hippocampus. *J. Neurosci.* 29, 12255–12264. doi:10.1523/JNEUROSCI.2454-09.2009.
- Wallasch, C., Weiss, F. U., Niederfellner, G., Jallal, B., Issing, W., and Ullrich, A. (1995). Heregulin-dependent regulation of HER2/neu oncogenic signaling by heterodimerization with HER3. *EMBO J.* 14, 4267–4275.
- Wang, J. Y., Frenzel, K. E., Wen, D., and Falls, D. L. (1998). Transmembrane neuregulins interact with LIM kinase 1, a cytoplasmic protein kinase implicated in development of visuospatial cognition. *J. Biol. Chem.* 273, 20525–20534. doi:10.1074/jbc.273.32.20525.
- Wang, L., Zhou, K., Fu, Z., Yu, D., Huang, H., Zang, X., et al. (2017). Brain development and Akt signaling: the crossroads of signaling pathway and neurodevelopmental diseases. *J. Mol. Neurosci.* 61, 379–384. doi:10.1007/s12031-016-0872-y.
- Weber, T., Böhm, G., Hermann, E., Schütz, G., Schönig, K., and Bartsch, D. (2009). Inducible gene manipulations in serotonergic neurons. *Front. Mol. Neurosci.* 2, 24. doi:10.3389/fneuro.02.024.2009.
- Weickert, C. S., Tiwari, Y., Schofield, P. R., Mowry, B. J., and Fullerton, J. M. (2012). Schizophrenia-associated HapICE haplotype is associated with increased NRG1 type III expression and high nucleotide diversity. *Transl Psychiatry* 2, e104. doi:10.1038/tp.2012.25.
- Wen, D., Peles, E., Cupples, R., Suggs, S. V., Bacus, S. S., Luo, Y., et al. (1992). Neu differentiation factor: A transmembrane glycoprotein containing an EGF domain and an immunoglobulin homology unit. *Cell* 69, 559–572. doi:10.1016/0092-8674(92)90456-M.
- Wen, D., Suggs, S. V., Karunakaran, D., Liu, N., Cupples, R. L., Luo, Y., et al. (1994). Structural and functional aspects of the multiplicity of neu differentiation factors. *Mol. Cell. Biol.* 14, 1909–1919. doi:10.1128/MCB.14.3.1909.Updated.
- Wersinger, S. R., Ginns, E. I., O'Carroll, A.-M., Lolait, S. J., and Young, W. S. (2002). Vasopressin V1b receptor knockout reduces aggressive behavior in male mice. *Mol. Psychiatry* 7, 975–984. doi:10.1038/sj.mp.4001195.
- Wersinger, S. R., Temple, J. L., Caldwell, H. K., and Young, W. S. (2008). Inactivation of the

- oxytocin and the vasopressin (Avp) 1b receptor genes, but not the Avp 1a receptor gene, differentially impairs the Bruce effect in laboratory mice (*Mus musculus*). *Endocrinology* 149, 116–121. doi:10.1210/en.2007-1056.
- Willem, M., Garratt, A. N., Novak, B., Citron, M., Kaufmann, S., Rittger, A., et al. (2006). Control of peripheral nerve myelination by the  $\beta$ -secretase BACE1. *Science* 314, 664–666. doi:10.1126/science.1132341.
- Williams, C. C., Allison, J. G., Vidal, G. A., Burow, M. E., Beckman, B. S., Marrero, L., et al. (2004). The ERBB4/HER4 receptor tyrosine kinase regulates gene expression by functioning as a STAT5A nuclear chaperone. *J. Cell Biol.* 167, 469–478. doi:10.1083/jcb.200403155.
- Wilson, T. W., Hernandez, O. O., Asherin, R. M., Teale, P. D., Reite, M. L., and Rojas, D. C. (2008). Cortical gamma generators suggest abnormal auditory circuitry in early-onset psychosis. *Cereb. Cortex* 18, 371–378. doi:10.1093/cercor/bhm062.
- Winkler, D., Daher, F., Wüstefeld, L., Hammerschmidt, K., Poggi, G., Seelbach, A., et al. (2017). Hypersocial behavior and biological redundancy in mice with reduced expression of PSD95 or PSD93. *Behav. Brain Res.* doi:10.1016/j.bbr.2017.02.011.
- Wonders, C. P., and Anderson, S. (2006). The origin and specification of cortical interneurons. *Nat. Rev. Neurosci.* 7, 687–296.
- Woo, R. S., Li, X. M., Tao, Y., Carpenter-Hyland, E., Huang, Y. Z., Weber, J., et al. (2007). Neuregulin-1 enhances depolarization-induced GABA release. *Neuron* 54, 599–610. doi:10.1016/j.neuron.2007.04.009.
- Wright, I. C., Rabe-Hesketh, S., Woodruff, P. W. R., David, A. S., Murray, R. M., and Bullmore, E. T. (2000). Meta-Analysis of regional brain volumes in schizophrenia. *Am. J. Psychiatry* 157, 16–25. doi:10.1176/ajp.157.1.16.
- Wu, G. Y., Deisseroth, K., and Tsien, R. W. (2001). Spaced stimuli stabilize MAPK pathway activation and its effects on dendritic morphology. *Nat. Neurosci.* 4, 151–158. doi:10.1038/83976.
- Wynn, J. K., Light, G. A., Breitmeyer, B., Nuechterlein, K. H., and Green, M. F. (2005). Event-related gamma activity in schizophrenia patients during a visual backward-masking task. *Am. J. Psychiatry* 162, 2330–2336. Available at: <http://ajp.psychiatryonline.org>.
- Yang, X. L., Huang, Y. Z., Xiong, W. C., and Mei, L. (2005). Neuregulin-induced expression of the acetylcholine receptor requires endocytosis of ErbB receptors. *Mol. Cell. Neurosci.* 28, 335–346. doi:10.1016/j.mcn.2004.10.001.
- Yarden, Y., and Sliwkowski, M. X. (2001). Untangling the ErbB signalling network. *Nat. Rev. Mol. Cell Biol.* 2, 127–137. doi:10.1038/35052073.
- Yin, D.-M., Sun, X.-D., Bean, J. C., Lin, T. W., Sathyamurthy, A., Xiong, W.-C., et al. (2013a). Regulation of spine formation by ErbB4 in PV-positive interneurons. *J. Neurosci.* 33,

- 19295–19303. doi:10.1523/JNEUROSCI.2090-13.2013.
- Yin, D. M., Chen, Y. J., Lu, Y. S., Bean, J. C., Sathyamurthy, A., Shen, C., et al. (2013b). Reversal of behavioral deficits and synaptic dysfunction in mice overexpressing neuregulin 1. *Neuron* 78, 644–657. doi:10.1016/j.neuron.2013.03.028.
- Yokozeki, T., Wakatsuki, S., Hatsuzawa, K., Black, R. A., Wada, I., and Sehara-Fujisawa, A. (2007). Meltrin  $\beta$  (ADAM19) mediates ectodomain shedding of Neuregulin  $\beta$ 1 in the Golgi apparatus: Fluorescence correlation spectroscopic observation of the dynamics of ectodomain shedding in living cells. *Genes to Cells* 12, 329–343. doi:10.1111/j.1365-2443.2007.01060.x.
- Yoon, J. H., Maddock, R. J., Rokem, A., Silver, M. A., Minzenberg, M. J., Ragland, J. D., et al. (2010). GABA concentration is reduced in visual cortex in schizophrenia and correlates with orientation-specific surround suppression. *J. Neurosci.* 30, 3777–3781. doi:10.1523/JNEUROSCI.6158-09.2010.
- Young, W. S., Li, J., Wersinger, S. R., and Palkovits, M. (2006). The vasopressin 1b receptor is prominent in the hippocampal area CA2 where it is unaffected by restraint stress or adrenalectomy. *Neuroscience* 143, 1031–1039. doi:10.1016/j.neuroscience.2006.08.040.
- Zambrowicz, B. P., Imamoto, A., Fiering, S., Herzenberg, L. A., Kerr, W. G., and Soriano, P. (1997). Disruption of overlapping transcripts in the ROSA beta geo 26 gene trap strain leads to widespread expression of beta-galactosidase in mouse embryos and hematopoietic cells. *Proc. Natl. Acad. Sci. U. S. A.* 94, 3789–3794. doi:10.1073/pnas.94.8.3789.
- Zhang, J., Zhao, J., Jiang, W.-J., Shan, X.-W., Yang, X.-M., and Gao, J.-G. (2012). Conditional gene manipulation: Cre-ating a new biological era. *J. Zhejiang Univ. Sci. B* 13, 511–524. doi:10.1631/jzus.B1200042.
- Zhang, Z. J., and Reynolds, G. P. (2002). A selective decrease in the relative density of parvalbumin-immunoreactive neurons in the hippocampus in schizophrenia. *Schizophr. Res.* 55, 1–10. doi:10.1016/S0920-9964(01)00188-8.
- Zhou, W., and Carpenter, G. (2000). Heregulin-dependent trafficking and cleavage of ErbB-4. *J. Biol. Chem.* 275, 34737–34743. doi:10.1074/jbc.M003756200.
- Ziff, E. B. (1997). Enlightening the postsynaptic density. *Neuron* 19, 1163–1174.

**Curriculum vitae**

Surname, first name: Soto Bernardini, María Clara  
Date of birth: 01. September 1982  
Place of birth: San José, Costa Rica  
Nationality: Costa Rican, Italian  
Home address: Hannoversche str. 137a  
37077 Göttingen, Germany

**Education:**

03.2013 – present Graduate student at the Max Planck Institute of Experimental Medicine, Department of Neurogenetics  
Thesis: “Modelling schizophrenia endophenotypes by over-expression of Neuregulin-1 isoforms in transgenic mice”  
Student of the program Molecular Physiology of the Brain (GGNB).

01.2005 – 03.2008 Master in Biology with emphasis in Genetics and Molecular Biology.  
Graduation with honors. University of Costa Rica, Costa Rica.

03.2000 – 06.2004 Bachelor in Biology: University of Costa Rica, Costa Rica.

02.1995 – 02.1999 Bachelor in Medium Education: Saint Francis High School, Costa Rica.

**Professional experience:**

2008 – 2012 Lecturer at the Costa Rican Institute of Technology.

2008 – 2012 Research scientist in psychiatric genetics projects. Center for Research in Cellular and Molecular Biology (CIBCM), University of Costa Rica.

- 2005 – 2007                      Research assistant in projects of genetics of neuropsychiatric diseases. CIBCM, University of Costa Rica.
- 2002-2004                      Research assistant, sequencing laboratory. CIBCM, University of Costa Rica.

**Publications:**

- Gummert M.\*, Zhang M.\*, **Soto-Bernardini M. C.\***, Unterbarnscheidt T., Radyushkin K., El-Kordi A., Ehrenreich H., Nave K.-A., Zhang W., Schwab M. H. (2016). Elimination of ErbB4 from postnatal projection neurons suggests cell-autonomous functions in excitatory networks. *In prep.*
- Soto-Bernardini M. C.**, Unterbarnscheidt T., Dere E., Altas B., Rhee J. S., Ehrenreich H., Nave K.-A., Schwab M. H. (2016). Endophenotype profiling in a conditional transgenic mouse model of NRG1 type I-mediated cortical ErbB4 hyperstimulation. *In prep.*
- Wehr M. C., Hinrichs W., Brzozka M. M., Unterbarnscheidt T., Herholt A., Wintgens J. P., **Soto-Bernardini M. C.**, Kravchenko M., Zhang M., Nave K.-A., Wichert S. P., Falkai P., Zhang W., Schwab M. H., Rossner M. J. (2016). Spironolactone is an antagonist of NRG1-ERBB4 signaling and schizophrenia-relevant endophenotypes in mice. *Submitted to EMBO Mol. Med.*
- Marballi K., Quinones M. P., Jimenez F., Escamilla M. A., Raventós H., **Soto-Bernardini M. C.**, Ahuja S. S., Walss-Bass C. (2010). *In Vivo* and *in Vitro* Genetic Evidence of Involvement of Neuregulin 1 in Immune System Dysregulation. *J. Mol. Med.* 88, 1133-1141.
- Walss-Bass C., **Soto-Bernardini M. C.**, Johnson-Pais T., Leach R. J., Ontiveros A., Nicolini H., Mendoza R., Jerez A., Dassori A., Chavarria-Siles I., Escamilla M.A. y Raventós H. (2008). Methionine sulfoxide reductase: A novel schizophrenia candidate gene. *Am J Med Genet B Neuropsychiatr Genet.* 150, 219-225.

\*Co-first authors

**Funding:**

- 04-06.17 Bridging Fund from the Göttingen Graduate School for Neurosciences, Biophysics, and Molecular Biosciences (GGNB).
- 12-16.10.2016 Travel grant from the GGNB to attend SfN meeting. San Diego, USA.
- 04.2016-03.2017 Scholarship from the Ministry of Science, Technology and Telecommunications of Costa Rica (MICITT) to finish PhD project.
- 10.2012-03.2016 DAAD fellowship (Deutscher Akademischer Austausch Dienst) for PhD studies.
- 06-07.2007 Fellowship from the National Institute of Mental Health (NIMH) for the internship in psychiatric genetics at the South Texas Psychiatric Genetics Research Center (STPGRC) of the University of Texas Health Science Center at San Antonio (UTHSCSA).
- 07.2005 Fellowship from the Fundación Carolina to attend the workshop Genomics at the Universidad Complutense, Madrid.

**Founded projects:**

- 2018-2020: Investigation of neuronal signaling pathways downstream of Neuregulin-2. Vice presidency of Research, Costa Rican Institute of Technology (01.2018-12.2020 / 135 000 USD)
- 2018-2021: Profiling and validation of molecular pathophysiology downstream of NRG1-ErbB4 hyperstimulation with relevance for schizophrenia Vice presidency of Research, Costa Rican Institute of Technology (01.2018-12.2021 / 150 000 USD)

**International activities:**

- 2016 Society for Neuroscience Meeting. San Diego, USA.  
November 12-16
- 2015 Workshop/collaboration. Structural expression analysis of the  
NRG1/ErbB4 signaling module at CNS synapses. Department  
of Experimental Medicine. University of de Lleida, Spain.  
March 9-20.
- 2007 Internship at the South Texas Psychiatric Genetics Research  
Center (STPGRC) of the University of Texas Health Science  
Center at San Antonio (UTHSCSA). San Antonio, USA.  
June-July.
- 2005 Workshop Genomics. Escuela Complutense de Verano,  
Universidad Complutense, Madrid, Spain. July 4-29.